Phenotyping C9-ALS/FTD iPSC-derived cortical neurons



By

Malina Graf

A thesis submitted for the degree of

Doctor of Philosophy

New College

Nuffield Department of Clinical Neurosciences

University of Oxford

Declaration

I declare that this thesis is entirely my own work. Except where otherwise stated, this dissertation describes my own research.

Malina Graf, New College

Issues arising from the COVID-19 pandemic

This work was heavily affected by the COVID-19 pandemic. During the first lockdown in March 2020, the department was closed, and I was unable to conduct any experiments for five months. When the lab closed, I had to freeze the cells from an ongoing differentiation and thaw them when the lab re-opened, which led to a decrease in purity in those cell cultures. As I had passed my transfer of status milestone not long before, I only had about two weeks' worth of data to analyse and figures to make during my time away from the lab.

During the second lockdown in November 2020, I had to shield because I was in an at-risk group myself and lived with someone who had to shield. Therefore, I did home office during the day and my cell culture work at night when I was alone at the lab. This took a toll on my mental well-being. During the third lockdown in early 2021, I pushed off starting a differentiation in our small cell culture lab until I received my first vaccine in March. Instead, I focused on running Western blotting and immunofluorescence experiments in our lab.

While I received 4.5 months of the university’s COVID-19 Scholarship Extension Funding, this did not cover all the experimental time I had lost due to the pandemic.

Abstract

The GGGGCC hexanucleotide expansion in the C9orf72 gene (C9-HRE) is the most frequent genetic cause of amyotrophic lateral sclerosis (ALS) and frontotemporal dementia (FTD). C9-ALS/FTD describes the condition in which patients suffer from both ALS and FTD, which are described as the degeneration of motor or cortical neurons, respectively. While the molecular phenotype caused by the C9-HRE is relatively well established in motor neurons, little work has been done to understand the molecular effect of the C9-HRE on cortical neurons.

This study aims at furthering our understanding of the molecular impairments caused by the C9-HRE in patient cortical neurons. To this end, I differentiated C9-ALS/FTD-patient induced pluripotent stem cells (iPSCs) into cortical neurons. In these cells, I measured stress granule formation, autophagic flux, ER stress, excitability, Ca^{2+} signalling, and mitochondrial integrity and function, which are pathways that are commonly affected in C9-HRE-carrying motor neurons.

I found no evidence of altered stress granule formation, autophagic flux, and ER stress in C9-iPSC-derived cortical neurons. Furthermore, I discovered changes in excitability, excitation latency, and cytosolic Ca^{2+} clearance after glutamate and KCl stimulation due to changes in GluA1 expression in cortical neurons. In addition, C9-iPSC-derived cortical neurons displayed mitochondrial impairments. The mitochondrial membrane potential was reduced causing increased mitophagy which results in a reduction in mitochondrial mass. The mitochondrial fission apparatus was downregulated, and the anterograde axonal transport machinery was overexpressed. Mitochondrial respiration remained unaltered in patient cortical neurons.

Together this data suggests the C9-HRE causes a distinct phenotype in iPSC-derived cortical neurons, stressing the need to study the FTD pathomechanism in the respective cell type. The molecular early-disease phenotype of C9-FTD includes impairments in excitability and mitochondrial processes. This study serves as a foundation for future FTD research using iPSC-derived cortical neurons.

Acknowledgements

I want to thank my funding bodies, the Alzheimer's Society and the Oxford Motor Neurone Disease Centre for sponsoring this project. I want to thank my primary supervisor Prof. Kevin Talbot for supporting me throughout my degree with his scientific knowledge and wide view of the MND field. I want to thank my secondary supervisor Dr Ruxandra Dafinca for passing on her vast skills, for all the practical day-to-day support, and for steadily keeping me on the right track. I also want to thank everybody at the lab who helped me out: Paola, Jakub, Carlota, Stephen, Max, Nidaa, and Dr Sally Cowley.

I want to thank New College, especially Ros Temple for all her advice and perspective in good and bad times. I would like to thank the New College MCR for offering me a home and community I could be part of and shape. I want to thank my Oxford family for all the unforgettable memories, early morning rowing, dinners, lockdown walks, trips, and last-minute-panic scientific advice.

I want to thank Rob for being my home and my rock, for providing me with meals when I worked all day, and for making all issues seem a little smaller when my differentiations went wrong… It is hard to put into words everything you have done for me.

I want to thank Jim and Janet for opening their home to me when I had to leave Oxford. I want to thank my family for always believing in me and making me the person I am today. I want to thank everyone who got on a plane to visit me on an island that kept creeping further and further away from the continent.

Abbreviations

ALS	amyotrophic lateral sclerosis
ALS-FTD	amyotrophic lateral sclerosis with comorbid frontotemporal dementia
AMPAR	α-amino-3-hydroxy-5-methyl-4-isoxazolepropionic acid receptor
ASO	antisense oligonucleotide
ATF4	activating transcription factor 4
BAC	bacterial artificial chromosome
Bcl-2	B-cell lymphoma 2
BDNF	brain-derived neurotrophic factor
BiP	binding immunoglobulin protein
C9-CNs	C9-HRE carrying iPSC-derived cortical neurons
C9-HRE	C9orf72 hexanucleotide repeat expansion
C9-MNs	C9-HRE carrying iPSC-derived motor neurons
C9orf72	chromosome 9 open reading frame 72
C9-RNA	C9-HRE-containing RNA
CACNA2D1	calcium voltage-gated channel auxiliary subunit alpha 2 delta 1
CBS	corticobasal syndrome
CCCP	carbonyl cyanide *m*-chlorophenyl hydrazone
CCh	carbachol
CHMP2B	charged multivesicular protein 2B
CHOP	C/EBP homologous protein
ClCasp3	cleaved caspase 3
CN or CNs	cortical neuron or cortical neurons
CNS	central nervous system
COX IV	Cytochrome C oxidase subunit 4
CTIP1	B-cell lymphoma/leukaemia 11A
CTIP2	B-cell lymphoma/leukaemia 11B
CytC	cytochrome C
DAPI	4’,6-diamidino-2-phenylindole
DCTN1	dynactin subunit 1
DPR	dipeptide repeat protein

DRP1	dynamin-related protein 1
eIF2α	eukaryotic translation initiation factor 2
ER	endoplasmic reticulum
FTD	frontotemporal dementia
FTLD	frontotemporal lobar degeneration
GDNF	glial cell-derived neurotrophic factor
GFAP	glial fibrillary acidic protein
GluA1	glutamate ionotropic receptor AMPA type subunit 1
GluN1	glutamate ionotropic receptor NMDA type subunit 1
GPCR	G-protein coupled receptor
GRN	granulin
IP_3	inositol trisphosphate
iPSCs	induced pluripotent stem cells
KIF5	kinesin-related protein 5
LAMP2A	lysosomal-associated membrane protein 2A
LC3B	microtubule-associated proteins 1A/1B light chain 3B
lvPPA	logopenic variant primary progressive aphasia
MAPT	microtubule-associated protein tau
MCU	mitochondrial calcium uniporter
Mfn	mitofusin
MND	motor neuron disease
mtDNA	mitochondrial DNA
mTORC1	mammalian target of rapamycin complex 1
$NaAsO_2$	sodium arsenite
nfvPPA	non-fluent primary progressive aphasia
NMDAR	N-methyl-D-aspartate receptor
OCR	oxygen consumption rate
OMM	outer mitochondrial membrane
OPA1	optic atrophy-1
OPTN	optineurin
OXPHOS	oxidative phosphorylation
PABP	poly(A)-binding protein

PARL	presenilin-associated rhomboid-like protein
PERK	protein kinase RNA-like ER kinase
PINK1	PTEN-induced kinase 1
PPA	primary progressive aphasia
P-Ub (Ser65)	ubiquitin chains phosphorylated at serin 65
PSD95	post-synaptic density 95
RAN translation	repeat-associated non-ATG-dependent translation
RBP	RNA-binding protein
ROS	reactive oxygen species
RyR	ryanodine receptor
SERCA	sarco/endoplasmic reticulum Ca^{2+}-ATPase
SG	stress granule
SQSTM1, p62	sequestosome 1
svPPA	semantic variant primary progressive aphasia
TBK1	TANK-binding kinase 1
Tbr1	T-box, brain 1
TDP-43	TAR DNA-binding protein 43
TIA1	T cell-restricted intracellular antigen-1
TOMM20	translocase of the outer mitochondrial membrane complex subunit 20
Tuj1	βIII-tubulin
UBQLN2	ubiquilin 2
ULK1	Unc-51 like autophagy activating kinase 1
UPR	unfolded protein response
VCP	valosin-counting protein
VDAC	voltage-dependent anion channel
VENs	von Economo neurons
VGCC	voltage-gated calcium channel
VGluT1	Vesicular glutamate transporter 1

Table of Contents

1 Introduction 10

1.1 Frontotemporal Dementia 10

1.1.1 Clinical presentation 10

1.1.2 Current therapeutic strategies 12

1.1.3 Comorbidities 12

1.1.4 The ALS-FTD spectrum 13

1.1.5 Pathology 14

1.1.5.1 TDP-43 proteinopathy 14

1.1.5.2 Tau pathology 16

1.1.5.3 FUS pathology 17

1.1.6 Disease-associated mutations 17

1.1.6.1 *C9orf72* 18

1.1.6.2 *MAPT* and *GRN* 19

1.1.6.3 *SOD1* and *TARDBP* 21

1.1.6.4 Other mutations 22

1.2 The GGGGCC hexanucleotide repeat expansion in the *C9orf72* gene 24

1.2.1 Loss of function 24

1.2.2 Gain of function 25

1.2.2.1 RNA foci 25

1.2.2.2 Dipeptide repeat proteins 26

1.2.3 Affected cellular mechanisms in neurons 28

1.2.3.1 Apoptosis 29

1.2.3.2 ER stress 31

1.2.3.3 Stress granule formation 32

1.2.3.4 Autophagy 33

1.2.3.5 Excitotoxicity 37

1.2.3.6 Mitochondrial function 40

1.2.3.7 Dynamics of mitochondrial morphology 42

1.2.3.8 Mitophagy 44

1.2.3.9 Axonal transport 46

1.2.4 Non-neuronal involvement 48

1.2.4.1 Microglia 49

1.2.4.2 Astrocytes 50

1.2.4.3 Oligodendrocytes 51

1.2.5 Therapeutic strategies for C9-ALS/FTD in development 51

1.3 C9-Research models 54

1.3.1 Post-mortem brain tissue 54

1.3.2 Animal models 55
1.3.2.1 Mice 55
1.3.2.2 Zebrafish 56
1.3.2.3 Drosophila 57
1.3.3 Induced pluripotent stem cells (iPSCs) 59
1.3.4 Pathomechanisms of C9-ALS/FTD research models 61
1.3.4.1 Human post-mortem tissue 61
1.3.4.2 Mice 62
1.3.4.3 Zebrafish 63
1.3.4.4 Drosophila 63
1.3.4.5 Induced pluripotent stem cells 64
1.4 Aims of this thesis 66
2 Methods 68
2.1 Cell culture 68
2.1.1 hiPSC lines 68
2.1.2 hiPSC culture 68
2.1.3 Differentiation 69
2.2 Basic methods 70
2.2.1 Immunofluorescence 70
2.2.2 Western Blot 70
2.2.3 Calcium imaging 71
2.3 Characterising iPSC-derived cortical neurons 72
2.4 Analysis of protein-associated cellular stress 74
2.5 Analysis of excitability 74
2.6 Analysis of mitochondrial function 75
2.6.1 Measuring mitochondrial protein levels 75
2.6.2 Measuring mitochondrial depolarisation 75
2.6.3 Measuring axonal transport 76
2.6.4 Seahorse XF Cell Mito Stress Test 76
2.6.5 ROS assay 78
2.7 Statistical analysis 78
3 *C9orf72* patient-derived induced pluripotent stem cells are differentiated into layer V/VI cortical neurons with features of C9-ALS/FTD pathology 80
3.1 iPSC-derived cultures are neuronal and glutamatergic on day 55 83
3.2 A high proportion of cells in iPSC-derived cultures show properties of layer V/VI cortical neurons 86
3.3 C9-ALS/FTD cortical neurons show an increase in apoptosis 90
3.4 C9-ALS/FTD cortical neurons do not show TDP-43 mislocalisation 97
3.5 Conclusion 98
4 C9-ALS/FTD-derived CNs do not show features of protein-associated cellular stress 102

4.1 Stress granule formation was not upregulated in iPSC-derived C9-CNs 103
4.2 No evidence for ER stress was found in iPSC-derived C9-CNs 105
4.3 Intracellular Ca^{2+} signalling is disturbed in iPSC-derived C9-CNs 107
4.4 No changes in autophagic flux were observed in iPSC-derived C9-CNs 109
4.5 Conclusion 112
5 Excitability is significantly altered in C9-ALS/FTD-derived CNs 117
5.1 iPSC-derived C9-CNs demonstrate changes in excitability 118
5.2 GluA1 levels were significantly altered in iPSC-derived C9-CN 121
5.3 iPSC-derived C9-CNs demonstrate changes in calcium clearance 127
5.4 Conclusion 130
6 Mitochondrial processes are significantly altered in C9-ALS/FTD-derived CNs 133
6.1 Mitochondrial fission apparatus proteins are downregulated in stressed iPSC-derived C9-CNs 135
6.2 The mitochondrial mass is reduced in iPSC-derived C9-CNs 139
6.3 The mitochondrial membrane potential is reduced in iPSC-derived C9-CNs 143
6.4 Mitophagy initiators were upregulated in iPSC-derived C9-CNs after 24h CCCP treatment 145
6.5 Reactive oxygen species levels are not increased in iPSC-derived C9-CNs 147
6.6 Mitochondrial respiration is not altered in iPSC-derived C9-CNs 148
6.7 The anterograde axonal transport machinery is overexpressed in iPSC-derived C9-CNs 152
6.8 Conclusion 157
7 Discussion 162
7.1 Which disease phenotypes did I discover in iPSC-derived C9-CNs? 162
7.2 Which phenotypes might be the primary defect caused by the *C9orf72* hexanucleotide expansion? 165
7.3 Is the disease phenotype in C9-CNs the same as in C9-MNs? 168
7.4 Are iPSC-derived C9-CNs a useful disease model? 172
7.5 Which further experiments are needed? 174
8 References 177
9 Appendices 211
9.1 Appendix 1: Chromosomal aberrations in iPSCs 211
9.2 Appendix 2: Optimising the concentration of treatments 212
9.2.1 Thapsigargin treatment 213
9.2.2 Bafilomycin treatment 214
9.2.3 Rapamycin treatment 215
9.2.4 $NaAsO_2$ treatment 216
9.2.5 CCCP treatment 217
9.3 Appendix 3: Materials 218

1 Introduction

1.1 Frontotemporal Dementia

1.1.1 Clinical presentation

Dementia is a major global health challenge. It is the leading cause of death in the UK, causing about 75k deaths in 2017. It remains the only condition in the top 10 causes of death in the UK without an available treatment to cure, prevent, or slow its progression (National Records of Scotland, 2018; Northern Ireland Statistics and Research Agency, 2018; Office for National Statistics, 2018) The global burden of dementia is expected to increase almost 4-fold between 2016 and 2060 (Sleeman et al., 2019). After Alzheimer's Disease, Frontotemporal Dementia (FTD) is the second most common form of dementia, with an age of onset of typically 45-65 years. The mean duration of the illness is eight years, ranging from 2 to 20 years, depending on comorbidities and affected brain areas (Warren et al., 2013). Due to its early onset and long duration, FTD causes a substantial socioeconomic cost and burden on families and carers (Warren et al., 2013).

FTD is a heterogeneous neurodegenerative disease characterised by the progressive degeneration of cortical neurons in the frontal and temporal lobes (Woollacott & Rohrer, 2016). Roughly half of the cases present with behavioural variant FTD (bvFTD), which is characterised by a progressive decline in social skills, such as loss of sympathy or empathy, an emergence of abnormal behaviours, such as disinhibition, apathy, and compulsive behaviour, as well as a decline in executive function (Woollacott & Rohrer, 2016). bvFTD is caused by atrophy in the frontal lobe, often in combination with anterior temporal lobe atrophy. The extent and severity of atrophy may vary widely (Warren et al., 2013).

The other half of patients present with a decline of language skills termed primary progressive aphasia (PPA), which is caused by progressive atrophy commonly in the left temporal lobe with varying extent and severity. There are three forms of PPA, non-fluent variant PPA (nfvPPA), semantic variant PPA

(svPPA), and logopenic variant PPA (lvPPA). nfvPPA is characterised by impaired speech production, such as effortful non-fluent speech with frequent articulatory and grammatical errors. svPPA is characterised by a progressive breakdown of semantic memory, which is the memory of objects and concepts, and initially typically presents as a lack of knowledge of the meaning of words. In advanced cases, it can also impact visual information such as impaired recognition of faces or objects or the recognition of odours and flavours. lvPPA presents as hesitant but grammatically correct speech with frequent word-finding pauses, phonological errors and impaired phonological working memory (difficulty repeating phrases rather than single words). Most lvPPA patients suffer from underlying Alzheimer's disease (Warren et al., 2013; Woollacott & Rohrer, 2016).

For an overview of FTD subtypes, see Figure 1. Comorbidities, characteristic pathologies, and associated mutations will be described in the following sections (1.1.3 - 1.1.6).

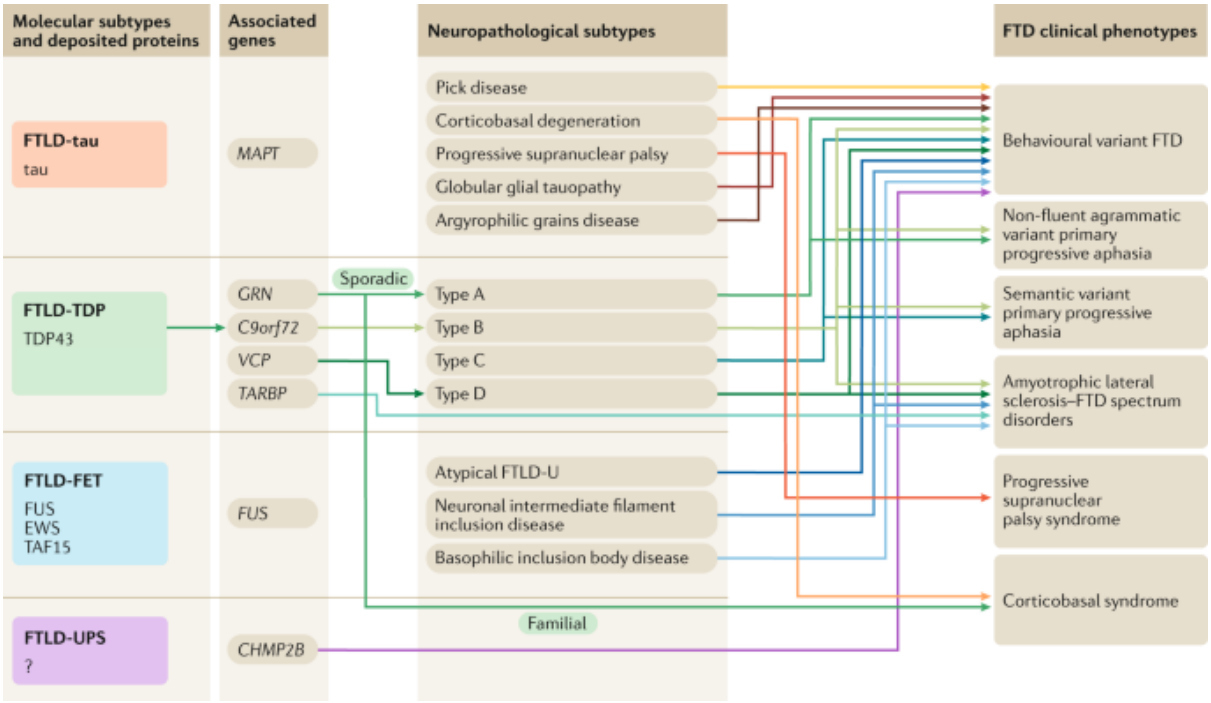


Figure 1: Overview of pathological, genetic, and clinical subtypes of FTD. This image was taken from Panza et al. (2020) and altered.

1.1.2 Current therapeutic strategies

There are currently no disease-modifying treatments available for FTD. Instead, treatments focus on managing symptoms. Antidepressants such as selective serotonin reuptake inhibitors (SSRIs) have been described as effective in treating behavioural symptoms such as agitation, disinhibition, depression, and obsessive-compulsive behaviours in some patients suffering from bvFTD (Jicha & Nelson, 2011; Khoury et al., 2021). For patients that do not respond to SSRIs and present aggressive and psychotic features, antipsychotic medication may be used. However, this class of drugs can cause severe adverse effects such as stroke and cardiac complications, especially in elderly patients. Therefore, they are generally only used if the behaviour of patients poses an immediate threat to safety (Jicha & Nelson, 2011; Khoury et al., 2021; Tsai & Boxer, 2014). Other treatments which are used in Alzheimer's disease and Parkinson's disease, such as cholinesterase inhibitors, NMDAR-antagonists, and dopaminergic therapies, do not have a beneficial effect on FTD but might worsen behavioural or cognitive symptoms (Tsai & Boxer, 2016).

Non-pharmacological treatments are equally crucial, such as speech therapy for patients suffering from PPA. Furthermore, exercise benefits mood, cognition, and overall health in dementia. Physical therapy for balance training and gait, and swallow evaluations are critical for patients with motor difficulties (Tsai & Boxer, 2016). Not every symptom can be addressed effectively by these symptomatic treatments. Moreover, none of these therapies halts the disease progression of FTD.

1.1.3 Comorbidities

Several overlap syndromes, all with motor symptoms, are known. Parkinsonism, a syndrome characterised by tremors at rest, muscle rigidity, and bradykinesia (slowness of movement), is observed in about 20% of FTD cases (Galvan & Wichmann, 2008; Woollacott & Rohrer, 2016). Progressive supranuclear palsy syndrome is a further common comorbidity of FTD (Woollacott & Rohrer, 2016). This tauopathy is characterised by supranuclear gaze palsy (the inability to look in a

vertical direction), postural instability, akinesia (the inability to perform voluntary movements), and cognitive dysfunction (M. J. Armstrong, 2018). A further tauopathy is often associated with FTD: corticobasal syndrome (CBS) cases present with asymmetrical Parkinsonism, muscle spasms, involuntary muscle jerks, alien limb phenomena, apraxia (the inability to perform learned movements on command), and cortical sensory deficits (Constantinides et al., 2019).

The comorbidity of FTD with motor neuron disease (MND) is common, particularly amyotrophic lateral sclerosis (ALS). ALS is the most common form of MND, with an incidence of 1.5 to 2.7 per 100,000 people per year, and is characterised by progressive degeneration of upper and lower motor neurons, causing progressive muscle atrophy and paralysis. The most common cause of death in ALS patients is respiratory failure. The average survival is 30 months from symptom onset but ranges from <1 to over 10 years (Salameh et al., 2015). Patients suffering from ALS with comorbid FTD (ALS-FTD) have a shorter survival (23 months) on average than ALS without (34 months) cognitive dysfunction (Elamin et al., 2011). Similarly, FTD with comorbid ALS (FTD-ALS) has a survival of approx. 2.5 years in contrast to about eight years for bvFTD (Kansal et al., 2016).

1.1.4 The ALS-FTD spectrum

There is a significant overlap in the clinical profile of ALS and FTD. About 60% of FTD patients show some motor neuron impairment, and 10-15% meet ALS diagnostic criteria. Similarly, at least 50% of ALS patients show cognitive or behavioural symptoms and 10-20% meet the diagnostic criteria for FTD (Woollacott & Rohrer, 2016). Up to 40% of ALS patients have detectable mild cognitive changes (Phukan et al., 2012).

In addition, FTD and ALS share many disease-causing genetic mutations and pathological hallmarks. Therefore, FTD and ALS, with TDP-43 proteinopathy are now conceptualised as aspects of a disease continuum, with FTD-only and ALS-only cases representing the extremes of the spectrum (see Figure

2) (Strong et al., 2017). Mutations associated with the ALS-FTD spectrum and pathological features will be discussed in the following sections.

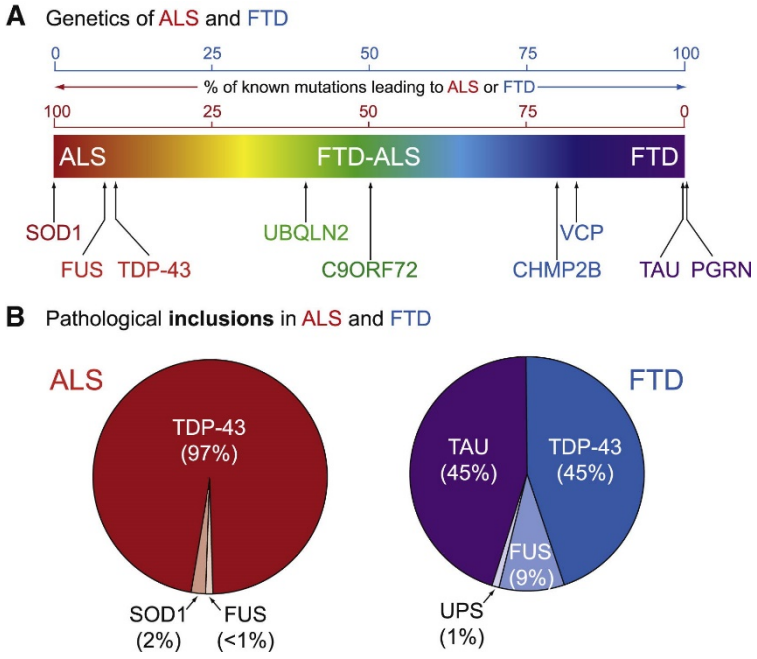


Figure 2: FTD and ALS represent a disease continuum with FTD- and ALS-only variants as the end of the spectrum. (A) Genetic causes of ALS and FTD overlap. Major genetic causes are plotted to reflect the ratio of known disease presentation. (B) Percentage of patients with ALS and FTD showing TDP-43, FUS, SOD1, or ubiquitin (UPS) protein aggregates. This image was taken from Ling et al. (2013).

1.1.5 Pathology

1.1.5.1 TDP-43 proteinopathy

In up to 97% of ALS cases and about 45-50% of FTD cases, nuclear and cytoplasmic transactive response DNA-binding protein 43 (TDP-43) positive inclusions are found in neurons and glia (Arai et al., 2006; Bodansky et al., 2010; Neumann et al., 2006; H. P. Nguyen et al., 2018). The distribution of TDP-43 inclusions correlates with brain areas affected by ALS or FTD pathology (Neumann et al., 2006). Aggregates were detected in the primary motor cortex, brainstem motor nuclei, and spinal cord in ALS (Bodansky et al., 2010; Davidson et al., 2007; I. R. A. Mackenzie et al., 2007), and neocortex and dentate granule cells of the hippocampus in FTD (Davidson et al., 2007; Neumann et al., 2006). These

inclusions are ubiquitin- and p62-positive and contain hyperphosphorylated, ubiquitinated and truncated TDP-45 fragments (Arai et al., 2006; Hiji Masanori et al., 2008; Neumann et al., 2006). Mislocalisation of the nuclear protein TDP-43 to the cytoplasm and cytosolic and nuclear aggregation are known as TDP-43 proteinopathy.

TDP-43 is an RNA- and DNA-binding protein regulating RNA metabolism in many aspects, such as transcription (Ou et al., 1995), splicing (Buratti et al., 2001), miRNA biogenesis (Kawahara & Mieda-Sato, 2012), mRNA transport (I. F. Wang et al., 2008), and mRNA stabilisation (see Figure 3) (Strong et al., 2007). Due to the mislocalisation of TDP-43 into the cytosol, loss of function of TDP-43 causes altered RNA metabolism (A. L. Ji et al., 2017; Prpar Mihevc et al., 2016). Furthermore, mislocalised TDP-43 could lead to the mislocalisation of bound mRNA molecules preventing their processing and maturation (E. B. Lee et al., 2012). This could cause a loss of function of downstream molecules.

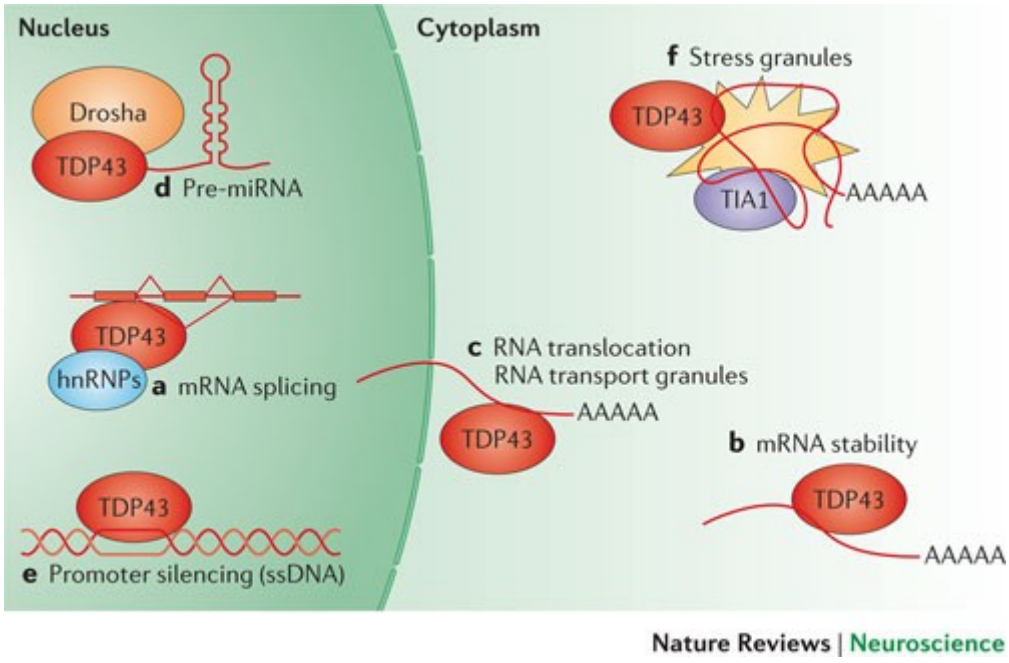


Figure 3: TDP-43 is involved in mRNA splicing, mRNA stability, RNA translocation, miRNA processing, gene silencing, and stress granule formation. This figure was taken from E. B. Lee et al. (2012).

TDP-43 pathology also leads to a gain of function of toxic aggregates. For example, cytosolic TDP-43 aggregates were shown to impair nucleocytoplasmic transport and recruit other proteins, thus

impairing their normal function (Woerner et al., 2016). Additionally, aggregations of misfolded TDP-43 proteins were shown to disrupt the conformation of other TDP-43 proteins in a prion-like fashion (Nonaka et al., 2013; Smethurst et al., 2016). Small soluble TDP-43 assemblies could be transmitted to neighbouring cells, causing a spread of toxicity (Nonaka et al., 2013; Smethurst et al., 2016). Furthermore, it has been shown that both overexpression and underexpression of TDP-43 have a toxic effect (Kabashi et al., 2009; White et al., 2018). Therefore, the autoregulation of TDP-43 involved in processing its mRNA is an essential feedback mechanism for TDP-43 expression and could aggravate TDP-43 pathology (E. B. Lee et al., 2012; White et al., 2018).

Through these pathological mechanisms, TDP-43 pathology disrupts gene expression. TDP-43 dysfunction affects pathways which involve the CREB transcription factor leading to defects in dendritic branching (Herzog et al., 2020). RNAseq showed that dysregulated mechanisms include synapse assembly, signal transduction, and positive regulation of GTPase activity (Herzog et al., 2020).

1.1.5.2 Tau pathology

Tau pathology is described as the pathological aggregation of hyperphosphorylated tau in neurofibrillary tangles (X. Zhang et al., 2018). One study found that 59% of patients with ALS, 44% of patients with FTD and ALS and 43% of patients with FTD display significant tau pathology (Behrouzi et al., 2016). Tau pathology is found in cases of C9-HRE-associated frontotemporal lobar degeneration (Bieniek et al., 2013). In decreasing abundance, tau pathology was observed in the entorhinal cortex, hippocampus, temporal cortex, frontal cortex, and occipital cortex (Behrouzi et al., 2016). However, the role of tau pathology in ALS/FTD pathogenesis remains to be confirmed and is not universally agreed to be a prominent feature of ALS.

Tau is a protein stabilising microtubules and axonal maintenance (see 1.1.6.2) (Olszewska et al., 2016; Y. Wang & Mandelkow, 2016). The hyperphosphorylation of tau leads to its disintegration from microtubules, resulting in neuronal dysfunction (X. Zhang et al., 2018). In addition,

hyperphosphorylated tau is prone to accumulate and form tangles (X. Zhang et al., 2018). Tau pathology is found in multiple syndromes called tauopathies, including Alzheimer's disease, progressive supranuclear palsy, and CBS (see 0).

1.1.5.3 FUS pathology

FUS pathology is present in 5-10% of FTD patients and is usually observed in patients with TDP-43- and tau-negative subtypes of FTD (I. R. A. MacKenzie & Neumann, 2012; Urwin et al., 2010). FUS pathology in FTD leads to severe early-onset bvFTD (Neumann et al., 2009; Urwin et al., 2010). One study showed that in FTD, FUS-positive inclusions are also positive for TATA-binding protein-associated factor 15 (TAF15) and Ewing's sarcoma protein (EWS) which make up the FET family of DNA/RNA binding proteins with functional homology. In ALS, FUS pathology is negative for TAF15 and EWS, suggesting that the pathomechanism of FUS pathology differs between ALS and FTD (I. R. A. MacKenzie & Neumann, 2012). Equally, mutations in the FUS gene are associated with ALS but rarely cause FTD (A. L. Ji et al., 2017).

The FUS protein is a DNA/RNA binding protein which ubiquitously expressed (Andersson et al., 2008). In most cells, FUS is located in the nucleus and cytoplasm, but in neurons, FUS is mainly nuclear, while FUS in glial cells is exclusively nuclear (Andersson et al., 2008; I. R. A. Mackenzie & Neumann, 2017). FUS is involved in various cellular processes such as DNA repair, transcription regulation, RNA splicing, and RNA transport (I. R. A. Mackenzie & Neumann, 2017). In the central nervous system (CNS), FUS has been described to bind to more than 5500 genes (Lagier-Tourenne et al., 2012). FUS is involved in cell proliferation, neural plasticity, and the maintenance of dendrites (I. R. A. Mackenzie & Neumann, 2017).

1.1.6 Disease-associated mutations

30-50% of patients report a positive family history of FTD; a definitive autosomal dominant inheritance is found in 10-15% of patients (Woollacott & Rohrer, 2016). The most common mutations worldwide

in order of frequency affect the chromosome 9 open reading frame 72 (*C9orf72*) gene, the progranulin (*GRN*) gene, and the microtubule-associated protein tau (*MAPT*), which account for up to 60% of familial FTD cases (Le Ber, 2013). Each of these disease-associated genes accounts for approximately 5-10% of all FTD cases, but there is geographical variability (Greaves & Rohrer, 2019). For example, *GRN* mutations are more common in Italy, Spain, and Brazil, while *C9orf72* mutations are more frequent in Sweden and Finland (Öijerstedt et al., 2019). While *C9orf72* mutations are similarly common in ALS, GRN and MAPT mutations are not associated with ALS (A. L. Ji et al., 2017)

Furthermore, in recent years less common disease-associated genes have been identified, which cumulatively account for less than 5% of all FTD cases, such as *VCP* (2004), *CHMP2B* (2005), *TARDBP* (2008), *FUS* (2009), *SQSTM1* (2012), *CHCHD10* (2014), *TBK1* (2015), *OPTN* (2015), *CCNF* (2016), and *TIA1* (2017) (Greaves & Rohrer, 2019). Most of these rare mutations have also been found in ALS, although some are more common in FTD, such as mutations in *VCP* and *CHMP2B*, while others are more common in ALS, such as mutations in *FUS* and *TARDBP*. Again, there are geographical differences in frequencies. For example, one study of FTD in Sardinia found *TARDBP* mutations in 8% of patients due to a genetic founder effect (Floris et al., 2015).

1.1.6.1 *C9orf72*

The most common FTD and ALS-causing mutation in Europe and North America is a mutation in the *C9orf72* gene, with about 25% of familial FTD cases and about 6% of sporadic FTD cases, 39% of familial ALS cases, and 7% of sporadic ALS cases (Majounie et al., 2012). The terms for *C9orf72*-associated ALS or FTD are C9-ALS and C9-FTD. *C9orf72*-associated ALS and FTD comorbidity is termed C9-ALS/FTD.

The mutation in the *C9orf72* gene is a heterozygous repeat expansion of the hexanucleotide GGGGCC in intron 1 of the *C9orf72* gene (DeJesus-Hernandez et al., 2011; Majounie et al., 2012; Renton et al., 2011). Whereas healthy individuals usually carry between 2-20 hexanucleotide repeats with an average number of 3.0 (DeJesus-Hernandez et al., 2011; Renton et al., 2011), carriers of the *C9orf72*

hexanucleotide repeat expansion (C9-HRE) carriers are believed to have about 400-4400 repeats, with most containing thousands (Majounie et al., 2012. Due to this large number of repeats, determining the exact number remains technically challenging.

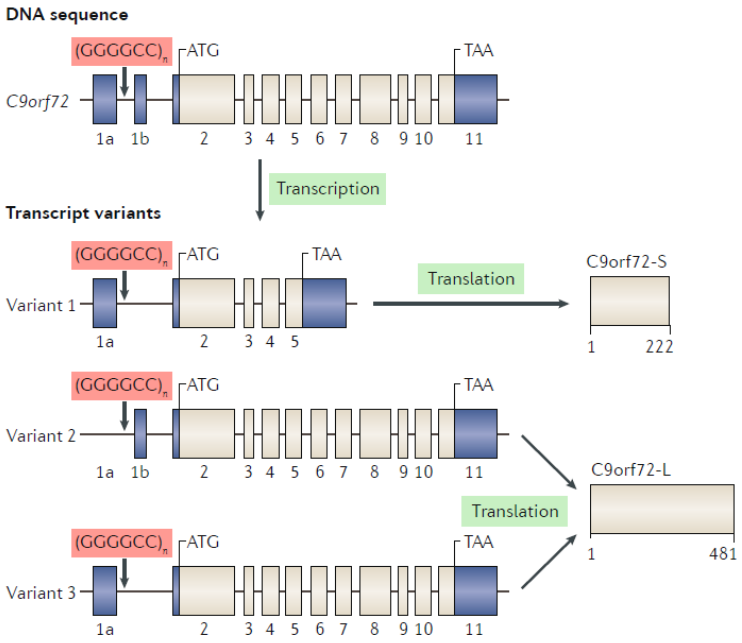


Figure 4: Schematic representation of the *C9orf72* DNA sequence, multiple transcript variants and their protein isoforms. Non-coding exons are displayed in blue; coding exons are shown in grey (not to scale). This image was taken from **Balendra & Isaacs (2018).**

The *C9orf72* gene is expressed across all tissues. Due to alternative splicing, three transcript variants exist, which produce two protein isoforms (see Figure 4) (Balendra & Isaacs, 2018). The short ~25 kDa isoform is localised to the nuclear membrane and is believed to play a role in nucleocytoplasmic transport. The long ~50 kDa isoform plays a significant role in autophagy and endosomal trafficking (Amick et al., 2016; Beckers et al., 2021). The effects of the *C9orf72* HRE on a cellular level are described in section 1.2.

1.1.6.2 *MAPT* and *GRN*

After the C9-HRE, mutations in the *MAPT* and *GRN* genes are the next most common familial causes of FTD. Both genes are associated with FTD but not with ALS.

Mutations in the *MAPT* gene cause 10-20% of familial FTD and up to 3% of sporadic FTD (Olszewska et al., 2016). *MAPT* encodes for the microtubule-associated protein tau, which is involved in stabilising microtubules and axonal maintenance (Olszewska et al., 2016; Y. Wang & Mandelkow, 2016). Tau also interacts with various cellular compartments and therefore plays a role in other processes such as neurogenesis, neuronal activity, and iron export (Y. Wang & Mandelkow, 2016). Tau mutations include intronic mutations that affect splicing and missense mutations that impair the normal function of tau and result in pathological aggregates of hyperphosphorylated tau.

Tau pathology is found in several syndromes called tauopathies, including Alzheimer's disease, progressive supranuclear palsy, and CBS (see 1.1.3 Comorbidities). *MAPT*-associated FTD most commonly presents as bvFTD with late parkinsonism (Olszewska et al., 2016).

Mutations in the *GRN* gene are associated with approximately 16% of familial FTD cases and 7% of all FTD cases (C. E. Yu et al., 2010). bvFTD is most common in *GRN*-associated FTD, while nfvPPA and CBS are less frequent. The *GRN* gene encodes for progranulin, which is processed into granulin (GRN). The majority of mutations lower the protein levels or function of granulin (Baker et al., 2006; Cruts et al., 2006; Gass et al., 2006; Götzl et al., 2016; Greaves & Rohrer, 2019; Shankaran et al., 2008).

GRN colocalises with LAMP1 and plays a crucial role in lysosomal function (Belcastro et al., 2011; Götzl et al., 2014; Hu et al., 2010). Interestingly, heterozygous GRN loss of function causes FTD. In contrast, a homozygous GRN loss of function leads to neuronal ceroid lipofuscinosis (NCL), a rare lysosomal storage disorder, which links FTD to lysosomal storage disorders (Anderson et al., 2013; Götzl et al., 2016; Smith et al., 2012). Additionally, GRN is also secreted from cells and functions as a growth factor involved in several processes such as neuronal survival (Van Damme et al., 2008), wound repair (He et al., 2003), and inflammation (J. Zhu et al., 2002). Loss of function of GRN was shown to induce TDP-43 pathology, as GRN-associated FTD cases present TDP-43 and ubiquitin-positive inclusions (R. A. Armstrong et al., 2010; Cairns et al., 2007).

1.1.6.3 *SOD1* and *TARDBP*

Besides the C9-HRE, mutations in the *SOD1* and *TARDBP* genes are the most common causes of familial ALS but rare in FTD.

Mutations in the *SOD1* gene account for 15-30% of familial ALS and <2% of sporadic ALS cases, but only very few known FTD cases (Katz et al., 2012; Mejzini et al., 2019; Zou et al., 2017). The superoxide dismutase 1 (SOD1) protein is a metalloenzyme that acts as an antioxidant defence mechanism in the cytosol and intermembrane space of mitochondria (McCord & Fridovich, 1969; Mejzini et al., 2019). The majority of the >180 different mutations in the *SOD1* gene that have been identified are missense mutations (Mejzini et al., 2019; Yamashita & Ando, 2015). Patients with *SOD1*-associated ALS often have less cognitive impairment than sporadic ALS or non-*SOD1* familial ALS cases (Wicks et al., 2009).

TARDBP encodes the nuclear protein TAR DNA-binding protein 43 (TDP-43). Despite the high prevalence of TDP-43 pathology, especially in ALS cases, *TARDBP* mutations are a relatively uncommon trigger of the disease. About 1% of all ALS cases and 4% of familial ALS cases are caused by mutations in *TARDBP* (Lagier-Tourenne et al., 2010). Few cases of *TARDBP* mutant-associated FTD are known (Caroppo et al., 2016; Floris et al., 2015). Whereas 60% of *TARDBP*-associated FTD patients do not develop ALS (Caroppo et al., 2016), *TARDBP*-associated ALS cases rarely develop cognitive impairments (Lagier-Tourenne et al., 2010).

Nonsense mutations or missense mutations in the RNA-binding domain disturb the normal function of TDP-43 in RNA metabolism (A. L. Ji et al., 2017; Prpar Mihevc et al., 2016). Additionally, mutations in *TARDBP* have a gain of function effect by causing TDP-43 mislocalisation and aggregation in patients (Van Deerlin et al., 2008). Since patients without *TARDBP* mutations show TDP-43 pathology, other factors such as *C9orf72* mutations might cause TDP-43 mislocalisation and aggregation.

1.1.6.4 Other mutations

Several rare FTD and ALS-associated genes have been identified. Their prevalence adds up to less than 5% of all FTD cases (Greaves & Rohrer, 2019). Although rare, disease-associated genes provide information on disease-associated cellular mechanisms. The following disease-associated genes are note-worthy:

The *sequestosome 1* (*SQSTM1*) gene encodes for p62, an essential autophagy protein involved in the ubiquitin-mediated degradation of protein aggregates, mitochondria, viral capsids, and other structures (reviewed by Lamark et al., 2017). Many of its functions are dependent on liquid-liquid phase separation (Sun et al., 2018). However, defective p62 is prone to aggregate and form p62-positive, ubiquitin-positive inclusions causing ALS and FTD (Arai et al., 2003; Mizuno et al., 2006).

The *valosin-counting protein* (*VCP*) gene encodes for VCP/p97, a chaperone-like ATPase with numerous functions in protein degradation, such as autophagy and degradation through the ubiquitin-proteasome system and ER-associated degradation (Colpo et al., 2017). Rare VCP mutations can cause ALS and FTD.

Charged multivesicular protein 2B (*CHMP2B*) gene mutations are believed to be associated with ALS/FTD. While the function of CHMP2B has not been established yet, its yeast orthologue is a component of the endosomal secretory complex required for transport (ESCRTIII). ESCRTIII is essential for trafficking proteins between the trans-Golgi network, vacuoles and lysosomes, and the plasma membrane (Cox et al., 2010).

The *UBQLN2* gene encodes for ubiquilin 2, an essential mediator in protein degradation via the ubiquitin-proteasome system and autophagy (Renaud et al., 2019). Ubiquilin recognises proteins and aggregates tagged for degradation and shuttles substrates to the proteasome (Hjerpe et al., 2016). Ubiquilin also acts as a chaperone for transmembrane domains and is involved in targeting mitochondrial transmembrane proteins for degradation if they are not transported to the correct

location (Itakura et al., 2016). Furthermore, ubiquilin 2 is involved in cell signalling and cell cycle regulation and associates with cytoskeletal elements (Oh et al., 2018). Rare UBQLN2 mutations cause ALS and ALS-FTD. Additionally, ubiquilin 2 positive inclusions can form in affected neurons of some familial and sporadic ALS and ALS-FTD patients (Renaud et al., 2019).

Mutations in the *TIA1* gene, which encodes for the 3' UTR mRNA binding protein T cell-restricted intracellular antigen-1 (TIA1), have been identified in ALS and ALS-FTD patients. As a component of stress granules (SGs), the low complexity domain of the TIA1 protein is essential in promoting SG assembly (Gilks et al., 2004; Kedersha et al., 2000; Panas et al., 2016). ALS- and FTD-associated mutations affect the low complexity domain and delay SG disassembly, which causes TDP-43 to accumulate in non-dynamic SGs (I. R. Mackenzie et al., 2017).

Mutations in the *optineurin* (*OPTN*) gene cause FTD, ALS, and glaucoma. The OPTN protein is involved in multiple cellular mechanisms. It acts as an adaptor protein in autophagy and mitophagy (Toth & Atkin, 2018). OPTN is also relevant for Golgi maintenance, vesicular trafficking, receptor recycling, secretion, and innate immune response (Toth & Atkin, 2018).

Mutations in the *TANK-binding kinase 1* (*TBK1*) gene have been associated with ALS and FTD. TBK1 is involved in innate immunity signalling pathways as an inducer of type-1 interferons (Oakes et al., 2017). In addition, TBK1 plays a role in autophagy and mitophagy. TBK1 phosphorylates autophagy adapters and is essential for efficient cargo recruitment. This function might be disrupted by TBK1 mutations, which could lead to autophagy impairment and aggregate accumulation (Oakes et al., 2017). These pathways link impairments in protein degradation, RNA metabolism, and innate immune signalling to the pathogenesis of ALS and FTD.

1.2 The GGGGCC hexanucleotide repeat expansion in the *C9orf72* gene

Three mechanisms of C9-HRE toxicity have been proposed: C9orf72 haploinsufficiency, RNA foci, and dipeptide repeat protein (DPR) accumulation (see Figure 5).

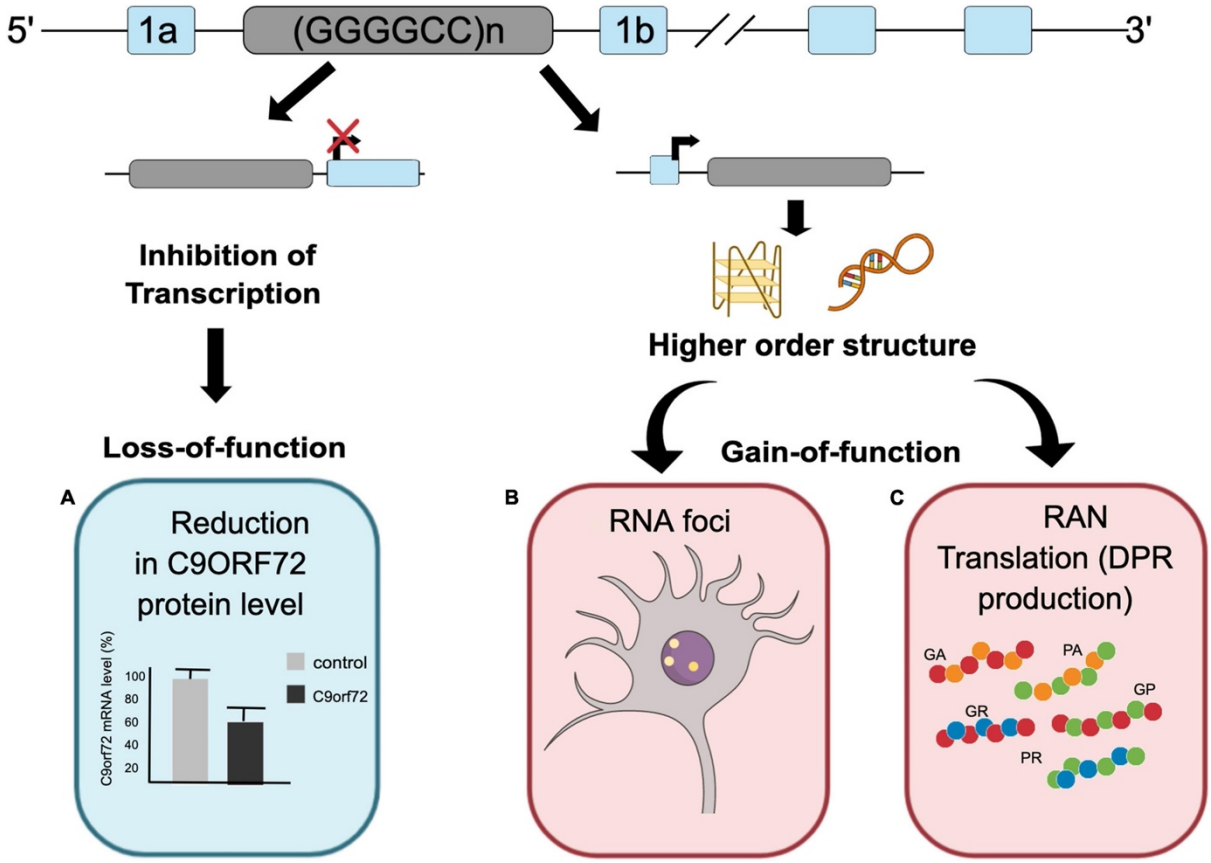


Figure 5: The pathomechanisms of C9-HRE are loss of function through the reduced expression of the C9orf72 protein and gain of function of foci containing higher-order structure RNA and DPR production via RAN translation. This image was taken from Schmitz et al. (2021).

1.2.1 Loss of function

The C9-HRE leads to reduced levels of the C9orf72 protein. This was previously shown in the frontal cortex, the motor cortex, the cerebellum, the hippocampus and spinal cord, and induced pluripotent stell cell (iPSC)-derived neurons (Donnelly et al., 2013; Waite et al., 2014). While the exact mechanism by which the C9-HRE reduces C9orf72 expression is unknown, multiple factors have been suggested,

such as reduced binding of transcription factors and methylation status (Beckers et al., 2021; Belzil et al., 2013; Gijselinck et al., 2015; Xi et al., 2013).

Several studies have found that the C9orf72 protein regulates autophagy by forming complexes with proteins essential for autophagy initiation (Ho et al., 2019; Sellier et al., 2016; Sullivan et al., 2016; Webster et al., 2016). As a result, C9orf72 haploinsufficiency decreases autophagy and promotes the accumulation of dysfunctional organelles or proteins such as dipeptide repeat proteins (Shi et al., 2018). Since synaptic plasticity depends on the lysosomal degradation of glutamate receptors, C9-haploinsufficiency also causes an accumulation of glutamate receptors which leads to excitotoxicity (Selvaraj et al., 2018; Shi et al., 2018).

1.2.2 Gain of function

1.2.2.1 RNA foci

The transcription of the expansion leads to repeat-containing RNA (C9-RNA), which forms RNA foci in the nucleus. RNA foci were found in the frontal cortex, motor cortex, spinal cord, hippocampus, and cerebellum (Haeusler et al., 2016). Patients with more RNA foci were described to have an earlier age of symptom onset in a small number of C9-FTD patients (Mizielinska et al., 2013). Both sense and antisense RNA foci were observed (Mizielinska et al., 2013). RNA foci are mainly found in neuronal nuclei and occasionally in the cytoplasm. RNA foci can also be found in glial cells (Balendra & Isaacs, 2018; Haeusler et al., 2016).

RNA foci sequester RNA-binding proteins (RBPs) and thus might lead to altered nucleolar function, impaired nucleocytoplasmic transport, and altered RNA processing (Haeusler et al., 2016). Several studies have identified a range of RBPs which interact with RNA foci with limited consensus. The most commonly identified interacting RBPs are heterogeneous nuclear ribonucleoproteins (hnRNPs), particularly hnRNP H which causes dysregulated splicing (Balendra & Isaacs, 2018; Conlon et al., 2016). Another interactor of RNA foci is hnRNP A1, which is believed to result in stress granule dysregulation.

Additionally, hnRNP a3 has been shown to interact with RNA foci (Clarke et al., 2021). The function of hnRNP A3 in FTD is not well understood, but one study showed that the knockdown of hnRNP A3 caused an increase in C9-RNA and DPR production (Mori et al., 2016).

Studies on the effect of RNA foci on cellular functions show varied results. In HEK cells expressing $(GA)_{65}$, adding a $(G_4C_2)_{73}$ transgene caused a reduction in viability, nuclear mRNA export, and protein biogenesis (Frottin et al., 2021). Another study used *Drosophila* flies which express ~100 repeat sense or antisense RNA either in the cytoplasm or in nuclei, or >1000 repeat sense RNA in nuclei (Moens et al., 2018). *Drosophila* neurons showed sequestration of RBP but not toxicity, suggesting that the role of RNA foci on disease pathogenesis is limited. Therefore, the extent of the contribution of RNA foci to neurodegeneration is still unclear.

1.2.2.2 Dipeptide repeat proteins

C9-RNA is translated via repeat-associated non-ATG-dependent translation (RAN translation). Depending on the reading frame and sense or antisense translation, five different DPRs are produced (Mori et al., 2013). These are, in order of abundance: poly-GA, poly-GP, poly-GR, poly-PA, and poly-PR (I. R. A. Mackenzie et al., 2015). Poly-PR and poly-GR are believed to be highly toxic. Poly-GA shows moderate toxicity, whereas poly-PA and poly-GP show little toxicity (Freibaum & Taylor, 2017).

DPR pathology has been observed in brain tissue years before disease onset preceding TDP-43 pathology, suggesting that DPR inclusions might be tolerated by some cells (Scaber & Talbot, 2016; Vatsavayai et al., 2016). In end-stage post-mortem tissue, DPR pathology is highest in the cerebellum and neocortical regions, including the frontal and motor cortex, hippocampus, and thalamus. Moderate pathology was described in subcortical areas, while few inclusions were observed in lower motor neurons (I. R. MacKenzie et al., 2013; Schludi et al., 2015). Discrepancies between areas affected by DPR pathology and neurodegeneration might result from methodological issues (Freibaum

& Taylor, 2017). Importantly, several studies describe DPR pathology early in the disease process, suggesting a contribution to disease pathogenesis (Freibaum & Taylor, 2017).

Table 1: Summary of the properties of DPRs. This table was taken from Sharpe et al. (2021).

	Alanine-proline (AP)	Glycine-alanine (GA)	Glycine-proline (GP)	Glycine-arginine (GR)	Proline-arginine (PR)
Biochemical properties	Flexible coil	Beta sheets, fibrils, highly insoluble	Flexible coil	High hydrophilicity	High hydrophilicity
Charge	Neutral	Neutral	Neutral	Positive	Positive
Relative abundance (1 = most) in patient post-mortem brains	4	1	2	3	4
Cellular localization	Diffuse cytoplasmic	Cytoplasmic stellate aggregates	Cytoplasmic	Cytoplasmic	Nuclear and cytoplasmic
Toxicity inferred from current models	Majority of models suggest low toxicity	Toxic in some models	Insufficient evidence	Universally most toxic	Universally most toxic
Main pathways implicated currently	NA	Proteasome inhibition	NA	Disruption of stress granule dynamics. Translational inhibition. Nucleocytoplasmic transport defects. DNA damage/repair.	Translational inhibition. Nucleocytoplasmic transport defects. DNA damage/repair.

Poly-GA is lipophilic and forms aggregates (see Table 1) (Chang et al., 2016; May et al., 2014). Although its interactome is limited, poly-GA has been shown to increase endoplasmic reticulum (ER) stress, inhibit the proteasome, induce apoptosis by activating caspase 3, and reduce dendritic branching (Freibaum & Taylor, 2017; May et al., 2014; Y. J. Zhang et al., 2014).

Poly-GR and poly-PR are highly charged and primarily toxic in polymeric conformation (Y. Lin et al., 2016). Whereas poly-GR is more abundant than poly-PR, poly-GR is relatively unstable with a half-life of less than 30 min, whereas poly-PR has a half-life of about 72 h. Poly-PR is localised in the nucleolus, whereas poly-GR is localised in both the nucleolus and the cytoplasm (K. H. Lee et al., 2016). Both have a large interactome, of which they share about 40% (K. H. Lee et al., 2016). Both DPRs impair ribosome biogenesis and suppress global translation (K. H. Lee et al., 2016; Tao et al., 2015). They are implicated in triggering stress granule formation by suppressing translation and binding to RBPs, which mediate the formation of membrane-less organelles such as stress granules (K. H. Lee et al., 2016; Lopez-Gonzalez et al., 2016; Tao et al., 2015; Wen et al., 2014). Moreover, they are believed to impair nucleocytoplasmic trafficking defects (K. H. Lee et al., 2016).

Poly-GR also impairs rRNA synthesis (K. H. Lee et al., 2016; Tao et al., 2015). Moreover, it colocalises with mitochondria and binds to mitochondrial ribosomal proteins causing oxidative stress (Lopez-Gonzalez et al., 2016).

Additionally, different DPR species might have a combinatorial effect. Co-expression of poly-GA with poly-PR has been described to increase cytoplasmic localisation of poly-PR and rescue poly-PR toxicity (Darling et al., 2019). Furthermore, studies suggested that the presence of DPRs in combination with C9orf72 haploinsufficiency aggravates autophagy impairment causing increased sensitivity to autophagy inhibitors and elevated p62 levels (Gao et al., 2017; Sellier et al., 2016). In mice expressing a *C9orf72* transgene with 450 repeats, haploinsufficiency combined with the presence of C9-RNA leads to DPR accumulation, accelerated death, cognitive defects, glial activation, and hippocampal neuron loss (Q. Zhu et al., 2020).

1.2.3 Affected cellular mechanisms in neurons

Various cellular mechanisms have been identified to be impaired in cells carrying the C9-HRE, such as in neurons, oligodendrocytes, and microglia. These impairments include ER stress, autophagy and lysosomal dysfunction, ubiquitin-proteasome system impairment, DNA damage, nucleolar dysfunction, nucleocytoplasmic transport dysfunction, translation inhibition, stress granule formation, altered liquid-liquid phase separation, mitochondrial dysfunction, axonal and vesicular transport dysfunction, neuronal branching and growth cone defects, and hypo- and hyperexcitability (see Figure 6) (Balendra & Isaacs, 2018). In this section, I will focus on the mechanisms which will be relevant to this study.

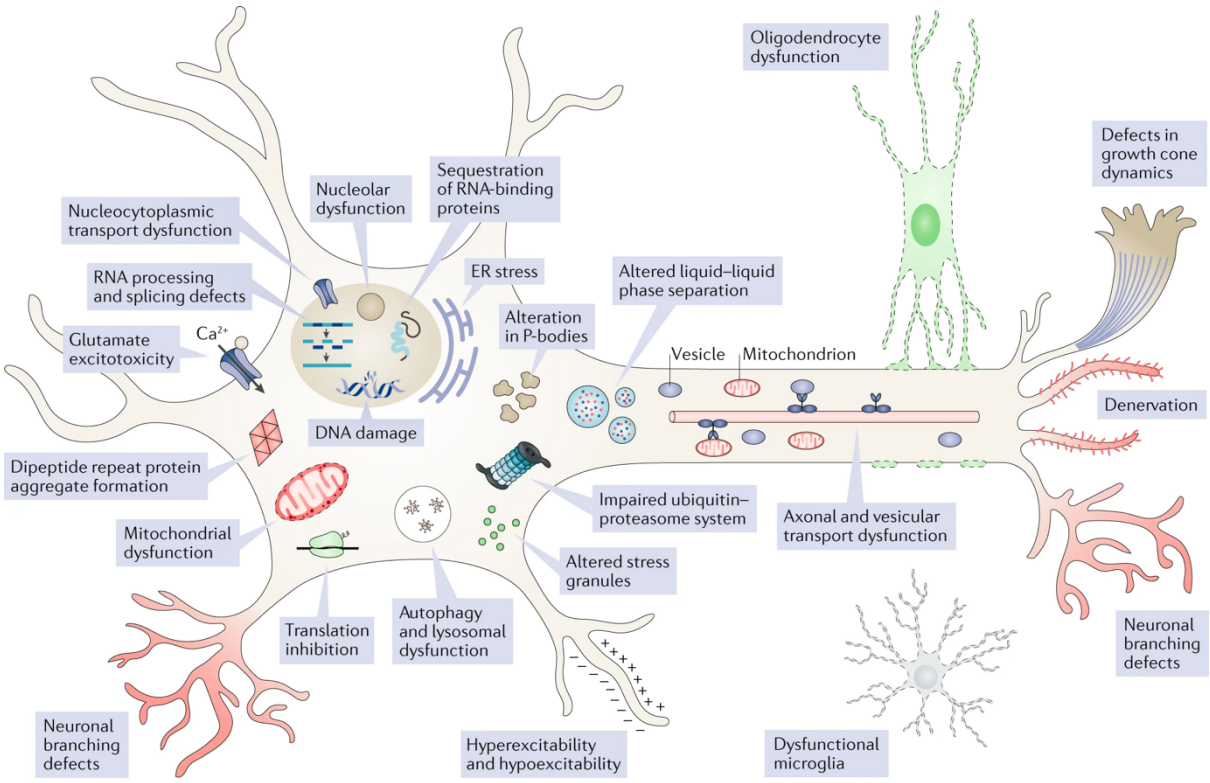


Figure 6: Cellular mechanisms affected by C9-HRE toxicity. These mechanisms are targeted by the effectors of the C9-HRE, namely haploinsufficiency, RNA foci, and DPRs. This figure was taken from **Balendra & Isaacs (2018).**

1.2.3.1 Apoptosis

Loss of integrity of functional nervous system connections due to degeneration of cortical or motor neurons is the primary cause of symptoms in ALS/FTD patients. The first reported patient with FTD with behavioural and cognitive impairment was a 71-year-old man described by Arnold Pick (1851-1924) in 1892. At autopsy, the patient's brain showed atrophy in the temporal lobe (Ferrari et al., 2011). Since then, atrophy in the frontal or temporal lobe has been considered a pathological hallmark of frontotemporal lobar degeneration (FTLD) (Olney et al., 2017). Similarly, in ALS, atrophy of lower or upper motor neurons is the defining pathology (Hardiman et al., 2017).

There are multiple cellular pathways of cell death. The main pathway in C9-ALS/FTD is intrinsic apoptosis, which is initiated by various cellular perturbations including ER stress, oxidative stress, replication stress, and DNA damage (X. Chen et al., 2012; Kaufmann et al., 2007; Pihán et al., 2017;

Vitale et al., 2017). When an apoptotic stimulus is present, the outer membrane of mitochondria is irreversibly permeabilised (Galluzzi et al., 2018). This step is regulated by the B-cell lymphoma 2 protein family (BCL-2 family), consisting of proapoptotic and antiapoptotic members. The expression of pro- versus anti-apoptotic BCL-2 family proteins determines cell fate (Galluzzi et al., 2018). Pro-apoptotic members of the BCL-2 family are expressed or undergo post-translational modifications when the homeostasis of cellular compartments is disrupted (Galluzzi et al., 2014, 2018). Anti-apoptotic BCL-2 family members, such as Bcl-2 and Bcl-X_L, antagonise pro-apoptotic BCL-2 family members by directly binding pro-apoptotic BCL-2 family members. Anti-apoptotic BCL-2 family members are generally located in the outer mitochondrial membrane (Galluzzi et al., 2018; Yin et al., 1994). Bcl-X_L is also implicated in regulating ER Ca^{2+} homeostasis, regulating redox homeostasis, and promoting mitochondrial energetics (Y. Chen et al., 2011; Galluzzi et al., 2018; Y. Rong & Distelhorst, 2008).

Permeabilisation of the outer mitochondrial membrane leads to the release of proteins such as cytochrome C (CytC) from the mitochondrial intermembrane space into the cytosol. There, CytC binds to pro-caspase 9 and apoptotic peptidase activating factor 1 (APAF1) to form the apoptosome complex, which causes the autocatalytic activation of pro-caspase 9 (Li et al., 1997). Activated caspase 3 cleaves and activates caspase 3 (ClCasp3) and caspase 7, which execute the demolition of the cell during intrinsic apoptosis (Julien & Wells, 2017).

The degeneration of neurons evident in ALS and FTD patients has been replicated in mouse primary cortical neurons expressing GFP-$(GA)_{50}$, with significantly upregulated ClCasp3 levels (Y. J. Zhang et al., 2014, 2016). Similarly, in C9-iPSC-derived motor neurons (C9-MNs) and cortical neurons (C9-CNs), ClCasp3 was found to be upregulated (Dafinca et al., 2016). Additionally, in C9-MNs, the anti-apoptotic proteins Bcl-2 and Bcl-X_L were downregulated while the pro-apoptotic protein BAK was upregulated (Dafinca et al., 2016). Furthermore, C9-MNs in culture exhibit reduced survival over time (Shi et al., 2018).

1.2.3.2 ER stress

ER stress describes the accumulation of unfolded or misfolded proteins in cells. It can be caused by conditions such as a decreased degradation of misfolded proteins through the proteasome or low activity of chaperones. For example, low Ca^{2+} levels in the ER decrease the activity of Ca^{2+}-dependent chaperones. ER stress is alleviated through several mechanisms, such as ER biogenesis, ER-associated degradation, protein folding, protein entry to the ER, autophagy, secretion, etc. Irreversible ER stress causes the cell to undergo apoptosis through the mitochondrial pathway (Hetz, 2012).

ER stress triggers the unfolded protein response (UPR) to reduce the load of unfolded proteins. Consequently, proteins involved in the UPR are valuable markers for studying ER stress. Key initiators of the UPR are protein kinase RNA-like ER kinase (PERK), activating transcription factor 6 (ATF6), and inositol-requiring protein 1 (IRE1), which control transcriptional and non-transcriptional responses to ER stress (Ron & Walter, 2007). A downstream target of PERK is the transcriptional factor C/EBP homologous protein (CHOP), the expression of which indicates the activation of the PERK-CHOP signalling pathway of ER stress (Y. J. Zhang et al., 2014). Another downstream target of PERK is the eukaryotic translation initiation factor 2 (eIF2α), which causes a global halt of translation with the preferential translation of activating transcription factor 4 (ATF4), a regulator of the transcription of genes involved in autophagy, apoptosis, amino acid metabolism and antioxidant response (B'chir et al., 2013; Guan et al., 2014; Hetz, 2012). A downstream effect of IRE1 and ATF6 is the expression of binding immunoglobulin protein (BiP), a Ca^{2+}-independent chaperone that is expressed in response to an accumulation of unfolded proteins in the ER (Enogieru et al., 2019).

In cellular C9-ALS/FTD models, an increase in ER stress has been described. In mouse primary cortical neurons, GFP-GA_{50} expression inhibits proteasome activity and therefore triggers the UPR. Specifically, it caused an increase in the levels of BiP, phosphorylated PERK, and CHOP, but not ATF6 (Y. J. Zhang et al., 2014). Additionally, in C9-iPSC-derived MNs, ER Ca^{2+} levels and BiP expression were found to be increased (Dafinca et al., 2016).

Interestingly, the RAN translation of DPRs was described to be stimulated by eIF2α. As poly-GA was shown to induce ER stress and eIF2α activation, the interplay between RAN translation and ER stress suggests a feedforward loop, where both processes stimulate each other (Baradaran-Heravi et al., 2020; Cheng et al., 2018; Green et al., 2017). Moreover, targeting activated PERK and eIF2α reduced DPR levels suggesting a potential therapeutic strategy (Westergard et al., 2019).

1.2.3.3 Stress granule formation

Inhibition of translation, e.g., through ER-stress-associated eIF2α activity, can cause the generation of cytosolic SGs, which are insoluble aggregates of mRNAs and RBPs. While SG formation is a healthy process of the cell to conserve cellular resources by storing transcripts, when translation is stalled due to chronic cellular stress or when the regulation of stress granules is aberrant, SGs can cause harm by sequestering essential RBPs and causing aggregate formation (Gao et al., 2017).

When the cellular stress is relieved, SGs dissolve again. If cellular stress persists, SGs are degraded via autophagy. The C9orf72 protein is recruited to SGs and plays a role in the SG assembly and degradation through autophagy. In the absence of the C9orf72 protein, cells are hypersensitive to stress signals like ER stress (Maharjan et al., 2016).

Stress granule formation can also be caused in the absence of ER stress. For example, arginine-rich DPRs can interact with low-complexity domains of RBPs and cause them to phase transition into aggregates in cellular C9-ALS/FTD models (Boeynaems et al., 2017; K. H. Lee et al., 2016).

Aberrant stress granule formation has been observed in iPSC-derived C9-ALS/FTD patient cells. The percentage of C9-MNs and C9-CNs displaying stress granules at base conditions was described to be significantly increased in one study (Dafinca et al., 2016), while another study found that the number of stress granules per neuron was increased in C9-MNs (Abo-Rady et al., 2020).

1.2.3.4 Autophagy

Autophagy is a cellular mechanism of selective and non-selective proteolytic degradation of misfolded or aggregated proteins, damaged organelles, and intracellular pathogens. There are three types of autophagy: macro-autophagy, micro-autophagy, and chaperone-mediated autophagy (Glick et al., 2010).

In macro-autophagy, cytoplasmic cargo is delivered to the lysosome through an intermediary vesicle, the autophagosome, which fuses with the lysosome to form the autolysosome (see Figure 7) (Glick et al., 2010). Macro-autophagy is negatively regulated by Mammalian target of rapamycin complex 1 (mTORC1), which indirectly inhibits the nucleation, autophagosome, and the fusion of the autophagosome with the lysosome (Dossou & Basu, 2019). In neurons, it has been demonstrated that autophagosomes are formed in the distal axon both *in vitro* and *in vivo*. Once formed, autophagosomes are transported towards the soma via dynein and dynactin, underlining the importance of functioning axonal transport (Evans & Holzbaur, 2019; Maday et al., 2012; Neisch et al., 2017).

A key protein in selective macro-autophagy is the adapter protein sequestosome-1 (p62/SQSTM1), which recognises cellular waste labelled by ubiquitination. p62 binds to intracellular waste and causes its inclusion in the autophagosome, where p62 is degraded together with its cargo (Rusten & Stenmark, 2010). Thus, measuring p62 levels are a useful tool for studying the macro-autophagic flux. Another essential protein is microtubule-associated protein 1A/1B light chain 3 (LC3), an autophagosomal membrane protein critical for membrane elongation in autophagosome formation. LC3-II sequesters p62 to localise its cargo in the autophagosome. LC3-I is a cytosolic protein conjugated to phosphatidylethanolamine and inserted into the autophagosomal membrane to generate its active form LC3-II. Hence, the ratio of LC3-I to LC3-II is a valuable marker for macro-autophagic flux (Kadowaki & Karim, 2009; Tanida et al., 2004).

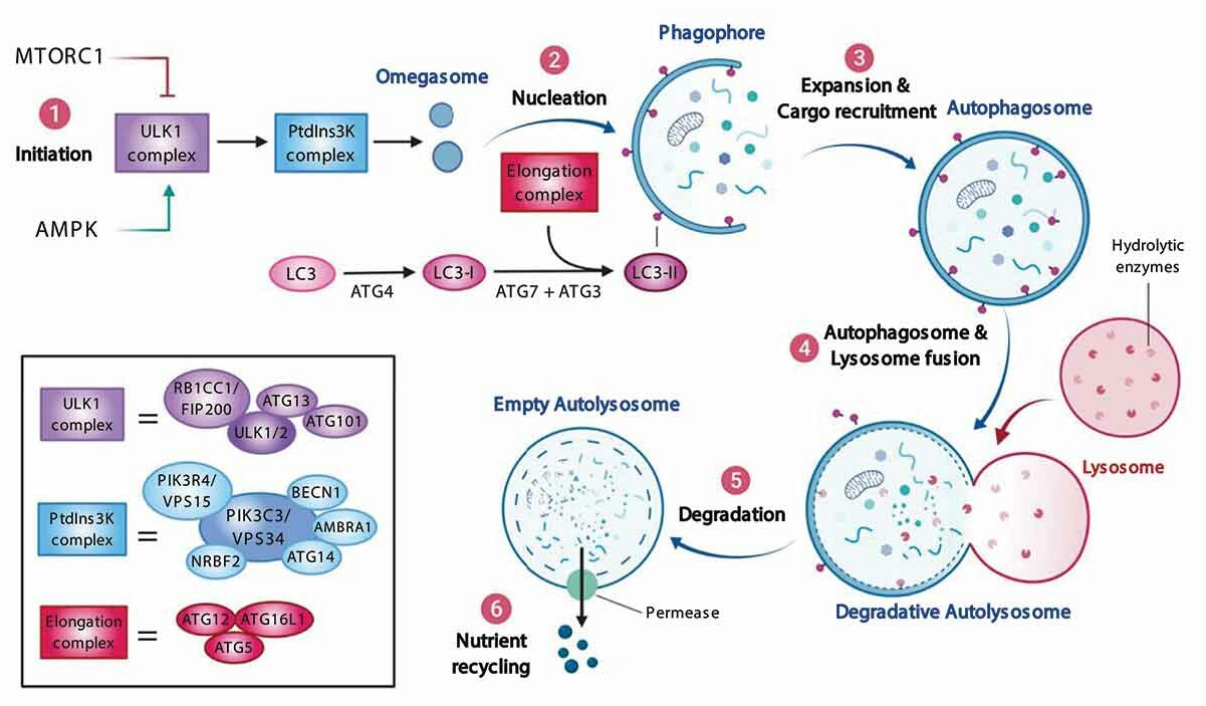


Figure 7: In macro-autophagy, cargo is engulfed by the autophagosome, which lyses with the lysosome to degrade its content. The ULK1 complex is responsible for initiating autophagy and is inhibited by MTORC1. This figure was taken from Beckers et al. (2021).

In micro-autophagy, the cytosolic component is taken up by the lysosome directly. Both macro- and micro-autophagy can take up large structures for degradation (Glick et al., 2010). In chaperone-mediated autophagy, proteins targeted for degradation form a complex with chaperone proteins which is recognised by the lysosomal membrane receptor lysosomal-associated membrane protein 2A (LAMP2A), leading to the unfolding, insertion into the lysosome, and degradation (Glick et al., 2010; Saftig et al., 2008). LAMP2A also plays a role in the maturation of autophagosomes in macro-autophagy as well as in protecting the lysosomal membrane from the luminal environment (Saftig et al., 2008).

Autophagy impairment is strongly linked to C9-ALS/FTD. The C9orf72 protein has a multifaceted function in regulating autophagy, both positively and negatively (Figure 8). C9orf72 is involved in initiating autophagy by interacting with the Unc-51 Like Autophagy Activating Kinase 1 (ULK1) complex. Thus, C9orf72 haploinsufficiency decreases autophagic flux (Webster et al., 2016). However,

loss-of-function C9orf72 seems to alter mTORC1 signalling, thus activating the autophagic pathway in C9orf72 knockout models (Y. J. Ji et al., 2017). Most studies suggest an overall decrease in autophagic flux when C9orf72 levels are subtly reduced in models (Beckers et al., 2021). This reduction in autophagic flux aggravates the accumulation of DPRs, suggesting a double-hit pathogenic mechanism. Autophagy activation can prevent neuronal cell death induced by DPR accumulation (Boivin et al., 2020).

In iPSC-derived C9-cortical neurons, increased sensitivity to autophagy inhibitors and elevated levels of p62 have been described, suggesting a decreased autophagic flux (Almeida et al., 2013). Similarly, iPSC-derived C9-motor neurons exhibit increased p62 levels (Dafinca et al., 2016). Additionally, C9orf72 has been described as an essential regulator of post-synaptic GluA1 receptor levels, and loss of C9orf72 contributed to excitotoxicity in C9-ALS/FTD in mouse models (Xiao et al., 2019).

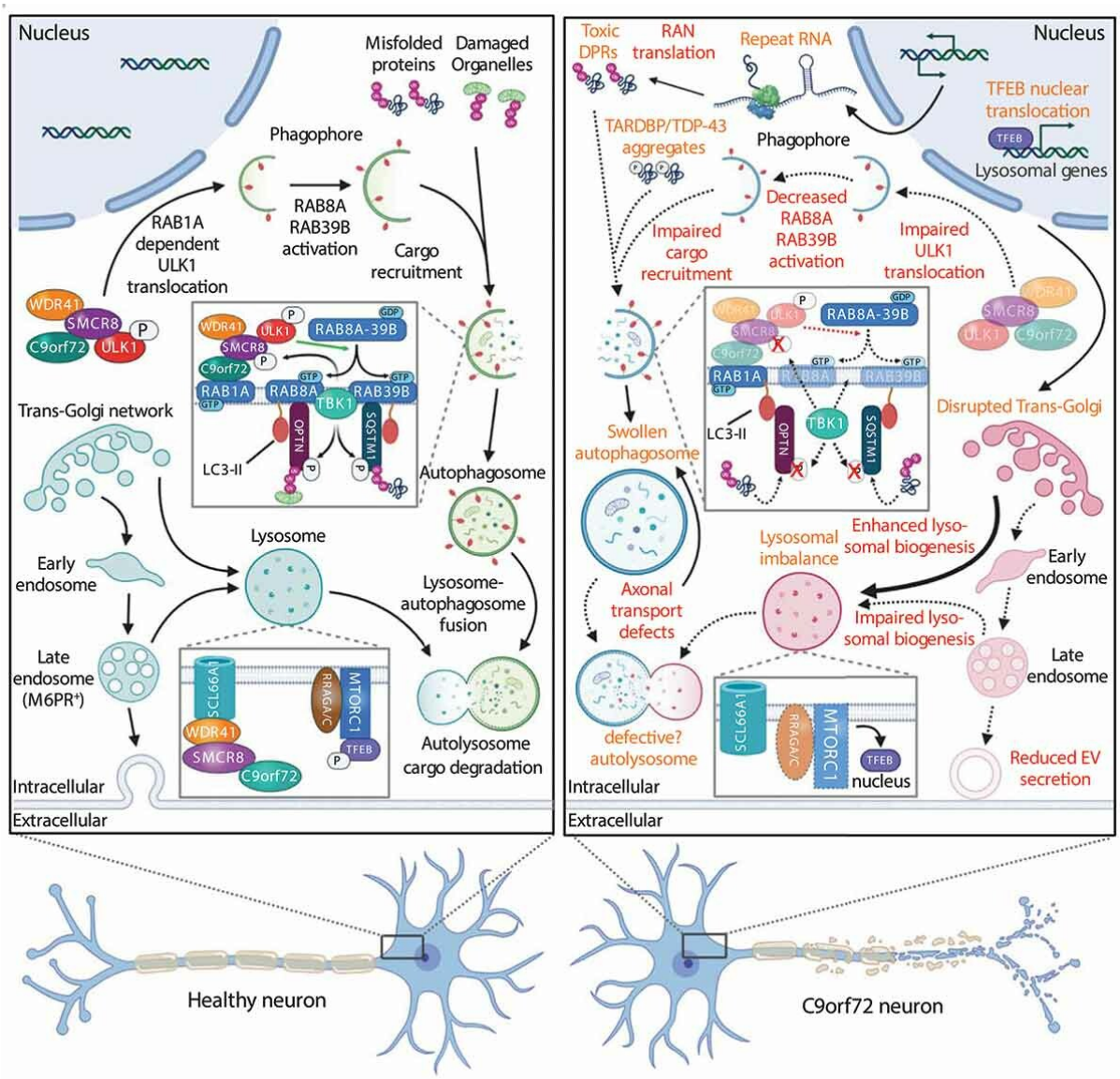


Figure 8: Overview of the function of the C9orf72 protein in autophagy. As a component of the ULK1 complex, the C9orf72 protein modulated autophagy initiation. It is also recruited to the lysosome. In neurons carrying the C9-HRE, autophagy is impacted by several mechanisms. First, the reduced expression of C9orf72 reduces autophagy initiation by the ULK1 complex. Second, C9orf72 deficiency reduces MTORC1 function, resulting in increased activation of the autophagic flux. Additionally, toxic dipeptide repeat proteins are disruptive to several cellular mechanisms, such as axonal transport of the autophagosome. A disruption in autophagy results in reduced clearance of DPR and TDP-43 aggregates. This figure was taken from Beckers et al. (2021).

1.2.3.5 Excitotoxicity

Neurons are connected with synapses to pass on action potentials. When an action potential reaches a synaptic terminal, the depolarisation of the pre-synapse causes the opening of voltage-gated calcium channels (VGCCs). In neurons, two types of VGCCs are involved in this process, N-type VGCCs and P/Q-type VCGGs (Lipscombe et al., 2004; Weber et al., 2010). The resulting influx of Ca^{2+} ions into the pre-synaptic terminal causes the release of neurotransmitters from vesicles into the synaptic cleft.

In glutamatergic synapses, ligand-gated and voltage-gated ion channels and metabotropic receptors are located in post-synaptic densities to receive signals from connected neurons (Popoli et al., 2011). Released glutamate binds and opens the cation channel α-amino-3-hydroxy-5-methyl-4-isoxazolepropionic acid receptor (AMPAR). AMPARs are tetramers consisting of four types of subunits, GluA1, GluA2, GluA3, and GluA4. AMPARs are permeable to Na^+, K^+, and, depending on the composition of subunits, Ca^{2+} ions (Wright & Vissel, 2012). GluA1 plays an essential role in synaptic plasticity and is downregulated in the frontal cortex with increasing age (T. Lu et al., 2004).

Glutamate release also causes the opening of N-methyl-D-aspartate receptors (NMDARs). Glutamate binding and depolarisation of the post-synaptic neuron causes NMDARs to open, causing an influx of Na^+ ions and, preferentially, Ca^{2+} ions (Xin et al., 2005). NMDARs are composed of four subunits, two GluN1 subunits and two GluN2 or GluN3 subunits (Salussolia et al., 2011). Additionally, glutamate binding causes the opening of the third type of glutamate-activated ion channel, the kainate receptor. This ion channel is not involved in excitatory post-synaptic signalling (Contractor et al., 2011).

The depolarisation of the post-synapse by glutamate binding to ion channels causes the opening of L-type VGCCs. This contributes to the flux of Ca^{2+} ions in the cytosol of post-synaptic neurons. Cytosolic Ca^{2+} ions cause the opening of Ca^{2+}-gated channels in the ER, leading to a further increase in cytoplasmic Ca^{2+} (Araya, 2014).

Excitotoxicity is defined as toxicity induced by excessive exposure of the brain to glutamate (Starr & Sattler, 2018). Excess glutamate in the synaptic cleft causes an over-stimulation of post-synaptic NMDARs, AMPARs, and metabotropic glutamate receptors (X. X. Dong et al., 2009). The prolonged overactivation of Ca^{2+} permeable channels causes downstream effects such as oxidative stress, mitochondrial membrane depolarisation, and apoptosis or necrosis (X. X. Dong et al., 2009; Fan & Raymond, 2007).

Toxicity by hyperexcitability is believed to be a major disease mechanism leading to the degeneration of motor neurons in ALS (Starr & Sattler, 2018). A study conducted in iPSC-derived C9-MNs found that cells first display hyperexcitability followed by a gradual loss in synaptic activity and action potential output the longer cells are kept in culture (Devlin et al., 2015). Similarly, a study using a 24-day motor neuron differentiation protocol observed hyperexcitability in C9-MNs (Wainger et al., 2014), while a study using a differentiation protocol of at least 39 days described reduced excitability (Sareen et al., 2013). Additionally, increased cell death was observed in C9-MNs treated with glutamate (Cheng et al., 2019). Little is known about the contribution of excitotoxicity to FTD (Starr & Sattler, 2018).

Several mechanisms of excitotoxicity in ALS have been proposed. One study found the expression of the glutamate transporters to be lost in astrocytes of SOD1-mutant rodent models of ALS and samples from patients with familial and sporadic ALS (Bruijn et al., 1997; Howland et al., 2002; Rothstein et al., 1995). Consequently, astrocytes fail to take up and remove glutamate from the synaptic cleft, causing a prolonged glutamate stimulation of post-synaptic neurons (Taylor et al., 2016). Another mechanism suggests that astrocytes protect motor neurons from excitotoxicity by releasing factors which induce the upregulation of GluA2 in neurons, reducing the permeability of AMPARs to calcium. The expression of mutant SOD1 by astrocytes was found to impair the regulation of GluA2 expression, thus compromising their neuroprotective function (van Damme et al., 2007). Alternatively, one study suggests a defect in synaptic vesicle cycling caused by a posttranscriptional reduction in Hsc70-4/HSPA8 chaperone levels in C9-MNs (Coyne et al., 2017). Impaired pre-synaptic vesicle dynamics

results in an enhanced synaptic output but a shorter burst duration (Perkins et al., 2021). Additionally, an increase in GluA1 AMPAR expression has been identified in C9-MNs, leading to an enhanced vulnerability to excitotoxicity (Selvaraj et al., 2018). A study using RNAseq in C9-MNs showed an increased expression of the AMPAR subunits GluA1, GluA2, and GluA3, the NMDA subunit GluN2A, and the metabotropic glutamate receptor subunits mGluR2 and mGluR4 in C9-MNs (Dafinca et al., 2020). The upregulation of calcium-permeable AMPAR and NMDAR subunits was confirmed using qPCR in C9-MNs. Despite this, the intake of calcium was reduced in C9-MNs stimulated with glutamate, while calcium intake was enhanced in C9-MNs stimulated with KCl (Dafinca et al., 2020).

One mechanism which could lead to the long-term hypoexcitability seen in C9-MNs is aberrant AMPAR recycling. AMPAR recycling is a pathway for regulating the strength of glutamatergic synapses, in which AMPARs are removed from post-synaptic densities, internalised, and later returned to synapses (N. Zheng et al., 2015). Under chronic glutamate signalling, AMPARs are not returned to synapses but are degraded via autophagy. This causes a long-term downregulation of AMPARs at the synapse, which leads to a decrease in synaptic strength (see Figure 9) (Ehlers, 2000; Huganir & Nicoll, 2013). Defects in autophagy cause the accumulation of glutamate receptors on the surface (G. Wang et al., 2012).

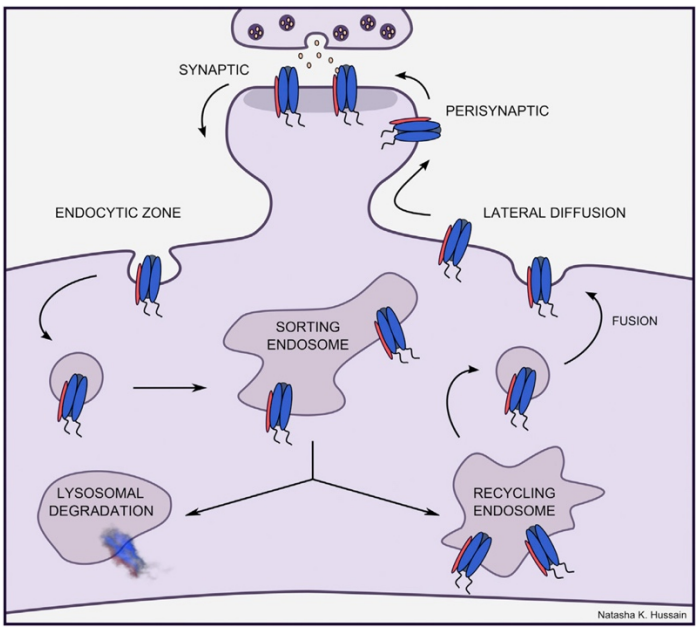


Figure 9: Schematic depiction of AMPAR recycling and degradation. AMPAR (blue) are internalised and sorted for recycling or lysosomal degradation, thus providing a mechanism for short-term or long-term decrease in synaptic strength. This image was taken from **Huganir & Nicoll (2013).**

C9orf72 haploinsufficiency-associated autophagy defects have been shown to cause an increase in the number of glutamate receptors in glutamatergic neurons (Shi et al., 2018). C9orf72 is an essential regulator of post-synaptic GluA1 receptor levels, and loss of C9orf72 contributed to excitotoxicity in C9-ALS/FTD in mouse models (Xiao et al., 2019).

In C9-iPSC-derived MNs from my group, C9-MNs stimulated with glutamate were hypoexcitable, while C9-MNs stimulated with KCl were hyperexcitable. Additionally, the clearance of calcium from the cytosol was delayed as a result of reduced mitochondrial calcium buffering due to a downregulation of mitochondrial calcium uniporters (Dafinca et al., 2020).

1.2.3.6 Mitochondrial function

Mitochondria have multiple roles in cells. They are primarily responsible for ATP production through oxidative phosphorylation (OXPHOS). Additionally, mitochondria regulate apoptosis, free radical production, protein and lipid biosynthesis, iron processing, haem and steroid synthesis, etc (Filler et al., 2014; Pieczenik & Neustadt, 2007). Mitochondria also play a role in regulating calcium homeostasis (Ivannikov et al., 2010; Zenisek & Matthews, 2000). Thus, mitochondrial dysfunction causes a lack of energy supply, cell death, oxidative stress, and excitotoxicity (Filler et al., 2014; Pieczenik & Neustadt, 2007; Prentice et al., 2015). Mitochondrial dysfunction can be the result of oxidative stress, mutations in the mitochondrial DNA (mtDNA), or aberrant proteins or protein aggregates (Cha et al., 2015; C. Y. Guo et al., 2013; B. Lu & Guo, 2020; Nowicka et al., 2021).

Mitochondrial function is particularly essential in neurons since neurons have a very high ATP demand, for example, due to the use of ATP-dependent ion pumps in the recovery from depolarisation (Kann & Kovács, 2007). During neuronal differentiation, cells switch from mainly generating ATP through

glycolysis to relying primarily on mitochondrial OXPHOS, as glycolysis becomes too inefficient (X. Zheng et al., 2016). Neurons use both pyruvate produced by internal glycolysis and pyruvate derived from lactate, which is provided by astrocytes *in vivo* (Kann & Kovács, 2007).

Mitochondrial dysfunction is a crucial disease mechanism associated with neurodegeneration, including ALS (C. Y. Guo et al., 2013). ALS- and FTD-associated protein aggregates co-localise with mitochondria and trigger a disease phenotype. Mutant SOD1 has an increased tendency to localise at the mitochondrial membrane and is sufficient to cause mitochondrial damage (Cozzolino et al., 2009; Tafuri et al., 2015). FUS interacts with the mitochondrial chaperone Hsp60, which promotes the induction of the FUS-associated neurodegenerative phenotype in *Drosophila* expressing mutant FUS (Deng et al., 2015). Wild-type and mutant TDP-43 colocalise with mitochondria and impair mitochondrial function in primary motor neurons (W. Wang et al., 2013). In C9-ALS, $(GR)_{80}$ has been shown to interact with mitochondrial ribosomal proteins and induce oxidative stress in C9-MNs (Lopez-Gonzalez et al., 2016).

One study observed an increase in mitochondrial polarisation and a decrease in mitochondrial content in fibroblasts from sporadic ALS patients (Kirk et al., 2014). Similarly, a study found an increase in mitochondrial polarisation and reactive oxygen species (ROS), as well as a rise in oxygen consumption and ATP production in fibroblasts from C9-ALS patients (Onesto et al., 2016). In contrast, the same study found no changes in oxygen consumption rate and a decrease in mitochondrial membrane potential in TARDBP fibroblasts, suggesting that mitochondrial dysfunction is present in different types of ALS but with other pathological mechanisms (Onesto et al., 2016). My group has observed a reduction in mitochondrial membrane potential, basal respiration and ATP production in C9-MNs (Dafinca et al., 2016; Dr Paola Barbagallo, unpublished).

1.2.3.7 Dynamics of mitochondrial morphology

Mitochondria are highly dynamic, with continuously ongoing fusion and fission processes to adapt mitochondrial morphology to the metabolic needs of cells (Westermann, 2012). Fusion plays a role in spreading enzymes and metabolites across mitochondria and functions as a repair mechanism for mildly damaged mitochondria. On the other hand, fission is vital for producing new mitochondria and the degradation of depolarised mitochondria via autophagy (Westermann, 2012).

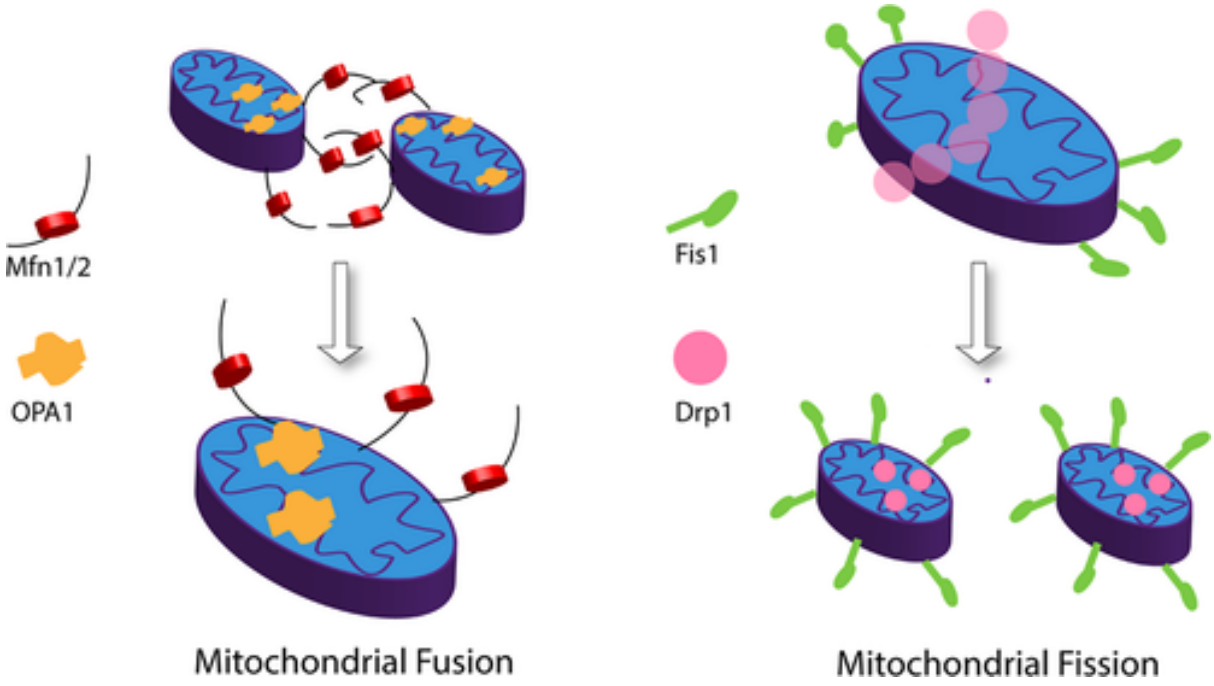


Figure 10: Mitochondria constantly undergo mitochondrial fusion mediated by Mfn1/2 and OPA1 and fission mediated by Fis1 and Drp1. This image was taken from Y. Wang et al. (2019).

Mitofusins (Mfns) are mitochondrial transmembrane proteins which mediate mitochondrial fusion. Of its two isoforms, Mfn2 is predominantly expressed in the brain (Eura et al., 2003). Depletion of Mfn2 causes mitochondrial fragmentation, as well as a reduction in mitochondrial membrane potential, oxygen consumption rate, and the expression of OXPHOS complexes (Bach et al., 2003; H. Chen et al., 2003; Pich et al., 2005). Additionally, Mfns are also required for mitochondrial DNA replication (H. Chen et al., 2010). While the primary function of Mfns is to control the plastic behaviour of mitochondria, Mfn2 is also involved in tethering mitochondria and ER, thus regulating the Ca^{2+}

exchange and lipid transfer between both organelles (de Brito & Scorrano, 2008; Hernandez-Resendiz et al., 2020). During mitophagy, phosphoubiquitination of Mfn2 destroys the contact between mitochondria and ER, which is a prerequisite for mitophagy (McLelland et al., 2018).

To protect intact mitochondria from fusion with dysfunctional mitochondria, which could damage functional mitochondria, mitochondrial fusion is tightly regulated. Mfn2 is a target for ubiquitination by parkin. It is extracted from the OMM and degraded via the proteasome prior to mitochondrial degradation to avoid the fusion of damaged mitochondria with healthy mitochondria (McLelland et al., 2018). Optic atrophy-1 (OPA1) is also involved in regulating mitochondrial fusion. The long isoform L-OPA1 carries out mitochondrial fusion when the mitochondrial membrane potential is intact. L-OPA1 is cleaved to inactive short isoforms when mitochondria are depolarised, preventing mitochondrial fusion. This leads to a fragmentation of dysfunctional mitochondria (Gilkerson et al., 2021).

Mitochondrial fission relies on Dynamin-Related Protein 1 (DRP1), which forms oligomers that wrap around the OMM to scission mitochondria (Fonseca et al., 2019). Another protein which plays an important role in fission is Fis1, which binds Mfns and OPA1 and inhibits the fusion machinery, which leads to mitochondrial fragmentation (R. Yu et al., 2019). Therefore, mitochondrial fragmentation in neurons could be caused by either upregulation of DPR1 or Fis1, downregulation of Mfn2 and OPA1, or mitochondrial depolarisation.

Several studies found an association between an ALS phenotype and aberrant fusion and fission and mitochondrial morphology. The proteins CHCHN10 and DNAJC11 are involved in the formation and organisation of mitochondrial cristae, which undergo constant dividing and fusing. Mutations have been identified in both genes, which cause the disorganisation of mitochondrial cristae and lead to a motor neuron pathology similar to ALS (Ioakeimidis et al., 2014; Straub et al., 2018). SOD1 mutant mice and cultured cells display increased levels of fission proteins and decreased levels of fusion proteins. Inhibiting DRP1 to block mitochondrial fission rescues mitochondrial functionality in SOD1 G93A rat spinal cord motor neurons. Additionally, it has been shown that the expression level of TDP-

43 correlates to the length and density of mitochondria in the neurites of cultured primary neurons. This effect is exacerbated by TDP-43 mutants Q331K and M337V, while the co-expression of Mfn2 abolished TDP-43-induced abnormalities in mitochondrial dynamics (W. Wang et al., 2013). A recent paper showed that ER-mitochondria tethering is impaired in iPSC-derived C9-CNs and mutant C9-transgenic mice. Poly-GA, poly-GR, and poly-PR impair the interaction of the tethering proteins VABP and PTPIP51 and disrupt the delivery of ER Ca^{2+} to mitochondria (Gómez-Suaga et al., 2019). Furthermore, in experiments from my group using iPSC-derived C9-MNs, we observed both enlarged mitochondria and cristae, as well as increased mitochondrial fragmentation in the C9-2 line in iPSC-derived MNs (Dr Ruxandra Dafinca, unpublished; Dafinca et al., 2016).

1.2.3.8 Mitophagy

The physiological process in which mitochondria are degraded via macro-autophagy is called mitophagy. This process primarily serves as a quality control mechanism which recognises damaged mitochondria to prevent a spill of ROS, which might cause apoptosis or inflammation. Mitophagy is also a way of responding to changes in energy demand by removing mitochondria or renewing the mitochondrial stock (Weil et al., 2018). An imbalance in mitophagy causes pathologies such as neurodegeneration, cancer, or organ failure (Weil et al., 2018).

An essential protein in mitophagy initiation is PTEN-induced kinase 1 (PINK1), which is constantly produced and degraded by presenilin-associated rhomboid-like protein (PARL) in healthy mitochondria (Martinez-Vicente, 2017). In damaged mitochondria, however, the drop in membrane potential inhibits PARL causing an increase in PINK1 levels in the outer mitochondrial membrane (OMM). PINK1 activates the E3 ubiquitin ligase parkin (see Figure 11) (Koyano et al., 2014). Parkin ubiquitinates outer OMM proteins such as translocase of outer mitochondrial membrane 20 (TOMM20), mitofusin 1 and 2 (Mfn1/2), DRP1, Fis1, and Miro1/2, which are responsible for protein integration, mitochondrial motility, transport, etc (Desai et al., 2018; H. Wang et al., 2011). PINK1 then phosphorylates the ubiquitinated products of parkin at Ser65 to label mitochondria for degradation

(Desai et al., 2018; Koyano et al., 2014). Autophagy receptors recognise these phosphorylated poly-ubiquitin chains and recruit additional components of the macro-autophagy machinery (Desai et al., 2018). In short, mitochondrial depolarisation activates PINK1, which phosphorylates ubiquitin and parkin at serin 65, while parkin amplifies the degradation signal (Martinez-Vicente, 2017). Mitochondrial depolarisation can be caused by cellular stress such as ROS and aggregation of toxic proteins.

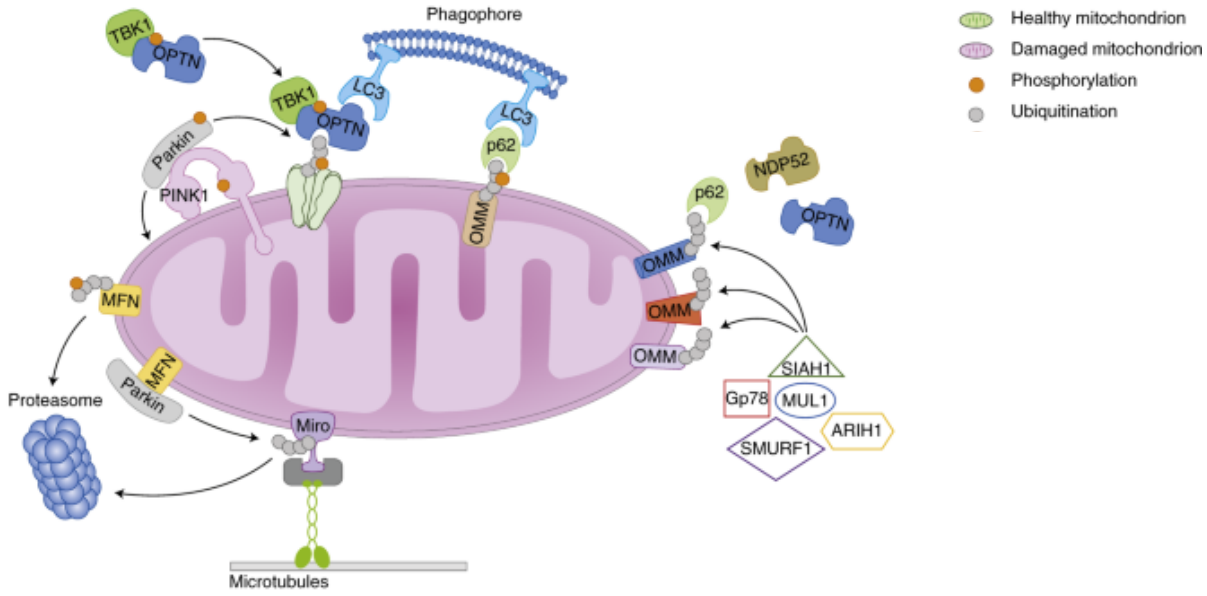


Figure 11: Schematic depiction of mitophagy initiation following mitochondrial depolarisation. This image was taken from Palikaras et al. (2018).

Aberrant regulation of mitophagy is associated with neurodegeneration. In Parkinson's Disease, parkin- and PINK1-mutations in fly models cause a Parkinson's Disease phenotype, including mitochondrial dysfunction and motor deficits (Burman et al., 2012; Greene et al., 2003; Pesah et al., 2004; Yang et al., 2006). Changes in protein quality control and autophagy are also associated with Alzheimer's Disease and Huntington's Disease (Martinez-Vicente, 2017).

Mitophagy has not been studied in detail in ALS or FTD, although several disease-associated mutations affect proteins associated with mitophagy. TBK1 phosphorylates adapter proteins. Mutations in TBK1

have been identified to cause ALS and FTD (Oakes et al., 2017). OPTN functions as an adapter protein between ubiquitin and LC3 and is essential for the recruitment of damaged mitochondria to the phagophore (Weil et al., 2018). While five adapter proteins can bind ubiquitin and LC3, including p62, previous studies found that only OPTN and NDP52 expression can rescue mitophagy when all adapters are depleted (Lazarou et al., 2015). ALS-associated OPTN mutations affect the ubiquitin-binding ability and prevent the recruitment of damaged mitochondria (Weil et al., 2018). Other autophagic factors such as the ULK1 complex, which were discussed previously, also play an essential part in the degradation of mitochondria. Furthermore, VCP is a protein which localises to mitochondria in response to the ubiquitination of mitochondria by parkin (N. C. Kim et al., 2013). It is required for the degradation of Mfns by the proteasome at the onset of mitophagy. VCP knockdown reportedly disrupts the degradation of damaged mitochondria in MEFs (N. C. Kim et al., 2013). Mutations in the VCP gene are associated with various neurodegenerative diseases, including ALS and FTD (Koppers et al., 2012). In addition, PINK1 and parkin have been identified as interactors of FUS, and their down-regulation partially rescued neurodegeneration in FUS transgenic flies (Y. Chen et al., 2016).

1.2.3.9 Axonal transport

Due to the morphological compartmentalisation and unique energy demand of neurons, mitochondria need to be transported to distal areas such as axonal branches and synapses where there is a high demand for energy and Ca^{2+} buffering. One-third of axonal mitochondria are motile in mature neurons. Mitochondria move bi-directionally with frequent pauses and changes in direction. Stationary mitochondria function as a local energy supply and Ca^{2+} buffer. The balance between stationary and motile mitochondria adapts quickly to changes in energy demands (M. Y. Lin & Sheng, 2015).

Axonal transport relies on motor proteins that move along microtubules in retrograde (minus-end directed, towards the soma) or anterograde (plus-end directed, towards synaptic terminals) fashion. The main motor proteins for the anterograde transport of mitochondria are members of the kinesin-

related protein 5 (KIF5), which consists of three isoforms (KIF5a, KIF5b, KIF5c) (Hirokawa et al., 2010; Kurd & Saxton, 1996; Pilling et al., 2006; Tanaka et al., 1998). While KIF5a and KIF5c are exclusively expressed in neurons, KIF5b is expressed ubiquitously (M. Y. Lin & Sheng, 2015).

Cytoplasmic dynein is the main motor protein for retrograde transport along axons with the support of dynactin. Dynactin binds to dynein, microtubules, and mitochondria and is essential for mitochondrial retrograde transport in *D. melanogaster* (Pilling et al., 2006). While the exact function of dynactin in axonal transport is unknown, the disruption of dynactin has been shown to interrupt both anterograde and retrograde transport, suggesting a role of dynactin in both anterograde and retrograde transport (Haghnia et al., 2007). Since mitochondria commonly change direction during axonal trafficking and dynein colocalises with mitochondria moving in either direction, it is believed that kinesin and dynein both coordinate the transport of mitochondria (Hirokawa et al., 1990).

Mitochondria are connected to axonal transport machinery by adapter proteins such as Miro1 (also called RhoT), a transmembrane protein of the OMM (Fransson et al., 2006). Miro1 is also a parkin target, which prevents the transport of dysfunctional mitochondria.

Thus, mitochondrial dysfunction disrupts axonal transport in several ways: the induction of mitophagy disrupts the binding between mitochondria and motor proteins. In addition, a decrease in Ca^{2+} buffering disrupts the microtubule network, and a decrease in ATP production disrupts the function of motor proteins, which have a high energy demand. Therefore, mitochondrial dysfunction also disrupts the transport of functional mitochondria, which could replace damaged mitochondria (W. Guo et al., 2020).

Motor neurons are particularly vulnerable to defects in axonal transport due to their long axons (Hegedus et al., 2007). Various evidence has been uncovered pointing towards the involvement of axonal transport in ALS disease mechanisms. Studies in ALS patients and animal models show axonal degeneration is present long before symptom onset (Fischer et al., 2004; Fischer & Glass, 2007;

Fischer-Hayes et al., 2013). Additionally, an abnormal accumulation of kinesins, cargos, and hyperphosphorylated neurofilaments has been found in the soma of motor neurons in post-mortem tissue (de Vos & Hafezparast, 2017). The aberrant transport of mitochondria and ER vesicles has also been identified in various *C9orf72* drosophila models (Baldwin et al., 2016).

Additionally, several ALS-causing genetic mutations affect axonal transport. Mutations in the FUS protein are common in familial ALS but not FTD. Mutations in FUS have been shown to affect mitochondrial axonal transport (W. Guo et al., 2017). FUS also regulates the expression of motor proteins such as KIF5b and KIF5c (W. Guo et al., 2020). Less common mutations, such as mutations in KIF5a or the $p150^{Glued}$ subunit of the dynein/dynactin complex, are associated with ALS (Burk & Pasterkamp, 2019).

Furthermore, neurofibrillary tangles consisting of hyperphosphorylated tau protein are commonly found in the frontal and temporal lobes of C9-HRE carriers (Bieniek et al., 2013). The tau protein stabilises microtubules and maintains axons (Olszewska et al., 2016; Y. Wang & Mandelkow, 2016). Its hyperphosphorylation causes the disintegration of microtubules X. Zhang et al., 2018). Therefore, tau pathology is a sign of unstable microtubules affecting axonal transport. The contribution of axonal transport to FTD pathogenesis is not well understood.

1.2.4 Non-neuronal involvement

Apart from neurons, microglia, astrocytes, and oligodendrocytes show a C9-dependent phenotype (see Figure 12).

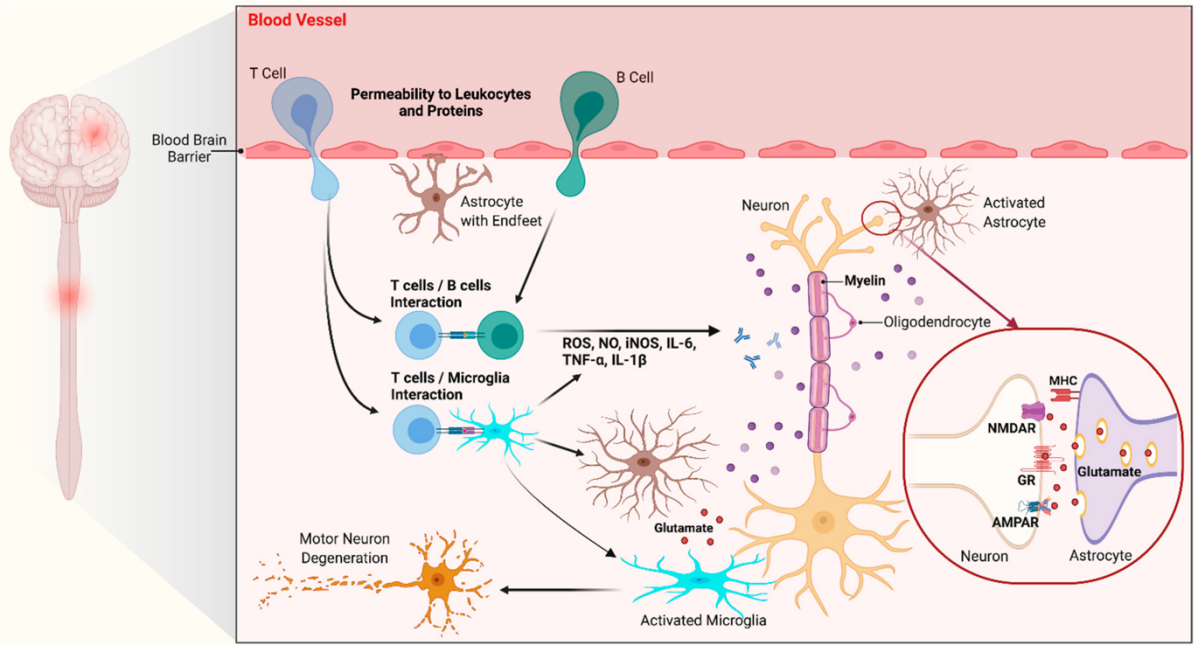


Figure 12: Overview of glial cell toxicity in ALS/FTD. Overactive microglia and astrocytes become neurotoxic and produce excess pro-inflammatory factors and glutamate. C9-oligodendrocytes become dysfunctional, which leads to myelin damage. This image was taken from Ghasemi et al. (2021)

1.2.4.1 Microglia

Microglia are glial cells responsible for synaptic pruning, tissue development, phagocytosis of debris and apoptotic cells, assisting myelination, and giving trophic support to neurons (Y. Dong & Yong, 201919). Microglial have a resting state in which they patrol their environment and become activated by endogenous or exogenous inflammatory stimuli (see Figure 12) (Nimmerjahn et al., 2005).

Microglia are associated with C9-ALS/FTD as this cell type has the highest expression of C9orf72 of any cell type in the brain and has been reported to be increasingly activated in post-mortem tissue of C9-ALS/FTD patients (O'Rourke et al., 2016). While mice models with a single or double knockdown of *C9orf72* did not exhibit evidence of neurodegeneration, C9orf72 haploinsufficiency caused the upregulation of microglial activation genes towards a pro-inflammatory pathway (O'Rourke et al., 2016).

Microglia present RNA foci, but their impact on microglial functions has not been investigated yet (Vahsen et al., 2021). DPR aggregates have so far not been reported in microglia in post-mortem tissue and C9-animal models (Vahsen et al., 2021). Instead, microglia are activated by neuronal GA expression and potentially PR expression in DPR-expressing mouse models (Hao et al., 2019; LaClair et al., 2020; Vahsen et al., 2021). Thus, DPR release from C9-neurons and C9orf72 haploinsufficiency might induce a neurotoxic phenotype in microglia, causing additional damage to neurons (Vahsen et al., 2021).

1.2.4.2 Astrocytes

Astrocytes are a type of glial cell vital for controlling ion and neurotransmitter homeostasis and supporting neuronal metabolism by supplying neurons with energy substrates, synthesising glycogen, and regulating local blood flow (Verkhratsky & Nedergaard, 2018). Together with microglia, they carry out synaptic pruning and give trophic support to neurons (Vahsen et al., 2021).

The presence of activated astrocytes has been described to be increased in post-mortem brain tissue of ALS patients. C9-astrocytes display RNA foci and RAN translation (Zhao et al., 2020). C9-astrocytes show a loss of metabolic flexibility due to a reduction in enzymes involved in adenosine, fructose, and glycogen metabolism. Additionally, the transport of energy substrates into mitochondria is disrupted (Allen et al., 2019). During bioenergetic stress, metabolic flexibility is essential for cell survival. Thus, these effects contribute to starvation-induced toxicity in C9-astrocytes (Allen et al., 2019).

A major function of astrocytes is the uptake of glutamate from the synaptic cleft to prevent excess glutamate stimulation of neurons. In astrocytes, glutamate is converted to glutamine, released, and taken up by neurons. In cellular models with C9-knockdown, the expression of glutamine synthetase is reduced, which disturbs glutamate conversion and leads to an accumulation of intracellular glutamate (Fomin et al., 2018). Additionally, in C9-ALS patient tissue, the expression of the glutamate

uptake transporters by astrocytes is decreased, which could result in excitotoxicity (see Figure 12) (Fomin et al., 2018).

Furthermore, C9-astrocytes cause oxidative stress in motor neurons due to the C9-HRE-dependent downregulated secretion of antioxidant proteins (Birger et al., 2019). C9-astrocytes in co-culture with motor neurons induce a progressive loss of action potential output in motor neurons (Zhao et al., 2020).

1.2.4.3 Oligodendrocytes

Oligodendrocytes make up the majority of glial cells (Vahsen et al., 2021). The primary function of oligodendrocytes is to myelinate axons of neurons in the CNS. Together with other glial cells, they provide metabolic and trophic support to neurons, maintain axonal integrity, and modulate immune responses (Raffaele et al., 2021; Vahsen et al., 2021).

Oligodendrocytes are believed to be affected by C9-pathology, as they display TDP-43 inclusions (Nolan et al., 2020). In addition, the activity of the promoter for the mouse *C9orf72* ortholog is increased in brain regions which are affected in ALS (Langseth et al., 2017). In a SOD1 G93A mouse model, myelin damage and oligodendrocyte degeneration have been described in the spinal cord at a pre-symptomatic phase (Kang et al., 2013). Additionally, the maturation of oligodendrocytes precursor cells in response to the degeneration of mature oligodendrocytes is impaired. Myelin abnormalities have also been observed in the spinal cord and motor cortex of ALS patients (Kang et al., 2013).

1.2.5 Therapeutic strategies for C9-ALS/FTD in development

Several strategies are being investigated to develop disease-modifying treatments targeting the *C9orf72* hexanucleotide repeat expansion and its effectors. One approach is to reduce C9-HRE-containing transcripts. A phase I clinical trial (NCT03626012) assessed the effectiveness of the

antisense oligonucleotide (ASO) BIIB078. This ASO targets sense C9-HRE transcripts to reduce sense G_4C_2 RNA foci without reducing C9-mRNA (Hautbergue et al., 2021). Although BIIB078 was shown to reduce DPRs and selectively protect iPSC-derived C9-MNs from excitotoxicity, the clinical study found no clinical benefit (Biogen Inc. & Ionis Pharmaceuticals Inc., 2022; Boros et al., 2022; J. Jiang et al., 2016). A similar clinical study using the stereopure ASO WVE-004 is ongoing (NCT04931862). Early results reported a reduction in poly-GR after a single dose but no change in clinical outcome measures (Boros et al., 2022; WAVE Life Science Ltd., 2022). Similarly, a study found that Adeno-Associated Virus (AAV)-delivered miRNAs targeting repeat transcripts reduced C9-HRE transcripts and RNA foci levels in iPSC-derived frontal brain-like neurons and BAC transgenic mice (Martier et al., 2019). C9-HRE transcripts can also be reduced by limiting their expression. The deletion of the promoter driving the expression of C9-HRE using CRISPR/Cas9 has been shown to reduce DPR levels and rescue neurodegeneration (Krishnan et al., 2020). Similarly, targeting the C9-HRE with deactivated Cas9 inhibits the transcription of C9-HRE regions, reduces RNA foci, and lowers poly-GP levels (Pinto et al., 2017).

Another approach to target the effects of the C9-HRE pharmaceutically is to reduce DPR levels. Anti-GA antibodies have been shown to minimise poly-GA aggregate formation and seeding in patient fibroblasts and primary neurons (Zhou et al., 2017). In BAC transgenic mice expressing sense and antisense C9-HRE transcripts, anti-GA antibodies reduce neuroinflammation, improve motor and behaviour symptoms, and reduce motor neuron loss. They also cause a reduction in poly-GP and poly-GR proteins, possibly due to increased proteasome function (Hautbergue et al., 2021; L. Nguyen et al., 2020). Since the activation of the UPR causes an increase in RAN translation, DPR levels can be modified by targeting proteins involved in the UPR. The inhibition of the UPR protein kinase R (PKR) decreases DPR levels and improves behavioural and neuropathological deficits in *C9orf72* BAK transgenic mice (Zu et al., 2020). One inhibitor of PKR is the FDA-approved drug metformin, which is currently in a phase II clinical trial (NCT04220021; Zu et al., 2020). A different strategy is to inhibit the nuclear export of C9-HRE transcripts by targeting the nuclear export adaptor Serine/Arginine-Rich

Splicing Factor 1 (SRSF1) using gene therapy. SRSF1 inhibition prevents neurodegeneration and motor deficits in a *Drosophila* C9-HRE model and suppresses cell death in patient-derived MNs and astrocytic-mediated neurotoxicity (Hautbergue et al., 2017). Additionally, the levels of DPRs can be reduced by stimulating their clearance. The overexpression of the Small Heat Shock Protein B8 (HSPB8) has been shown to reduce the accumulation of most insoluble DPR species by promoting their autophagy in MNs (Cristofani et al., 2018). An ongoing clinical trial (NCT03359538) is assessing the use of the autophagy-stimulator rapamycin in sporadic and familial ALS patients (Gittings & Sattler, 2020).

Alternatively, the repeat expansion in the *C9orf72* gene could be targeted directly via gene editing using CRISPR/Cas9. One study showed a reversal of excitotoxicity by homology-directed repair of the C9-HRE site with wild-type repeats (Ababneh et al., 2020). However, gene-editing the C9-HRE region in patients is technically challenging. The delivery of CRISPR/Cas9 systems to the relevant areas, the problematic accuracy of gene editing, and the low efficacy of homology-directed repair present hurdles for this approach that still need to be overcome (Hautbergue et al., 2021; Krishnan et al., 2020).

A general approach to treating C9-ALS/FTD is supplementing neurotrophic factors to support neuronal growth and survival. While several preclinical studies showed promising results for this strategy in SOD1-ALS, this strategy has so far not been tried in C9-ALS/FTD (Hautbergue et al., 2021).

Clinical trials that are open to but not limited to C9-ALS/FTD patients include a phase 1 trial (NCT03945279) of the compound BIIB100, which inhibits the nuclear export receptor Exportin 1 (XPO1) (Hautbergue et al., 2021). In addition, a phase 2 clinical trial (NCT03987295) of the recombinant antibody AL001 specific to sortilin (SORT1), a glycoprotein involved in progranulin trafficking, is being carried out in FTD patients with *C9orf72* or *granulin* mutations (Hautbergue et al., 2021).

Other therapeutical developments which do not target the C9-HRE include targeting TDP-43 or FUS pathology, increasing progranulin levels in patients carrying *GRN* mutations, or targeting tau in patients with *MAPT* mutations (Panza et al., 2020).

1.3 C9-Research models

1.3.1 Post-mortem brain tissue

Post-mortem brain tissue from patients gives vital insight into understanding FTD and ALS on a microscopic level, such as the connection between cellular disease pathologies and symptoms. Post-mortem brain tissue is commonly used to study disease pathologies. For example, it is used to examine protein aggregation pathologies such as DPR aggregates in different cell types or to study specific cell type vulnerability (E. J. Kim et al., 2012; Quaegebeur et al., 2020; Santillo & Englund, 2014). These findings often serve as a useful starting point for *in vitro* and *in vivo* studies in disease models.

While patient brain tissue is the most accurate substrate for investigating C9-ALS/FTD, its applications are limited. Post-mortem brain tissue only serves as a snapshot at the end-stage of the disease, making it impossible to study early disease drivers (Giacomelli et al., 2022). It may also mainly reflect on neurons which are less susceptible to degeneration since susceptible neurons might have degenerated in an earlier disease stage (Giacomelli et al., 2022). Furthermore, studying end-stage patient tissue makes it hard to distinguish between disease drivers and compensatory mechanisms (Giacomelli et al., 2022). Since it is a static state, post-mortem brain tissue cannot be used for methods which require functional neurons. In addition, the genetic heterogeneity between patients makes it imperative to study brain tissue samples from several patients to gain reliable results. The availability of patient brain tissue, however, is very limited.

1.3.2 Animal models

Animal models offer valuable information on pathogenic pathways in the context of intact tissues, such as the cortex in its entire composition or the neuromuscular synapse (Giacomelli et al., 2022). In addition, animal models enable the study of complex symptoms such as motor or cognitive deficits. Animal models can also be a source for primary neurons to study in culture, which are more mature than iPSC-derived cultures.

However, animal models might not always recapitulate human biology faithfully, especially in species with genes with low homology to human orthologues. Furthermore, genetic manipulation usually leads to the overexpression of disease genes in animal models, which may not replicate disease pathways appropriately and might exacerbate interspecies differences (Giacomelli et al., 2022).

Therefore, animal models are essential for studying diseases but must be complemented by human models. Various types of C9-ALS/FTD animal models exist.

1.3.2.1 Mice

Mice are commonly used as disease models. Approximately 90% of the mouse and human genomes have synteny, and orthologous genes share 78.5% identity (Monaco et al., 2015). Well-established methods exist to study complex behavioural and motor impairment, making this the ideal model to study the effect of disease transgene expression on behavioural or motor defects.

The disadvantages of mouse disease models are that they are costly and high maintenance. Generating genetically altered mice which express the transgene of interest is a lengthy process. Thus, mouse models are not viable for high-throughput screening. In addition, the life span of mice is not long enough to study physiological neurodegeneration.

To model C9-ALS/FTD in mice, parts of the C9-HRE or its effectors are introduced into mice via different genetic techniques. Bacterial artificial chromosome (BAC) transgenic mice are a C9-disease model in

which parts of the human *C9orf72* gene-containing repeats are integrated into the mouse genome. BAC mice can carry endogenous regulatory sequences of transcription and can express different splice variants (Batra & Lee, 2017). BAC transgenic mice were created to study C9-RNA and DPR toxicity. This disease model exhibits repeat-length dependent expression of sense and antisense RNA foci (Batra & Lee, 2017). Along with RNA foci, BAC transgenic mice also display DPR expression, particularly poly-GP and poly-GA, and, to a lesser extent, poly-GR (Batra & Lee, 2017). Despite these commonly observed pathological features, very few models show signs of motor deficits and reduced survival (le Bras, 2021).

Another type of C9-mouse model relies on the delivery of G4C2-repeat DNA by somatic transduction using AAVs (Batra & Lee, 2017). Different versions of this AAV-G4C2-repeat expression mouse model have been created, which carry different repeat lengths. The severity of the C9-HRE phenotype is found to be dependent on the repeat length. Mouse models with a long repeat length, such as AAV-G4C2-149 mice show a stronger phenotype than mouse models with a shorter repeat length, such as the AAV-G4C2-66 mouse model (Batra & Lee, 2017; Chew et al., 2019; Gendron et al., 2013).

Similarly, AAV-mediated mouse models of DPR expression exist. A mouse model expressing $(GR)_{50}$ and $(GR)_{100}$ displayed a length-dependent reduction of survival of cortical and motor neurons. This mouse model exhibited sex-specific phenotypes with more pronounced neuron loss and gait impairment in female mice (Verdone et al., 2022).

1.3.2.2 Zebrafish

In addition to mouse models, zebrafish are commonly used. Zebrafish are 70% genetically homologous to humans, making them significantly less physiologically relevant than mice. They are easily genetically manipulated, their translucency offers simple visualisation of organs, and they can be used for high-throughput drug screening (Fortier et al., 2020). Additionally, ageing zebrafish show similar

senescence in age as humans, making them a valuable model for studying C9-disease drivers in an ageing model (Kishi et al., 2009).

Loss-of-function C9-models include zebrafish in which the transcription of the zebrafish orthologue *C9orf72* is transiently inhibited using injected antisense morpholino oligonucleotides (MOs) (Ciura et al., 2013). Gain-of-function zebrafish models can be generated by injecting constructs containing repeats (Y.-B. Lee et al., 2013). Alternatively, DPR constructs can be introduced into zebrafish (Ohki et al., 2017).

1.3.2.3 Drosophila

Drosophila C9orf72 models are commonly used due to their low cost, rapid generation times, and easy genetic manipulation. *Drosophila* flies are low maintenance and have a short life span which allows for the examination of phenotypes throughout their life cycle and for studying ageing. While some behaviour and motor test exist for *Drosophila*, this methodology is less advanced than that for mice.

These flies have an orthologue of 75% of human genes. Thus, some downstream interactors of RNA foci or DPRs may not be conserved. *Drosophila* flies do not carry a *C9orf72* orthologue, making loss-of-function studies impossible. However, it allows for studying gain-of-function mechanisms without complications from endogenous expression (Sharpe et al., 2021). The transgene expression in *Drosophila* eyes is a useful tool for genome-wide modifier genetic screens. It is also beneficial for investigating dose- and length-dependent toxicity and for studying transgene expression at a level that would be lethal if expressed globally (Sharpe et al., 2021). However, as the expression in the eye, is less pathologically relevant than global expression or the expression in all neurons, this method is not ideal for studying disease mechanisms or viability (Sharpe et al., 2021).

Several types of disease models exist. Pure repeat models express the G_4C_2 sequence and thus produce C9-RNA and DPRs via RAN translation. The expression of 36 repeats or more in the eye causes toxicity which worsens in a repeat-length-dependent fashion (Mizielinska et al., 2014). RNA-only *Drosophila*

models express C9-RNA without expressing DPRs using a transgene interspersed with stop codons to prevent RAN translation. One eye-specific RNA-only model, which exhibits RNA foci but no antisense RNA, did not demonstrate an eye phenotype or lethality (Mizielinska et al., 2014). Another RNA-only model, which exhibits antisense foci in the nucleus and sense foci in the cytoplasm, equally shows no lethality of motor deficits (Moens et al., 2018).

Drosophila models are mainly used to study DPR toxicity. Models expressing poly-GP, poly-AP, or poly-GA have not shown a degenerative eye phenotype or DPR toxicity, even though poly-GA is often toxic in other disease models (Sharpe et al., 2021). Only one study found that the expression of $(AP)_{1000}$ caused toxicity in the eye, electrophysiological defects, and motor impairments (West et al., 2020). The expression of poly-PR or poly-GR has been found to cause severe eye degeneration and lethality from as little as $(PR)_{36}$ or $(GR)_{36}$ on (Mizielinska et al., 2014). One study showed that the pan-neuronal expression of $(PR)_{1000}$ or $(GR)_{1000}$ reduced the longevity of flies (West et al., 2020). The expression of $(PR)_{1000}$ or $(GR)_{1000}$ in the eye was not lethal. Only homozygous expression in the eye or an increase in temperature to 29^{o}C caused a severe degenerative phenotype (West et al., 2020). Interestingly, the expression of long DPRs was less toxic than short DPR constructs used in other publications (Mizielinska et al., 2014; Sharpe et al., 2021; West et al., 2020). The same study showed TDP-43 mislocalisation in larval salivary glands in *Drosophila* expressing $(GR)_{64}$ or $(GR)_{1000}$ without direct co-localisation of GR and TDP-43 (West et al., 2020). Co-expressing two DPRs in *Drosophila* eyes showed that the combination of $(GR)_{1000}$ and $(PR)_{1000}$ was more toxic than the homozygous expression of $(GR)_{1000}$ (West et al., 2020). The pan-neuronal co-expression of two DPRs caused motor deficits for each combination but $(AP)_{1000}/(GA)_{1000}$. Motor symptoms were most severe in *Drosophila* expressing $(AP)_{1000}/(GR)_{1000,}$ which was lethal at a young age. Co-expression of alanine- and arginine-rich DPRs also caused seizures in flies (West et al., 2020).

Since overexpression defects and interspecies differences might skew findings from animal models, it is important to confirm results from animal models in a human disease model, such as patient-derived iPSCs.

1.3.3 Induced pluripotent stem cells (iPSCs)

iPSCs are a valuable research tool which enables the examination of disease pathways in the human cell types involved in C9-ALS/FTD. iPSCs derived from C9-ALS/FTD patients contain the full unmodified C9-HRE expressed at a physiological level (Giacomelli et al., 2022). Therefore, patient-derived iPSCs are essential to gaining full knowledge of disease processes. C9orf72 protein expression is often unaltered in iPSC-derived C9-MNs (Beckers et al., 2021). RNA foci and DPRs, however, are commonly observed in C9-MNs (Dafinca et al., 2016; Haeusler et al., 2016).

iPSCs are differentiated into the respective cell type, such as cortical neurons or motor neurons, via months-long differentiation. Thus, working with iPSCs is a time-intensive and costly method. The resulting iPSC-derived neurons replicate a young and immature biological state, making them ideal for studying developmental defects or early-disease phenotypes. While artificial methods to induce ageing phenotypes in iPSC-derived neurons are being investigated to study late disease phenotypes, generating a physiological replicate of aged neurons remains challenging (Giacomelli et al., 2022).

Additionally, high levels of variability between differentiated iPSC cultures make working with iPSCs challenging. A study found that the leading cause for variability is genetic variation between individuals, such as differences in epigenetics, leading to differences in gene expression. Additional sources for the variability are copy number alterations acquired during the reprogramming process and the effects of cell culture conditions. Minor contributors to variability are the effects of gender and passage number (Giacomelli et al., 2022; Kilpinen et al., 2017).

Several strategies exist to overcome genetic variability. First, the number of control and patient lines can be vastly increased. Extensive multicentre efforts are needed for best results, which are costly and

can induce additional variation by conducting experiments with different methods or experimenters (Giacomelli et al., 2022). Second, the repeat sequence in the *C9orf72* gene can be deleted from patient cell lines to create isogenic lines as controls. Due to the complexity of the C9-HRE, off-target effects, and deleterious on-target effects such as loss of heterozygosity or mono-allelic deletions, generating isogenic lines is challenging (Ababneh et al., 2020; Giacomelli et al., 2022). Several isogenic cell lines in which the C9-HRE was knocked out have been used in studies (Selvaraj et al., 2018). My group has developed the only isogenic cell line in which the C9-HRE expansion was corrected by replacing it with the number of repeats from the healthy allele to generate a physiological C9-corrected line (Ababneh et al., 2020). Alternatively, the disease-causing mutation can be engineered into well-characterised control lines to generate C9-lines (Giacomelli et al., 2022). However, due to the size and complexity of the C9-HRE, this has never been successfully done to our knowledge.

In addition to genetic variability, variation in cell culture composition regarding maturity, number, and cell type between differentiations compromise experiments with iPSCs (Giacomelli et al., 2022). Strategies to overcome this type of variation are more limited. Single-cell characterisation allows the generation of heterogenous monocultures. However, this strategy introduces cell stress, causing significant cell death, which might bias analysis (Giacomelli et al., 2022). Alternatively, translating ribosome affinity purification (TRAP) is another method to purify cultures which has recently been successfully applied to iPSC-derived MNs for the first time by my group (Dr Chaitra Sathyaprakash; unpublished).

In this study, C9-iPSC-derived cortical neurons will be used. This model was chosen because I aimed to examine the disease phenotype in a model that is as physiologically relevant as possible. Patient-derived iPSCs are human, carry no genetic alterations to the C9-HRE site, and can be differentiated to the specific cell type associated with FTD.

1.3.4 Pathomechanisms of C9-ALS/FTD research models

After discussing the molecular effect of the C9-HRE and disease models commonly used to study C9-ALS/FTD, I will now discuss aspects of the molecular phenotype found in the most common ALS/FTD disease models.

1.3.4.1 Human post-mortem tissue

Post-mortem tissue from ALS/FTD patients displays a reduction in the expression levels of the C9orf72 protein in the frontal cortex, the motor cortex, the cerebellum, the hippocampus and the spinal cord (Donnelly et al., 2013; Waite et al., 2014). Both sense and antisense RNA foci are present in post-mortem brains in neurons and glial cells (Balendra & Isaacs, 2018; Haeusler et al., 2016). In addition, both DPR pathology and TDP-43 pathology is present in human post-mortem tissue (Scaber & Talbot, 2016; Vatsavayai et al., 2016). Furthermore, neurofibrillary tangles are commonly observed in the frontal and temporal lobes of C9-HRE carriers (Bieniek et al., 2013). The most affected brain areas in end-stage ALS/FTD include the frontal and motor cortex, hippocampus, and thalamus (I. R. MacKenzie et al., 2013; Schludi et al., 2015).

These C9-effectors cause several atrophy of the frontal or temporal lobe in patients with frontotemporal lobar degeneration (FTLD) (Olney et al., 2017). In ALS, the atrophy of lower or upper motor neurons is observed (Hardiman et al., 2017). Additionally, axonal deficits have been identified in post-mortem tissue including an abnormal accumulation of kinesins, cargos, and hyperphosphorylated neurofilaments (de Vos & Hafezparast, 2017).

Apart from neuronal deficits, increasing evidence from human post-mortem tissue suggests a glial component to ALS/FTD. Activated astrocytes are commonly observed in post-mortem tissue of ALS patients which display both RNA foci and RAN translation (Zhao et al., 2020). Moreover, myelin abnormalities due to aberrant oligodendrocytes have been observed in the spinal cord and motor cortex of ALS patients (Kang et al., 2013).

1.3.4.2 Mice

There are many versions of mouse C9-ALS/FTD models engineered in different ways with different molecular phenotypes. Hence, I will discuss the phenotype of a selection of mouse C9-ALS/FTD models.

One mouse model expressing a *C9orf72* transgene with 450 repeats displays C9orf72 haploinsufficiency, C9-RNA, and DPR accumulation. These effects lead to accelerated death, cognitive defects, glial activation, and hippocampal neuron loss (Q. Zhu et al., 2020). Another study using the same mouse model identified impaired ER-mitochondria tethering (Gomez-Suaga et al., 2022).

A transgenic mouse was engineered to express GFP-PR_{28} specifically in neurons. Heterozygous mice show brain atrophy, loss of Purkinje cells and lower motor neurons, inflammation in the spinal cord and cerebellum, microglia activation, and motor imbalance, accompanied by the differential expression of genes linked to synaptic transmission. Homozygous mice have a reduced life span (Hao et al., 2019).

In AAV-G4C2-149 mice, sense and antisense RNA foci, DPR expression, phospho-TDP-43 inclusions, and the dysregulation of stress granules were observed. This mouse model showed cognitive and motor deficits along with gliosis and neurodegeneration (Chew et al., 2019). An AAV-G4C2-66 mouse model also exhibited RNA foci, RAN translation, and phosphorylated TDP-43 in a small number of neurons. This model showed mild neurodegeneration, as well as motor and cognitive deficits (Batra & Lee, 2017; Gendron et al., 2013).

Additionally, primary neurons extracted from mice and then transduced to carry transgenes are useful research tools. For example, primary mouse models expressing GFP-$(GA)_{50}$ have significantly upregulated ClCasp3 levels suggesting increased apoptosis (Y. J. Zhang et al., 2014, 2016). Moreover, these cells display reduced proteasome activity which triggers the UPR, causing an increase in the levels of BiP, phosphorylated PERK, and CHOP (Y. J. Zhang et al., 2014).

1.3.4.3 Zebrafish

Zebrafish C9-ALS/FTD models are less common due to their low genetic homolofy to humans. The suppression of C9orf72 expression in loss-of-function models leads to behavioural and motor deficits along with axonal degeneration (Ciura et al., 2013). In a gain-of-function model, the expression of 72 G4C2 repeats in zebrafish embryos induces measurable RNA foci, while the expression of 35 or 72 G4C2 repeats causes apoptosis (Y.-B. Lee et al., 2013). Another gain-of-function zebrafish model expressing $(GA)_{80}$-GFP displays RNA foci and toxicity (Ohki et al., 2017).

1.3.4.4 Drosophila

Similar to mice, there are many different versions of *Drosophila* genetically engineered to reflect an aspect of C9-ALS/FTD. I will discuss the phenotype of some of these *Drosophila* models.

One study using a *Drosophila* model expressing 8, 28, or 58 G4C2-repeat-containing transcripts, identified a dosage-dependent, repeat-length-dependent translation of DPRs and neuronal degeneration. The group identified morphological changes in the nuclear envelope and a defect in RNA export suggesting that nucleocytoplasmic transport is a major disease mechanism in this *Drosophila* model (Freibaum et al., 2015).

One *Drosophila* model caries a ~100 repeat sense or antisense RNA transgene, which was genetically modified to allow the accumulation of RNA foci but disable RAN translation, termed an RNA-only transgene. This model displayed the sequestration of RBP but not toxicity, suggesting that RNA foci on their own do not cause a toxic phenotype in *Drosophila* (Moens et al., 2018).

One study tested *Drosophila* carrying 3 or 36 G4C2 repeats, an RNA-only transgene, or PR_{36}. This study found that the axonal transport of mitochondria was downregulated in *Drosophila* carrying 36 G4C2 repeats *Drosophila* expressing PR_{36}. The axonal transport of vesicles was downregulated in *Drosophila* carrying 3 G4C2 repeats, 36 G4C2 repeats, or PR_{36}. The motor function of larvae and adults was only

reduced in *Drosophila* expressing PR_{36} (Baldwin et al., 2016). These results imply that axonal transport is a disease mechanism in *Drosophila* models of C9-ALS/FTD.

1.3.4.5 Induced pluripotent stem cells

Human iPSCs carrying the C9-HRE are useful disease models for human neuron cultures. iPSC-derived motor neurons, cortical neurons, and glial cells are commonly used. Depending on cell types, the molecular phenotypes induced by the C9-HRE differ. Additionally, changes in differentiation protocols can alter the disease phenotype. Particularly, the length of differentiation and use of growth factors affects molecular phenotypes. For example, a study conducted in iPSC-derived C9-MNs investigating synaptic transmission found that cells first display hyperexcitability followed by a gradual reduction in synaptic activity the longer cells are kept in culture (Devlin et al., 2015). Thus, a study using a 24-day motor neuron differentiation protocol identified hyperexcitability in C9-MNs (Wainger et al., 2014), while a study using a differentiation protocol of at least 39 days observed reduced excitability (Sareen et al., 2013). In this section, I will discuss the molecular phenotype commonly observed in iPSC-derived C9-MNs and C9-CNs.

Human iPSC-derived C9-MNs display RNA foci and DPR expression (Dafinca et al., 2016). Due to the low sensitivity of available anti-C9orf72 antibodies, it is difficult to determine C9orf72 haploinsufficiency in cell cultures. Apoptosis markers are present in C9-MNs, such as the upregulation of ClCasp3, the downregulation of anti-apoptotic proteins Bcl-2 and Bcl-X_L proteins, and the upregulation of the pro-apoptotic protein BAK. In addition, the survival of C9-MNs is reduced over time (Shi et al., 2018). Stress granule formation is increased in C9-MNs (Abo-Rady et al., 2020; Dafinca et al., 2016). Furthermore, C9-MNs display ER stress markers, such as the downregulation of ATF4, CHOP and PERK expression, upregulation of BiP expression, and increase in ER Ca^{2+} levels (Dafinca et al., 2016; Dr Paola Barbagallo, unpublished). While ER Ca^{2+} levels were upregulated, Ca^{2+} release through the IP_3 receptor was reduced in response to CCh stimulation, suggesting a defect in IP_3 signalling (Dafinca et al., 2021).

A further major disease mechanism is defective excitability. C9-MNs treated with glutamate lead to neurodegeneration (Cheng et al., 2019). At first, C9-MNs first display hyperexcitability, but the longer cells are kept in culture, the more reduced their excitability becomes (Devlin et al., 2015). On day 30, C9-MNs from my group stimulated with glutamate were hypoexcitable, whereas C9-MNs stimulated with KCl were hyperexcitable. The efficiency of cytosolic calcium clearance was reduced, as the downregulation of mitochondrial calcium uniporters lead to a reduction in mitochondrial calcium buffering (Dafinca et al., 2020). Using RNAseq of these cells, my group identified an increased expression of the AMPAR subunits GluA1, GluA2, and GluA3, the NMDA subunit GluN2A, and the metabotropic glutamate receptor subunits mGluR2 and mGluR4 in C9-MNs (Dafinca et al., 2020). The increase in the number of glutamate receptors has also been linked to C9orf72 haploinsufficiency-associated autophagy defects (Shi et al., 2018). p62 levels are increased in C9-MNs suggesting a reduction in autophagic flux (Dafinca et al., 2016). Moreover, C9-astrocytes in co-culture with MNs reduce the excitability of MNs (Zhao et al., 2020).

Additionally, mitochondrial dysfunction has been identified in C9-MNs. C9-MNs display mitochondrial depolarisation and a decrease in basal respiration and ATP production while showing no change in mitochondrial mass (Dr Ruxandra Dafinca, unpublished; Dr Paola Barbagallo, unpublished; Dafinca et al., 2016; Mehta et al., 2021). In addition, morphological changes were observed in the mitochondria of C9-MNs. Both enlarged mitochondria and cristae and increased mitochondrial fragmentation were identified (Dr Ruxandra Dafinca, unpublished; Dafinca et al., 2016). Moreover, some studies suggest mitochondrial transport impairments, specifically a reduced number of motile mitochondria along axons in C9-MNs (Mehta et al., 2021). Preliminary experiments in my research group using C9-MNs did not show any significant changes in the speed or direction of mitochondrial axonal transport (Dr Jakub Scaber, unpublished).

Therefore, in iPSC-derived C9-MNs, the C9-ALS/FTD phenotype consists of an increase in apoptosis, stress granule formation, ER stress, altered calcium signalling, changes in excitability including altered

post-synaptic glutamate channel expression and impaired calcium buffering, as well as aberrant mitochondrial function due to morphological changes, depolarisation and altered axonal transport.

Studies on the pathomechanism in iPSC-derived CNs are limited. In iPSC-derived CNs, DPRs and RNA foci are present (Almeida et al., 2013). iPSC-derived C9-CNs express apoptosis markers, such as upregulated ClCasp3 and cytosolic CytC levels (Dafinca et al., 2016). C9-CNs display elevated p62 levels and increased sensitivity to autophagy inhibitors in iPSC-derived CNs (Almeida et al., 2013; Dafinca et al., 2016). Furthermore, increased stress granule formation has been identified at base conditions (Dafinca et al., 2016). Recent evidence for disruptions in the interaction between IP3R and mitochondrial voltage-dependent anion channel (VDAC) has been identified in iPSC-derived CNs (Gomez-Suaga et al., 2022). In addition, one study identified the upregulation of transcripts encoding for the GluA2 and GluA4 but not GluA1 and GluA3 AMPAR subunits causing an imbalance between Ca^{2+}-permeable and impermeable AMPARs (Gascon et al., 2014). Therefore, the main mechanisms identified so far are increased apoptosis, stress granule formation, reduced autophagic flux, and the imbalance in post-synaptic glutamate receptor levels.

1.4 Aims of this thesis

Extensive characterisation of spinal motor neurons differentiated from iPSCs derived from ALS/FTD patients with the C9-HRE has demonstrated a range of reproducible molecular phenotypes of disease relevance. However, if these disease phenotypes are present in cortical neurons in the context of C9-FTD is much less understood. Moreover, little work has been done to determine whether cortical neurons can serve as a useful disease model for FTD or ALS/FTD.

This study aims at establishing a molecular phenotype caused by the *C9orf72* hexanucleotide expansion in ALS/FTD patient cortical neurons by:

i) Studying whether iPSC-derived cortical neurons in culture reflect FTD characteristics

ii) Characterising iPSC-derived cortical neurons for phenotypes associated with C9-HRE pathology

iii) Testing the hypothesis that C9-cortical neurons show a similar disease phenotype as iPSC-derived motor neurons, namely alterations in cellular stress and protein handling (autophagy), Ca^{2+} signalling and excitability, and bioenergetics

2 Methods

2.1 Cell culture

2.1.1 hiPSC lines

All cell lines used were derived from clinically well-characterised patients seen at the Oxford Motor Neuron Disorders Clinic and collected under ethical approval (South Wales Ethics Committee, Ref No. 12WA/0186). Cell lines were reprogrammed from fibroblasts by Dr Sally Cowley, James Martin Stem Cell Facility. The genetically corrected cell line, clones 59-2 and 59-3, was produced by Dr Nida'a Ababneh and is derived from the C9-02-02 cell line (Ababneh et al., 2020).

Table 2: The passage number of iPSC lines.

NAME	TECHNICAL NAME	PASSAGE NUMBER UPON THAWING	PASSAGE NUMBER AT THE END OF THE DIFFERENTIATION
WT-1	SFC180-01-01	27 or 29	+5
WT-2	SFC840-03-03	24, 25, or 31	+5
WT-3	SFC856-03-04	30	+5
ISO-2	59-2 or 59-3	46 or 48	+5
C9-1	OXC9-01-07 or OXC9-01-06	24 or 26	+5
C9-2	OXC9-02-02	31 or 48	+5
C9-8	SFC853-03-03	21 or 23	+5

2.1.2 hiPSC culture

iPSCs were grown on Geltrex-coated plates in mTeSR1 with antibiotic-antimycotic. Cells were passaged using 0.5 mM EDTA, centrifuged in PBS at 200*xg* for 5min, resuspended in mTeSR1 containing 10 μM Y-26732, and transferred to a Geltrex-coated plate. Y-26732 was removed after 24h. The medium was changed daily.

Cells were cryopreserved in 50% mTeSR with 10 µM Y-26732 and 50% freeze mix (60% ES grade serum, 20% DMSO, 20% KO-DMEM, 10 µM Y-26732) and transferred to -80 °C. After a few days, cells were transferred into liquid nitrogen.

2.1.3 Differentiation

iPS cells were differentiated into CNs following a previously published protocol (Shi et al., 2012). Briefly, cells were grown on Geltrex-coated plates as monolayers. For passaging, 10 µM Y-26732 was added to the medium for 24h. iPS cells were expanded, split once, and then again expanded in mTeSR until 100% confluent. The differentiation was induced by switching to the neural maintenance medium (0.5x DMEM/F12 GlutaMAX, 0.5x Neurobasal, 0.5x N2 supplement, 0.5x B27 supplement minus vitamin A, 2.5 µg/mL insulin, 50 µM NEAA, 50 µM 2-mercaptoethanol, antibiotic-antimycotic) supplemented with 1 µM dorsomorphin and 10 µM SB-431542 with daily medium changes. After 9 days, cells were split with Accutase 1:3. The next day, the medium was changed to the neural maintenance medium without supplements. When neural rosettes appeared, the medium was supplemented with 20 ng/mL FGF2 for 4 days. Afterwards, cells were split with Accutase 1:2 and the medium was changed every other day.

Once the neurons started growing dendrites (day 26-31), cells were split 1:6. Excess cells were cryopreserved in the neural maintenance medium supplemented with 10% (vol/vol) DMSO, 20 ng/mL FGF2, and 10 µM Y-26732 and stored in liquid nitrogen. Later, they were thawed, and their differentiation continued. Every 2-3 days, 2/3s of the medium was changed. Cells were differentiated for 55 days until fixation for immunocytochemistry or harvest of proteins for western blotting. Neurons were grown for 56-59 days for live imaging and functional assays.

Where applicable, cells were treated with 250 nM bafilomycin, 200 nM rapamycin, 1.5 µM thapsigargin, or 10 µM CCCP 24h before fixation or protein harvest (d54). Cells were treated with 0.5 mM sodium arsenite ($NaAsO_2$) for 1h before fixation or protein harvest. These compounds were added

to the treatment medium consisting of 0.5x DMEM/F12 GlutaMAX, 0.5x Neurobasal, 0.5x N2 supplement, and 0.5x B27 supplement minus vitamin A. Details of how these concentrations for treatments were established can be found in 0

Appendix 2: Optimising the concentration of treatments.

2.2 Basic methods

2.2.1 Immunofluorescence

During the last split of differentiation (day 26-31), cells were plated on Geltrex-coated coverslips. Mature CNs on day 55 were fixed using 4% PFA in 50% PBS/medium for 10 min. Cells were washed with PBS three times and then stored at 4°C.

Coverslips were incubated with 10% Normal Goat Serum (NGS) in 0.2% Triton/PBS for 1h at room temperature. Then, cells were incubated with primary antibodies (see Table 8, appendix 3) and 1% NGS in 0.1% Triton/PBS overnight at 4°C. All coverslips were counterstained with anti-Tuj1.

Coverslips were washed with 0.1% Triton/PBS three times for 10min. Then, cells were incubated with Alexa Fluor 488 or 568 or 647 conjugated secondary antibodies (see Table 8, appendix 3) in 1% NGS in 0.1% Triton/PBS for 1h at room temperature. Nuclei were stained with 4',6-Diamidino-2-Phenylindole (DAPI) for 10min. Coverslips were washed with 0.1% Triton/PBS three times for 10min.

Coverslips which were blinded to genotype were imaged using confocal microscopy. Three to five images were taken per coverslip with a magnification of 40x or 63x. For each coverslip, approx. 300-500 cells were analysed.

2.2.2 Western Blot

CNs in PBS were scraped off the bottom of wells and centrifuged at 4000 rpm for 3min at 4°C. The pellet was resuspended in RIPA buffer with protease and phosphatase inhibitors, sonicated, and

incubated for 30min on ice. Samples were centrifuged at 5000 rpm for 10min at 4°C. Protein concentrations of the supernatant were assessed using a BCA protein assay following the manufacturer's instructions. Samples were prepared at 1 µg/µL with LDS sample buffer, sample reducing agent, and PBS, and boiled at 95°C for 5min.

10 µg protein per sample was loaded onto a 4-12% bis-tris gradient gel. Electrophoresis was performed under the constant current of 125 mA for about 75min using MES as a running buffer and an XCell mini-cell electrophoresis system. An iBlot-2 gel transfer device was used for transferring proteins onto a PVDF membrane using 20 V for 7min.

Membranes were blocked with 5% skimmed milk powder in TBST (10% 10xTBS, 0.1% Tween20 in dH_2O) for 1h at room temperature, rocking. Then, they were incubated with primary antibodies (see Table 8, appendix 3) in 1% milk TBST overnight at 4°C, rocking. Membranes were washed with TBST three times for 10min each and incubated with secondary antibodies (see Table 8, appendix 3) in 1% milk in TBST for 1h at room temperature on a rocker. After washing membranes with TBST three times for 10min, membranes were incubated with Immobilon Western Chemiluminescent HRP substrate for 3min, then imaged using a ChemiDoc MP Imaging System.

Membranes were washed with TBST and stripped using Restore PLUS Western Blot Stripping Buffer and washed three times with TBST for 5min. Membranes were re-blocked, incubated with primary and secondary antibodies, and imaged as described above.

2.2.3 Calcium imaging

Calcium transients in iPSC-derived CNs were measured using the fluorescent probe Fluo 4-AM. Neurons were incubated with 20 µM Fluo 4-AM in Hank's Balanced Salts Solution (HBSS) with Ca^{2+} and Mg^{2+} supplemented with Hepes for 45min at 37°C. Cells were washed twice with HBSS with Ca^{2+} and Mg^{2+}. The Fluo 4-AM intensity was recorded by fluorescence microscopy with an excitation of 488 nm at room temperature.

For glutamate and KCl stimulation, cells were perfused with HBSS with Ca^{2+} and Mg^{2+} for 30sec, then with either 0.2 mM glutamate or 50 mM KCl in HBSS with Ca^{2+} and Mg^{2+} for 30sec. The stimulant was washed out for 90sec with HBSS with Ca^{2+} and Mg^{2+}.

For CCh stimulation, cells were perfused with HBSS depleted of Ca^{2+} and Mg^{2+} for 30sec, then with 0.1 mM CCh in HBSS without Ca^{2+} and Mg^{2+} for 30sec. The stimulant was washed out for 2min with HBSS without Ca^{2+} and Mg^{2+}.

The Fluo 4-AM traces of single cells were analysed. Fluorescence measurements are expressed as a ratio ($\Delta F/F_0$) of the change in fluorescence (ΔF) of a cell relative to the resting fluorescence of the cell before stimulation (F_0). The latency was calculated by measuring the time between the addition of the stimulant and the time of maximum Fluo 4-AM intensity. The clearance time was calculated by measuring the time between maximum Fluo 4-AM intensity and recovery to baseline Fluo 4-AM intensity.

2.3 Characterising iPSC-derived cortical neurons

Fixed coverslips were stained for the protein(s) of interest, with anti-Tuj1 and DAPI (for antibodies see Table 8, appendix 3) and imaged as described in 2.2.1. The protein markers were analysed as follows:

- To study the number of neurons, the number of Tuj1-positive cells versus the number of nuclei stained with DAPI was counted manually.
- To study the glutamatergic identity of neurons, the signal of the VGluT1 staining was measured within the Tuj1-positive area of the image and normalised to the area. (*)
- To study the number of astrocytes, the number of GFAP-positive cells versus the number of DAPI-positive cells was counted manually. To ensure objectivity, a threshold for GFAP-positivity was set.

- To study cortical identity using Tbr1, the signal of the Tbr1 staining was measured within the Tuj1-positive area of the image and normalised to the area. Additionally, the number of Tbr1-positive cells was counted manually at the time point of the maximum Tbr1 signal for each cell line.

- To study cortical identity using CTIP1 and CTIP2, the number of CTIP1- or CTIP2-positive cells versus the number of nuclei stained with DAPI was counted manually.

- To study apoptosis using ClCasp3, the number of ClCasp3- and Tuj1-positive cells versus the number of ClCasp3-negative and Tuj1-positive cells was counted manually.

- To study apoptosis using CytC localisation, the CytC signal was measured within the TOMM20-positive area within the Tuj1-positive area. For this experiment, both untreated cells and cells treated with 0.5 mM $NaAsO_2$ for 1h before fixation were tested. (*)

- To study TDP-43 localisation, the signal of TDP-43 was measured within the DAPI-positive area and within the DAPI-negative, Tuj1-positive area. (*)

Additionally, Western blots were performed staining for Bcl-2, ClCasp3, CytC, TDP-43 and actin or GAPDH and imaged as described in 2.2.2. Where applicable, cells were treated with stressors as described in 2.1.3. The signal of the relevant protein band was measured using ImageJ.

For Western blots and all immunostaining experiments marked with (*), the measurements for each cell line of each differentiation were normalised to the measurement of the untreated WT-1 line unless the differentiation of the WT-1 line failed for a specific differentiation, in which case all measurements were normalised to the untreated WT-2 line. Where applicable, statistical analysis was performed as described in 2.7.

2.4 Analysis of protein-associated cellular stress

To study the number of stress granules, fixed coverslips were stained with anti-PABP, anti-Tuj1, and DAPI (for antibodies see Table 8, appendix 3) and imaged as described in 2.2.1. For each image, 10 to 15 cells with strong Tuj1 signals were chosen. The number of PABP-positive granules per neuron was counted manually within the cell soma and the beginning of the dendrites. Additionally, Western blots were performed staining for BiP, CHOP, ATF4, p62, LC3B, LAMP2A and actin or GAPDH and imaged as described in 2.2.2. Where applicable, cells were treated with stressors as described in 2.1.3. The signal of the relevant protein band was measured using ImageJ. For all markers but ATF4 and LC3B, the measurements for each cell line of each differentiation were normalised to the measurement of the untreated WT-1 line unless the differentiation of the WT-1 line failed for a specific differentiation, in which case all measurements were normalised to the untreated WT-2 line. For ATF4, measurements were normalised to thapsigargin-treated WT-1 or WT-2, or to $NaAsO_2$-treated WT-1. For LC3B, the intensity of the lower LC3BII band was divided by the intensity of the higher LC3BI band for each sample. Furthermore, calcium imaging of cells stimulated with CCh was performed and analysed as described in 2.2.3. Where applicable, statistical analysis was performed as described in 2.7.

2.5 Analysis of excitability

Western blots were performed staining for GluN1, GluA1, CACNA2D1, MCU, and actin or GAPDH and imaged as described in 2.2.2. Where applicable, cells were treated with stressors as described in 2.1.3. The signal of the relevant protein band was measured using ImageJ. Additionally, to study the expression levels of PSD95, fixed coverslips were stained with anti-PSD95, anti-Tuj1, and DAPI (for antibodies see Table 8, appendix 3) and imaged as described in 2.2.1. The signal of the PSD95 staining was measured within the Tuj1-positive area of the image and normalised to the area. For Western blots and all immunostaining experiments, the measurements for each cell line of each differentiation were normalised to the measurement of the untreated WT-1 line unless the differentiation of the WT-1 line failed for a specific differentiation, in which case all measurements were normalised to the

untreated WT-2 line. Furthermore, calcium imaging of cells stimulated with glutamate and KCl was performed and analysed as described in 2.2.3. Where applicable, statistical analysis was performed as described in 2.7.

2.6 Analysis of mitochondrial function

2.6.1 Measuring mitochondrial protein levels

Western blots were performed staining for TOMM20, COX IV, P-DRP1, Mfn2, PINK1, P-Ub, DCTN1, KIF5a, and actin or GAPDH and imaged as described in 2.2.2. Where applicable, cells were treated with stressors as described in 2.1.3. The signal of the relevant protein band was measured using ImageJ.

Additionally, immunofluorescence experiments with coverslips stained with anti-TOMM20, anti-Tuj1, and DAPI (for antibodies see Table 8, appendix 3) and imaged as described in 2.2.1. The signal of the TOMM20 staining was measured within the Tuj1-positive area of the image and normalised to the area. For Western blots and all immunostaining experiments, the measurements for each cell line of each differentiation were normalised to the measurement of the untreated WT-1 line unless the differentiation of the WT-1 line failed for a specific differentiation, in which case all measurements were normalised to the untreated WT-2 line. Where applicable, statistical analysis was performed as described in 2.7.

2.6.2 Measuring mitochondrial depolarisation

Day 55 cells were treated with 0.5 mM $NaAsO_2$ for 1h or kept untreated. Then cells were incubated with 100 nM MitoTracker™ Red CMXRos (Invitrogen) for 45min. Cells were washed with PBS, then fixed and stained with anti-TOMM20 and anti-Tuj1 as described in section 2.2.1. Stained cells were imaged using confocal microscopy within one week. The intensity of MitoTracker was measured within the Tuj1-positive area and divided by TOMM20 intensity to normalise the mitochondrial mass. The measurements for each cell line of each differentiation were normalised to the measurement of the

untreated WT-1 line unless the differentiation of the WT-1 line failed for a specific differentiation, in which case all measurements were normalised to the untreated WT-2 line. Statistical analysis was performed as described in 2.7.

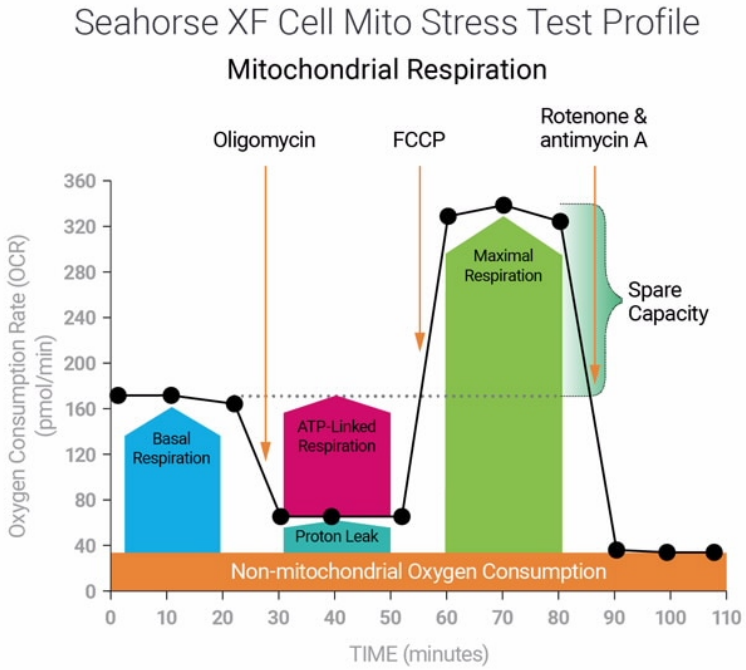
2.6.3 Measuring axonal transport

During the last split of the cortical neuron differentiation on around day 29, cells were plated onto one side of microfluidic chambers. The next day, 10 ng/mL BDNF and 10 ng/mL GDNF were added to the cell-free side of the microfluidic chambers. Cells were differentiated in microfluidic chambers for 2 weeks to allow axons to grow through the microchannels. The day before imaging, BDNF and GDNF were removed from the medium. On day 43, cells were incubated with 100 nM MitoTracker™ Green FM (Invitrogen) in a live imaging solution for 30min. Cells were washed with a live imaging solution. Mitochondrial axonal trafficking was imaged using a spinning disc confocal microscope recording for 5min. For each microfluidic chamber, three different areas were recorded. Then, neurons were stimulated with a 1mM glutamate solution and axonal transport was recorded again for 5min in three different areas. For analysis, the number of stationary and motile mitochondria was counted for each recording and the percentage of motile mitochondria was calculated. In addition, the overall direction of motile mitochondria was analysed.

2.6.4 Seahorse XF Cell Mito Stress Test

During the last split of the differentiation, cells were plated onto 96-well plates. On days 56-58, cells were used to measure mitochondrial respiration. Cells were treated with 10 μM CCCP for 24h, 0.5 mM $NaAsO_2$ for 1h, or remained untreated. The differentiation efficiency in 96-well plates was lower than in other cell culture formats. Therefore, wells which had been overtaken by undifferentiated cells as seen through light microscopy were excluded. The Seahorse XF Cell Mito Stress Test (Agilent) was carried out according to the manufacturer's instructions using 2.5 μM oligomycin, 1 μM carbonyl cyanide-p-trifluoromethoxyphenylhydrazone (FCCP), and 0.5 μM Rotenone/Antimycin A. After

performing the Seahorse XF Cell Mito Stress Test, cells were stored at -80°C. Then, the CyQUANT Cell Proliferation Assay (Invitrogen) was performed to analyse the number of cells in each well. Seahorse XF Cell Mito Stress Test measurements were normalised to the CyQUANT Cell Proliferation Assay measurements and multiplied by 30,000. Then, the mean normalised oxygen consumption rate of three wells was taken. The non-mitochondrial O_2 consumption, basal respiration, maximum respiration, H^+ leak, ATP production, and spare respiratory capacity were calculated as depicted in Figure 13. Statistical analysis was performed as described in 2.7.



Parameter Value	Equation
Non-mitochondrial Oxygen Consumption	Minimum rate measurement after Rotenone/antimycin A injection
Basal Respiration	(Last rate measurement before first injection) – (Non-Mitochondrial Respiration Rate)
Maximal Respiration	(Maximum rate measurement after FCCP injection) – (Non-Mitochondrial Respiration)
H+ (Proton) Leak	(Minimum rate measurement after Oligomycin injection) – (Non-Mitochondrial Respiration
ATP Production	(Last rate measurement before Oligomycin injection) – (Minimum rate measurement after Oligomycin injection)
Spare Respiratory Capacity	(Maximal Respiration) – (Basal Respiration)
Spare Respiratory Capacity as a %	(Maximal Respiration) / (Basal Respiration) × 100
Acute Response	(Last rate measurement before oligomycin Injection) – (Last rate measurement before acute injection)
Coupling Efficiency	ATP Production Rate) / (Basal Respiration Rate) × 100

Figure 13: How parameters were derived from oxygen consumption rates measured using the Seahorse XF Cell Mito Stress Test. This image was taken from Agilent Technologies (2019).

2.6.5 ROS assay

During the last split of the differentiation, cells were plated onto 96-well plates. On days 56-58, cells were used to measure oxidative stress. Cells were treated with 10 μM CCCP for 24h, 0.5 mM $NaAsO_2$ for 1h, or remained untreated. The Cellular ROS Assay (Red) (abcam) was performed according to the manufacturer's instructions. Then, cells were stored at -80°C before the CyQUANT Cell Proliferation Assay (Invitrogen) was performed to analyse the number of cells in each well. Cellular ROS Assay results were normalised to the CyQUANT Cell Proliferation Assay measurements. Then, the mean normalised ROS Red intensity was taken from three wells and normalised to the measurement of the untreated WT-1 line. Statistical analysis was performed as described in 2.7.

2.7 Statistical analysis

Statistical analysis was carried out using GraphPad Prism 8. For each data set, I checked for outliers using the GraphPad Prism Identify Outliers function. Outliers were removed from data sets before statistical analysis.

For the analysis of the differentiation efficiency, all cell lines were compared to each other with a one-way ANOVA using Dunnett's *post-hoc* test. For all other experiments, the measurements of the WT-1, WT-2, and WT-3 cell lines were pooled and portrayed as one sample (WT), while the C9-1 and C9-8 cell lines were pooled and portrayed as one (C9-1+8). Then, pooled WT controls were compared to pooled C9-1+8 patient lines, and ISO-2 was compared to C9-2 using a one-way ANOVA with Sidak's *post-hoc* test. P-values < 0.05 were treated as significant.

Additionally, all experiments using several culture conditions, e.g. untreated and treatments, these cell culture conditions were compared using a two-way ANOVA using Dunnett's *post-hoc* test. P-values < 0.05 were treated as significant. If there were significant differences between conditions, they were included in the results figures. If the results figures do not display a comparison between conditions, no significant differences were identified.

3 *C9orf72* patient-derived induced pluripotent stem cells are differentiated into layer V/VI cortical neurons with features of C9-ALS/FTD pathology

In this study, C9-ALS/FTD patient-derived cortical neurons were used as a disease model. To this end, iPSCs derived from fibroblasts obtained from C9-ALS/FTD patients and neurologically healthy individuals were differentiated into mid-layer CNs according to a protocol developed by Shi et al. (2012) with some modifications and harvested on day 55 (Figure 14).

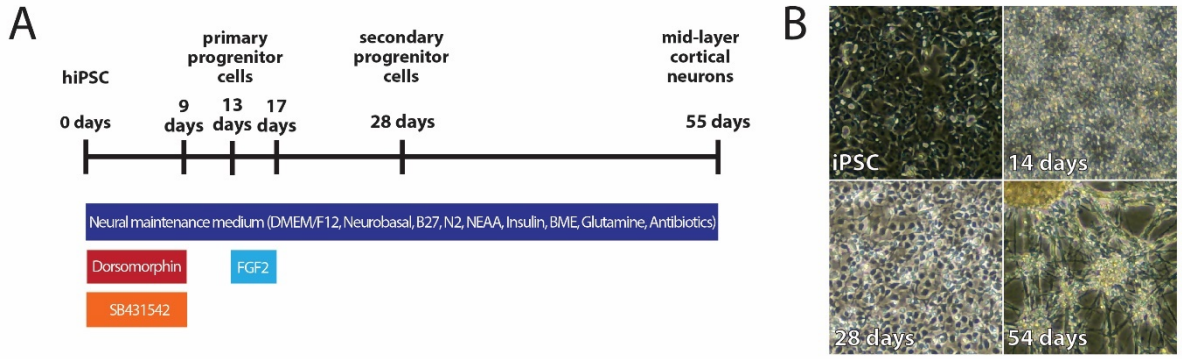


Figure 14: The differentiation of iPSCs to cortical neurons. (A) Schematic presentation of the cortical differentiation protocol after Shi et al. (2012) with modifications. (B) representative light microscopy images of cells at different stages of the differentiation.

In line with corticogenesis *in vivo*, cortical neuron cultures differentiated from iPSCs go through different stages of cortical layer identity during maturation. First, cells carry deep-layer cortical neuron markers. Then at a later timepoint, cells are positive for mid-layer markers such as the transcription factor Tbr1 expressed by layer VI neurons and the transcription repressors CTIP1 and CTIP2 expressed by layer V, until they resemble upper layer neurons expressing markers such as Brn1/2 (see Figure 15) (Mukhtar & Taylor, 2018). Hence, the length of CN differentiation determines the type of cortical neuron identity the iPSC-derived CNs will resemble.

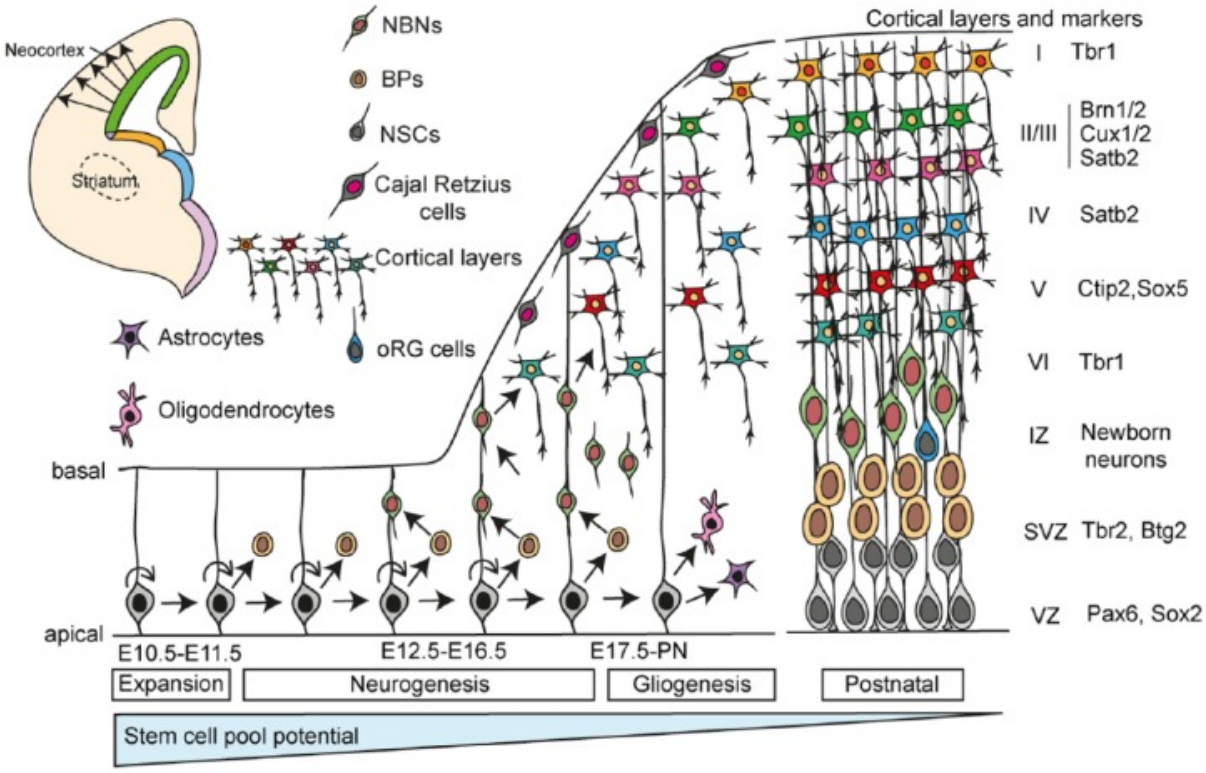


Figure 15: Scheme illustrating the development and organisation of the cerebral cortex. During neurogenesis, neural stem cells first form neurons of lower cortical layers, then mid-layer CNs, then upper-layer CNs. Each cell layer expresses specific proteins, mostly transcription factors, which can be used to characterise CNs. BPs=basal progenitors, IZ=intermediate zone, NBNs=newborn neurons, NSCs=neural stem cells, SVZ=subventricular zone, VZ=ventricular zone. This figure was taken from **Mukhtar & Taylor (2018).**

In previous studies using C9-ALS/FTD iPSC-derived CNs, little work has been previously done to characterise these iPSC-derived CNs in detail, such as which cortical layer they equate to (Almeida et al., 2013; Dafinca et al., 2016; Freibaum et al., 2015). Therefore, I carried out a detailed characterisation of cell types in iPSC-derived cortical neuron cultures. In FTD, cell death is most significant in upper cortical layers (II+III) and layer V neurons in frontal regions (Kersaitis et al., 2004; E. J. Kim et al., 2012; Santillo & Englund, 2014). While layers II and III are affected in early disease stages, cell death in layer V is commonly observed in late disease stages (Kersaitis et al., 2004). However, due to technical challenges and time limitations, I was unable to mature iPSC-derived CNs past layer V. Therefore, I decided to differentiate iPSC for 55 days, aiming to enrich for layer V CNs even though iPSC-derived CNs represent an early disease stage.

In order to assess whether these cortical neuron cultures show signs of neurodegeneration, I tested iPSC-derived C9-CNs for cell death through apoptosis as observed in iPSC-derived C9-motor neurons. In addition, I measured TDP-43 pathology as observed in up to 97% of ALS cases and about 45-50% of FTD cases (Arai et al., 2006; Bodansky et al., 2010; Neumann et al., 2006; Nguyen et al., 2018).

Thus, to gain an understanding of my cell cultures in comparison to similar cell cultures used in previous studies, I characterised iPSC-derived CN cultures in detail by analysing:

1. The proportion of neuronal cells
2. The glutamatergic identity of cells
3. The cortical identity of neurons
4. Which cortex layer the CNs are equivalent to

Additionally, I studied the neurodegenerative phenotype of iPSC-derived CN cultures by measuring:

1. Changes in apoptosis in C9-CNs
2. TDP-43 mislocalisation in C9-CNs

In this study, I used seven different iPSC lines. Most experiments were conducted without the WT-3 cell line, as I first tried using different control lines. However, their differentiation repeatedly failed, possibly due to aberrant pluripotency. I only managed to successfully differentiate the WT-3 towards the end of my experimental time. The demographics of the cell lines used are displayed in Table 3 below. The gender of all control line donors is female, as the differentiation of male control lines failed, as described above.

For the statistical analysis of the differentiation efficiency, I compared each cell line with each other cell line. For the statistical analysis of phenotypes, I compared the C9-2 line to its isogenic control ISO-2. As there were no isogenic control lines available for the C9-1 and C9-8 patient lines, I pooled the

measurements of the C9-1 and C9-8 cell line and compared them to the measurements of wild-type controls (WT-1, WT-2, WT-3) to improve the reproducibility and validity of any significant effects (see 2.7 Statistical analysis).

My group identified major chromosomal aberrations in some patient lines and the ISO-2 cell line during routine quality control at the end of my experimental time, which might have impacted the phenotype of this cell line throughout this study. Details on these chromosomal defects can be found in 9.1 Appendix 1: Chromosomal aberrations in iPSCs. Therefore, measurements from these cell lines were not included in the pooled controls and C9-ALS/FTD patient lines.

Table 3: Demographics of iPSC lines used in this study.

NAME	TECHNICAL NAME	CATEGORY	DISEASE	MUTATION	GENDER	AGE
WT-1	SFC180-01-01	Healthy control	NA	NA	Female	60
WT-2	SFC840-03-03	Healthy control	NA	NA	Female	67
WT-3	SFC856-03-04	Healthy control	NA	NA	Female	78
ISO-2	59-2 or 59-3	Isogenic control	NA	Isogenic control derived from C9-2 line	Female	62
C9-1	OXC9-01-07 or OXC9-01-06	patient line	C9-ALS/FTD	C9-HRE (~970 G_4C_2 repeats)	Male	72
C9-2	OXC9-02-02	patient line	C9-ALS/FTD	C9-HRE (~1000 G_4C_2 repeats)	Female	62
C9-8	SFC853-03-03	patient line	C9-FTD	C9-HRE (unknown)	Female	58

3.1 iPSC-derived cultures are neuronal and glutamatergic on day 55

To establish the neuronal identity of iPSC-derived cultures at day 55 of cortical differentiation, I used immunostaining with the neuron-specific antibody anti-βIII-tubulin (Tuj1). Tuj1 is expressed in all

neurons and forms part of the cytoskeleton, hence staining the cell body and dendrites (Katsetos et al., 2003). Immunostaining with anti-Tuj1 showed a percentage of neuronal cells in the cultures above 88% for all cell lines apart from the isogenic line ISO-2 (see Figure 16A). Thus, a high yield of neuronal cells was achieved using the cortical differentiation protocol, but a low amount of non-neuronal cells was present in all cell lines.

To measure whether there were differences in glutamatergic identity between cell lines, I stained cells for anti-vesicular glutamate transporter 1 (vGluT1). The expression of this synaptic protein is specific to glutamatergic neurons in the cortex, hippocampus, and cerebellar cortex, making it a marker for glutamatergic identity in these brain regions (E. Herzog et al., 2001; Kaneko & Fujiyama, 2002; Takamori et al., 2000). I observed no significant difference in glutamatergic identity between cell lines (Figure 16B). Thus, all cell lines differentiate into glutamatergic neurons to a similar extent.

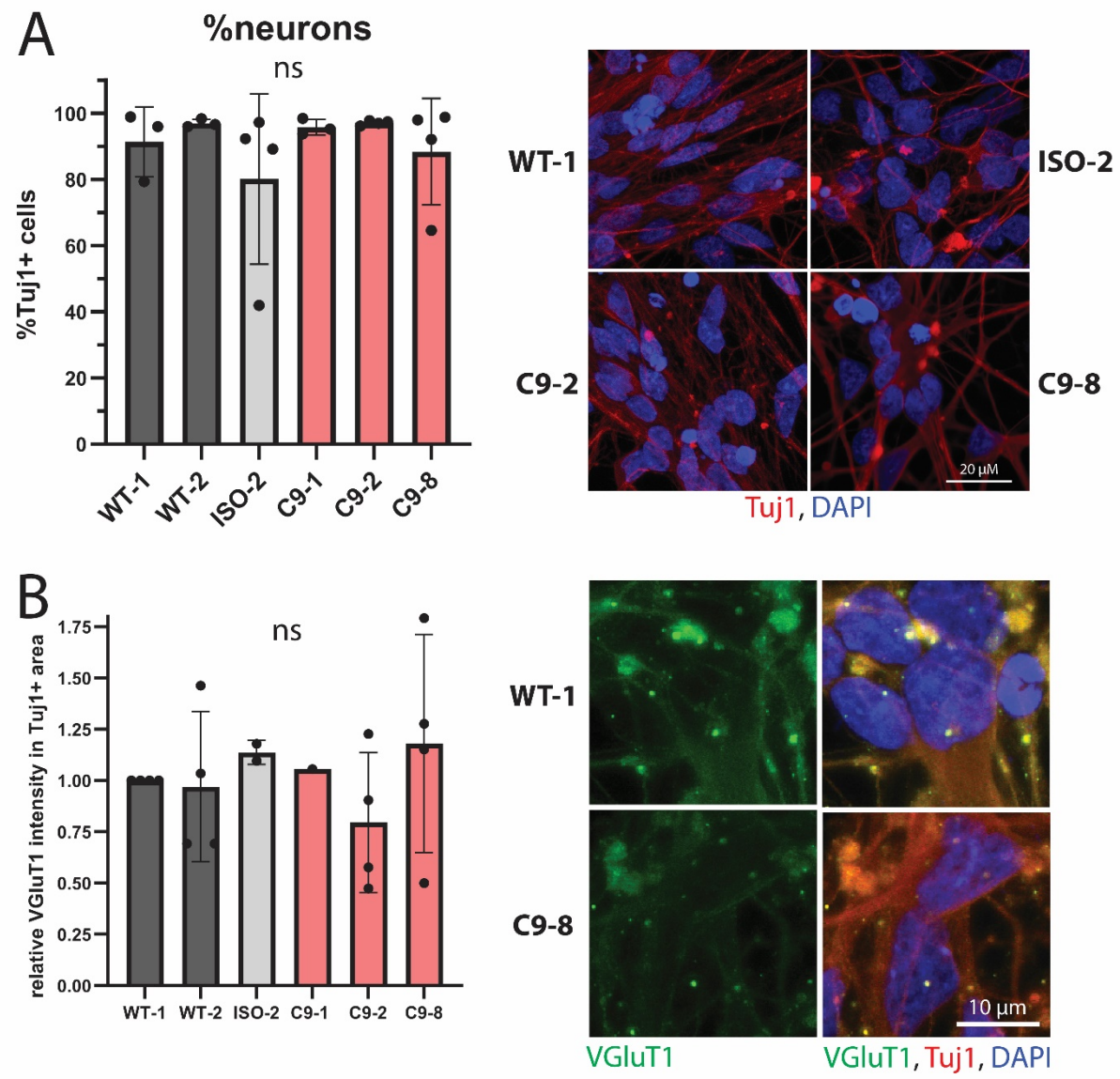


Figure 16: iPSCs differentiate into neuronal cultures with a high percentage of neurons and glutamatergic identity. (A) The percentage of neurons in differentiated cultures is >95% in WT-2, C9-1, and C9-2, with some differences in purity in differentiations in the WT01, ISO-2, and C9-8 cell lines. (B) The glutamatergic identity of neuronal cultures does not significantly differ between cell lines. (A-B) Right: Representative confocal image of cells stained for (A) Tuj1 (red) and DNA (blue), or (B) VGluT2 (green), Tuj1 (red), and DNA (blue). (A-B) Left: Each dot represents the measured protein level from one differentiation. Data were analysed with one-way ANOVA using Dunnett's *post-hoc* test.

Since the differentiation protocol for astrocytes shares similarities with cortical neuron protocols, such as dual SMADD inhibition, I also studied the number of astrocytes in these neuronal cultures. To this end, I stained the cultures for glial fibrillary acidic protein (GFAP), an intermediate filament protein selectively expressed in glial cells (Z. Yang & Wang, 2015).

I found that the percentage of glial cells in these cell cultures is low, apart from the isogenic cell line. ISO-2 cells from differentiations with low neuronal yield had a particularly high percentage of GFAP-positive cells (Figure 17).

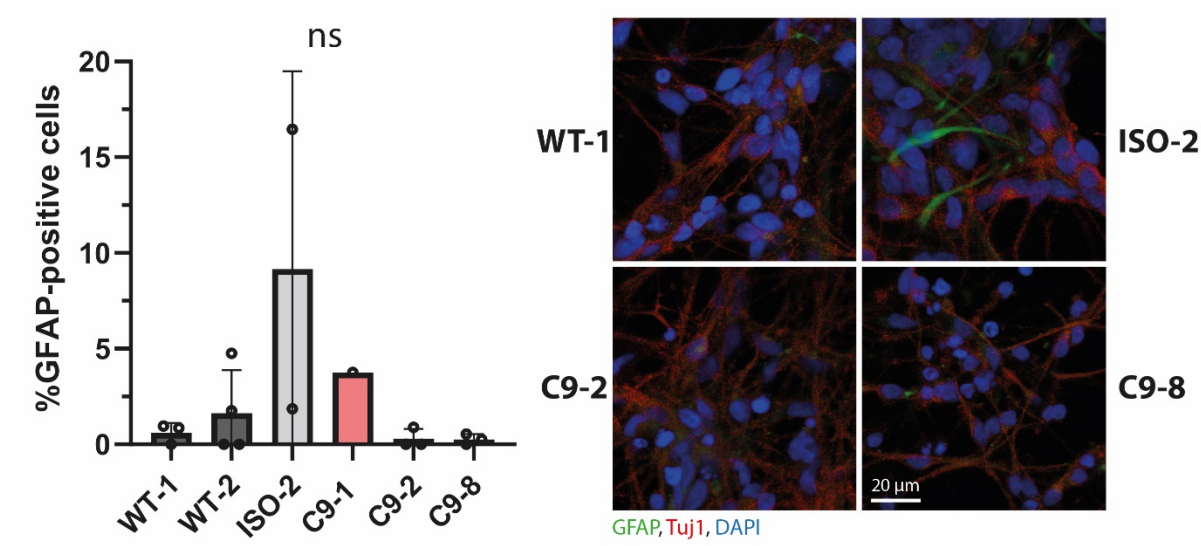


Figure 17: Neuronal cultures from all cell lines except the ISO-2 line contain a low number of GFAP-positive glial cells. Left: Each dot represents the measured protein level from one differentiation. Right: Representative image of cells stained for GFAP (green), Tuj1 (red), and DNA (blue). Data were analysed with one-way ANOVA using Dunnett's *post-hoc* test.

In summary, the percentage of neurons is very high in differentiated cultures at day 55 apart from the isogenic control line which varies in quality between differentiations. Similarly, the number of astrocytes in these cultures is very low apart from one differentiation of the isogenic cell line.

3.2 A high proportion of cells in iPSC-derived cultures show properties of layer V/VI cortical neurons

I stained differentiating cells at multiple time points with cortical layer markers T-box brain 1 (Tbr1; layer VI), B-cell lymphoma/leukaemia 11A (CTIP1; layer V), and B-cell lymphoma/leukaemia 11B (CTIP2; layer V) to track the differentiation progress, establish which cortical layer my differentiated cells equate to, and gain insight into the efficiency of the cortical differentiation.

Preliminary data shows that Tbr1 expression peaked between day 50 and day 55 of the cortical neuron differentiation in WT-1 and WT-2. For C9-2, Tbr1 expression is constant from day 40 to day 55 but drops off towards day 60. The expression of Tbr1 in C9-8 peaks at day 40 and then drops off, suggesting that this cell line might be more mature at day 55 than the other cell lines.

To analyse the maximum percentage of cells expressing Tbr1, I counted the number of Tbr1 cells on the day of maximum Tbr1 intensity for each cell line (see Figure 18). Tbr1 expression was highest on day 50 for WT-1, day 55 for WT-2, and day 40 for C9-2 and C9-8. The maximum percentage of cells expressing the cortical neuron marker is between 94.6% and 98.6%.

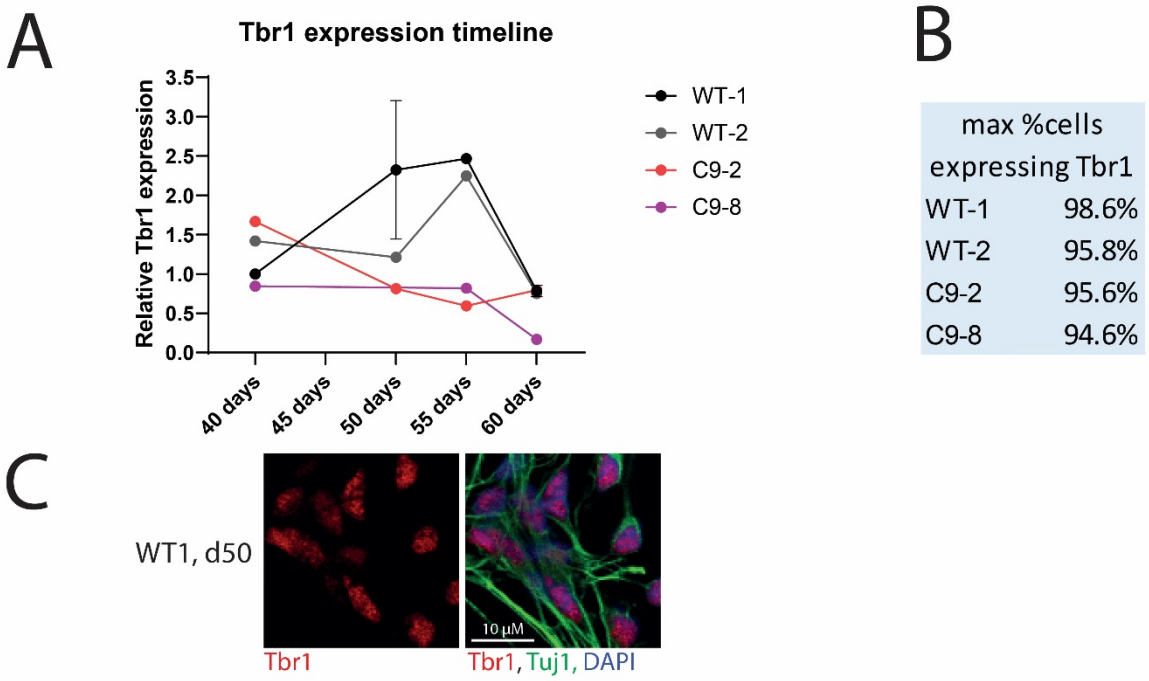


Figure 18: The percentage of differentiated cells expressing the cortical neuron marker Tbr1 is above 94% for all cell lines. (A) Expression of Tbr1 normalised to the Tbr1 levels of WT-1 at day 40. Tbr1 levels were measured on day 40, day 50, day 55, and day 60 of differentiation. Number of differentiations (n) used here: n(WT-1)=2 for day 40, 50, and 60, n(WT-1)=1 for day 55, n(WT-2)=1, n(C9-2)=1, n(C9-8)=1. error bars represent the standard deviation. (B) The percentage of cells expressing Tbr1 on the day of maximum expression levels. (C) Representative confocal image of cells stained for Tbr1 (red), Tuj1 (green), and DNA (blue). The WT-1 cell line is depicted on day 50.

The transcription factor CTIP1 regulates neocortical development by controlling projection neuron subtype identity. CTIP1 is expressed by postmitotic callosal and corticothalamic projection neurons. In the motor cortex, CTIP1 expression is limited to layer V neurons, while in the somatosensory cortex in mice, CTIP1 is expressed in all layers (Woodworth et al., 2016). CTIP2 shares approx. 60% sequence identity with CTIP1 (Woodworth et al., 2016). CTIP2 is expressed in subcerebral projection neurons and controls their connectivity in layer V neurons (Alcamo et al., 2008).

In these cultures, the maximum percentage of cells expressing CTIP1 was between 69.2% (ISO-2) and 90.5% (C9-01), whereas the maximum percentage of cells expressing CTIP2 was between 66.4% (C9-02) and 95.0% (C9-01) (see Figure 19). These findings suggest that most neuronal cells in culture express cortical neuron markers, with the C9-01 cell line being the purest cell culture and ISO-2 and C9-02 the cell lines with the most non-cortical cells.

CTIP1 and CTIP2 expression peaked between day 50 and day 55 in most cell lines, with a downward trend between day 55 and day 60. On day 55, CNs comprise both layer V and layer VI neurons. Due to the high percentage of Tbr1, CTIP1, and CTIP2 expressing cells, some cells probably express layer VI markers alongside layer V markers. Therefore, it is not possible to determine whether day 55 neuronal cultures contain more layer V or layer VI neurons.

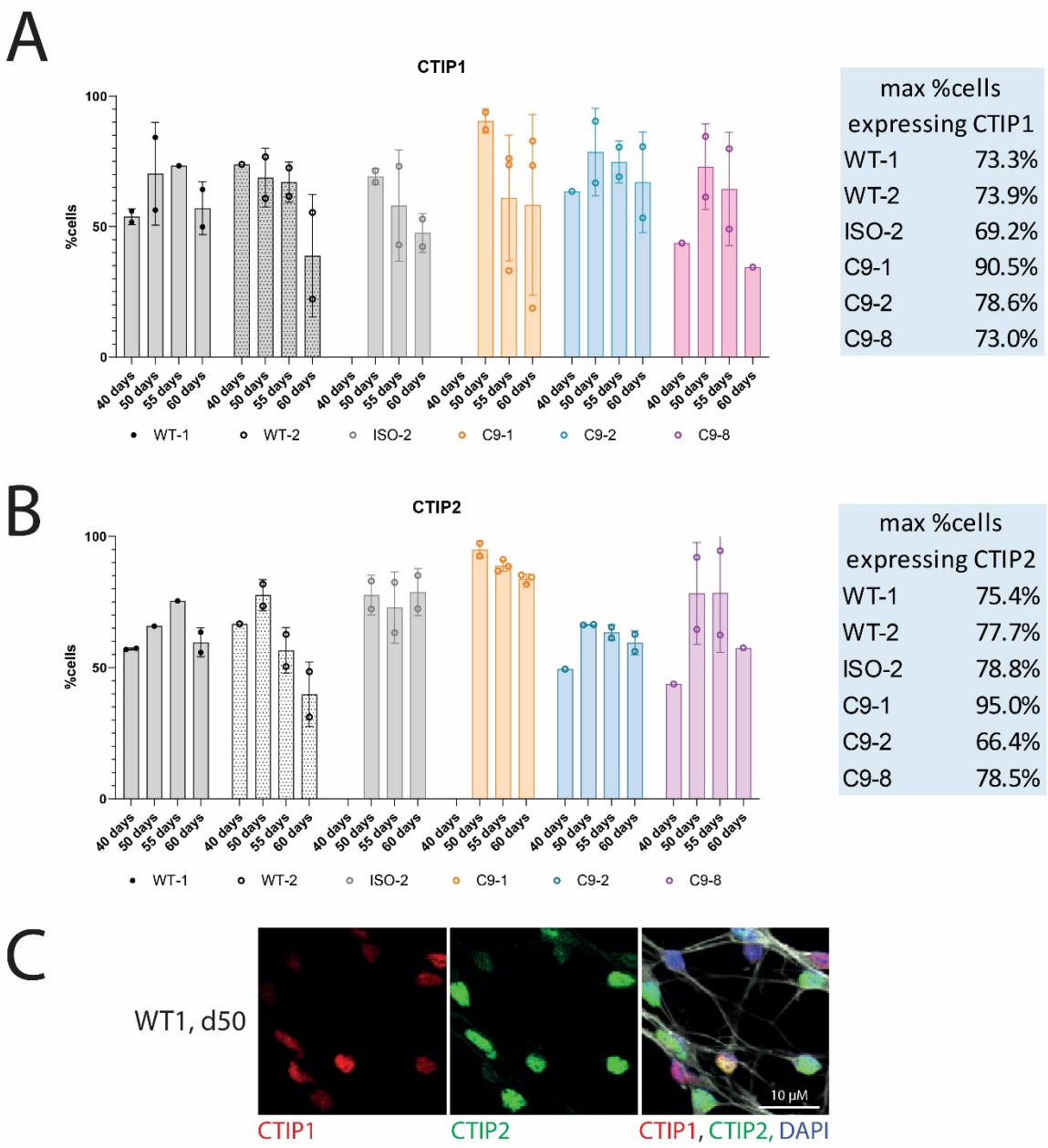


Figure 19: The percentage of differentiated cells expressing the cortical neuron marker CTIP1 and CTIP2 is above 69.2% and 66.4%, respectively. (A) The percentage of cells expressing CTIP1 was measured on day 40, day 50, day 55, and day 60 of differentiation. (B) The percentage of cells expressing CTIP2 was measured on day 40, day 50, day 55, and day 60 of differentiation. (A-B) The bars represent means. Error bars represent the standard deviation. Each dot represents the measured protein level from one differentiation. (C) Representative confocal image of cells stained for CTIP1 (red), CTIP2 (green), Tuj1 (white), and DNA (blue). The WT-1 cell line is depicted at day 50.

In summary, a high percentage of cells in differentiation cultures express the cortical neuron markers Tbr1, CTIP1, and CTIP2. On day 55, cultures display the expression profile of layer V/VI cortical neurons.

3.3 C9-ALS/FTD cortical neurons show an increase in apoptosis

I studied the expression of apoptotic markers to establish whether there is a difference in apoptosis between control lines and patient lines in these iPSC-derived CNs. To this end, I assessed the expression of the anti-apoptotic protein Bcl-2, the localisation of CytC, and the levels of ClCasp3 on day 55 CNs.

I conducted these experiments in both untreated neurons and neurons treated with 0.5 mM $NaAsO_2$ for 1h, or with 10 μM carbonyl cyanide *m*-chlorophenyl hydrazone (CCCP) for 24h, or with 1.5 μM thapsigargin for 24h. $NaAsO_2$ is an ATP synthase inhibitor that induces ATP depletion, leading to ER stress, mitochondrial dysfunction, and apoptosis (C. Chen et al., 2017; Yih et al., 1991). CCCP decouples the mitochondrial proton gradient, thus inhibiting oxidative phosphorylation (Demine et al., 2019). Thapsigargin is a small molecule which inhibits the sarco/endoplasmic reticulum Ca^{2+}-ATPase (SERCA), a Ca^{2+} pump located in the ER membrane that transports free Ca^{2+} ions from the cytosol into the ER, causing ER stress. This disruption of the homeostasis of the ER causes apoptotic stimuli to trigger mitochondrial membrane permeabilisation by BCL-2 family proteins. Therefore, these cellular stressors might exaggerate inherent cellular stress and reveal differential vulnerability to apoptotic stimuli.

I found the anti-apoptotic protein Bcl-2 to be significantly downregulated in the pooled C9-1+8 lines compared to WT controls, both without treatment and when treated with $NaAsO_2$ for 1h (Figure 20). This downregulation of the anti-apoptotic protein Bcl-2 implies an imbalance in anti- and pro-apoptotic proteins which causes increased apoptosis in C9-CNs. In CNs treated with CCCP, I did not

find a significant downregulation of Bcl-2 in patient lines, but rather a non-significant increase in Bcl-2 levels.

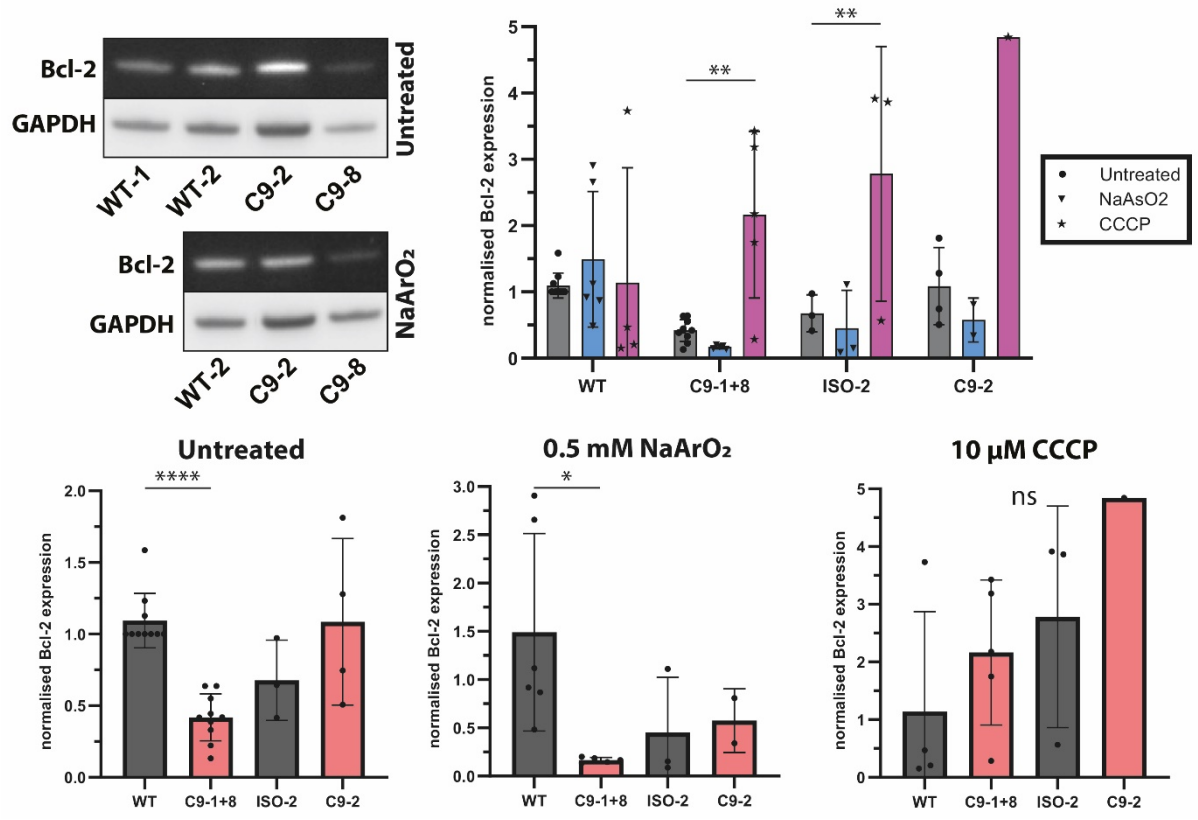


Figure 20: The expression of the anti-apoptotic protein Bcl-2 is significantly reduced in pooled C9-CNs. Western blot of Bcl-2 using untreated CNs and CNs treated with 0.5 mM $NaArO_2$ for 1h or with 10 µM CCCP for 24h. When comparing treatments, data were analysed with two-way ANOVA using Dunnett's *post-hoc* test. All other data were analysed with one-way ANOVA using Sidak's *post-hoc* test. The bars represent means. Error bars represent the standard deviation. Each dot represents the measured protein level from one differentiation. ns=not significant, *p<0.05, **p<0.01.

To investigate apoptosis further, I measured ClCasp3 levels in iPSC-derived CNs. First, I determined the number of ClCasp3-positive cells using immunofluorescence (Figure 21A). This method indicates an upregulation of ClCasp3 in C9-CNs. Due to the low number of replicates in this experiment, this upregulation was not significant. Then, I measured ClCasp3 levels using Western blotting with untreated cells and cells treated with thapsigargin (Figure 21B). In untreated cells, I found a significant upregulation of ClCasp3 levels in the pooled C9-1+8 CNs. I did not see a significant difference in

ClCasp3 levels in thapsigargin-treated cells, probably due to the low number of replicates for this condition.

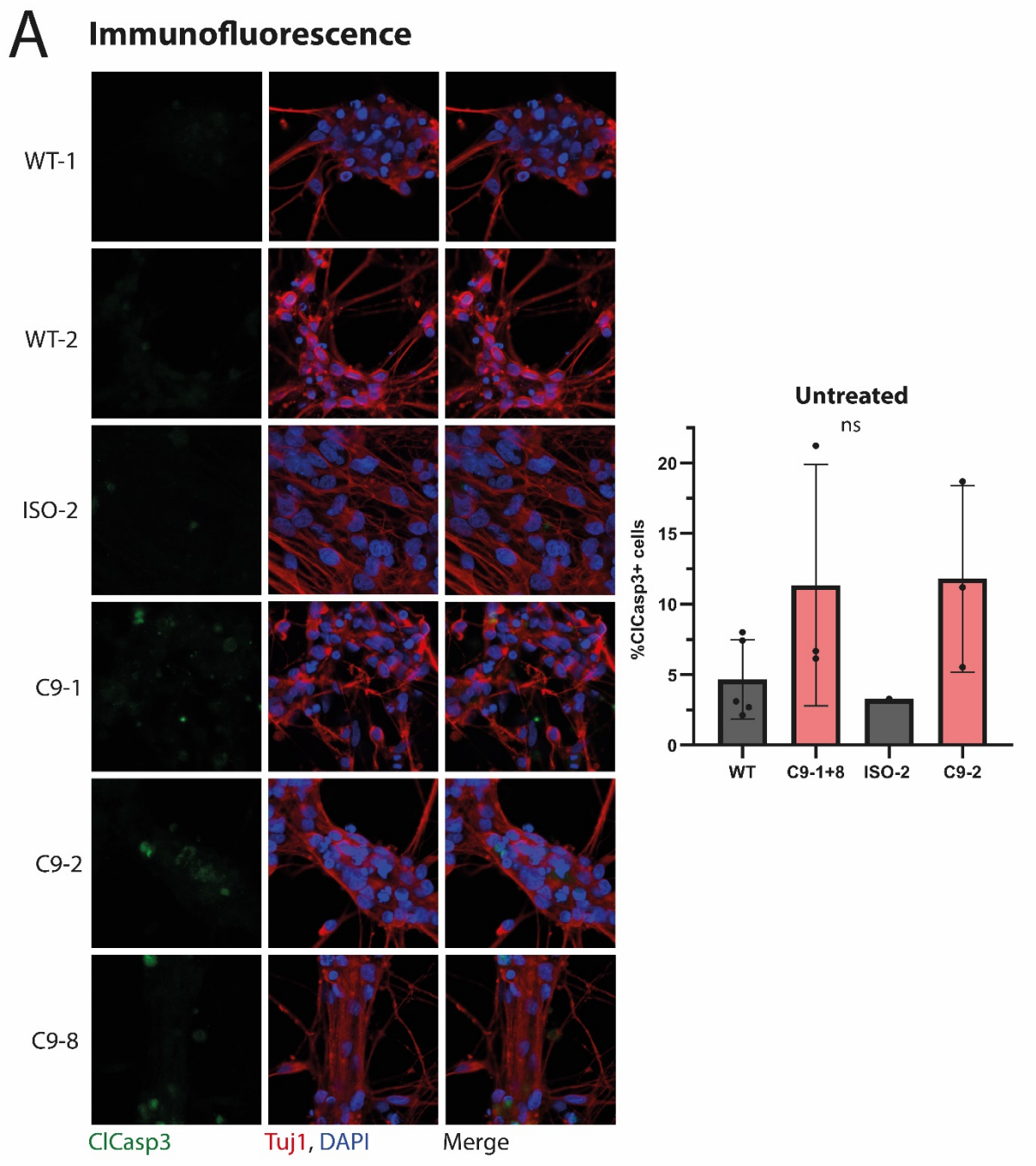


Figure 21: continued

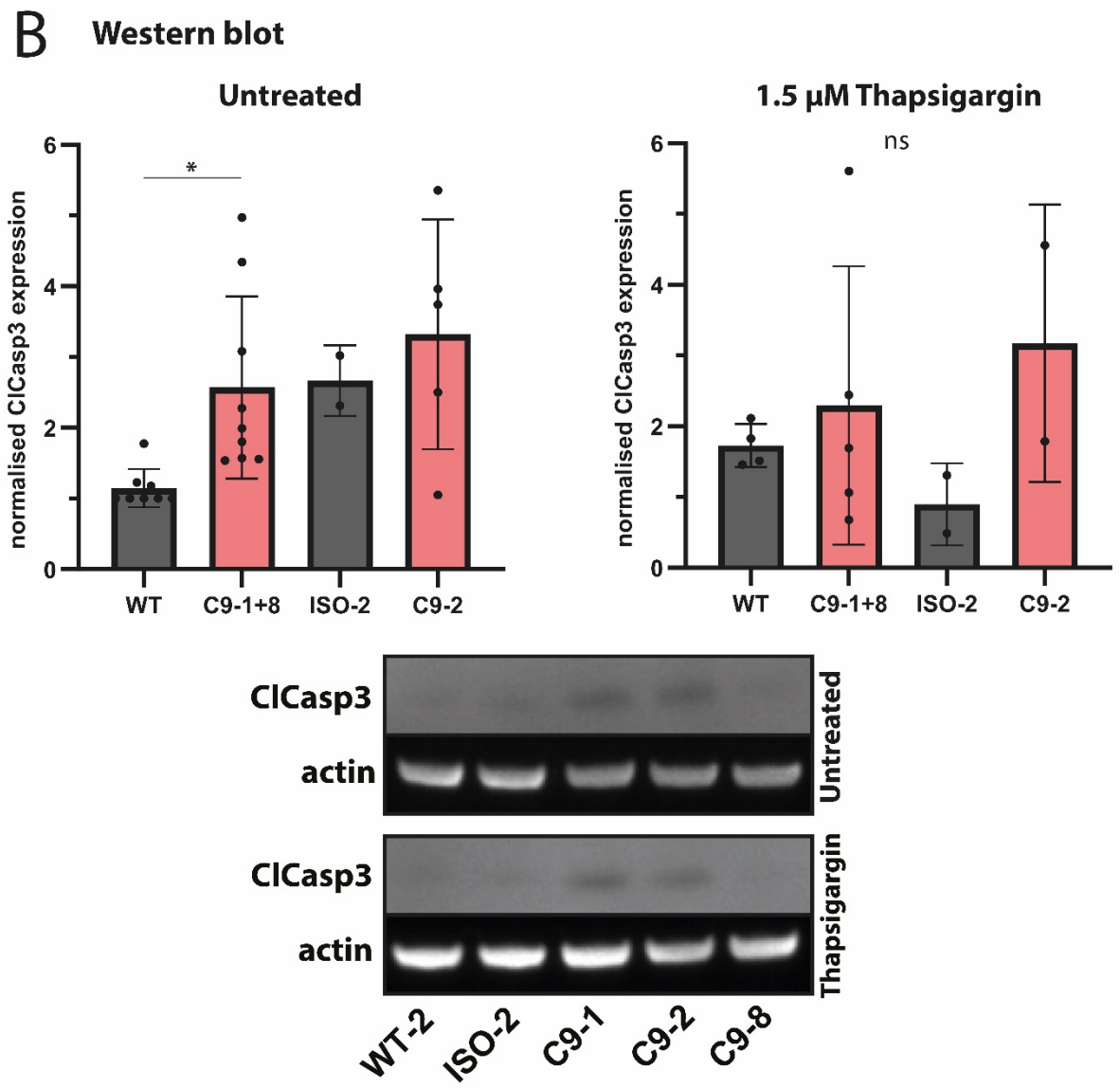


Figure 21: Cleaved caspase 3 levels are significantly altered in C9-CNs. (A) Immunofluorescent staining of ClCasp3 and Tuj1 using iPSC-derived CNs. The number of cells positive for ClCasp3 and Tuj1 was counted and divided by the total number of cells positive for Tuj1. (B) Western blot of ClCasp3 levels in untreated CNs and CNs treated with 1.5 µM thapsigargin for 24h. (A-B) Data were analysed with one-way ANOVA using Sidak's *post-hoc* test. The bars represent means. Error bars represent the standard deviation. Each dot represents the measured protein level from one differentiation. ns=not significant, *p<0.05.

To gain further evidence of increased apoptosis in C9-CNs, I attempted to measure the release of CytC into the cytosol. First, I stained iPSC-derived CNs for CytC and TOMM20, a protein of the outer mitochondrial membrane, and Tuj1 (Figure 22). I measured the intensity of CytC within TOMM20-stained mitochondria and the rest of the cell. I tested this novel method of measuring the localisation

of CytC to assess its usefulness. I observed a high percentage of CytC outside of mitochondria of about 40-60% in all cell lines. As CytC is a mitochondrial protein, it is unlikely to be present at such high levels in the cytosol in control cell lines, which do not show high levels of apoptotic ClCasp3-positive cells. Therefore, this method might exaggerate cytosolic CytC intensity due to the background intensity of unspecific binding of the CytC antibody or secondary antibody. Despite the high levels of background intensity, I would expect the percentage of cytosolic CytC to be increased in C9-CNs if CytC was released into the cytosol by a substantial amount. However, I observed no differences in the cytosolic CytC intensity between C9-CNs and control lines.

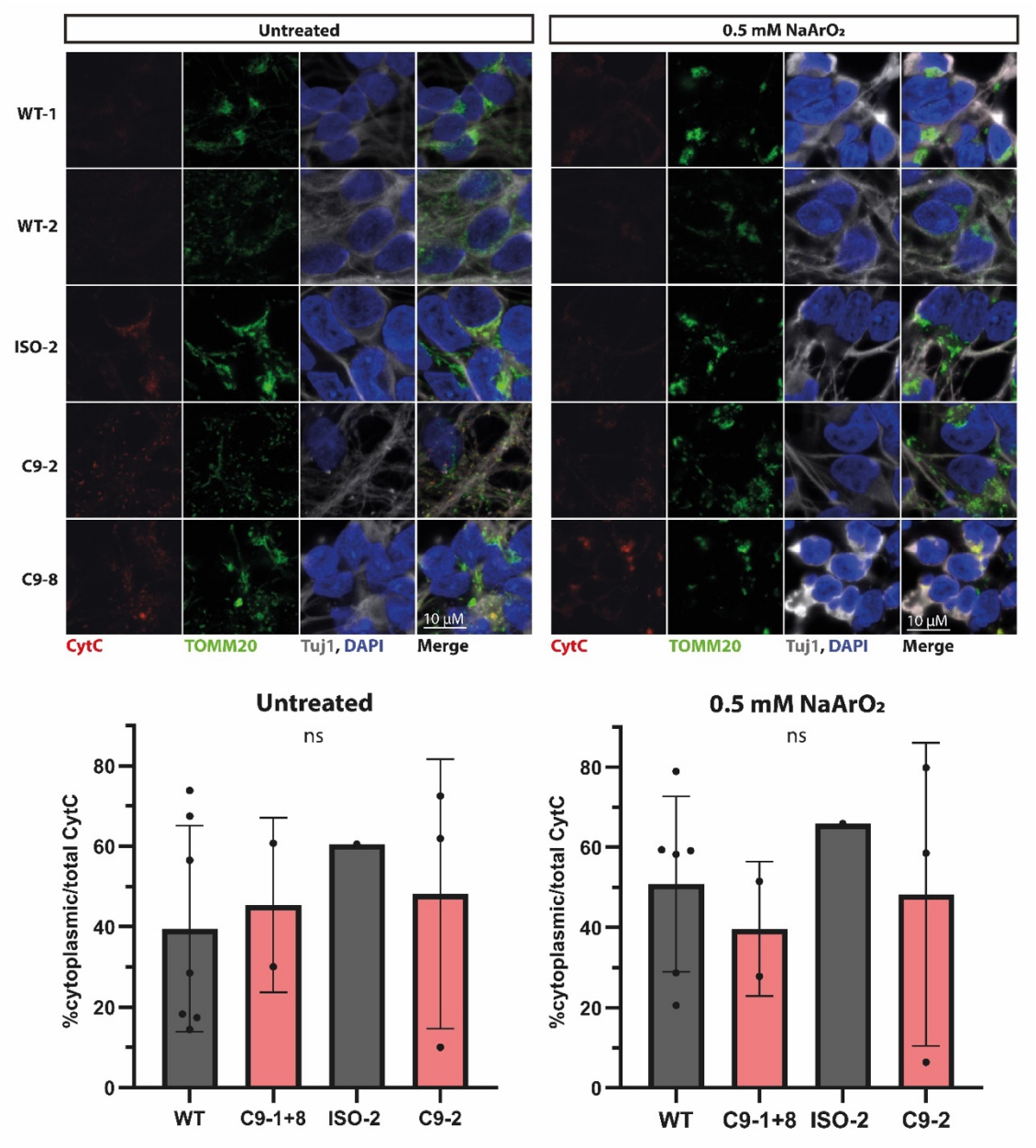


Figure 22: There is no significant difference in cytoplasmic CytC content in untreated C9-CN and C9-CNs treated with 0.5 mM $NaArO_2$ for 1h. Immunofluorescent staining of CytC, TOMM20, and Tuj1 using iPSC-derived CNs. The intensity of CytC staining was analysed outside of the TOMM20 staining but inside the Tuj1 staining. Data were analysed with one-way ANOVA using Sidak's *post-hoc* test. The bars represent means. Error bars represent the standard deviation. Each dot represents the value measured from one differentiation. ns=not significant.

Second, I measured the CytC levels in cells using Western blotting. Cells were lysed using RIPA buffer, which I expect not to extract all mitochondrial proteins. Therefore, Western blotting measures both cytosolic and mitochondrial CytC while underrepresenting mitochondrial CytC. If I assume the total expression of CytC to be the same in all cell lines, up or downregulation of CytC would represent the level of cytoplasmic CytC. However, the expression of CytC might differ between cell lines, which makes the results difficult to interpret. Despite this, I carried out this experiment, as previous work in my laboratory under similar Western blotting conditions showed a significant increase in CytC levels in one line of C9-CNs (Dafinca et al., 2016).

I studied CytC levels in untreated CNs and CNs treated with $NaAsO_2$ or CCCP. CCCP inhibits oxidative phosphorylation by decoupling the mitochondrial proton gradient (Demine et al., 2019). CCCP stresses mitochondria and causes mitophagy. I observed a minor significant reduction in CytC levels in the pooled C9-CNs in untreated cells (Figure 23). This reduction in CytC levels was not significant in treated CNs due to the lower number of measurements. Since CytC levels seemed to be reduced by an even bigger percentage in CCCP-treated cells (60.3%) compared to untreated cells (28.0%), I believe that additional technical replicates would make this reduction significant.

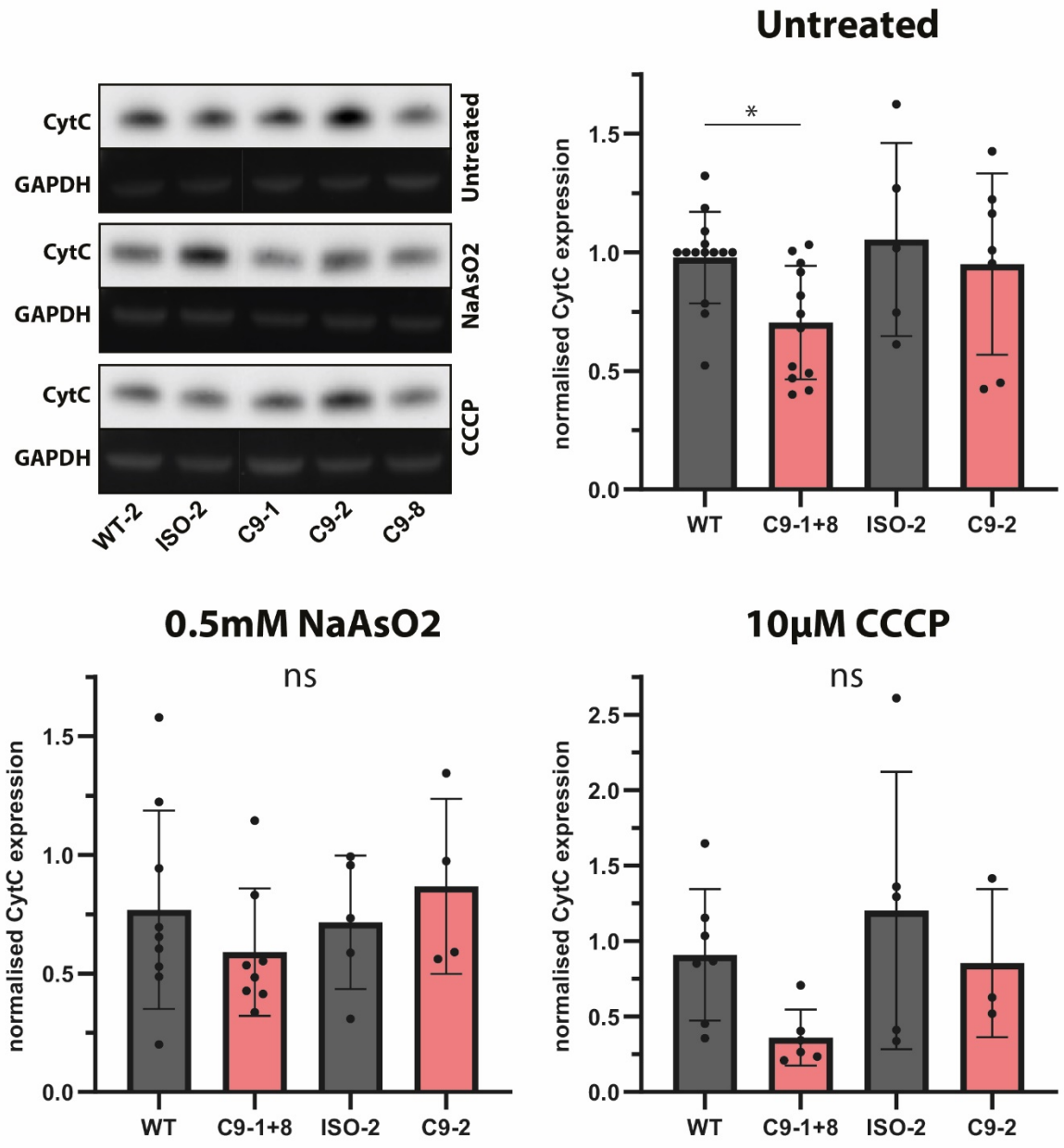


Figure 23: CytC levels are significantly downregulated in untreated C9-CNs. Western blot of CytC using untreated CNs and CNs treated with 0.5 mM $NaArO_2$ for 1h or with 10 µM CCCP for 24h. Data were analysed with one-way ANOVA using Sidak's *post-hoc* test. The bars represent means. Error bars represent the standard deviation. Each dot represents the measured protein level from one differentiation. ns=not significant, *p<0.05.

In summary, I found evidence for increased apoptosis in C9-CNs, namely a decrease in Bcl-2 expression and an increased number of ClCasp3-positive cells in the pooled C9-CNs. Thus, I found evidence for neuronal death in this early disease stage culture of layer V neurons. However, I did not identify any evidence for increased apoptosis in C9-2 CNs compared to its isogenic control, possibly due to the

chromosomal aberrations in these cell lines. In addition, I identified a reduction in CytC levels in pooled C9-CNs, which are most likely due to changes in mitochondrial mass (see Chapter 6).

3.4 C9-ALS/FTD cortical neurons do not show TDP-43 mislocalisation

I investigated whether TDP-43 mislocalisation was present in iPSC-derived C9-CNs, as it was observed in post-mortem C9-ALS/FTD patient neurons (Arai et al., 2006; Bodansky et al., 2010; Neumann et al., 2006; H. P. Nguyen et al., 2018). To this end, I first measured whether there were any differences in the overall expression of TDP-43 in untreated CNs and CNs treated with thapsigargin using Western blotting (Figure 24A). As detailed earlier (3.3), thapsigargin leads to ER stress, characterised by a disruption in protein folding and accumulation of unfolded proteins. Here, thapsigargin is used as a general cell stressor to exaggerate any disruptions in cellular mechanisms. As expected, I did not observe any differences in TDP-43 levels in untreated CNs and CNs treated with thapsigargin.

Next, I studied TDP-43 mislocalisation by measuring TDP-43 immunofluorescence outside the nucleus. I found no significant differences in TDP-43 localisation between cell lines (Figure 24B). Therefore, these iPSC-derived C9-CNs do not replicate the TDP-43 pathology found in patients.

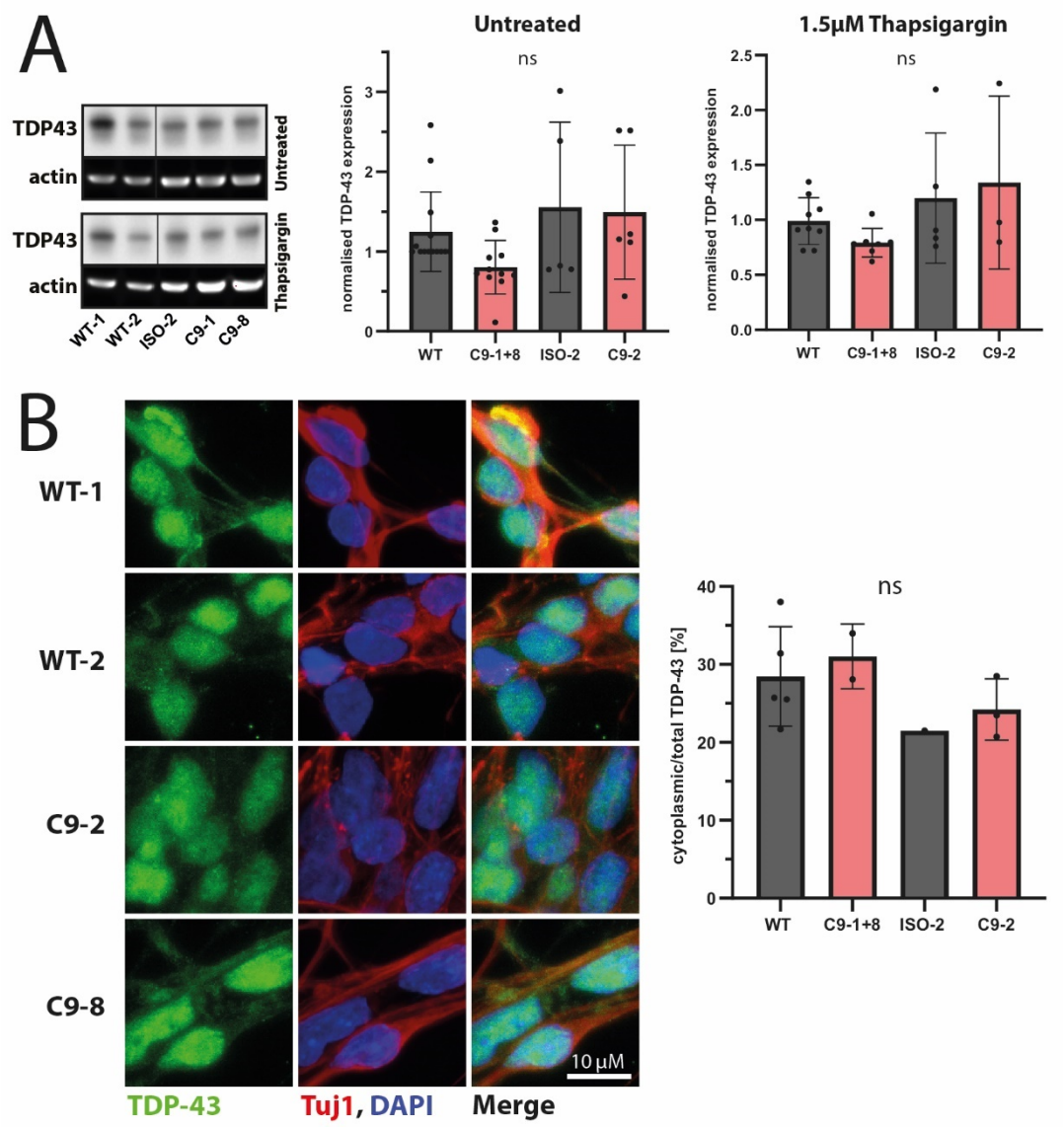


Figure 24: There are no significant changes to TDP-43 expression and localisation in C9-CNs. (A) Western blot of TDP-43 using untreated C9-CNs and C9-CNs treated with 1.5 µM thapsigargin for 24h. Data were analysed with one-way ANOVA using Sidak's *post-hoc* test. (B) Immunostaining of TDP-43 and Tuj1 using untreated iPSC-derived CNs. The intensity of TDP-43 outside the DAPI-positive area but inside the Tuj1-positive area was measured and divided by the intensity of TDP-43 inside the entire cell. Data were analysed with an unpaired two-tailed t-test. (A-B) The bars represent means. Error bars represent the standard deviation. Each dot represents the value measured from one differentiation. ns=not significant.

3.5 Conclusion

I successfully differentiated iPSCs into neurons, which show a high percentage of CNs and a low percentage of GFAP-positive glial cells. At day 55, cortical neuron cultures express layer VI and layer V

markers. Previous studies conducted in iPSC-derived C9-CNs do not analyse the identity of neuronal cultures in detail. One researcher in my group also studied the make-up of iPSC-derived cortical neuron cultures using a similar differentiation protocol. The only difference is that he added BDNF and GDNF when neurites appeared in culture (day 25-30) until the end of the differentiation. His cell cultures also expressed layer VI and layer V markers at day 55 (Dr Stephen Chen, unpublished), confirming my results.

Most of the following experiments were conducted with day 55 neurons. Thus, these experiments were carried out in a neuronal culture containing mainly layer V and layer VI CNs. Exceptions are the functional assays in Chapter 6 and calcium imaging in Chapters 4.3 and 1, which were conducted with day 56-60 neurons, and the axonal trafficking experiments in Chapter 6, which were carried out with day 43 neurons.

I observed a decreased differentiation efficiency in the ISO-2 cell line, which was also identified by another researcher in my group (Dr Stephen Chen, unpublished). This might be due to the passage number of this cell line which was roughly twice as high as the passage number of the other cell lines due to the gene-editing procedure (see Table 2). It could also be due to the chromosomal aberrations identified in this cell line (see 9.1 Appendix 1: Chromosomal aberrations in iPSCs).

Alternatively, the decrease in differentiation efficiency might be caused by an undesired genetic or epigenetic side-effect of gene editing, which might have decreased the pluripotency of this line. These deviations in the make-up of the ISO-2 cell culture between differentiations cause a skew in the data. Therefore, ISO-2 samples from problematic differentiations were excluded from Western blotting experiments, leading to fewer replicates of this cell line. ISO-2 data from these differentiations were included in immunocytochemistry and calcium imaging experiments, as non-neuronal cells could be excluded during the analysis. ISO-2 lines were also included in functional assays for which cells were grown in 96-well plates (data presented in Chapter 6), which caused lower differentiation efficiencies in all cell lines.

Further characterisation of cortical neuron cultures showed us that C9-CNs present some of the hallmarks of ALS and FTD. I observed a significant decrease in the expression of the anti-apoptotic Bcl-2 in pooled C9-CNs. Since I did not measure the expression levels of other anti-apoptotic and pro-apoptotic BCL-2 family members, it is not possible to determine if this reduction in Bcl-2 causes an imbalance in anti- and pro-apoptotic proteins, which triggers apoptosis. However, as I observed an increase in ClCasp3 in pooled C9-CNs, the reduction in Bcl-2 levels most likely causes an increase in apoptosis. This is evidence that cellular pathways are disrupted in C9-CNs, causing increased levels of apoptotic cells.

This finding corresponds well with other experiments which were conducted at my lab, showing a significant decrease in the expression of the anti-apoptotic proteins Bcl-2 and Bcl-X_L, a significant increase in the expression of pro-apoptotic BAK and subsequently an upregulation of ClCasp3 levels in C9-CNs and C9-MNs (Dafinca et al., 2016). However, I did not replicate any changes in CytC levels measured using Western blots, as were previously identified in my group in the C9-2 patient line in C9-CNs (Dafinca et al., 2016). As I used the same lysis buffer and protocol, these differences in results are probably due to the chromosomal aberrations identified in this cell line at the end of my experimental time, which were not present in this cell line when the previous study was conducted. Therefore, these chromosomal aberrations might have broad effects on the disease phenotype in this cell line.

Interestingly, in CNs treated with CCCP, I observed a non-significant increase in Bcl-2 levels in patient cell lines. Since I found that the CCCP treatment significantly increased Bcl-2 levels compared to untreated lines, this might be due to an unknown mechanism in which long-term mitochondrial permeabilisation induces an increase in Bcl-2 expression, possibly as a survival mechanism counteracting long-term low-level Bax and Bak presence.

Furthermore, I observed a minor significant reduction in CytC levels in the pooled C9-CNs in untreated cells (Figure 23). This indicates either the inhibition of apoptosis or a decreased level of mitochondrial

CytC levels, possibly due to increased mitophagy in C9-CNs. As I found evidence for differences in mitochondrial mass and increased mitophagy (discussed in Chapter 6), the reduction of CytC levels is most likely related to mitochondrial defects.

I did not identify any difference in expression or localisation of TDP-43, indicating that the increased apoptosis is independent of TDP-43 pathology. Difficulties with replicating a TDP-43 pathology phenotype are often described in cellular disease models. This is probably because I am working with an early disease model, suggesting that advanced neurodegeneration is necessary to observe TDP-43 pathology. Alternatively, technical issues might explain why TDP-43 pathology is commonly found in human C9-ALS/FTD post-mortem brain tissue, but not in hiPSC-derived neurons, such as the antibodies being less sensitive to low levels of TDP-43 in immunocytochemistry than in immunohistochemistry.

In summary, the work in this chapter suggests that iPSC-derived cortical neurons from patients carrying mutations in the *C9orf72* gene have the potential to be a valuable tool in studying FTD-specific pathophysiological pathways. However, not all phenotypes, especially TDP-43 mislocalisation, are present. Due to chromatic aberrations of the C9-2 and ISO-2 cell lines, results from these cell lines might be skewed. Therefore, phenotypes identified in pooled C9-1 and

In summary, the work in this chapter suggests that iPSC-derived cortical neurons from patients carrying mutations in the *C9orf72* gene have the potential to be a valuable tool in studying FTD-specific pathophysiological pathways. However, not all phenotypes, especially TDP-43 mislocalisation, are present. Due to chromatic aberrations of the C9-2 and ISO-2 cell lines, results from these cell lines might be skewed. Therefore, phenotypes identified in pooled C9-1 and C9-8 cells are more reliable.

4 C9-ALS/FTD-derived CNs do not show features of protein-associated cellular stress

Here, I define protein-associated stress as any stress a cell might exhibit in response to impaired protein homeostasis, such as translation inhibition, protein misfolding, or aberrant degradation. Specifically, I discuss stress granule formation, ER stress, and autophagy in C9-CNs, three processes which are closely related. SG formation can directly result from ER stress, and SGs can be degraded via autophagy. Similarly, ER stress can result from decreased degradation of misfolded proteins through the proteasome and can be alleviated via autophagy.

Increased stress granule formation has been observed in C9-iPSC-derived neurons. One study observed that the percentage of C9-MNs and C9-CNs displaying stress granules at base conditions is significantly increased (Dafinca et al., 2016). Another study using C9-MNs found that the number of stress granules per neuron was increased in patient cells (Abo-Rady et al., 2020).

In cellular C9-ALS/FTD models, ER stress was found to be increased. Previous studies observed increased ER Ca^{2+} levels and BiP expression in C9-iPSC-derived MNs (Dafinca et al., 2016). In mouse primary CNs expressing GFP-GA_{50}, the levels of BiP, phosphorylated PERK, and CHOP, but not ATF6, were found to be increased (Y. J. Zhang et al., 2014). Mechanistically, GFP-GA_{50} expression was found to inhibit proteasome activity, which triggers the accumulation of defective proteins and, thus, ER stress (Y. J. Zhang et al., 2014).

Autophagy impairment is strongly linked to C9-ALS/FTD. In previous studies, iPSC-derived C9-CNs exhibit increased sensitivity to autophagy inhibitors and a decreased autophagic flux, as suggested by elevated p62 levels (Almeida et al., 2013). Similarly, iPSC-derived C9-MNs exhibit increased p62 levels (Dafinca et al., 2016).

Due to this compelling evidence that SG formation, ER stress, and autophagy impairment are essential contributors to C9-ALS/FTD pathogenesis, I studied protein-associated cellular stress in C9-CNs. The aims of this chapter are to:

1. Establish whether stress granule formation is impaired in C9-CNs
2. Establish whether ER stress is present in C9-CNs
3. Study ER calcium release in C9-CNs
4. Establish whether autophagic flux is altered in C9-CNs

4.1 Stress granule formation was not upregulated in iPSC-derived C9-CNs

I studied the generation of SGs in response to the cellular stressor $NaAsO_2$. This ATP synthase inhibitor induces ATP depletion and disturbs Ca^{2+} homeostasis in the ER, leading to ER stress, mitochondrial dysfunction, and apoptosis (C. Chen et al., 2017; Yih et al., 1991). To this end, I visualised SGs by staining fixed CNs with anti-poly(A)-binding protein (PABP), an RBP commonly found as a component of SGs, and manually counted the number of SGs per cell (Mokas et al., 2009).

$NaAsO_2$ treatment effectively increased the number of stress granules per cell. However, no significant differences in the number of stress granules per neuron between C9-CNs and control CNs were found in untreated cells or cells treated with $NaAsO_2$ (Figure 25). Therefore, C9-CNs do not display an altered stress response phenotype.

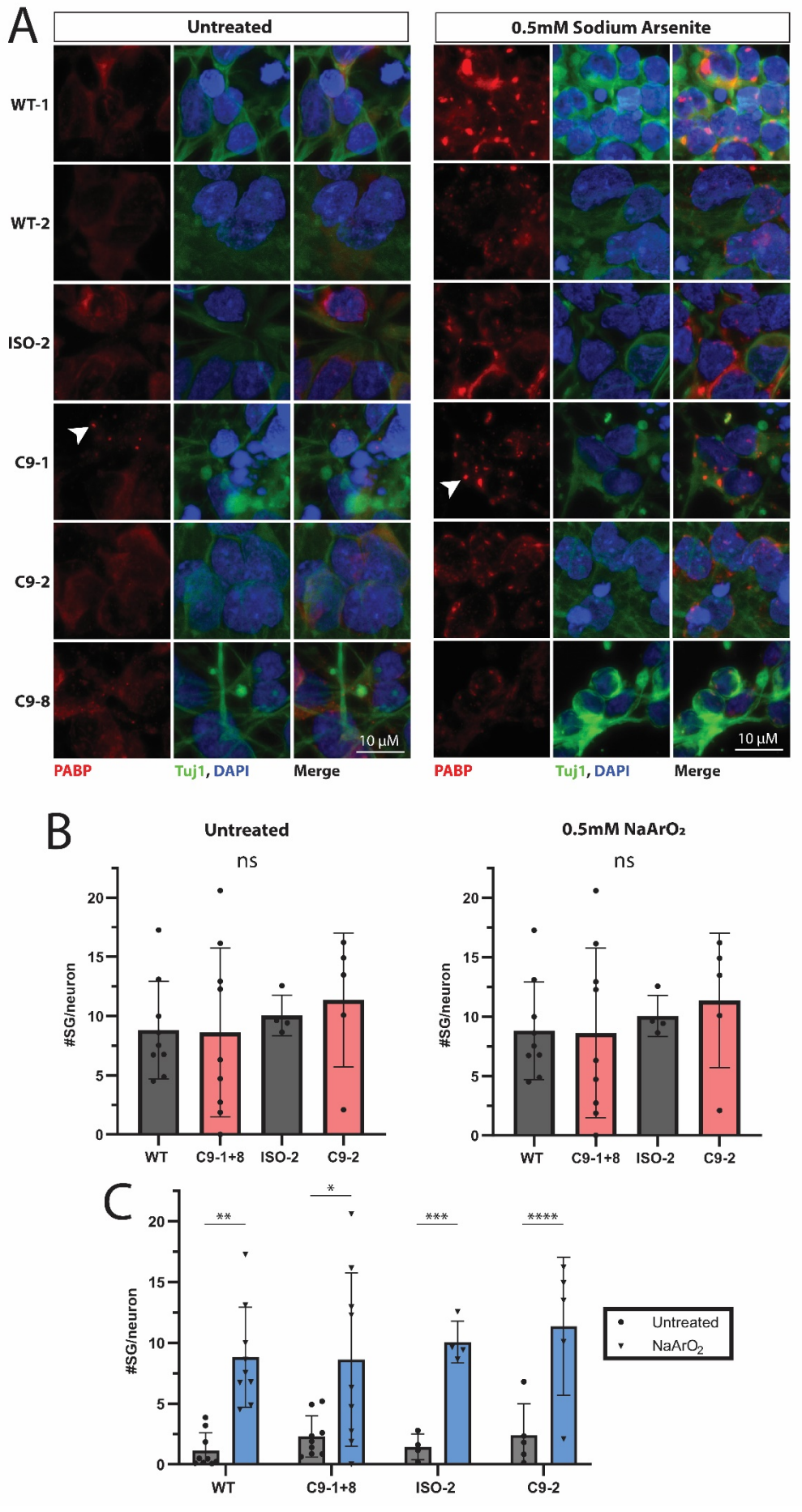

A
Untreated
0.5mM Sodium Arsenite
WT-1
WT-2
ISO-2
C9-1
C9-2
C9-8
10 µM
10 µM
PABP
Tuj1, DAPI
Merge
PABP
Tuj1, DAPI
Merge
B
Untreated
ns
0.5mM NaArO₂
ns
#SG/neuron
#SG/neuron
WT
C9-1+8
ISO-2
C9-2
C
**
*
***
****
#SG/neuron
Untreated
NaArO2
WT
C9-1+8
ISO-2
C9-2

Figure 25: No marked differences in stress granule formation were present in C9-CNs compared to control CNs. (A) Representative confocal images of CNs stained for PABP (red), Tuj1 (green) and DAPI. PABP aggregates were identified as stress granules (examples indicated with white arrowheads). (B) Quantification of the number of stress granules per Tuj1-positive neurons. Data were analysed with one-way ANOVA using Sidak's *post-hoc* test. (C) Incubating CNs with 0.5 mM $NaArO_2$ for 1h caused a significant increase in stress granules in all cell lines but WT-1. Data were analysed with two-way ANOVA using Dunnet's *post-hoc* test. (B-C) The bars represent means. Error bars represent the standard deviation. Each dot represents the value measured from one differentiation. ns=not significant, *p<0.05, **p<0.01, ***p<0.001, ****p<0.0001.

4.2 No evidence for ER stress was found in iPSC-derived C9-CNs

I measured various ER stress indicators to determine whether the C9-phenotype in iPSC-derived CNs included elevated ER stress, as seen in other cellular C9-ALS/FTD models. I examined untreated C9-CNs as well as the stress response to treatment with 1.5 μM thapsigargin. Thapsigargin is a small molecule which inhibits SERCA, a Ca^{2+} pump located in the ER membrane that transports free Ca^{2+} ions from the cytosol into the ER. Inhibiting SERCA leads to a reduced concentration of Ca^{2+} in the ER, which causes a decrease in the function of Ca^{2+}-dependent ER chaperones leading to an accumulation of unfolded proteins triggering the unfolded protein response. Equally, inhibiting SERCA increases the concentration of Ca2+ ions in the cytosol, causing Ca^{2+}-related toxicity.

To this end, I measured the IRE1 and ATF6 signalling-dependent activation of BiP expression by Western blot. I also analysed the activation of the PERK-CHOP signalling pathway of ER stress by measuring CHOP levels, as well as the PERK-eIF2α-dependent activation of ATF4 expression.

I did not find a significant difference in BiP levels, CHOP levels, or ATF4 levels between control and C9-ALS/FTD patient lines in untreated or stressed cells (Figure 26). These results indicate an absence of ER stress in this C9-ALS/FTD model. Additionally, I did not see a significant increase in the UPR in thapsigargin-treated cells compared to untreated cells in any of the cell lines. This suggests that the concentration of thapsigargin was not high enough to see a significant increase in the UPR response in iPSC-derived CNs.

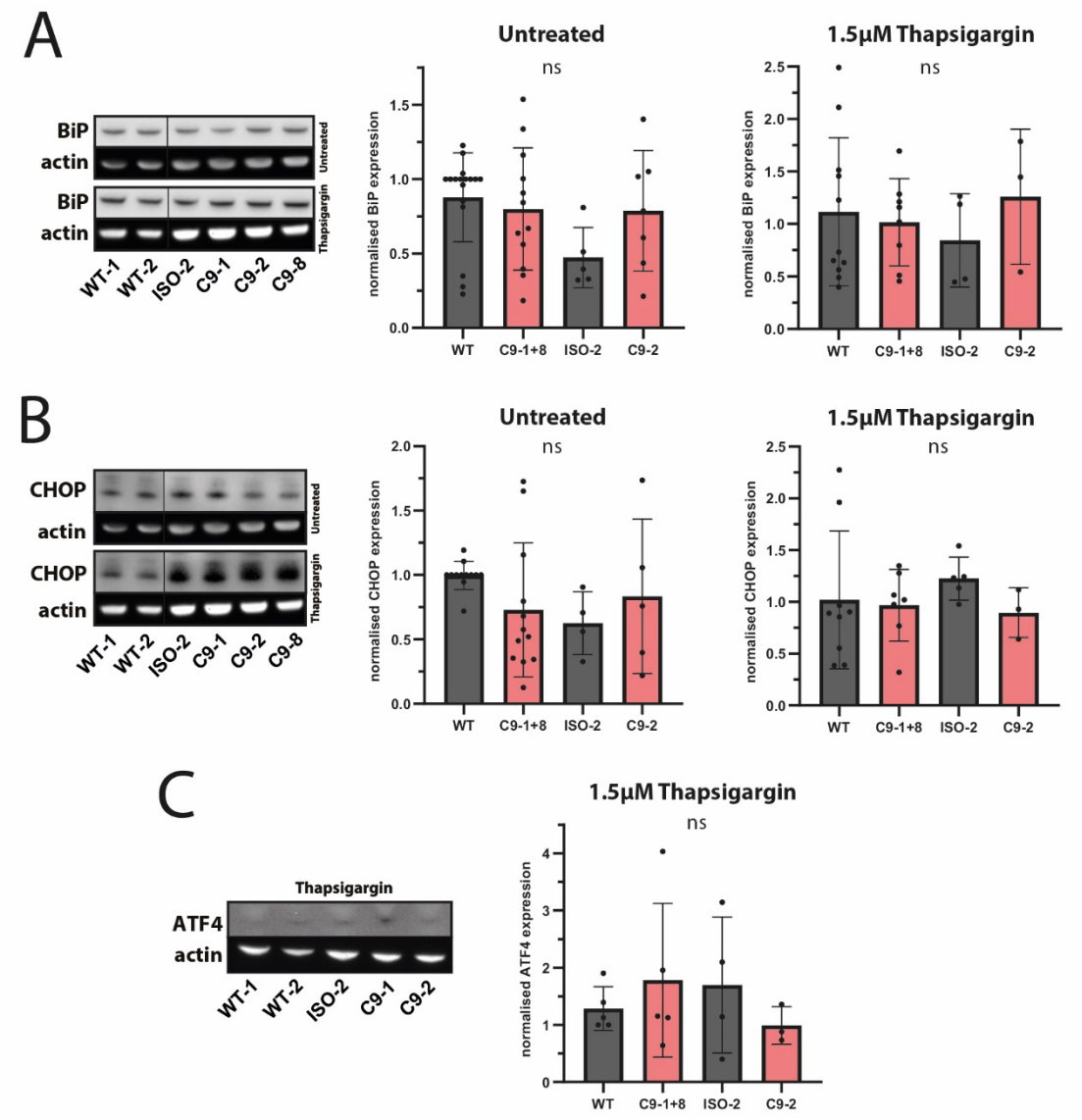


Figure 26: No ER stress was present in C9-CNs according to levels of key proteins of the ER stress response. (A) Western blot of BiP in untreated CNs and CNs treated with 1.5 µM thapsigargin for 24h. (B) Western blot of CHOP in untreated CNs and CNs treated with 1.5 µM thapsigargin for 24h. (C) Western blot of ATF4 in CNs treated with 1.5 µM thapsigargin for 24h. (A-C) Data were analysed with one-way ANOVA using Sidak's *post-hoc* test. The bars represent means. Error bars represent the standard deviation. Each dot represents the measured protein level from one differentiation. Vertical black lines running through the images of Western blot membranes indicate where the pictures of membranes were cut making this figure to exclude additional samples. The left and right parts of the images were taken from the same pictures. ns=not significant.

Given that stressing iPSC-derived CNs with 0.5 mM of $NaAsO_2$ for 1h significantly stimulated SG formation in all cell lines (Figure 25B), but there was no increase in ER stress in response to thapsigargin (Figure 26), I, therefore, investigated whether $NaAsO_2$ might be more effective than

thapsigargin in causing ER stress leading to ER stress-dependent SG formation. I performed preliminary tests on the effect of $NaAsO_2$ on the UPR response by Western blotting of ATF4 to rule out the ER stress phenotype in C9-CNs. Although Figure 27 shows preliminary results with a low number of differentiations, the expression of ATF4 appears to be similar in all cell lines, with no increased ATF4 expression in patient CNs. Thus, no significant ER stress or increased response to cellular stressors was found in C9-CNs.

The reason, the $NaAsO_2$ treatment effectively caused stress granule formation but no UPR response is probably that cells were only treated with $NaAsO_2$ for 1h and fixed immediately after. While this 1h treatment was enough to form induce stress granule formation, it was not long enough the increase the expression of a stress response protein.

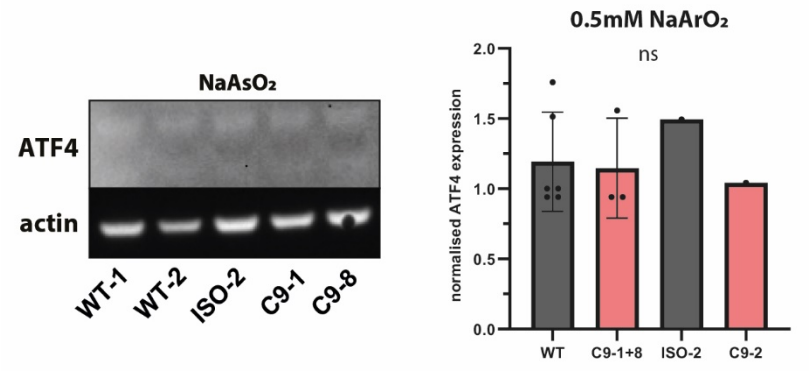


Figure 27: Preliminary data shows no differences in ATF4 expression between C9-CNs and control CNs treated with 0.5 mM $NaArO_2$ for 1h. Western blot of ATF4 in CNs treated with 0.5 mM NaArO2 for 1h. Data were analysed using an unpaired, two-tailed t-test. The bars represent means. Error bars represent the standard deviation. Each dot represents the measured protein level from one differentiation.

To conclude, I did not identify any signs of ER stress by measuring expression levels of UPR proteins.

4.3 Intracellular Ca^{2+} signalling is disturbed in iPSC-derived C9-CNs

Since altered ER Ca^{2+} levels cause the disruption of Ca^{2+}-dependent chaperone activity and thus ER stress, I examined the response of C9-ALS/FTD patient-derived CNs to 0.1 mM carbachol (CCh). CCh

activates G-protein coupled receptors (GPCRs), which stimulate phospholipase C (PLC) to generate inositol trisphosphate (IP_3). IP_3 triggers the release of Ca^{2+} from the ER by activating IP_3 receptors on the ER membrane (Belkacemi et al., 2018). Measuring the Ca^{2+} release into the cytoplasm informs us about the ER Ca^{2+} levels and IP_3 receptor signalling. A more direct approach to studying ER Ca^{2+} levels would be to measure the Ca^{2+} release into the cytoplasm after stimulating cells with an injection of thapsigargin, which inhibits SERCA. However, due to laboratory safety concerns with this approach, I decided to use a continuous stimulation of the cells with CCh instead.

We observed no significant differences in the amplitude of Ca^{2+} release from the ER after CCh stimulation between healthy and control lines (Figure 28B), suggesting that ER Ca^{2+} levels are not altered in FTD-patient-derived CNs. Similarly, we observed no differences in the time needed to clear Ca^{2+} from the cytosol (Figure 28D). This is further evidence, that no ER stress is present in iPSC-derived C9-CNs. However, the latency of Ca^{2+} release from the ER after CCh stimulation was significantly lower in C9-ALS/FTD patient CN lines compared to WT control CNs, which implies that the IP_3 pathway responded quicker to activation (Figure 28C).

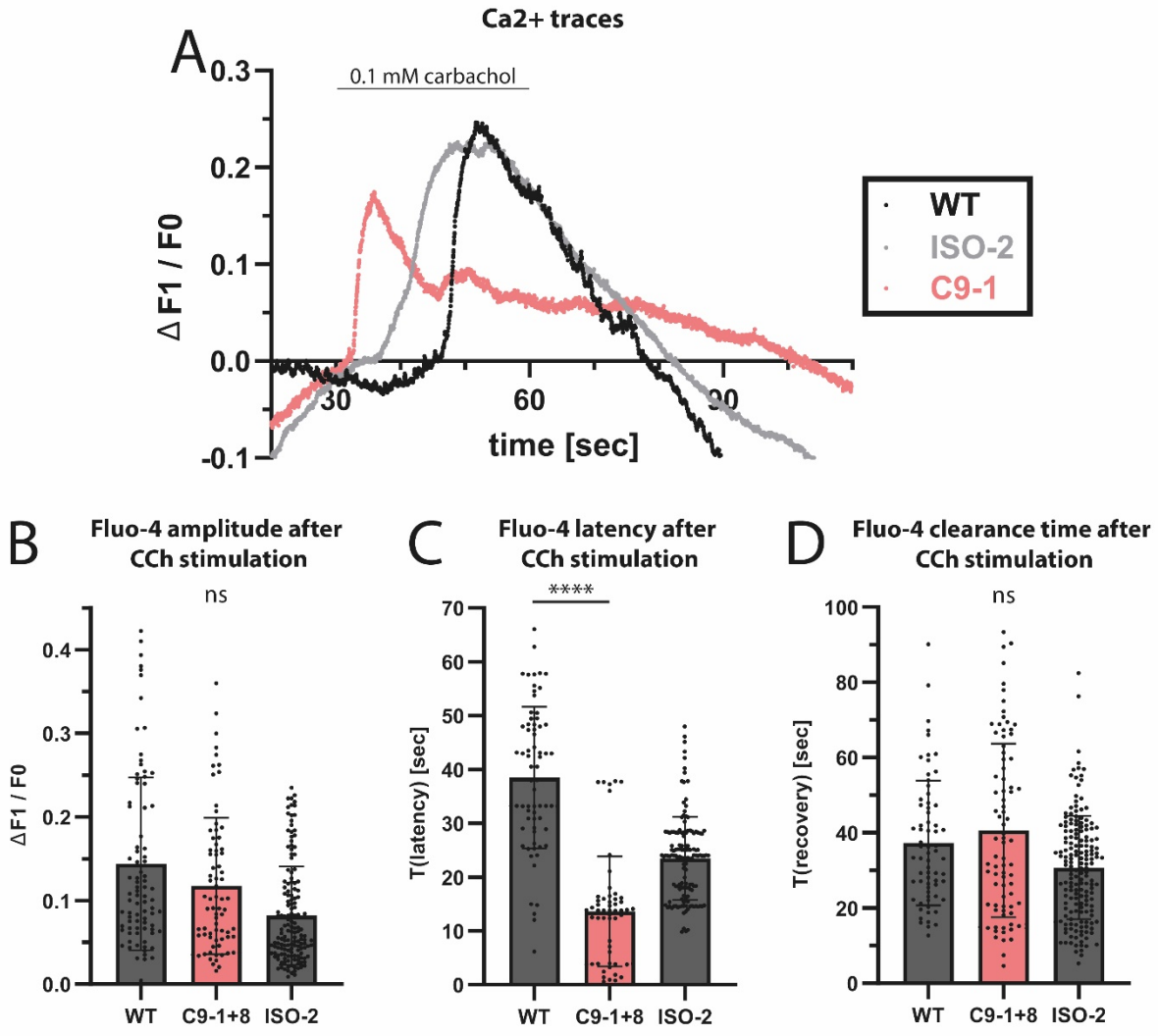


Figure 28: The release of Ca^{2+} from the ER after stimulation with 0.1 mM CCh is altered in C9-ALS/FTD patient-derived CNs compared to isogenic and wild-type controls. (A) Representative Ca^{2+} traces in Fluo-4 AM loaded CNs. 0.1 mM CCh was added after 30sec of recording for 30sec, then CCh was washed out for 2min. (B) The amplitude of cytosolic Ca^{2+} intake in Fluo-4 AM loaded CNs after the addition of carbachol. (C) The latency of ER Ca^{2+} release after the addition of carbachol. (D) the clearance time of cytosolic Ca^{2+} after the addition of carbachol. (B-D) The data is comprised of n differentiations: n(WT)=3, n(C9-1+8)=3, n(ISO-2)=3. Data were analysed with an unpaired two-sided t-test between WT and C9-1+8 cell lines. Each dot represents the measurements of one cell. The bars represent means. Error bars represent the standard deviation. ns=not significant, ****p<0.0001.

4.4 No changes in autophagic flux were observed in iPSC-derived C9-CNs

I studied autophagy since it is commonly dysregulated in C9-ALS/FTD models, including iPSC-derived C9-CN. I treated cells with the autophagy inhibitor bafilomycin and the autophagy stimulator

rapamycin to exaggerate any possible changes in autophagy. Bafilomycin inhibits autophagy by inhibiting the acidification of the lysosome and the fusion of the lysosome with the autophagosome (Mauvezin & Neufeld, 2015). Rapamycin inhibits mTOR, which causes a stimulation of the autophagic flux (Sarkar et al., 2008). I studied the protein levels of p62, which is responsible for binding cargo labelled for degradation and including it in the autophagosome (Rusten & Stenmark, 2010). p62 is degraded with the cargo. Thus a reduction in p62 levels implies high autophagic activity. I also measured the levels of LC3 converted from LC3-I to LC3-II, which is essential for autophagosome maturation and acts as a marker for autophagic flux (Kadowaki & Karim, 2009; Tanida et al., 2004). Lastly, I studied the levels of LAMP2A. This lysosomal protein plays a role in autophagosome maturation, chaperone-mediate autophagy, and protecting the lysosomal membrane from the luminal environment (Glick et al., 2010; Saftig et al., 2008).

Surprisingly, I did not observe any significant differences in p62 levels, LC3-I to LC3-II conversion, and LAMP2A levels in any of the tested conditions (Figure 29). Bafilomycin treatment effectively inhibited autophagic flux as observed as an increase in p62 levels and a reduction in the conversion of LC3BI to LC3BII. Still, bafilomycin did not cause an aberrant response in iPSC-derived C9-CNs. Rapamycin did not induce any significant changes in autophagic flux, suggesting that the concentration of rapamycin was not high enough for this experiment.

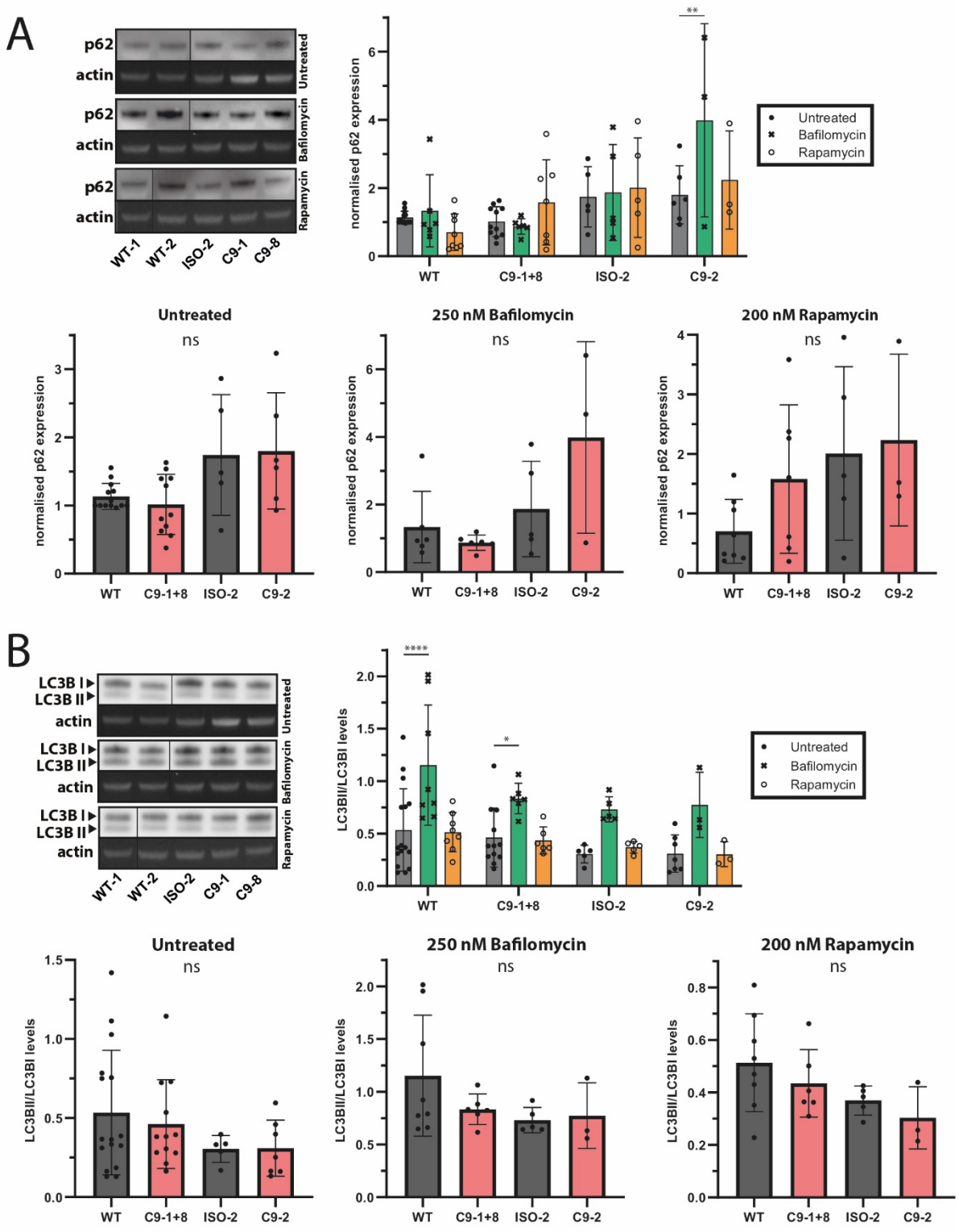


Figure 29A,B: continued

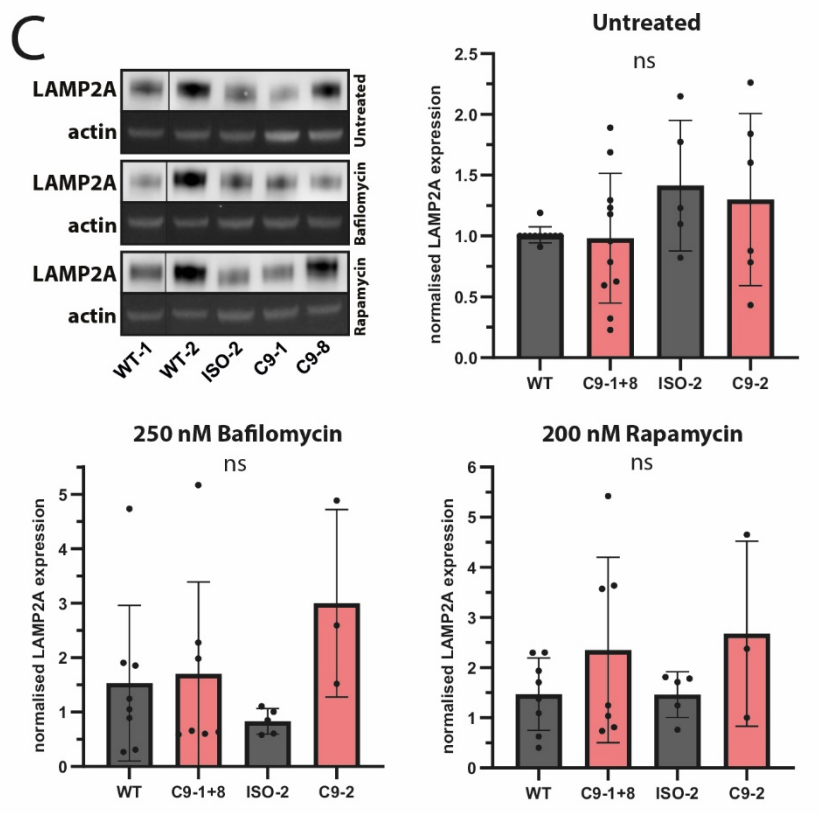


Figure 29: No differences in autophagic flux were identified in C9-CNs according to key autophagy proteins. (A) Western blot of p62 in untreated CNs and CNs treated with 250 nM bafilomycin or 200 nM rapamycin for 24h. (B) Western blot of the LC3-I to LC3-II conversion in untreated CNs and CNs treated with 250 nM bafilomycin or 200 nM rapamycin for 24h. (C) Western blot of LAMP2A in untreated CNs and CNs treated with 250 nM bafilomycin or 200 nM rapamycin for 24h (A-C) When comparing treatments, data were analysed with two-way ANOVA using Dunnett's *post-hoc* test. All other data were analysed with one-way ANOVA using Sidak's *post-hoc* test. The bars represent means. Error bars represent the standard deviation. Each dot represents the value measured from one differentiation. Vertical black lines running through the images of Western blot membranes indicate where the pictures of membranes were cut making this figure to exclude additional samples. The left and right parts of the images were taken from the same pictures. ns=not significant, *p<0.05, **p<0.01, ****p<0.0001.

4.5 Conclusion

Since aberrant stress granule formation and degradation is believed to be a contributor to neurodegeneration in ALS/FTD, I studied stress granule formation by measuring the accumulation of the RNA-binding protein PABP. In my iPSC-derived CNs cultures, I also did not determine an increase in the number of stress granules present in untreated cells and CNs treated with $NaArO_2$. Previous

work in my group showed an increase in the number of stress granule-positive cells in both C9-CNs and C9-MNs (Dafinca et al., 2016). Here, the number of SGs per cell rather than the number of SG-positive cells was counted. Therefore, I cannot directly compare these results. Additional work from my group showed preliminary results using two differentiations, in which the number of SGs per cell was non-significantly increased in C9-2 MNs (Dr Paola Barbagallo, unpublished). Similarly, I did not identify a significant increase in the number of SGs per cell.

I studied ER stress and UPR by measuring the protein levels of three UPR proteins which are upregulated in response to ER stress: BiP, CHOP, and ATF4. I did not identify any significant changes in UPR protein levels in untreated cells and cells treated with thapsigargin or $NaArO_2$. While a high deviation between differentiations might have covered minor changes in protein expression, I conclude that no significant differences in ER stress were present in these C9-CNs. These findings are in stark contrast to other ALS/FTD studies. In studies using primary cortical neurons expressing GFP-GA_{50}, increased levels of BiP and CHOP have been described (Y. J. Zhang et al., 2014). In C9-MNs, my group showed the significant downregulation of ATF4 in a C9-ALS/FTD patient line which was not used here and a reduction in CHOP and PERK levels in the C9-2 line and another patient line (Dr Paola Barbagallo, unpublished). Additionally, my group showed an increase in BiP levels in various patient cell lines not used here. Incidentally, C9-2 MNs also did not show a significant increase in BiP levels (Dafinca et al., 2016). Therefore, the work presented here is partially consistent with previous findings from C9-MNs.

As changes in ER Ca^{2+} levels trigger ER stress, I measured the release of ER Ca^{2+} through the IP_3 receptor in response to carbachol. I found no differences in amplitude between C9-CNs and healthy controls. This is further evidence that ER stress is not present in C9-CNs. In C9-MNs, my group identified a reduced amplitude of ER Ca^{2+} release after stimulation with carbachol in various cell lines, including the C9-1 and C9-2 cell lines (Dafinca et al., 2021). However, the C9-CN cultures used here do not replicate the ER stress phenotype identified in C9-MNs.

I observed that the latency of Ca^{2+} release from the ER after CCh stimulation was significantly lower in C9-CN lines compared to control CNs. This could point towards increased sensitivity of GPCRs or PLC, thus causing an increased generation of IP_3. Alternatively, IP_3 receptor levels might be raised, leading to maximum amplitude or Ca^{2+} release faster after activation of IP_3 receptors. However, one previous study found that the expression of IP_3 receptor 1, the isoform expressed in CNs, is not altered in C9-ALS/FTD-derived CNs (Gomez-Suaga et al., 2022). Previous studies have identified Bcl-2 and Bcl-X_L to inhibit IP_3-initiated IP3R opening and ER calcium release (Y. P. Rong et al., 2009; Rosa et al., 2021). My experiments together with other studies have shown a significant reduction in Bcl-2 and Bcl-X_L protein levels in iPSC-derived C9-CNs and C9-MNs (Dafinca et al., 2016). Thus, the reduced latency of CCh-induced ER Ca^{2+} release might be due to altered IP3R regulation, e.g. by BCL-2 family proteins or TMBIM family proteins (Rojas-Rivera & Hetz, 2014). Additional experiments would be necessary to determine the protein levels of GPCRs, PLCs, IP3 receptors, and their regulators to establish the cause for the decreased latency of ER Ca^{2+} release. However, due to time restrictions, I was unable to carry out these follow-up experiments.

Intracellular Ca^{2+} signalling is a vital regulator of various cellular processes, such as gene transcription, metabolism, autophagy, secretion, and cell death (Kania et al., 2017). The ER is the main storage organelle for intracellular Ca^{2+} and releases Ca^{2+} via IP3R or ryanodine receptors (RyRs) (Kania et al., 2017). The IP3R pathway stimulates Ca^{2+} release from the ER in response to neurotransmitters, hormones, growth factors, or antibodies (Kania et al., 2017). The IP3R is also constitutively active at a low level at basal conditions, which is necessary to maintain mitochondrial Ca^{2+} levels and sustain mitochondrial bioenergetics (Cárdenas et al., 2010). Additionally, IP3R has an inhibitory role in basal autophagy (Kania et al., 2017). In neurons, the IP_3 pathway regulates axonal growth, excitability, and brain rhythms (Berridge, 2016). Thus, the IP_3 signalling pathway is essential for neuronal function.

Changes in IP_3 signalling are associated with neurodegeneration. In Alzheimer's disease and Huntington's disease, enhanced IP_3 signalling contributes to neuronal loss (Berridge, 2016). Also, some

studies suggested that IP_3 signalling is altered in ALS. In SOD1 mutant ALS mouse models, the expression of PLCδ1, which generates IP_3, was increased (Staats et al., 2013). The survival was prolonged when PLCδ1 was knocked out (Staats et al., 2013), whereas the increase in IP3R expression reduced the life span (Staats et al., 2012).

Little is known about the impact of the C9-HRE on the IP_3 signalling pathway. Experiments from my group using C9-MNs showed a reduced amplitude of ER Ca^{2+} release after CCh stimulation, while ER Ca^{2+} levels remained unchanged, suggesting that Ca^{2+} release through the IP_3R is affected independently of ER Ca^{2+} levels (Dafinca et al., 2021). A recent study has identified disruptions in the interaction between IP3R and mitochondrial voltage-dependent anion channel (VDAC) in iPSC-derived CNs and *C9orf72* BAC transgenic mice. This disruption is possibly due to disrupted ER-mitochondria tethering as a result of poly-GA, poly-GR, and poly-PR toxicity (Gomez-Suaga et al., 2022). As ALS/FTD-associated aberrant IP_3 signalling has been observed in multiple disease models, but its molecular mechanism and role in C9-HRE toxicity are little understood, further experiments focusing on IP_3 signalling in C9-ALS/FTD are needed.

As autophagy disruption is commonly associated with C9-ALS/FTD, I studied the expression and activity of several proteins essential in the macro-autophagy: p62, LC3, and LAMP2A, while stimulating or inhibiting autophagic flux using rapamycin and bafilomycin. I did not observe any differences in autophagic flux. Thus, the C9-FTD phenotype in these cortical neuron cultures does not include an accumulation of cellular waste.

The absence of any indicators that autophagy might be dysregulated in these cortical neuron cultures contradicts several previous studies which identified significantly elevated p62 levels and increased sensitivity to autophagy inhibitors in iPSC-derived CNs, as well as elevated p62 levels in iPSC-derived MNs (Almeida et al., 2013; Dafinca et al., 2016). This includes a C9-CN study which also used the C9-2 cell line. In said study, the C9-2 which was found to be significantly upregulated compared to two of three WT control lines. The differentiation protocol for this study was similar to the protocol used

here, apart from the addition of brain-derived neurotrophic factor (BDNF) and glial cell-derived neurotrophic factor (GDNF) when neurons began to develop neurites until the end of differentiation (Dafinca et al., 2016). Another study which found elevated p62 levels in C9-CNs used a vastly different differentiation protocol involving embryoid bodies (Almeida et al., 2013).

As previously discussed (see chapter 1.2.3.4), mTOR signalling is an upstream regulator of autophagic flux. mTOR signalling also plays a vital role during neurogenesis and cortical development (Tee et al., 2016). Therefore, differences in growth factor exposure during iPSC differentiation using different differentiation protocols might account for differences in mTOR activity in iPSC-derived CNs, explaining why some studies have found aberrations in autophagy in C9-CNs, while I did not observe such an effect.

I also investigated if different lysis buffers were used in those previous studies. Only one of the two studies stated the lysis buffer used, which was identical to the lysis buffer used here. Therefore, I believe the differences in differentiation protocols to be the most likely reason for the different outcomes when studying autophagy.

These findings underline that reproducibility is low in phenotyping studies using iPSC-derived C9-neurons. Deviations between differentiations lead to high error bars, which might hide any significant effects. This is exacerbated in long differentiations, such as the differentiation to CNs, as mitotic undifferentiated cells are more likely to spread among post-mitotic neuronal cultures. Furthermore, there are differences in the phenotypes observed in various studies, both between C9-MNs and C9-CNs as well as between different studies using C9-CNs. This might be due to the use of different cell lines or cell culture conditions which impact the exposure to growth factors or cellular energetics. Stark deviations between differentiations will be an issue throughout this study.

5 Excitability is significantly altered in C9-ALS/FTD-derived CNs

Excitotoxicity is commonly associated with C9-ALS/FTD. Results from my laboratory from RNA sequencing of C9-ALS/FTD iPSC-derived MNs showed an upregulation of several Ca^{2+} permeable glutamate receptors, including GluA3 and GluN2 (manuscript under revision). Additionally, the upregulation of calcium-permeable AMPAR and NMDAR was identified using Western blotting in C9-ALS/FTD iPSC-derived MNs. Furthermore, mitochondrial calcium buffering was reduced due to the dysregulation of mitochondrial calcium uniporters (Dafinca et al., 2020). In these cells, calcium clearance from the cytosol was delayed due to decreased mitochondrial calcium buffering. However, while cytosolic calcium intake was increased in C9-ALS/FTD iPSC-derived MNs stimulated with KCl, calcium intake was reduced in C9-MNs stimulated with glutamate (Dafinca et al., 2020). Additionally, my group identified an increase in ER Ca^{2+} in iPSC-derived C9-MNs (Dafinca et al., 2016). Despite all this evidence in ALS, it is little understood if altered excitability contributes to neurodegeneration in C9-FTD CNs.

In this chapter, I investigated whether the increased apoptosis which I observed in C9-CNs might be caused by excitotoxicity by addressing the following scientific questions:

1. Whether excitability is altered in C9-iPSC-derived CNs
2. Whether levels of ionotropic receptors and other key proteins of synaptic transmission are altered
3. Whether cytosolic calcium clearance is altered in C9-iPSC-derived CNs
4. Whether cytosolic Ca^{2+} influx from the ER is altered

5.1 iPSC-derived C9-CNs demonstrate changes in excitability

To establish whether excitability is altered in C9-CNs, I carried out calcium imaging with CNs loaded with Fluo-4 AM. I stimulated cells with 0.2 mM glutamate to gain insight into the activity of post-synaptic Ca^{2+} AMPARs and NMDARs. Since the number of differentiations used in these calcium imaging experiments was low, the data presented in Figure 30 and Figure 31 is preliminary. However, due to the large number of cells I measured for each differentiation, careful conclusions can be drawn from the data.

I observed a significant downregulation of amplitude in response to glutamate stimulation in the C9-1 patient line compared to the pooled WT control lines, meaning that the presence of the C9-HRE causes hypoexcitability in this cell line (Figure 30). In the C9-2 line, I observed a significant upregulation of amplitude compared to its isogenic control line, suggesting hyperexcitability. In addition, I identified a significant decrease in latency in the C9-1 patient line and an increase in latency in the C9-2 patient line compared to its isogenic control. Thus, in the C9-1 patient line, the cytosolic Ca^{2+} peaked earlier and to a lower extent after glutamate stimulation compared to control lines and vice versa in the C9-2 patient line. This is potentially due to abnormal levels of glutamate-stimulated ion channels in the post-synapse of patient neurons.

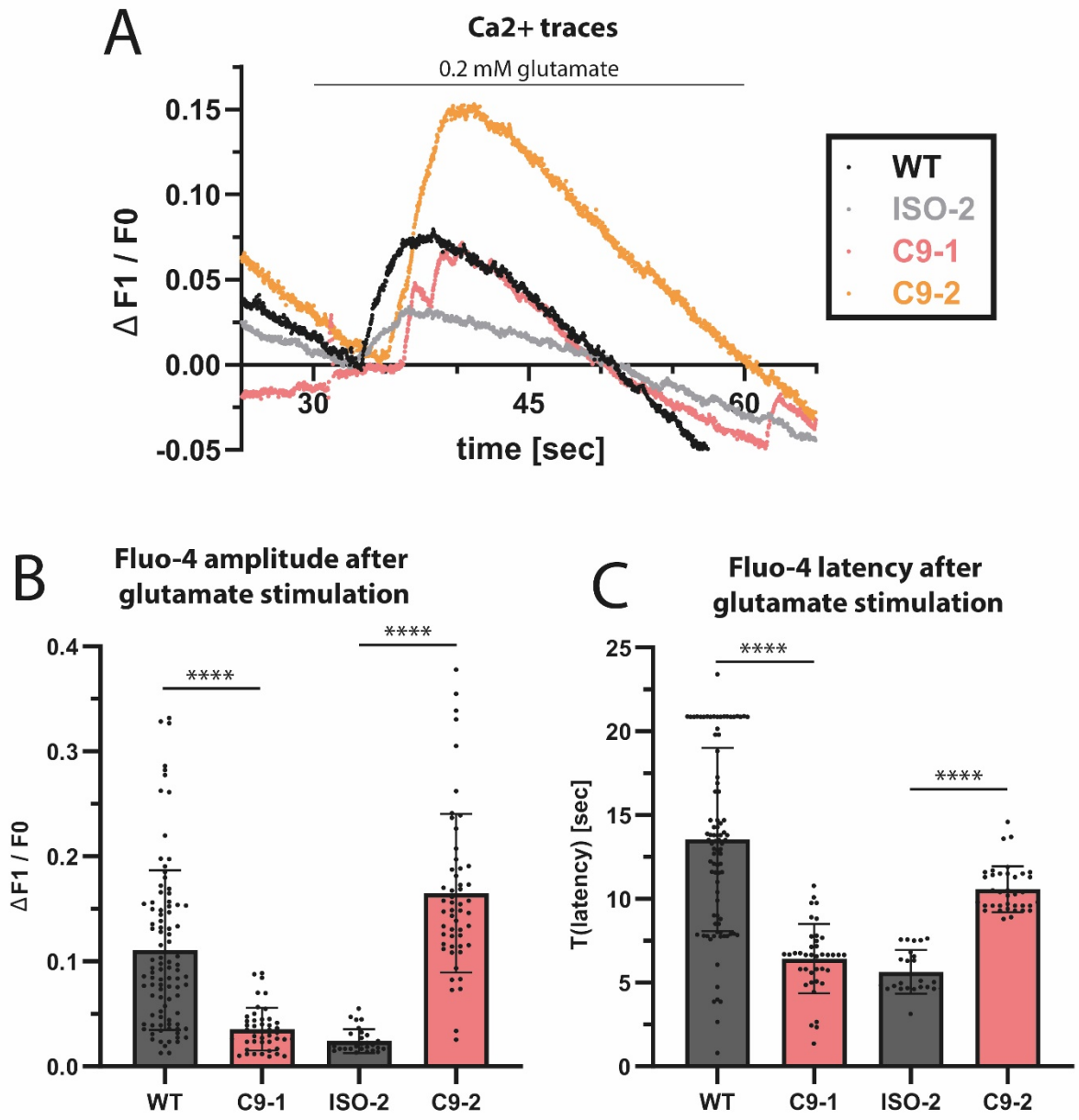


Figure 30: Glutamate-stimulated excitability is significantly altered in C9-CNs. (A) Representative Ca^{2+} traces in Fluo-4 AM loaded CNs. 0.2 mM glutamate was added after 30sec of recording for 30sec, then glutamate was washed out for 90sec. (B) The amplitude of cytosolic Ca^{2+} intake in Fluo-4 AM loaded CNs in response to glutamate stimulation. (C) The latency of cytosolic Ca^{2+} intake in Fluo-4 AM loaded CNs in response to glutamate stimulation. (A-C) The number of differentiations (n) used here was: n(WT)=5, n(C9-1)=4, n(ISO-2)=3, n(C9-2)=1. Data were analysed with one-way ANOVA using Sidak's *post-hoc* test. Each dot represents the measurements of one cell. The bars represent means. Error bars represent the standard deviation. ****p<0.0001.

Additionally, I studied cells stimulated with 50 mM KCl to gain insight into the function of VGCC to cause glutamate release. KCl stimulates both pre-synaptic VGCC, leading to the release of glutamate

into the synaptic cleft, and post-synaptic VGCC, causing an influx of Ca^{2+} into the cytosol. I identified a significant reduction in amplitude after KCl stimulation in all patient lines, which indicated either a decreased activity of pre- or post-synaptic VGCCs or a reduced response to pre-synaptic glutamate release (Figure 31). While I observed a slight reduction in latency in pooled C9-1+8 CNs, the latency of cytosolic Ca^{2+} intake after KCl stimulation was increased in the C9-2 patient line.

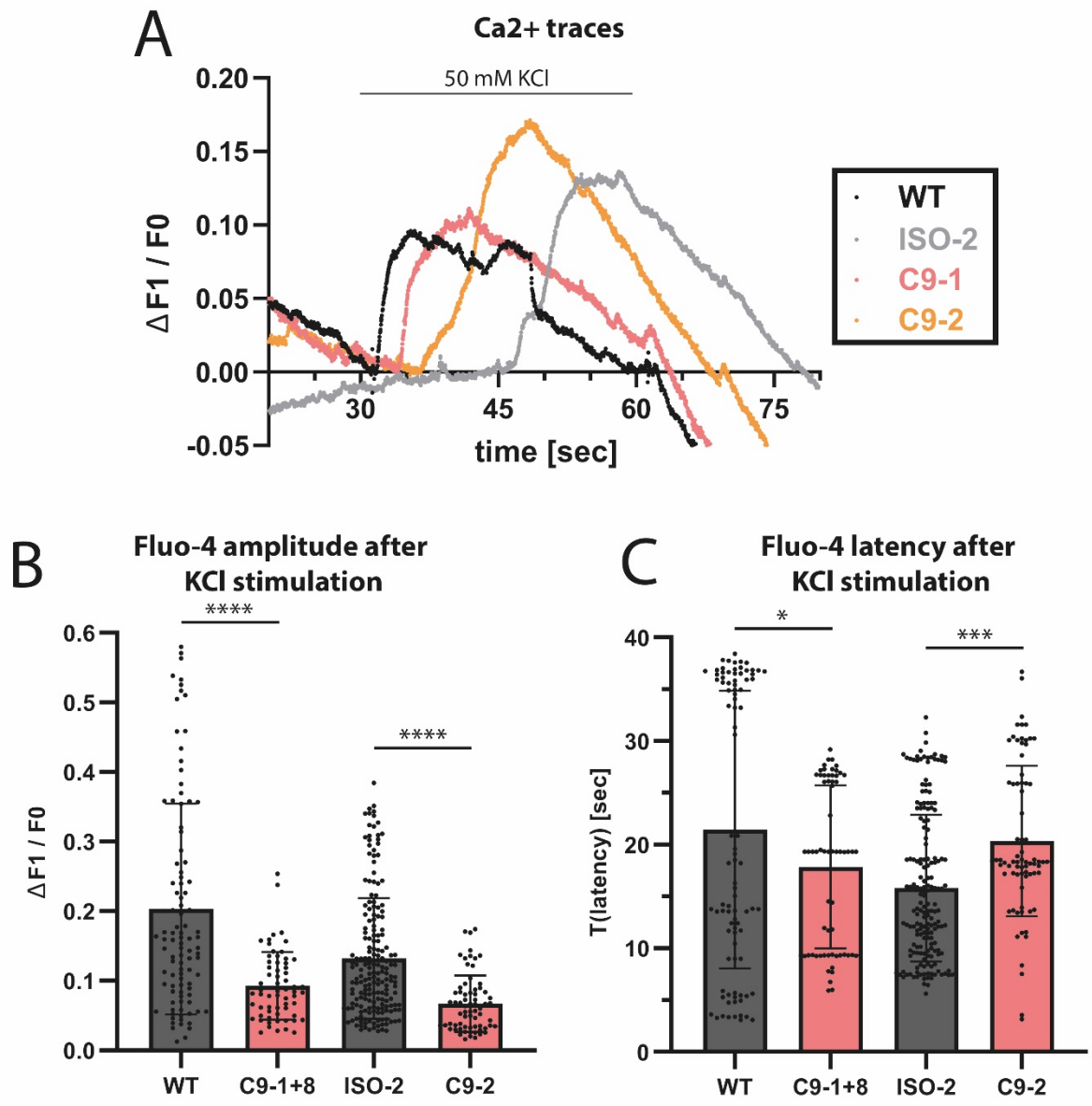


Figure 31: No consistent difference in excitability stimulated by KCl was identified between C9-CNs and control CNs. (A) Representative Ca^{2+} traces in Fluo-4 AM loaded CNs. 50 mM KCl was added after 30sec of recording for 30sec, then KCl was washed out for 90sec. (B) The amplitude of cytosolic Ca^{2+} intake in Fluo-4 AM loaded CNs in response to KCl stimulation. (C)

The latency of cytosolic Ca^{2+} intake in Fluo-4 AM loaded CNs in response to KCl stimulation. (A-C) The number of differentiations (n) used here is: n(WT)=3, n(C9-1+8)=2, n(ISO-2)=3, n(C9-2)=2. Data were analysed with one-way ANOVA using Dunnett's *post-hoc* test. Each dot represents the measurements of one cell. The bars represent means. Error bars represent the standard deviation. *p<0.05, ***p<0.001, ****p<0.0001.

In summary, the glutamate-induced excitation and its latency were reduced in the C9-1 patient line. In contrast, I found an increase in excitability and its latency after glutamate stimulation in the C9-2 line. These abnormal excitation levels hint at possible defects in glutamate receptor levels. Furthermore, the KCl-induced excitation was reduced in all C9-CNs, while the latency was reduced in pooled C9-1+8 CNs and increased in C9-2 CNs. This suggests an alteration in pre- and postsynaptic VGCC and glutamate receptor activity in these patient lines. Therefore, hypo- and hyperexcitability might contribute to C9-HRE toxicity in iPSC-derived C9-CNs.

5.2 GluA1 levels were significantly altered in iPSC-derived C9-CN

I measured the protein expression of post-synaptic Ca^{2+}-permeable receptors in the post-synapse to better understand the differences in excitability I found using calcium imaging and get a more consistent insight into neuronal excitability.

First, I measured glutamate ionotropic receptor NMDA type subunit 1 (GluN1) and glutamate ionotropic receptor AMPA type subunit 1 (GluA1) levels using Western blotting. GluN1 is a subunit of the NMDAR, making up two of four subunits. GluA1 is a Ca^{2+}-permeable subunit of AMPAR1, which plays a role in synaptic plasticity and is downregulated with increasing age (T. Lu et al., 2004). I studied GluN1 expression in untreated CNs and CNs treated with thapsigargin, which inhibits Ca^{2+} uptake into the ER, and $NaArO_2$, which causes mitochondrial damage, as cellular stressors.

I did not observe any significant differences in the expression of GluN1 between cell lines in untreated CNs and neurons treated with thapsigargin or $NaArO_2$ (see Figure 32). In thapsigargin-treated CNs, there seemed to be a downregulation of GluN1 in C9-CNs, which was not significant possibly due to

the low number of replicates. $NaArO_2$ treatment induced a significant upregulation of GluN1 levels across cell lines, but no significant differences between patient and control lines were identified.

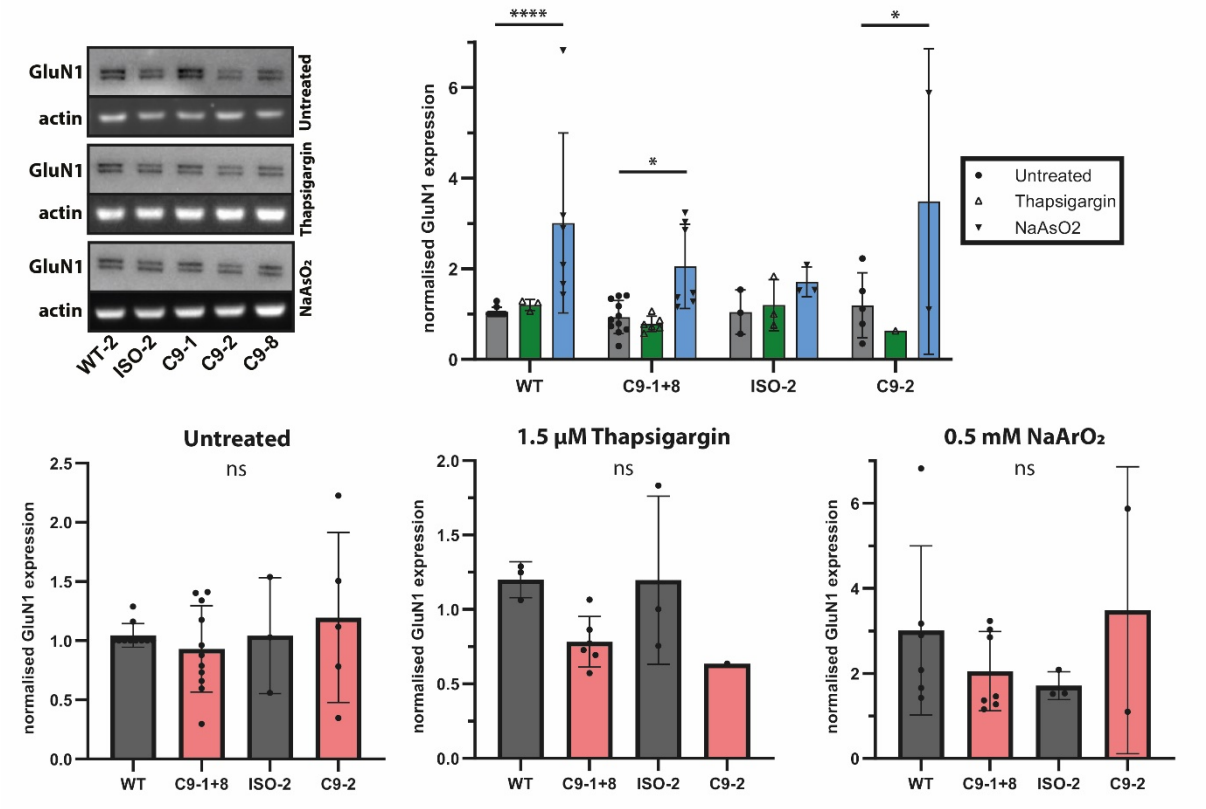


Figure 32: GluN1 levels are not significantly altered in C9-CNs. Western blot of GluN1 in untreated CNs, CNs treated with 1.5 µM thapsigargin for 24h, and CNs treated with 0.5 mM $NaArO_2$ for 1h. When comparing treatments, data were analysed with two-way ANOVA using Dunnett's *post-hoc* test. All other data were analysed with one-way ANOVA using Sidak's *post-hoc* test. The bars represent means. Error bars represent the standard deviation. Each dot represents the measured protein level from one differentiation. ns=not significant, *p<0.05, ****p<0.0001.

I used untreated cells and cells treated with thapsigargin to study GluA1. I established significantly decreased GluA1 levels in untreated pooled C9-CNs lines (Figure 33A). This change in GluA1 levels could account for the reduction in excitability and increased apoptosis in these C9-CNs. In C9-2 CNs, GluA1 seems to be slightly upregulated, albeit non-significantly, which might account for the significant hyperexcitability in response to glutamate stimulation identified in this cell line.

Treatment with thapsigargin caused a significant reduction in GluA1 levels in WT controls. However, thapsigargin treatment did not exacerbate differences in GluA1 levels between cell lines. The significant reduction in GluA1 levels in untreated pooled C9-CNs was not present in thapsigargin-treated cells, probably due to the low number of replicates.

To understand why GluA1 levels are downregulated, I decided to study GluA1 levels in the context of AMPAR recycling and degradation. I treated with the autophagy inhibitor bafilomycin and the autophagy stimulator rapamycin to determine whether those treatments exaggerate GluA1 dysregulation. Preliminary results show that the inhibition of autophagy with bafilomycin significantly increased GluA1 levels, confirming that GluA1 levels are tightly regulated by autophagy (Figure 33B). In pooled C9-CNs lines treated with the autophagy stimulator rapamycin, GluA1 levels are significantly reduced. Rapamycin treatment exacerbates the reduction in C9-CNs (84.6%) compared to untreated cells (55.9%). While this reduction is not significant due to the low number of technical replicates, preliminary results still suggest that GluA1 levels are reduced in C9-CNs due to increased degradation of AMPARs.

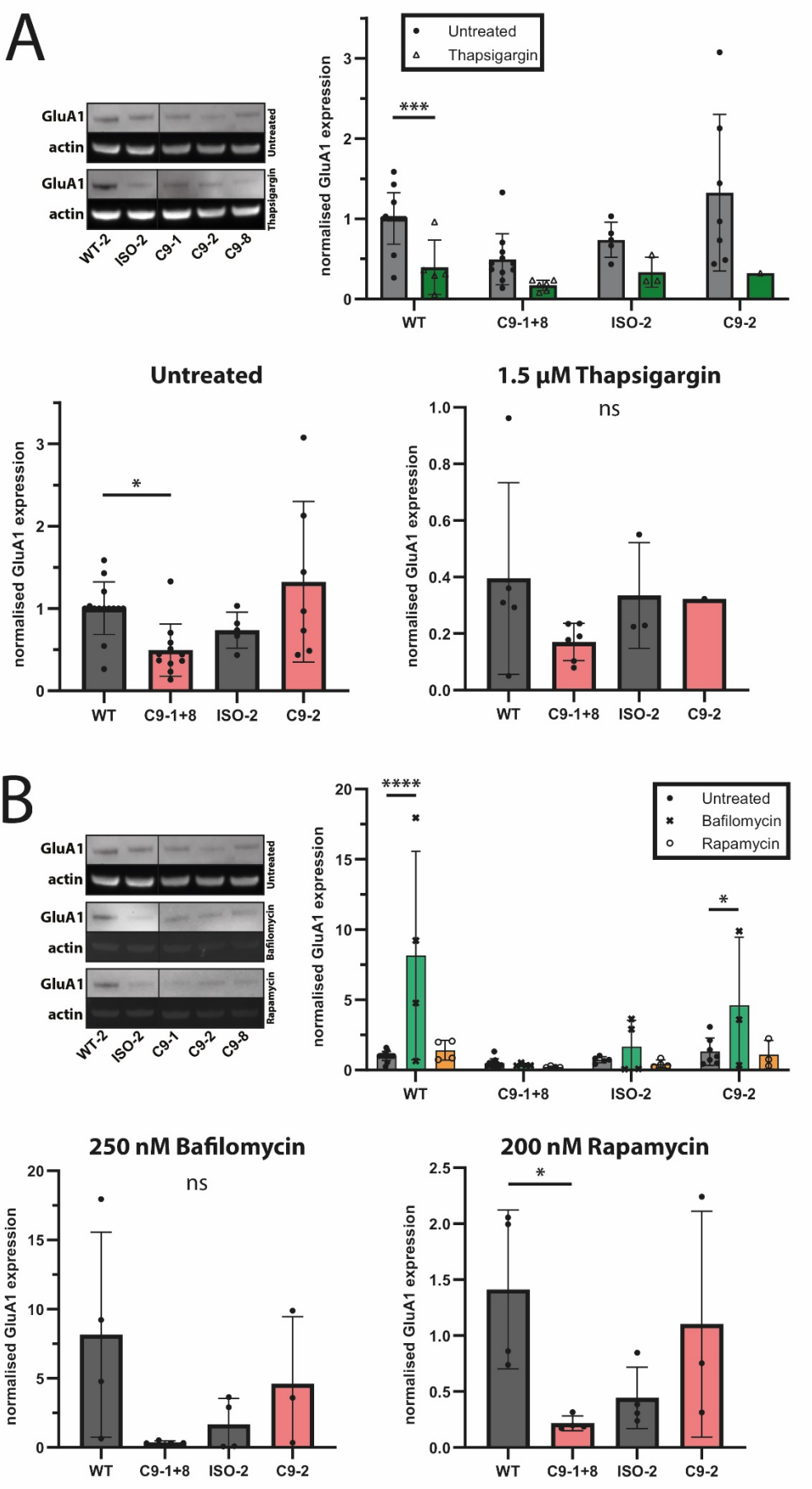

A
GluA1
actin
Untreated
GluA1
actin
Thapsigargin
WT-2
ISO-2
C9-1
C9-2
C9-8
Untreated
Thapsigargin
***
normalised GluA1 expression
WT
C9-1+8
ISO-2
C9-2
Untreated
*
1.5 µM Thapsigargin
ns
B
GluA1
actin
Untreated
GluA1
actin
Bafilomycin
GluA1
actin
Rapamycin
Untreated
Bafilomycin
Rapamycin
****
*
250 nM Bafilomycin
ns
200 nM Rapamycin
*

Figure 33: GluA1 levels are reduced in untreated C9-CNs due to increased degradation. (A) Western blot of GluA1 levels untreated CNs and CNs treated with 1.5 µM thapsigargin for 24h. (B) Western blot of GluA1 levels untreated CNs and CNs treated with 250 nM bafilomycin, or with 200 nM rapamycin for 24h. (A-B) When comparing treatments, data were analysed with two-way ANOVA using Dunnett's *post-hoc* test. All other data were analysed with one-way ANOVA using Sidak's *post-hoc* test. The bars represent means. Error bars represent the standard deviation. Each dot represents the measured protein level from one differentiation. Vertical black lines running through the images of Western blot membranes indicate where the pictures of membranes were cut making this figure to exclude additional samples. The left and right parts of the images were taken from the same pictures. ns=not significant, *p<0.05, ***p<0.001, ****p<0.0001.

Additionally, I studied the expression of post-synaptic density 95 (PSD95), a major component of glutamatergic synapses. It acts as a scaffolding protein which regulates the synaptic localisation of various channels, receptors, and signalling proteins. PSD95 regulates synaptic expression and transmission of NDMARs and AMPARs by direct or indirect interaction (Jeong et al., 2019). Preliminary results show no differences in PSD95 expression as measured using immunofluorescence in untreated CNs (Figure 34).

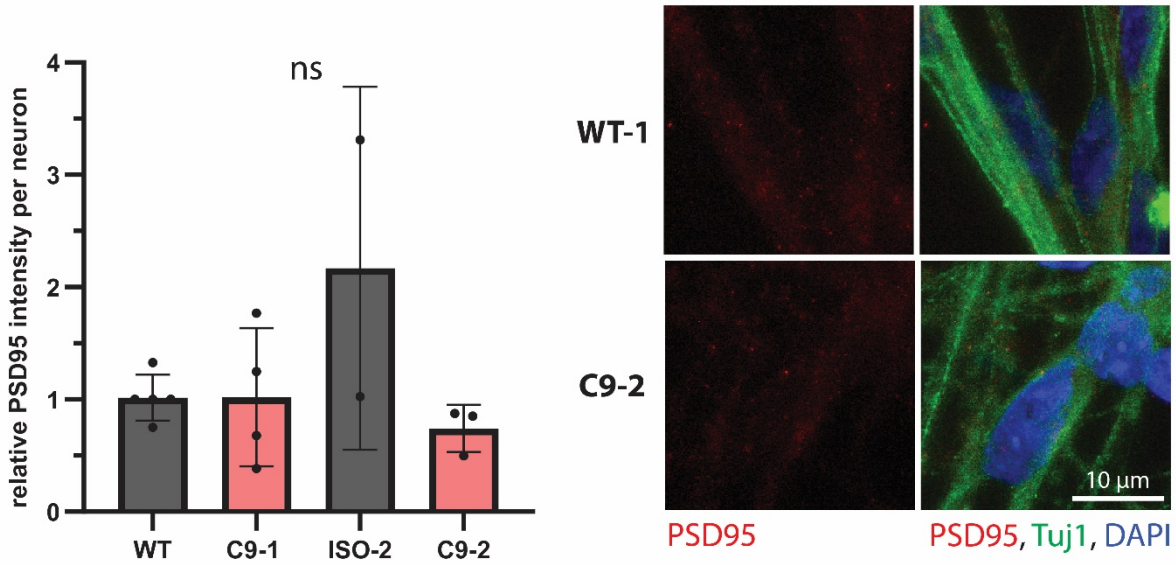


Figure 34: There are no differences in the expression of the post-synaptic protein PSD95. Immunocytochemistry of PSD95 and Tuj1. The intensity of PSD95 was measured within the Tuj1-positive area. The bars represent means. Error bars represent the standard deviation. Each dot represents the measured protein level from one differentiation. ns=not significant.

Furthermore, I measured the expression of calcium voltage-gated channel auxiliary subunit alpha 2 delta 1 (CACNA2D1), a subunit of the post-synaptic L-type VGCC, to better understand excitability in the context of KCl stimulation. To this end, I performed Western blotting with untreated cells and cells treated with thapsigargin or $NaArO_2$ as cellular stressors. $NaArO_2$ treatment caused a significant reduction in CACNA2D1 levels in pooled C9-1+8 lines (Figure 35). I did not observe any significant differences in CACNA2D1 expression between cell lines under any conditions. However, there seemed to be a non-significant increase in CACNA2D1 levels in untreated and thapsigargin-treated pooled C9-CNs, which might explain the significant reduction in latency of the Ca^{2+} influx after KCl stimulation I identified. Similarly, there seemed to be a non-significant reduction in CACNA2D1 levels in the C9-2 line across all treatment conditions, which could account for the reduction in amplitude and increase in latency of the Ca^{2+} influx after KCl stimulation. Additional technical replicates are needed to fully understand the differences in CACNA2D1 levels between C9-CNs and control lines.

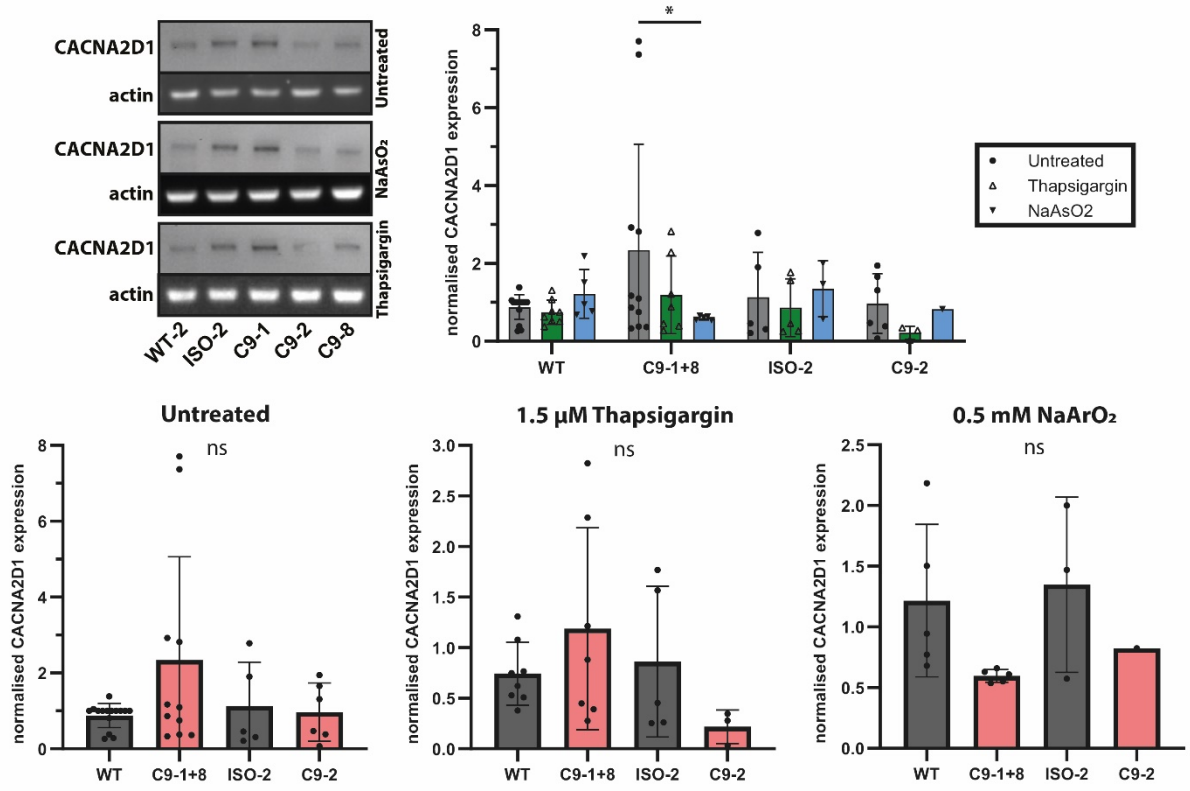


Figure 35: There are no differences in the expression of the L-type VGCC subunit CACNA2D1. Western blots of CACNA2D1 in untreated CNs, CNs treated with 1.5 µM thapsigargin for 24h, or with 0.5 mM $NaArO_2$ for 1h. When comparing treatments,

data were analysed with two-way ANOVA using Dunnett's *post-hoc* test. All other data were analysed with one-way ANOVA using Sidak's *post-hoc* test. The bars represent means. Error bars represent the standard deviation. Each dot represents the measured protein level from one differentiation. ns=not significant, *p<0.05.

To conclude, in pooled C9-1+8 CNs, no significant changes in GluN1 levels were identified, but a non-significant decrease in GluN1 levels was observed in thapsigargin-treated C9-CNs. GluA1 levels were significantly reduced in untreated CNs and CNs treated with bafilomycin. No significant changes in PSD95 and CACNA2D1 levels were observed, but CACNA2D1 expression seemed to be non-significantly increased in untreated CNs and CNs treated with thapsigargin. In C9-2 cells, no significant changes in GluN1 levels, GluA1 levels, PSD95, and CACNA2D1 levels were identified. However, CACNA2D1 levels seemed non-significantly reduced in untreated and treated CNs. Due to the high variation of measurements between differentiations, additional technical replicates are needed to understand if the non-significant changes are real. These changes in protein expression partly explain the changes in calcium imaging I observed with glutamate and KCl stimulation.

5.3 iPSC-derived C9-CNs demonstrate changes in calcium clearance

Besides an increase in excitability, defective calcium clearance from the cytosol can cause excitotoxicity. Thus, I studied the calcium clearance from the cytosol after glutamate and KCl stimulation. To this end, I measured the time between peak Ca^{2+} levels and recovery to original Ca^{2+} levels.

In pooled C9-1 and C9-8 CNs, I identified a reduction of clearance time both after glutamate and KCl stimulation (Figure 37). Since the amplitude of cytosolic Ca^{2+} influx after glutamate and KCl stimulation was greatly reduced in C9-1+8 CNs (Figure 30 and Figure 31), the smaller amount of cytosolic Ca^{2+} might be the reason for the faster clearance.

In contrast, I observed an increase in clearance time after glutamate, but not after KCl stimulation in C9-2 CNs. In this patient line, I found a greatly increased amplitude after glutamate stimulation but a

light reduction in amplitude after KCl stimulation. The significantly higher cytosolic Ca^{2+} levels might explain why I observed a higher clearance time only with glutamate stimulation and not with KCl stimulation.

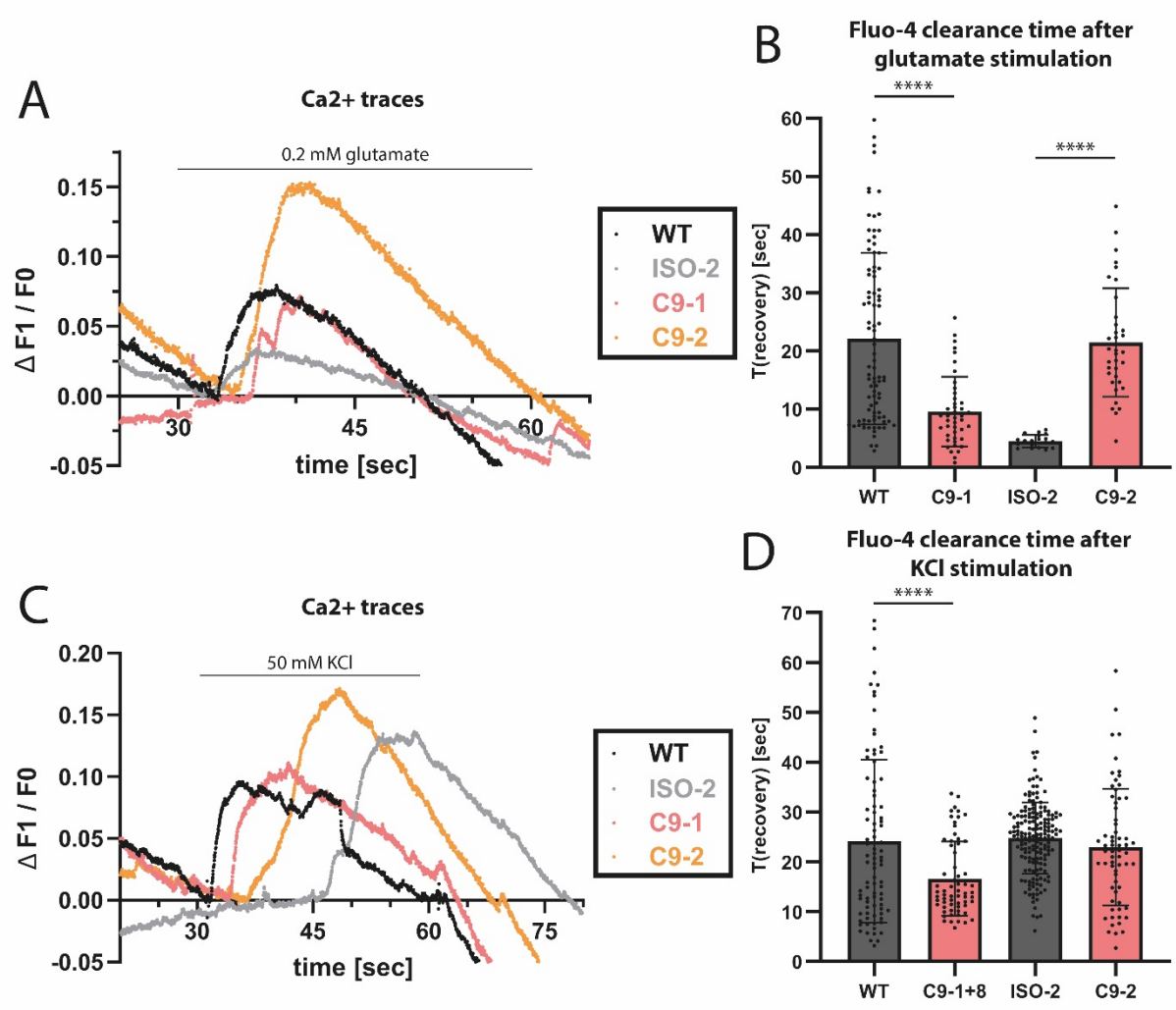


Figure 36: Calcium clearance was significantly altered in C9-CNs compared to control CNs. (A) Representative Ca^{2+} traces in Fluo-4 AM loaded CNs. 0.2 mM glutamate was added after 30sec of recording for 30sec, then glutamate was washed out for 90sec. (B) The clearance time of cytosolic Ca^{2+} in Fluo-4 AM loaded CNs stimulated with glutamate. The data is comprised of n differentiations: n(WT)=5, n(C9-1)=4, n(ISO-2)=3, n(C9-2)=1. (C) Representative Ca^{2+} traces in Fluo-4 AM loaded CNs. 50 mM KCl was added after 30sec of recording for 30sec, then KCl was washed out for 90sec. (D) The clearance time of cytosolic Ca^{2+} in Fluo-4 AM loaded CNs stimulated with KCl. The data is comprised of n differentiations: n(WT)=3, n(C9-1+8)=2, n(ISO-2)=3, n(C9-2)=2. (B+D) Data were analysed with one-way ANOVA using Sidak's *post-hoc* test. Each dot represents the measurements of one cell. The bars represent means. Error bars represent the standard deviation. ****p<0.0001.

Cytosolic Ca^{2+} is either transported into the ER by SERCA, transported out of the cell by plasma membrane Ca^{2+}-ATPase pumps or Na^{+}/Ca^{2+} exchangers, or to a lower extent, transported into mitochondria by mitochondrial calcium uniporters (MCUs) (Ivannikov et al., 2010; M. F. Wright et al., 2014; Zenisek & Matthews, 2000). As defects in calcium clearance have previously been described in C9-ALS/FTD iPSC-derived MNs due to reduced expression of MCU (Dafinca et al., 2020), I measured MCU expression levels in untreated CNs and CNs treated with $NaArO_2$ or CCCP to exaggerate any potential defects. I did not observe any significant differences in MCU levels between C9-CNs and control CNs (Figure 37).

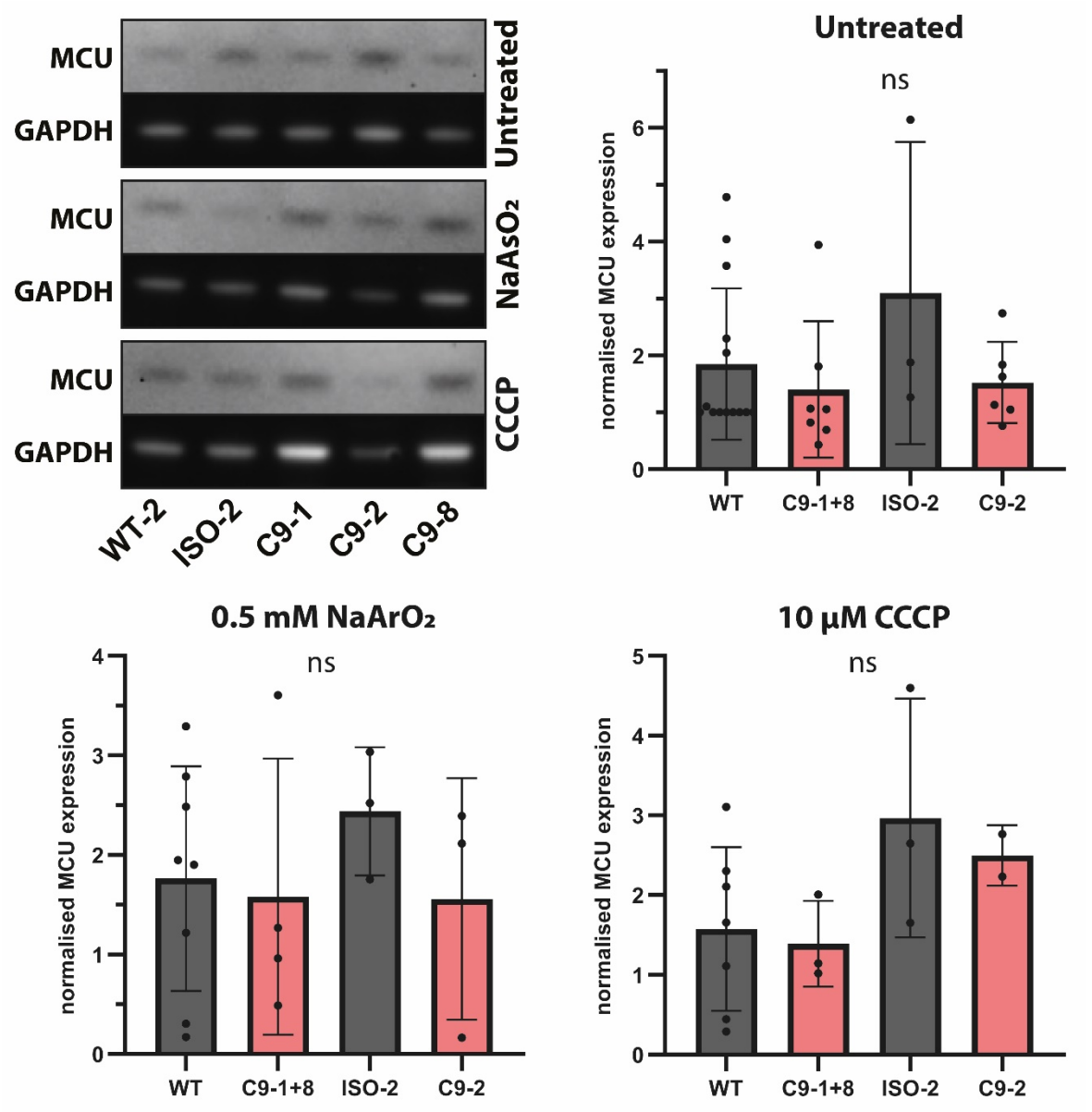


Figure 37: The expression levels of MCU are unaltered in C9-CNs. Western blots of MCU expression in untreated CNs and CNs treated with 0.5 mM $NaAsO_2$ for 1h or 10 μM CCCP for 24h. All data were analysed with one-way ANOVA using Sidak's *post-hoc* test. Each dot represents the measured protein level from one differentiation. The bars represent means. Error bars represent the standard deviation. ns=not significant.

To conclude, in the pooled C9-1+8 patient CNs, the cytosolic Ca^{2+} clearance after glutamate and KCl stimulation was reduced. In the C9-2 cell line, cytosolic Ca^{2+} clearance is prolonged after glutamate clearance. These changes in clearance time were not due to changes in MCU levels, but rather in line with the amount of Ca^{2+} influx in these cell lines.

5.4 Conclusion

I observed major deregulation of excitability in C9-CNs. When studying excitability using glutamate stimulation, I determined opposite effects between the C9-2 line and the C9-1 line. In the C9-2 patient line versus its isogenic control line, I observed a significantly increased amplitude and latency in Ca^{2+} influx after glutamate stimulation. This is most likely to be due to a non-significant increase in the levels of the AMPAR subunit GluA1, which leads to an increase in Ca^{2+}-permeable AMPARs, and possibly an increase of overall AMPAR levels in C9-2 CNs. Additionally, I found an increased clearance time after glutamate stimulation, which is probably due to the higher Ca^{2+} concentration in the cytosol.

In contrast, in C9-1 CNs, I observed a reduced amplitude and latency in Ca^{2+} influx after glutamate stimulation. We identified a significant reduction in GluA1 levels which might account for the reduction of the amplitude of Ca^{2+} influx. This reduction could point towards the increased inclusion of other, non-Ca^{2+}-permeable subunits into AMPAR, which would reduce the overall permeability of the post-synapse. Alternatively, it could represent a downregulation of AMPAR levels, for example, due to increased degradation of AMPARs. Rapamycin treatment exacerbates the reduction in pooled C9-1+8 CNs compared to untreated cells, suggesting that even though we saw no changes in the overall levels of autophagic flux, GluA1 levels or AMPAR levels could be specifically targeted by autophagy through a *C9orf72*-dependent mechanism. Alternatively, the expression levels of GluA1

could be altered on a transcriptional level in the C9-1+8 cell lines rather than due to increased AMPAR degradation. This hypothesis is supported by RNA sequencing data from C9-MNs from my laboratory, in which we saw an altered regulation of the expression of Ca^{2+} permeable glutamate receptors (Dafinca et al., 2020; Dr Ruxandra Dafinca, unpublished). Additionally, a study using iPSC-derived CNs derived from FTD patients with various genetic backgrounds also observed changes in the expression of AMPAR subunits at a transcriptional level (Gascon et al., 2014). The reduction in excitability in C9-CNs could also partially be due to a non-significant decrease in the NMDAR subunit GluN1, which I observed in thapsigargin-treated cells. I also found a reduced clearance time after glutamate stimulation, which is probably linked to the reduced cytosolic Ca^{2+} content rather than an abnormal expression of ion channels responsible for Ca^{2+} clearance.

Differences in excitability between patient lines might be due to differences in maturity. A previous study discovered that C9-MNs first display hyperexcitability followed by a gradual loss in synaptic activity and action potential output the longer cells are kept in culture (Devlin et al., 2015). I did not observe major differences in maturity on day 55-60, which is the age of the neuronal cultures used here. Still, subtle differences in maturity might affect the excitability of cell lines.

An alternative explanation of why the phenotype of the C9-2 cell line differs from other patient lines are the chromosomal aberrations identified in the C9-2 and ISO-2 cell line towards the end of my experimental time. However, the same cell lines were used for an excitability study in C9-MNs at around the same time I worked with these cells. In this study, the excitability phenotype of the C9-1 and C9-2 cell lines were the same (Dafinca et al., 2020). Thus, either chromosomal aberrations affect iPSC-derived CNs more than iPSC-derived MNs, or the differences in phenotypes could be due to the genetic heterogeneity between patients which is only apparent in cortical neurons.

In cells stimulated with KCl, the amplitude of cytosolic Ca^{2+} influx was reduced in all patient cell lines. Accordingly, the time needed to clear cytosolic Ca^{2+} from C9-CNs was significantly reduced in the pooled C9-CNs, which is probably directly linked to the low level of cytosolic Ca^{2+} in C9-CNs. KCl

stimulates both pre-synaptic VGCC causing a release of glutamate, and post-synaptic VGCC causing the increase of cytosolic Ca^{2+}. Therefore, differences in calcium imaging using KCl can be due to changes in pre-synaptic VGCCs, post-synaptic VGCCs, and post-synaptic glutamate receptors. Untangling the causes of changes in cytosolic Ca^{2+} influx after KCl stimulation is complex. We have observed a downregulation in glutamate receptors in pooled C9-1+8 CNs, which might account partially or fully for any changes in excitability in KCl stimulation for these cell lines. For the C9-2 cell lines, however, changes in VGCC levels might account for the reduced amplitude of cytosolic Ca^{2+} influx. However, we identified no significant changes in the CACNA2D1 subunit of post-synaptic L-type VGCCs. Increased technical replicates might make some of the non-significant differences in CACNA2D1 levels significant and might help to understand the changes in cytosolic Ca^{2+} influx after KCl stimulation.

No major differences in the latency of cytosolic Ca^{2+} influx were recorded, but the latency was slightly reduced in pooled C9-1+8 CNs and slightly increased in C9-2 CNs. The increase in latency in C9-2 patient lines might mean that the Ca^{2+} influx into the cytosol is mainly due to Ca^{2+}-activated presynaptic glutamate release rather than due to direct stimulation of post-synaptic VGCC, thus causing a delay in amplitude. In contrast, the reduced latency in pooled C9-CN implies that in these cell lines, the Ca^{2+} influx into the cytosol is mainly due to the direct stimulation of post-synaptic VGCC.

While studies have observed changes in cortical excitability in C9-ALS/FTD patients, specifically cortical hyperexcitability (Geevasinga et al., 2015), few studies exist studying excitability in cellular human FTD models. One study using FTD iPSC-derived CNs identified the upregulation of transcripts encoding for the GluA2 and GluA4 but not GluA1 and GluA3 AMPAR subunits causing an imbalance between Ca^{2+}-permeable and impermeable AMPARs (Gascon et al., 2014). While this study did not observe a reduction in GluA1 subunits as I identified in this study, my findings could also suggest an imbalance between Ca^{2+}-permeable and impermeable AMPARs.

Comparing the excitability phenotype in C9-CNs to C9-MNs, I found marked differences. The Ca^{2+} amplitude after glutamate stimulation was reduced in C9-1 and C9-2 MNs (Dafinca et al., 2020), similar to C9-1 CNs but not C9-2 CNs in my experiments. Cytosolic calcium clearance after glutamate stimulation was increased in C9-1 and C9-2 MNs (Dafinca et al., 2020), similar to C9-2 CNs but not C9-1 CNs. Assessing expression levels of glutamatergic receptors showed a reduced expression of GluA1 in C9-MNs (Dafinca et al., 2020). In C9-CNs, I observed a significant reduction in GluA1 in pooled C9-1+8 CNs, but not in C9-2 CNs. The Ca^{2+} amplitude after KCl stimulation was increased in C9-1 and C9-2 MNs (Dafinca et al., 2020), while in my experiments, the Ca^{2+} amplitude was reduced in pooled C9-1+8 CNs and C9-2 CNs. Cytosolic calcium clearance after KCl stimulation was increased in C9-1 and C9-2 MNs (Dafinca et al., 2020), while it was increased in C9-2 CNs and reduced in pooled C9-1+8 CNs, supporting the finding that C9-CNs have a unique excitability phenotype which differs from C9-MNs.

6 Mitochondrial processes are significantly altered in C9-ALS/FTD-derived CNs

Mitochondrial dysfunction is associated with neurodegenerative diseases, such as Parkinson's disease, Alzheimer's disease, and Huntington's disease (Islam, 2016; Johri & Beal, 2012). In addition, various studies have established that mitochondrial function is affected in ALS. One study using fibroblasts from sporadic ALS patients found an increase in mitochondrial polarisation and a decrease in mitochondrial content (Kirk et al., 2014). Another study using fibroblasts from C9-ALS patients has shown an increase in oxygen consumption, mitochondrial hyperpolarisation, and a rise in ROS and ATP (Onesto et al., 2016). Results from my lab using C9-MNs showed structural changes to mitochondria and a reduction in mitochondrial membrane potential (Dafinca et al., 2016). More recent experiments showed decreased basal respiration and ATP production in C9-MNs (Dr Ruxandra Dafinca, unpublished; Dr Paola Barbagallo, unpublished). Mechanistically, $(GR)_{80}$ has been identified to bind to mitochondrial ribosomal proteins and cause oxidative stress in iPSC-derived C9-motor neurons (Lopez-

Gonzalez et al., 2016). As mitochondrial function has not been studied in detail in C9-FTD cortical neurons, I assess mitochondrial polarisation, mitochondrial mass, respiration, and oxidative stress.

Several studies established aberrant fusion and fission and mitochondrial morphology as ALS phenotypes. In my group, we observed both enlarged mitochondria and cristae, as well as increased mitochondrial fragmentation in the C9-2 line in iPSC-derived MNs (Dr Ruxandra Dafinca, unpublished; Dafinca et al., 2016). Additionally, it has been shown that the expression level of TDP43 correlates to the length and density of mitochondria in the neurites of cultured primary neurons (W. Wang et al., 2013). Therefore, I study the fusion and fission apparatus in FTD cortical neurons.

In addition, various pieces of evidence have been uncovered pointing towards the involvement of axonal transport in ALS disease mechanisms. In post-mortem tissue, an abnormal accumulation of kinesins, cargos, and hyperphosphorylated neurofilaments has been observed in the soma of motor neurons (de Vos & Hafezparast, 2017). In *C9orf72* drosophila models, altered transport of mitochondria and ER vesicles have been identified (Baldwin et al., 2016). However, experiments from my group using C9-MNs did not show any significant changes in the speed or direction of mitochondrial axonal transport (Dr Jakub Scaber, unpublished). The contribution of axonal transport to FTD disease mechanisms is little understood.

Aberrant regulation of mitophagy is associated with neurodegeneration pathologies, such as Parkinson's Disease, Alzheimer's Disease, and Huntington's Disease (Burman et al., 2012; Greene et al., 2003; Martinez-Vicente, 2017; Pesah et al., 2004; Y. Yang et al., 2006). In ALS and FTD, several disease-associated mutations affect proteins associated with mitophagy, for example, TBK1 and OPTN (Oakes et al., 2017; Weil et al., 2018). Even though mitochondrial membrane depolarisation has been identified in ALS which triggers mitophagy, mitophagy has not been studied in ALS or FTD.

In summary, despite the overwhelming evidence that mitochondrial defects contribute to C9-toxicity, the contribution of mitochondrial defects to FTD pathology has not previously been studied in detail

in cellular C9-FTD models. Therefore, this chapter aims to establish whether the function of mitochondrial is altered in iPSC-derived C9-CNs by investigating:

1. Mitochondrial fusion and fission machinery in C9-CNs
2. The mitochondrial mass in C9-CNs
3. The mitochondrial membrane potential in C9-CNs
4. Mitophagic flux in C9-CNs.
5. ROS levels in C9-CNs
6. Mitochondrial respiration in C9-CNs
7. Axonal transport of mitochondria in C9-CNs

6.1 Mitochondrial fission apparatus proteins are downregulated in stressed iPSC-derived C9-CNs

Structural changes in mitochondria are commonly associated with ALS. My group observed both enlarged mitochondria and cristae and increased mitochondrial fragmentation in the C9-2 line in iPSC-derived MNs (Dr Ruxandra Dafinca, unpublished; Dafinca et al., 2016). I would require electron microscopy images of these iPSC-derived CNs to understand mitochondrial morphology fully. However, due to time constraints, I was not able to conduct electron microscopy experiments. Still, I gained some insight into mitochondrial fusion and fission by studying the proteins involved in those processes. DRP1 is responsible for mitochondrial fission, while Mfn2 is essential for mitochondrial fusion. DRP1 is located in the cytosol and translocates to mitochondria upon stimulus (Jo et al., 2017). Mfn2 is a protein of the OMM. It is mainly located in mitochondria, with a small portion located in the ER membrane (Casellas-D Iaz et al., 2021).

Mitochondrial fusion and fission can be cellular coping mechanisms for low-level mitochondrial stress. Stressed mitochondria fuse with healthy mitochondria to correct mitochondrial homeostasis. Fission is a necessary process to create new mitochondria and enables the removal of damaged mitochondria (Youle & van der Bliek, 2012). Therefore, I treated iPSC-derived CNs with the mitochondrial stressors $NaAsO_2$ or CCCP to exacerbate any potential fission or fusion defects.

Indeed, P-DRP1 levels are significantly increased in cells treated with $NaAsO_2$ for 1h compared to untreated cells, confirming that CNs upregulate fission as a coping mechanism for intense short-term mitochondrial dysfunction. I did not observe an upregulation in the pooled C9-1+8 patient lines, pointing towards an altered stress response in those patient lines. In untreated CNs, I saw no significant differences in P-DRP1 levels between cell lines, the activated form of DRP1 (Figure 38). However, in cells treated with $NaAsO_2$, I identified a significant downregulation of P-DRP1, implying that stressed C9-CNs are unable to upregulate fission as a coping mechanism against mitochondrial stress to generate new mitochondria. Fission is not upregulated in cells treated with CCCP for 24h, suggesting that for long-term mitochondrial stress, fission is not upregulated.

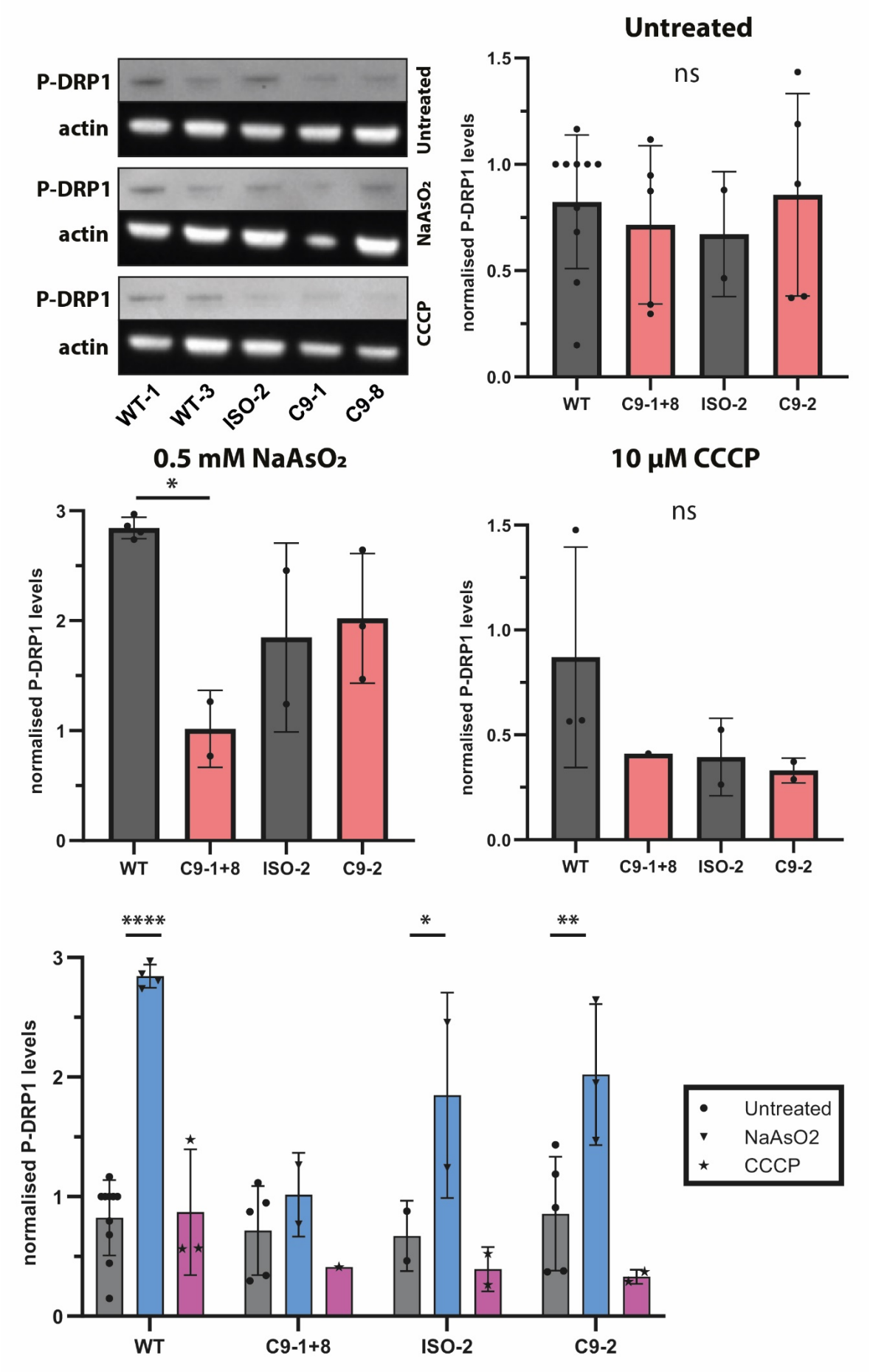

P-DRP1
actin
Untreated
P-DRP1
actin
NaAsO₂
P-DRP1
actin
CCCP
WT-1
WT-3
ISO-2
C9-1
C9-8
Untreated
ns
normalised P-DRP1 levels
1.5
1.0
0.5
0.0
WT
C9-1+8
ISO-2
C9-2
0.5 mM NaAsO₂
*
normalised P-DRP1 levels
3
2
1
0
WT
C9-1+8
ISO-2
C9-2
10 µM CCCP
ns
normalised P-DRP1 levels
1.5
1.0
0.5
0.0
WT
C9-1+8
ISO-2
C9-2
****
*
**
normalised P-DRP1 levels
3
2
1
0
WT
C9-1+8
ISO-2
C9-2
Untreated
NaAsO2
CCCP

Figure 38: P-DRP1 levels are significantly reduced in pooled C9-CNs treated with $NaAsO_2$ for 1h. Western blot of P-DRP1 in untreated CNs, CNs treated with 0.5 mM $NaAsO_2$ for 1h or 10 μM CCCP for 24h. When comparing treatments, data were analysed with two-way ANOVA using Dunnett's *post-hoc* test. All other data were analysed with one-way ANOVA using Sidak's *post-hoc* test. The bars represent means. Error bars represent the standard deviation. Each dot represents the measured protein level from one differentiation. ns=not significant, *p<0.05, **p<0.01.

I determined no significant changes in Mfn2 levels in untreated or treated C9-CN (Figure 39).

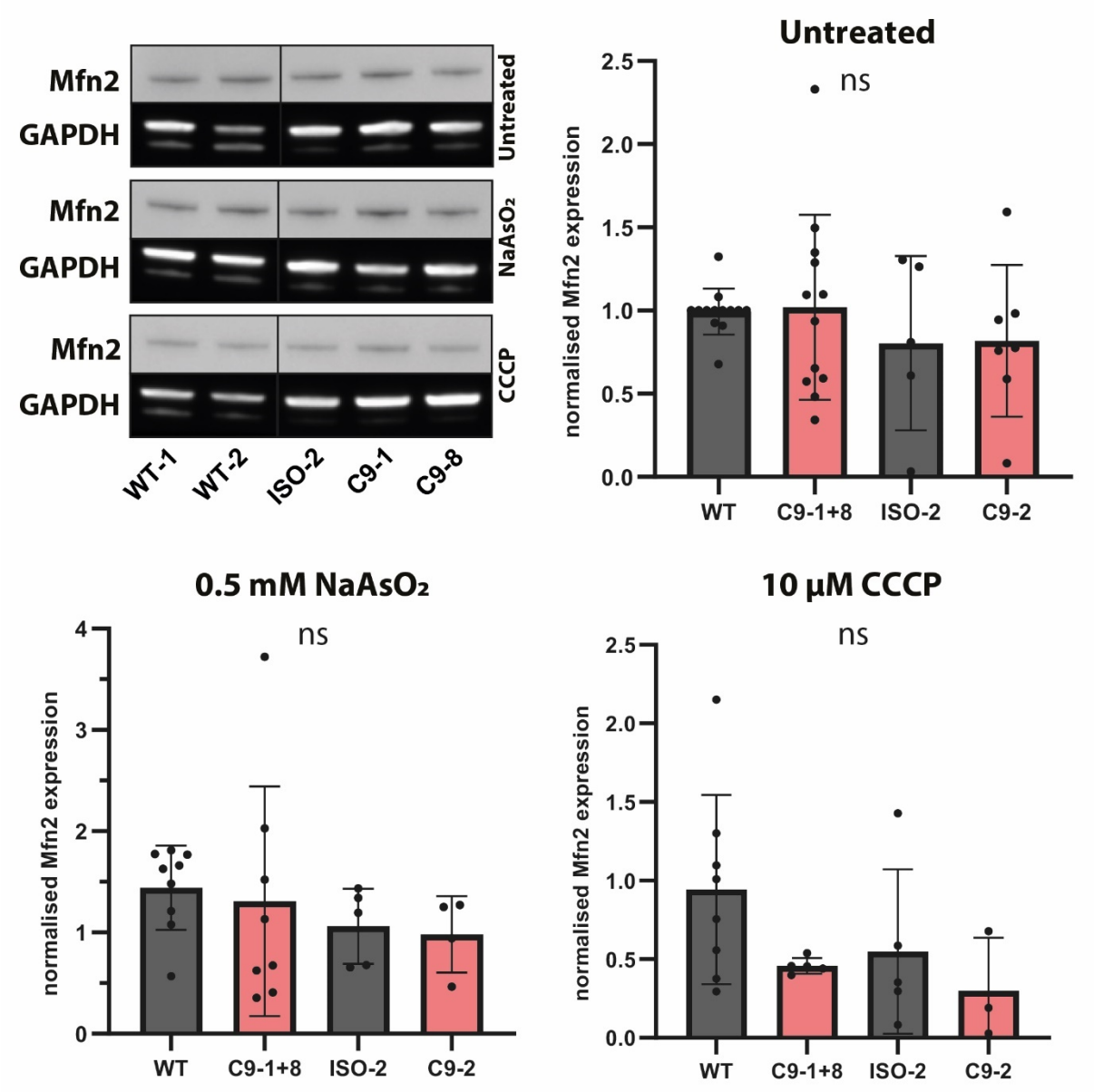


Figure 39: Mfn2 levels are not significantly changed in C9-CNs. Western blot of Mfn2 in untreated CNs, CNs treated with 0.5 mM $NaAsO_2$ for 1h or 10 μM CCCP for 24h. Data were analysed with one-way ANOVA using Sidak's *post-hoc* test. The bars represent means. Error bars represent the standard deviation. Each dot represents the measured protein level from one

differentiation. Vertical black lines running through the images of Western blot membranes indicate where the pictures of membranes were cut making this figure to exclude additional samples. The left and right parts of the images were taken from the same pictures. ns=not significant.

To conclude, I identified a significant decrease in P-DRP1 in C9-CNs treated with $NaAsO_2$, suggesting impaired fission in C9-CNs during mitochondrial stress. This might cause morphological changes in mitochondria and insufficient coping mechanisms for mitochondrial stress. I saw no changes in Mfn2 levels in patient CNs.

6.2 The mitochondrial mass is reduced in iPSC-derived C9-CNs

I studied mitochondrial mass to establish whether the quantity of mitochondria differs between control lines and C9-CNs, as changes in mitochondrial mass affect the energy generation of cells.

To this end, I measured the expression of mitochondrial proteins from several mitochondrial compartments. The OMM protein TOMM20 is involved in importing proteins produced by cytosolic ribosomes into mitochondria. Cytochrome C oxidase subunit 4 (COX IV) is a protein in the inner mitochondrial membrane, which is part of the respiratory chain. COX IV is nuclear-encoded (Barrientos et al., 2002). Both proteins are commonly used to measure mitochondrial mass. I treated iPSC-derived CNs to exacerbate mitochondrial defects with the mitochondrial stressors $NaAsO_2$ or CCCP. $NaAsO_2$ stresses mitochondria by inhibiting the ATP synthase, which causes oxidative stress and protein leak (Hong & Pedersen, 2008; X. Jiang et al., 2013; Luz et al., 2016). CCCP inhibits oxidative phosphorylation by decoupling the mitochondrial proton gradient. It causes mitochondrial depolarisation and mitophagy (Demine et al., 2019).

Both TOMM20 and COX IV levels were significantly downregulated in pooled C9-1+8 CN lines compared to WT controls in untreated cells (Figure 40). This indicates that the mitochondrial mass is reduced in C9-1+8 CNs compared to healthy controls. In cells treated with $NaAsO_2$ or CCCP, no significant effect was observed. For the Western blots of cells treated with mitochondrial stressors,

the number of replicates was lower and the standard deviation higher than in Western blots using untreated CNs. This is the most likely explanation of why I observed a significant decrease in TOMM20 and COX IV levels in untreated but not in treated CNs.

24h of CCCP treatment seems to increase mitochondrial protein levels. This effect is significant in pooled C9-1+8 CNs for TOMM20 and in WT controls and C9-1+8 CNs for COX IV. 1h of $NaAsO_2$ treatment induced a loss of TOMM20 in WT lines. In contrast, 1h of $NaAsO_2$ treatment leads to an increase in COX IV levels in C9-1+8 CNs and ISO-2 CNs. As $NaAsO_2$ inhibits the ATP synthase, cells might quickly upregulate the levels of respiratory chain proteins despite the potential initiation of mitophagy. No significant changes in the sensitivity to treatments were observed in C9-CNs for TOMM20 and COX IV.

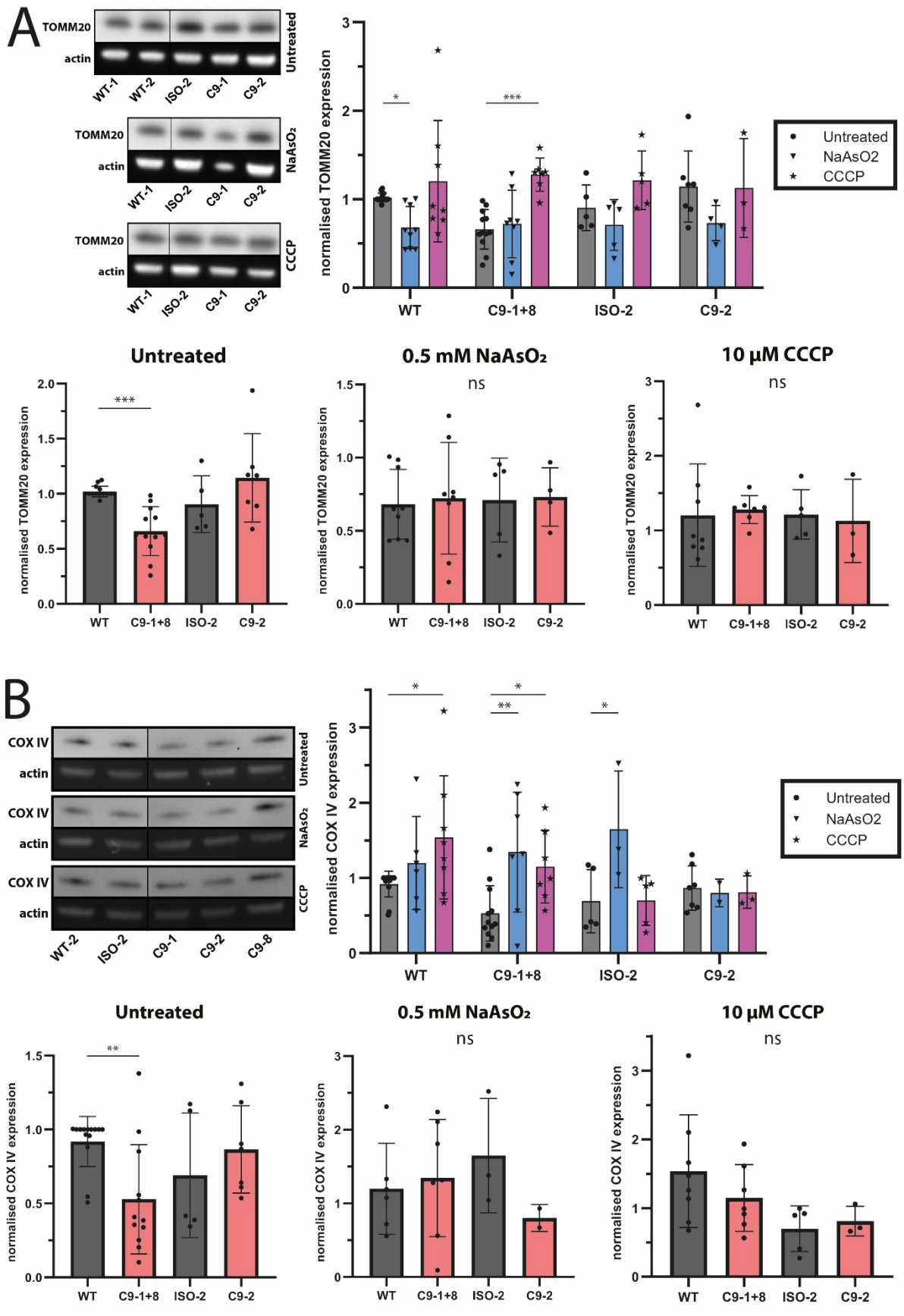

A
TOMM20
actin
Untreated
NaAsO₂
CCCP
WT-1
WT-2
ISO-2
C9-1
C9-2
normalised TOMM20 expression
Untreated
NaAsO2
CCCP
WT
C9-1+8
ISO-2
C9-2
0.5 mM NaAsO₂
10 µM CCCP
ns
B
COX IV
actin
WT-2
ISO-2
C9-1
C9-2
C9-8
normalised COX IV expression

Figure 40: TOMM20 and COX IV levels are significantly decreased in untreated C9-CNs. (A) Western blot of TOMM20 in untreated CNs, CNs treated with 0.5 mM $NaAsO_2$ for 1h or 10 μM CCCP for 24h. (B) Western blot of COX IV in untreated CNs, CNs treated with 0.5 mM $NaAsO_2$ for 1h or 10 μM CCCP for 24h. (A-B) When comparing treatments, data were analysed with two-way ANOVA using Dunnett's *post-hoc* test. All other data were analysed with one-way ANOVA using Sidak's *post-hoc* test. The bars represent means. Error bars represent the standard deviation. Each dot represents the measured protein level from one differentiation. Vertical black lines running through the images of Western blot membranes indicate where the pictures of membranes were cut making this figure to exclude additional samples. The left and right parts of the images were taken from the same pictures. ns=not significant, *p<0.05, **p<0.01, ***p<0.001.

I also analysed TOMM20 expression using immunocytochemistry (Figure 41). No significant changes in TOMM20 levels were identified, which might be due to the low number of replicates. Note the changes in mitochondrial morphology after treatment with $NaAsO_2$ for 1h, which might suggest changes in mitochondrial tethering upon mitochondrial stress in all cell lines.

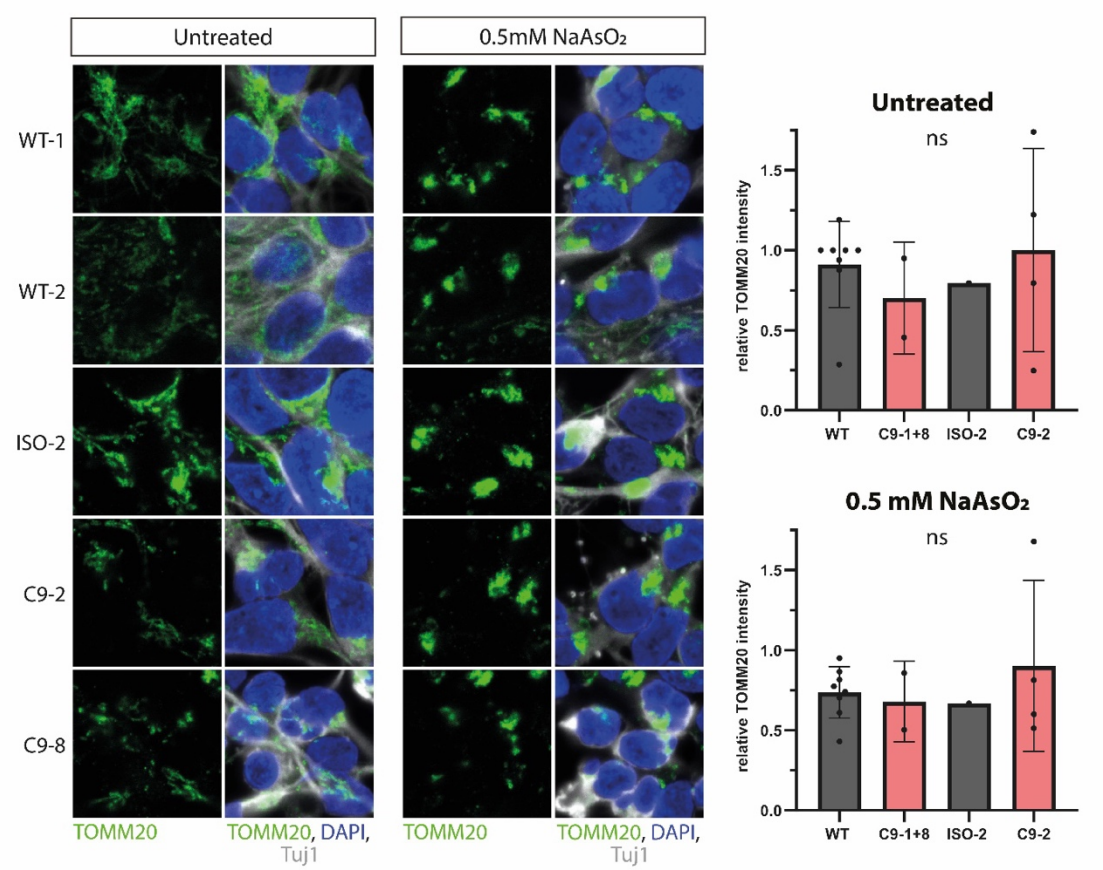


Figure 41: anti-TOMM20 stains mitochondria and shows no loss of mitochondrial mass. Representative confocal images of CNs stained with TOMM20 (green), Tuj1 (white) and DAPI on the left. Quantification of confocal images from untreated CNs

and CNs treated with 0.5 mM $NaAsO_2$ for 1h on the right. Data were analysed with one-way ANOVA using Sidak's *post-hoc* test. The bars represent means. Error bars represent the standard deviation. Each dot represents the value measured from one differentiation. ns=not significant

To conclude, I observed a reduction in mitochondrial proteins in C9-CNs using Western blotting, which most likely points toward a reduction in mitochondrial mass. This might be due to the increased degradation of mitochondria via mitophagy as a result of oxidative stress and mitochondrial depolarisation.

6.3 The mitochondrial membrane potential is reduced in iPSC-derived C9-CNs

I measured mitochondrial polarisation to investigate whether the reduction in mitochondrial protein levels is due to reduced mitochondrial membrane potential, which causes mitophagy. To this end, I stained cells with MitoTracker™ Red CMXRos before fixation. This dye stains polarised mitochondria. Thus I measured mitochondrial polarisation by analysing the intensity of MitoTracker. To exacerbate any potential differences in mitochondrial polarisation, I treated cells with $NaAsO_2$.

I observed significant depolarisation of mitochondria in all C9-CNs in untreated CNs (Figure 42). In cells treated with $NaAsO_2$, this reduction was not significant, probably due to the lower number of technical replicates. This indicates strongly that mitochondrial defects are present in C9-CNs.

Mitochondrial depolarisation acts as a trigger for mitophagy, which leads to a reduction in mitochondrial mass. Interestingly, I observed mitochondrial depolarisation both in the C9-CNs in which I established a loss of mitochondrial mass, and in the C9-2 patient line in which I observed no changes in mitochondrial mass.

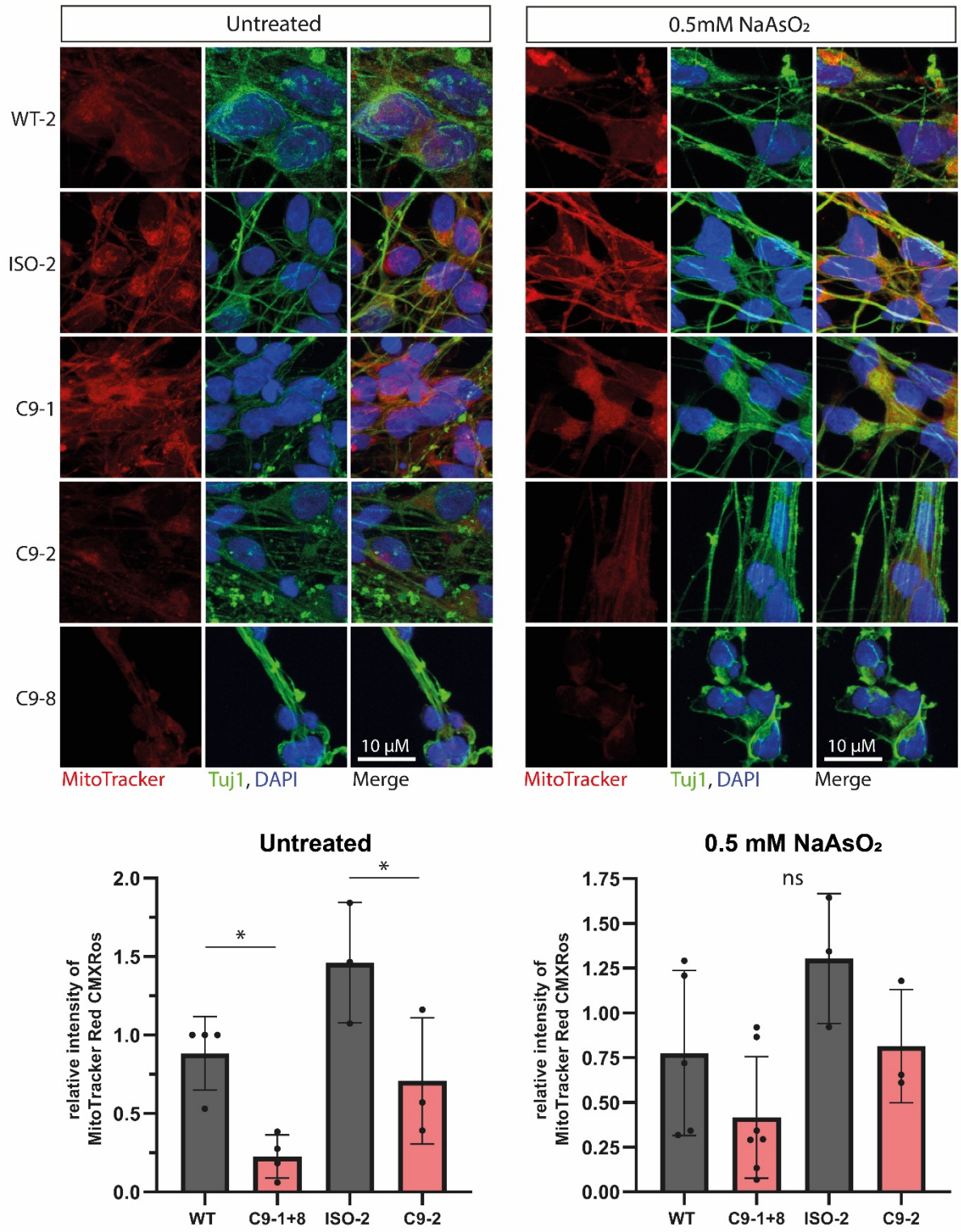


Figure 42: The mitochondrial potential is significantly reduced in untreated C9-CNs. Representative confocal images of CNs stained with MitoTracker™ Red CMXRos (red), Tuj1 (green) and DAPI at the top. The intensity of MitoTracker was measured in the TOMM20+ area to correct for the reduction in mitochondrial mass. Data were analysed with one-way ANOVA using

Sidak's *post-hoc* test. The bars represent means. Error bars represent the standard deviation. Each dot represents the measured MitoTracker intensity from one differentiation. ns=not significant, *p<0.05.

6.4 Mitophagy initiators were upregulated in iPSC-derived C9-CNs after 24h CCCP treatment

I studied proteins involved in mitophagy initiation to establish if the established depolarisation of mitochondria causes mitophagy, which would explain the reduction in mitochondrial markers in the pooled C9-1+8 cell lines. As explained in 1.2.3.8 Mitophagy, PINK1 levels increase as a result of mitochondrial depolarisation, which initiates mitophagy. PINK1 activates parkin by phosphorylating ubiquitin at serin 65. Parkin thus tags mitochondria for degradation by forming ubiquitin chains on OMM proteins, which are phosphorylated at serin 65 (P-Ub (Ser65)) by PINK1. Since CCCP induces mitochondrial depolarisation, it is commonly used to initiate mitophagy in *in vitro* experiments. Here, cells were treated with CCCP for 24h to exaggerate any differential mitophagy initiation.

Indeed, C9-1+8 CNs were overly sensitive to CCCP treatment, causing upregulated PINK1 levels specifically in C9-1+8 CNs compared to untreated cells (Figure 43A). PINK1 levels were significantly increased in CCCP-treated pooled C9-1+8 CNs compared to WT controls. Similarly, CCCP treated induced a significant increase in P-Ub (Ser65) in pooled C9-1+8 CNs compared to untreated cells, but not in other cell lines (Figure 43B). P-Ub (Ser65) levels were not significantly increased in pooled C9-1+8 CNs compared to WT controls, however, they seemed non-significantly increased in both untreated and CCCP-treated cell lines, suggesting that with additional technical replicates, this effect could be significant. Additionally, treating cells with CCCP for 6h instead of 24h could reveal a stronger upregulation of PINK1 and P-Ub (Ser65), as changes in PINK1 and P-Ub (Ser65) levels after mitophagy stimuli are time-dependent and peak at around 6h (data not shown).

The upregulation of mitophagy initiators and increased response to CCCP treatment indicates that the mitochondrial depolarisation in this cell line triggers mitophagy, which causes a decrease in mitochondrial mass.

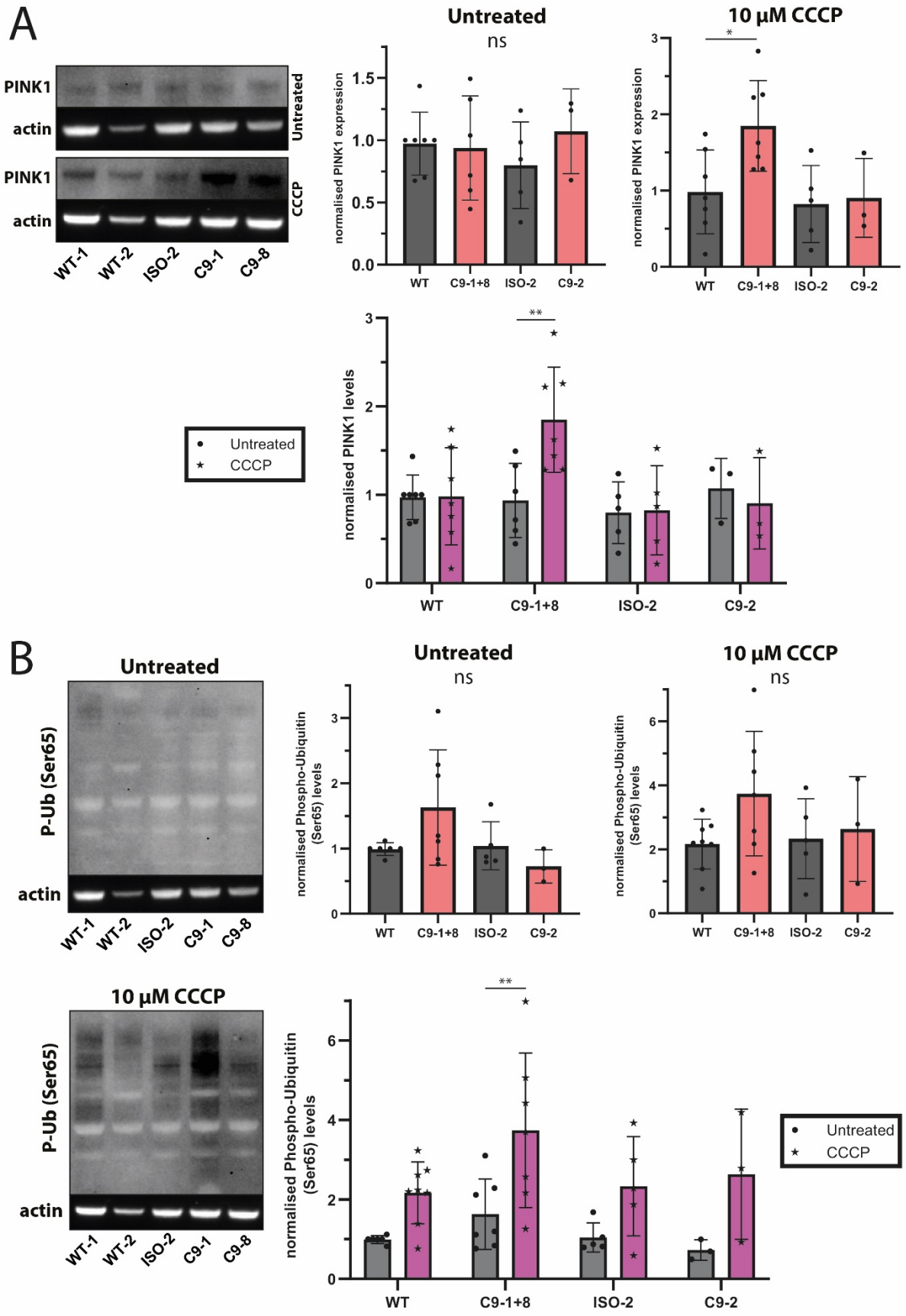

A
PINK1
actin
Untreated
PINK1
actin
CCCP
WT-1
WT-2
ISO-2
C9-1
C9-8
Untreated
ns
normalised PINK1 expression
WT
C9-1+8
ISO-2
C9-2
10 µM CCCP
*
normalised PINK1 expression
WT
C9-1+8
ISO-2
C9-2
**
normalised PINK1 levels
Untreated
CCCP
WT
C9-1+8
ISO-2
C9-2
B
Untreated
P-Ub (Ser65)
actin
WT-1
WT-2
ISO-2
C9-1
C9-8
Untreated
ns
normalised Phospho-Ubiquitin (Ser65) levels
WT
C9-1+8
ISO-2
C9-2
10 µM CCCP
ns
normalised Phospho-Ubiquitin (Ser65) levels
WT
C9-1+8
ISO-2
C9-2
10 µM CCCP
P-Ub (Ser65)
actin
WT-1
WT-2
ISO-2
C9-1
C9-8
**
normalised Phospho-Ubiquitin (Ser65) levels
Untreated
CCCP
WT
C9-1+8
ISO-2
C9-2

Figure 43: PINK1 and P-Ub (Ser65) levels are significantly upregulated in C9-CNs. (A) Western blot of PINK1 in untreated CNs and CNs treated with 10 mM CCCP for 24h. (B) Western blot of P-Ub (Ser65) in untreated CNs and CNs treated with 10 mM CCCP for 24h. (A-B) When comparing treatments, data were analysed with two-way ANOVA using Dunnett's *post-hoc* test. All other data were analysed with one-way ANOVA using Sidak's *post-hoc* test. The bars represent means. Error bars represent the standard deviation. Each dot represents the measured protein level from one differentiation. ns=not significant, *p<0.05, **p<0.01.

6.5 Reactive oxygen species levels are not increased in iPSC-derived C9-CNs

The mitochondrial depolarisation I established in C9-CNs might be caused by increased ROS levels. ROS may be produced by pro-oxidant enzymes or aberrant OXPHOS and ultimately cause cell death in C9-CNs. To establish whether ROS levels are increased in C9-CNs, I used a ROS Red Assay and normalised the results to the quantity of cells, which I measured using a CyQUANT GR Cell Proliferation Assay.

Cells were grown and differentiated in 96-well plates, which was technically challenging. I observed by visual examination that the percentage of neuronal cells in the wells was lower than when neural progenitor cells were differentiated in different formats. Since other cell types are less reliant on mitochondrial OXPHOS for their energy metabolism, non-neuronal cells might produce less ROS and might be less affected by it. Therefore, the lower neuronal yield across all wells makes this data less reliable as non-neuronal cells skew data. To minimise the impact of non-neuronal cells on this data, I excluded wells that seemed to contain an abundance of undifferentiated cells from my data, as judged using light microscopy. I treated cells with the mitochondrial stressors $NaAsO_2$ or CCCP to exacerbate ROS production. Due to time limitations, I only gained preliminary data of 1-2 differentiations per cell line.

I did not observe any significant differences in ROS levels between control lines and C9-CNs (Figure 44). ROS levels seemed to be slightly increased in C9-2 CNs, but due to the low number of technical replicates, this potential difference is impossible to interpret. The one measurement of ROS in the C9-

1 cell line is at an equal level to WT controls. Additional replicates are needed to draw any meaningful conclusions from this experiment.

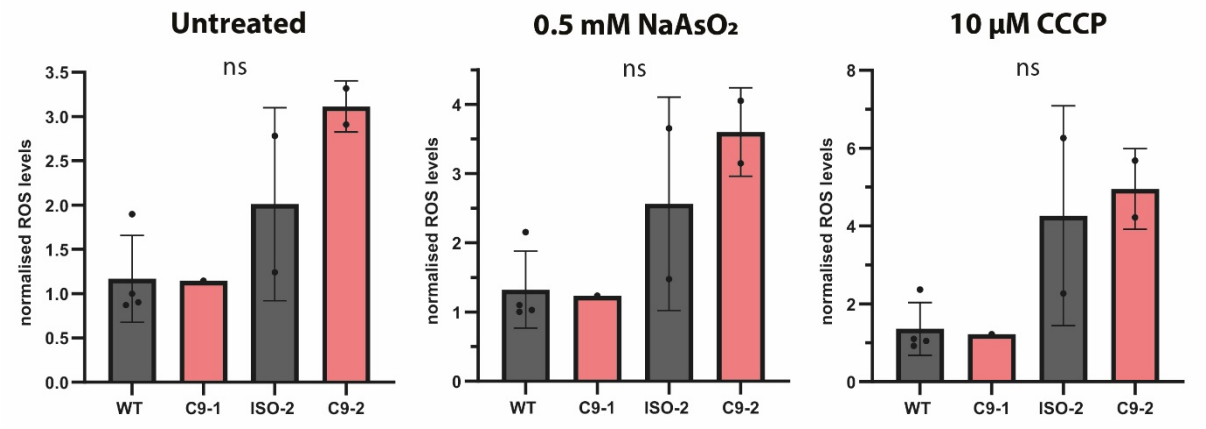


Figure 44: No significant differences in cellular ROS levels between C9-CNs and control CNs were found. ROS Red Assay measurements normalised to CyQUANT GR Cell Proliferation Assay measurements of CNs in different cell lines in untreated CNs, CNs treated with $NaAsO_2$, or with CCCP. Data were analysed with one-way ANOVA using an unpaired two-sided t-test. The bars represent means. Error bars represent the standard deviation. Each dot represents the value measured from one differentiation. ns=not significant.

6.6 Mitochondrial respiration is not altered in iPSC-derived C9-CNs

I investigated defects in mitochondrial energy production to measure whether the established mitochondrial defects, such as mitochondrial depolarisation and reduced levels of mitochondrial respiration proteins, cause a reduction in mitochondrial energy metabolism. Equally, assessing mitochondrial respiration will give us insight into whether mitochondrial dysfunction contributes to mitochondrial depolarisation and loss of mitochondrial mass.

To this end, I used the Seahorse XF Cell Mito Stress Test and normalised the results to the quantity of cells, which I determined using a CyQUANT GR Cell Proliferation Assay. The oxygen consumption rate (OCR) was measured over 73min in which cells were treated with several compounds. Oligomycin inhibits the ATP synthase and reduces all electron flow apart from the electron flow through proton leak. FCCP enables protons to cross the inner mitochondrial membrane along the proton gradient.

Rotenone inhibits mitochondrial complex I, thus blocking electron flow and causing the accumulation of electrons in the mitochondrial matrix. A range of parameters was calculated from the resulting OCR curves. I treated iPSC-derived CNs with the mitochondrial stressors $NaAsO_2$ or CCCP to exacerbate mitochondrial defects.

Again, cells were grown and differentiated in 96-well plates, which was technically challenging (see Chapter 6.5). Since other cell types are less reliant on mitochondrial OXPHOS for their energy metabolism, non-neuronal cells might skew the data. I excluded wells that seemed to contain an abundance of undifferentiated cells from my data, as judged using light microscopy. Still, the lower neuronal yield across all wells makes this data less reliable. Due to these differences in the quality of cells between differentiations, data from multiple differentiations varied widely (Figure 45).

I did not find any significant differences in basal respiration, maximum respiration, ATP production, spare respiratory capacity, proton leak, and non-mitochondrial oxygen consumption between control and patient lines under any treatment conditions. Additionally, there were no significant differences between untreated and treated cells, including treatment with $NaAsO_2$ which induces a high number of stress granules in all cell lines, and treatment with CCCP which causes the upregulation of mitophagy initiators.

This data suggests that C9-CNs are capable of normal mitochondrial energy metabolism despite the reduction in mitochondrial membrane potential and mitochondrial mass. However, the high standard deviation resulting from impure cell cultures might mask actual biological differences in mitochondrial function.

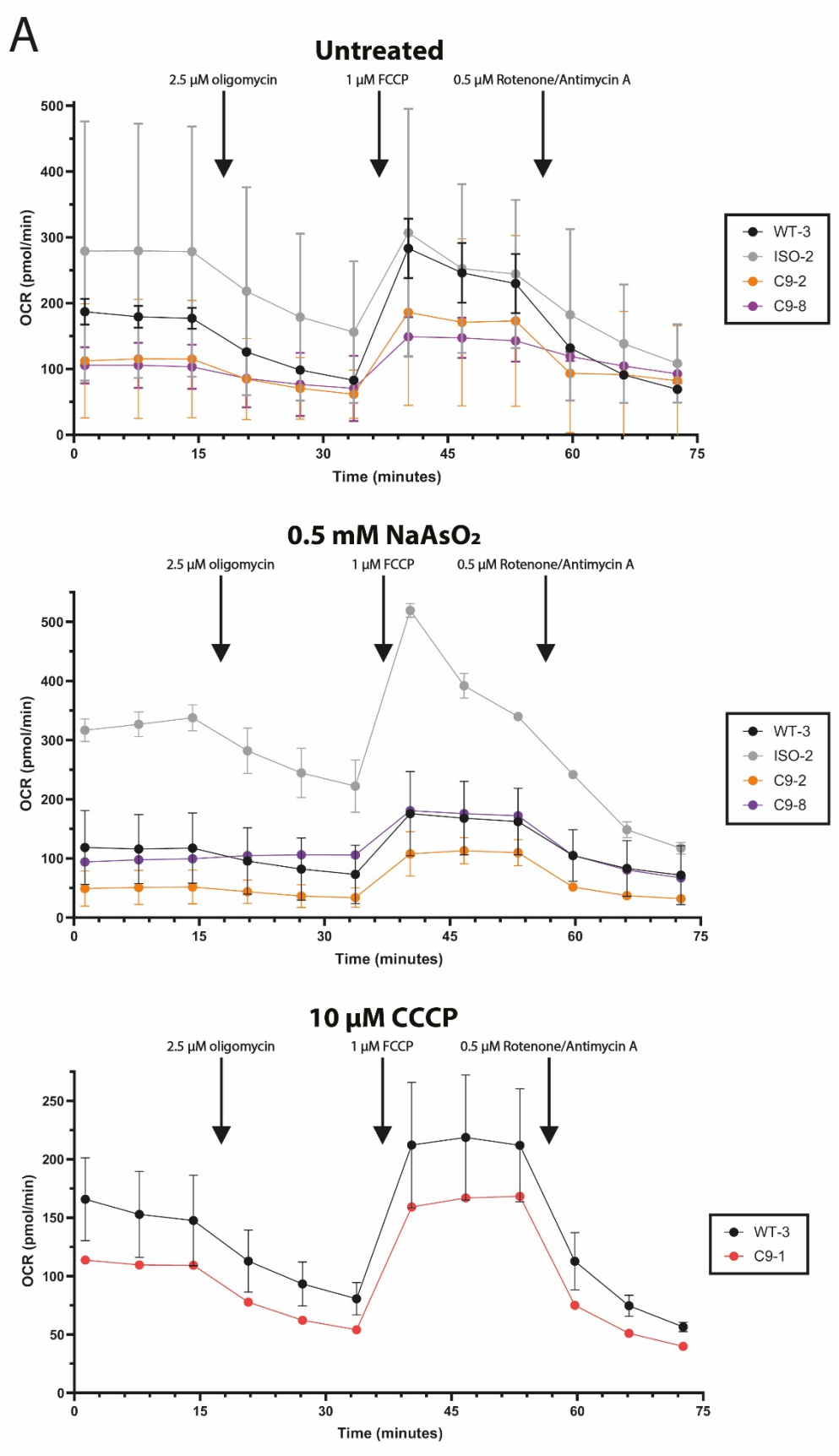


Figure 45A: continued.

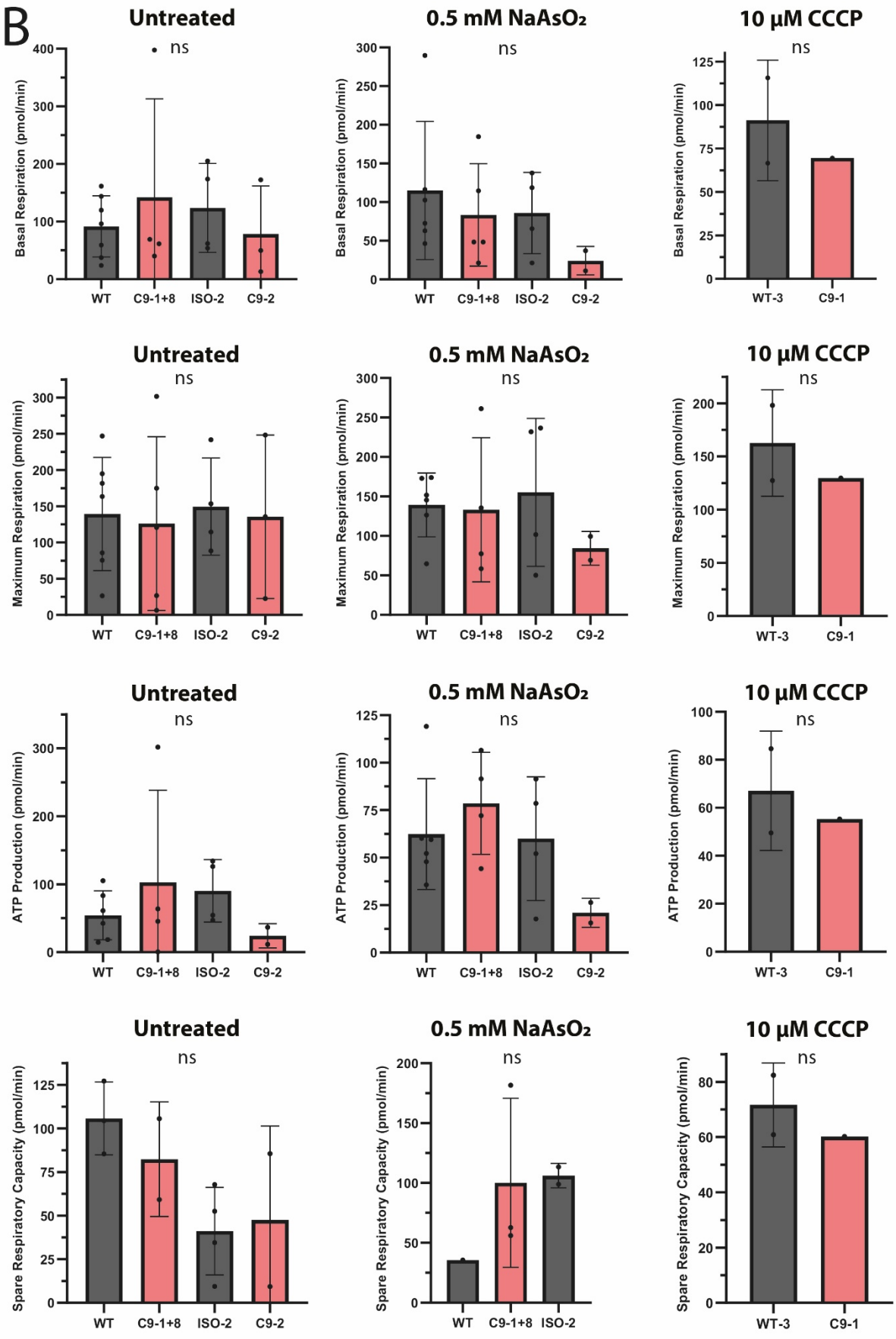


Figure 45B: continued.

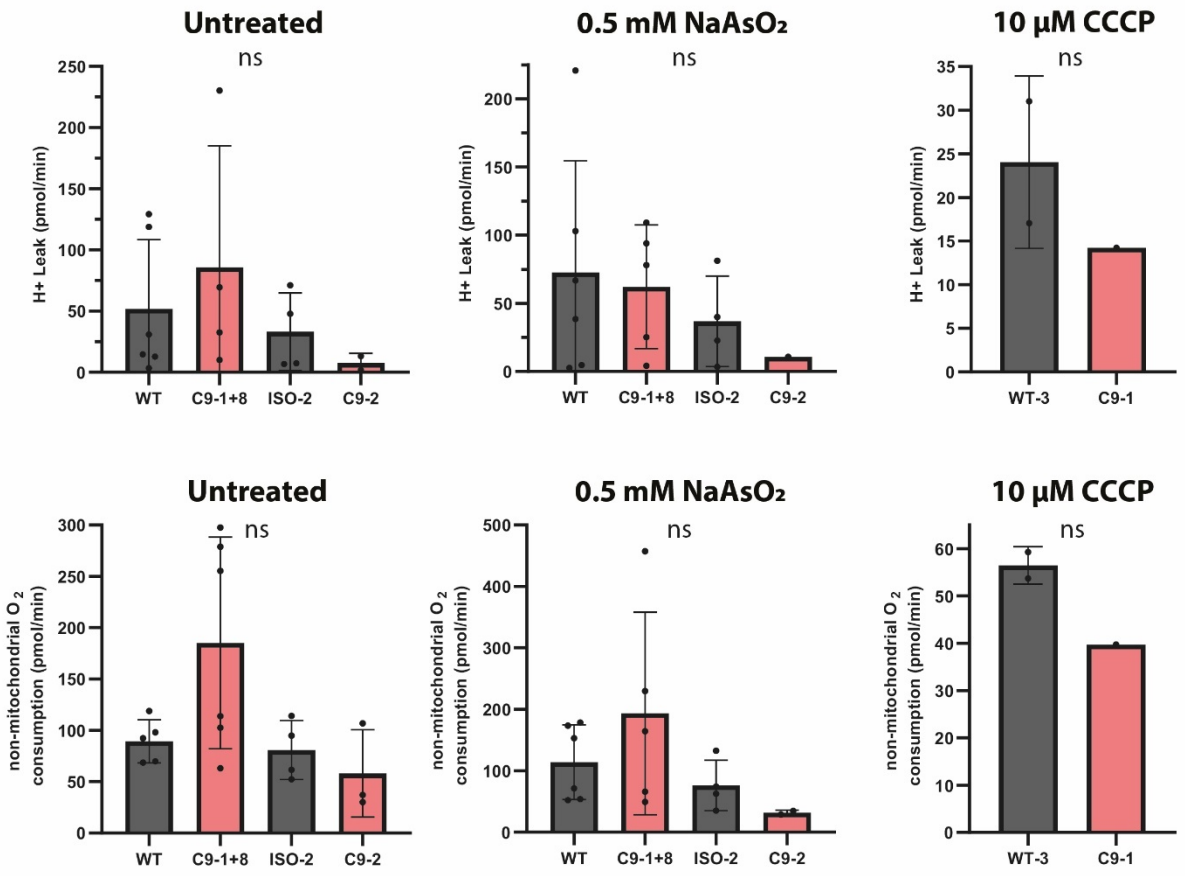


Figure 45: Mitochondrial respiration is not altered in C9-CNs. (A) Representative examples of oxygen consumption rate measured in different cell lines in untreated CNs, CNs treated with $NaAsO_2$, or with CCCP. (B) Various parameters were derived from OCR measurements. Data were analysed with one-way ANOVA using Sidak's *post-hoc* test. The bars represent means. Error bars represent the standard deviation. Each dot represents the value measured from one differentiation. ns=not significant.

6.7 The anterograde axonal transport machinery is overexpressed in iPSC-derived C9-CNs

Defects in axonal mitochondrial transport are commonly associated with ALS, while the role of axonal transport in FTD pathology is not well understood. Therefore I studied mitochondrial transport by Western blotting of microtubule-associated motor proteins and by live imaging of cells stained with MitoTracker™ Green FM. I treated CNs with the mitochondrial stressors $NaAsO_2$ or CCCP to exacerbate mitochondrial defects.

Dynactin subunit 1 (DCTN1) is involved in retrograde axonal transport, while KIF5a is the motor protein of anterograde transport. I observed no marked differences in DCTN1 levels between cell lines (Figure 46A). For KIF5a, I determined a significant upregulation of KIF5a expression in pooled C9-1+8 CNs in CCCP-treated cells (Figure 46B).

This upregulation of KIF5a expression might cause increased transport of mitochondria to synapses to compensate for dysfunctional mitochondria. In cells treated with CCCP, mitochondria are depolarised and degraded via mitophagy. Under this condition, KIF5a is significantly upregulated in C9-1+8 CNs to compensate for the lost mitochondria in synapses. Conversely, axonal transport requires ATP. Thus, mitochondrial dysfunction also limits axonal transport by not providing enough ATP.

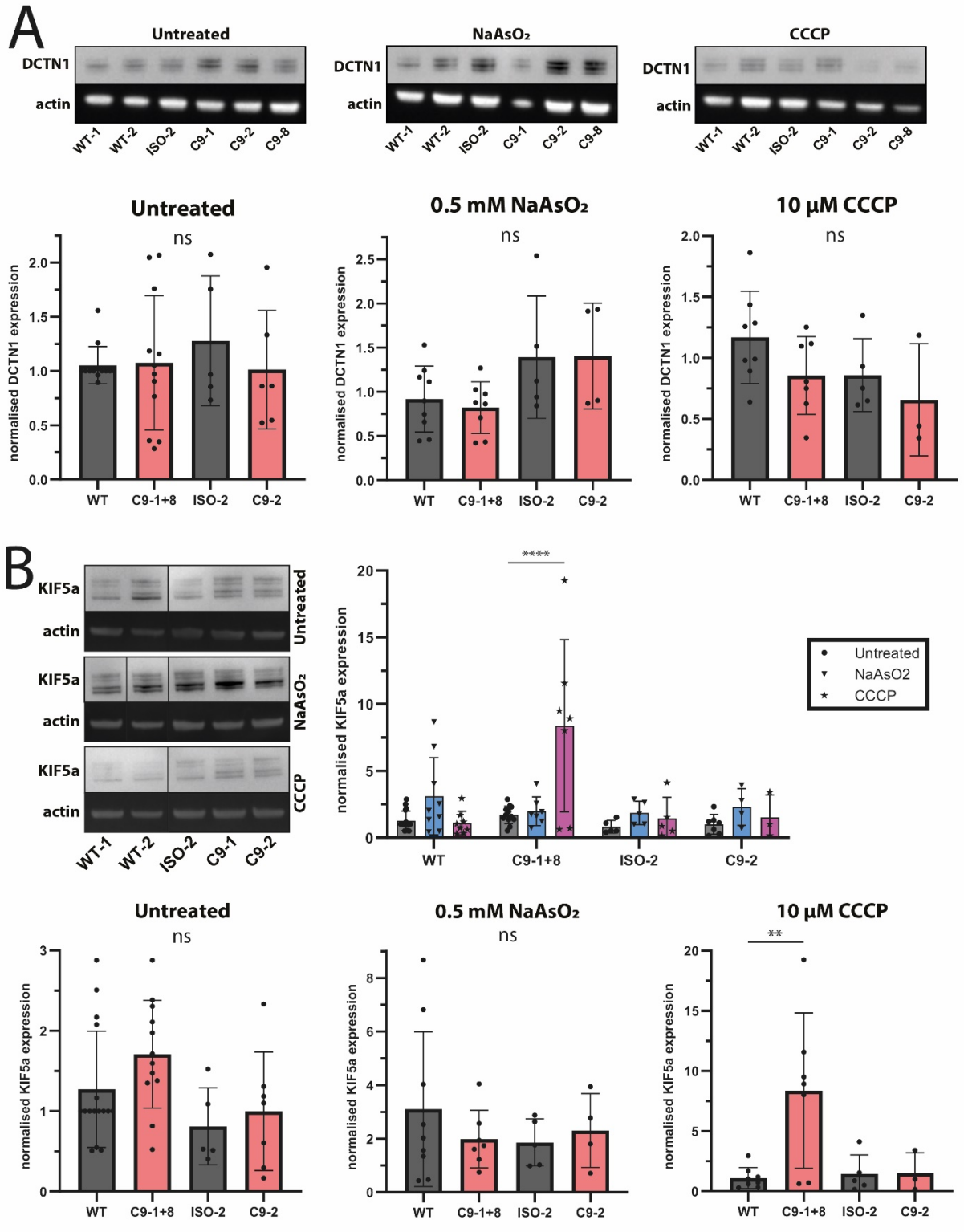


Figure 46: KIF5a expression is significantly increased in one C9-line, while DCTN1 levels are not significantly altered in C9-CNs. (A) Western blot of DCTN1 in untreated CNs and CNs treated with 0.5 mM $NaAsO_2$ or 10 µM CCCP. (B) Western blot of KIF5a in untreated CNs and CNs treated with 0.5 mM $NaAsO_2$ or 10 µM CCCP. (A-B) When comparing treatments, data were analysed with two-way ANOVA using Dunnett's *post-hoc* test. All other data were analysed with one-way ANOVA using

Sidak's *post-hoc* test. The bars represent means. Error bars represent the standard deviation. Each dot represents the measured protein level from one differentiation. Vertical black lines running through the images of Western blot membranes indicate where the pictures of membranes were cut making this figure to exclude additional samples. The left and right parts of the images were taken from the same pictures. ns=not significant, **p<0.01, ****p<0.0001.

I next investigated whether there were any differences in mitochondrial axonal transport using live imaging of axons stained with MitoTracker™ Green FM. Due to time limitations, I was only able to run this experiment with 1-2 differentiations. Therefore, the preliminary results of this experiment were not analysed statistically and I was unable to assess parameters such as speed. I first measured the axonal trafficking of mitochondria without stimulation. Then I added 1 mM glutamate to increase mitochondrial transport by increasing the excitation and thus energy demand in synapses.

In iPSC-derived CNs, only a small number of mitochondria were motile (Figure 47A), especially for patient lines. This was due to a reduced number of axonal mitochondria in patient lines, which is in line with the observation that mitochondrial mass is reduced. The percentage of motile mitochondria in axons was similarly low for all cell lines, apart from the WT-1 line, which had a high proportion of motile mitochondria (Figure 47B). In this cell line, several axons grew through single microchamber groves. The resulting high number of mitochondria complicated the analysis of motile and stationary mitochondria, which was done by eye. Thus, I may have overestimated the number of motile mitochondria or underestimated the number of stationary mitochondria.

By observing the overall direction of mitochondrial movement during a fixed timeframe, I identified an increase in anterograde transport in C9-CNs (Figure 47C). While this is a preliminary finding, it matches the significantly increased expression of the anterograde motor protein KIF5a in patient CNs.

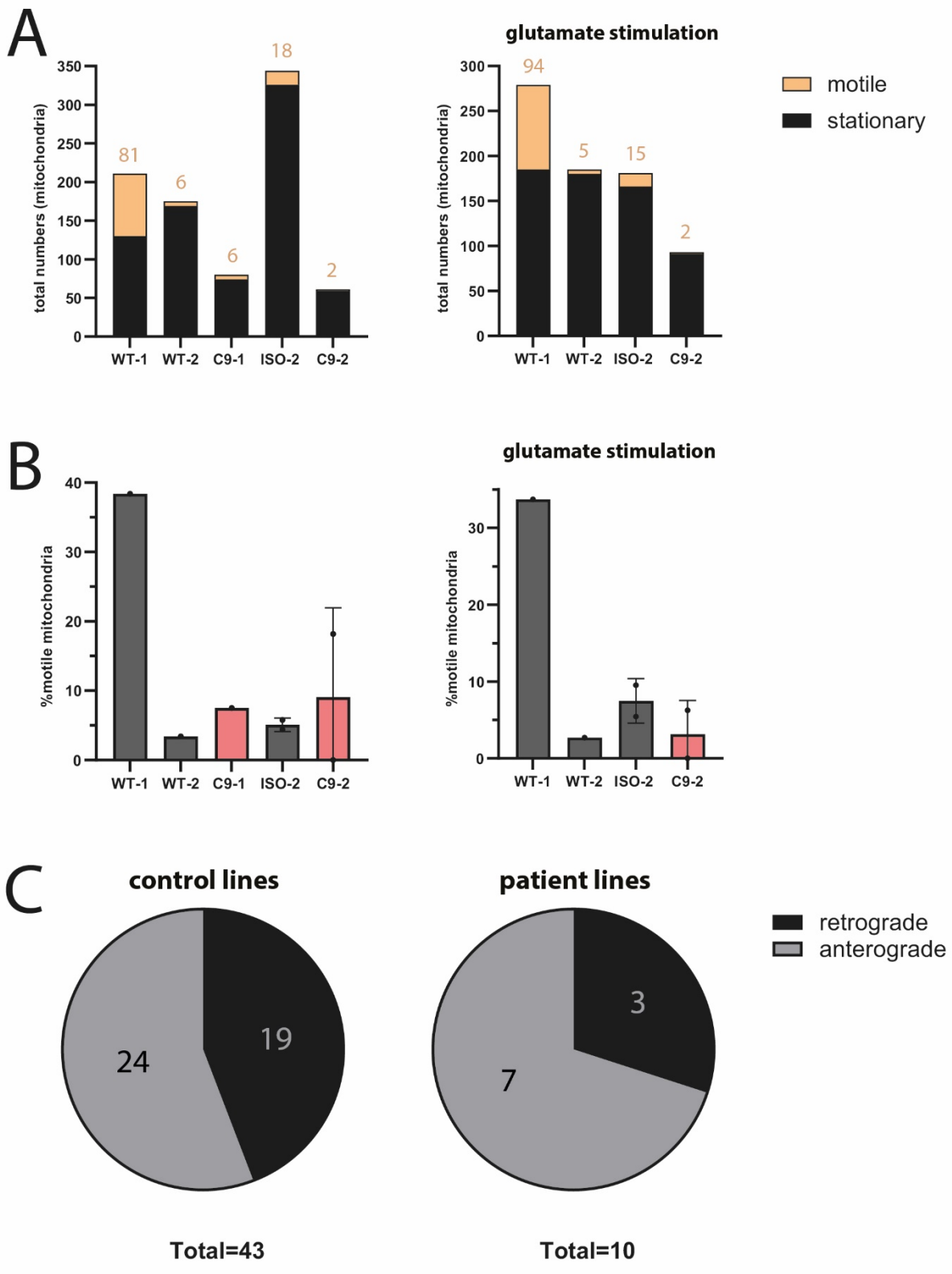


Figure 47: Despite a low number of motile mitochondria, this data suggests that anterograde transport is upregulated in C9-ALS/FTD patient CNs. (A) The number of motile mitochondria in unstimulated and glutamate-stimulated CNs. (B) The percentage of motile mitochondria in unstimulated and glutamate-stimulated CNs. (C) Retrograde vs anterograde axonal

transport in control lines and patient lines. Data from the WT-1 line was excluded. Results from unstimulated and stimulated cells were added up. (A-B) Each dot represents the value measured from one differentiation. The bars represent means. Error bars represent the standard deviation.

To conclude, I observed a significant upregulation of the anterograde motor protein KIF5a in pooled C9-1+8 CNs treated with CCCP. According to my preliminary data, this results in the upregulation of anterograde transport versus retrograde transport in patient CNs.

6.8 Conclusion

I observed the depolarisation of mitochondria in C9-CNs. This depolarisation could be caused by an increase in ROS. Previous studies using iPSC-derived MNs and zebrafish found that poly-GR expression causes oxidative stress through an unspecified mechanism which leads to mitochondrial depolarisation, mitochondrial dysfunction, and apoptosis (Lopez-Gonzalez et al., 2016; Riemslagh et al., 2021). However, my preliminary results showed no increase in ROS levels in CNs. Still, the results from the ROS assay were not reliable due to the high number of non-neuronal cells.

Alternatively, the mitochondrial depolarisation might be explained by the reduced cytosolic Ca^{2+} clearance time I observed in C9-1 and C9-8 CNs after glutamate and KCl stimulation (Figure 37). MCU levels were unaltered in untreated or stressed C9-CNs, although the levels of most mitochondrial proteins were significantly reduced due to a loss of mitochondrial mass. Thus, MCU expression might have been upregulated in remaining mitochondria, causing an increase in mitochondrial calcium uptake and subsequent mitochondrial depolarisation.

Mitochondrial depolarisation is a known trigger of mitophagy. I established an increase in the mitochondrial initiation protein PINK1 in C9-CNs treated with CCCP and an increased sensitivity to CCCP treatment for both PINK1 and P-Ub (Ser65) in C9-CNs. The upregulation of mitophagy leads to the loss of mitochondrial mass. PINK1 is not significantly upregulated in untreated cells, but since the mitochondrial loss is apparent in untreated cells and PINK1 levels are not significantly reduced in

untreated cells, PINK1 is probably slightly upregulated in untreated cells as well. I confirmed the loss of mitochondrial mass by measuring TOMM20 and COX IV levels. An apparent reduction in the number of axonal mitochondria may serve as further evidence for the reduced mitochondrial mass, however, as this was a preliminary study, further studies are required to confirm this finding.

A reduction in mitochondrial protein levels could also point towards a specific downregulation of the expression of mitochondrial nucleus-encoded proteins. A recent study established that the axonal accumulation of TDP-43 reduces the expression levels of nuclear-encoded mitochondrial proteins, including COX IV, by suppressing protein translation (Altman et al., 2021). While I did not study the accumulation of TDP-43 in axons specifically, I did not find any evidence of TDP-43 mislocalisation from the nucleus to the cell body. Thus, it is unlikely that axonal TDP-43 suppresses the expression of COX IV and TOMM20 here. Since I found evidence for mitochondrial depolarisation and mitophagy, I am confident that the loss of mitochondrial proteins is related to a loss in mitochondrial mass.

Additional mitochondrial proteins which were reduced in C9-1+8 patient CNs are CytC (Figure 23), which is located in the inter-membrane space, and Bcl-2 (Figure 20). Bcl-2 is located in mitochondrial membranes and the ER (Popgeorgiev et al., 2018). While I discussed CytC and Bcl-2 levels previously in the context of apoptosis, the reduction of CytC and Bcl-2 levels might result from a decrease in mitochondria. As I observed an increase in cytoplasmic ClCasp3 in addition to low Bcl-2 levels, evidence still suggests an increase in apoptosis in C9-CNs.

The decrease in mitochondrial mass resulted in the increased expression of anterograde transport machinery in C9-CNs treated with CCCP, which might increase the transport of healthy mitochondria to the synapses to compensate for the loss of depolarised mitochondria. The transport of mitochondria, mRNAs, proteins, and other organelles throughout the cell relies heavily on the availability of ATP (Dafinca et al., 2021). Therefore, axonal transport of mitochondria is necessary to replace dysfunctional mitochondria but is hindered by reduced ATP production. Even though I observed mitochondrial depolarisation and a reduction in mitochondrial mass in patient cells, I did not

find any significant changes in ATP production. Thus, mitochondrial regeneration and fast axonal transport of mitochondria might compensate for the mitochondrial damage in my young C9-CN cultures.

Since mitochondrial fusion and fission are important mechanisms for mitochondrial stress response and regeneration, I examined the protein levels of Mfn-2 and P-DRP1. Other proteins, such as OPA1 and Fis1 are also essential for regulating mitochondrial fusion and fission but were not studied here due to time constraints. I observed no differences in the levels of the mitochondrial protein Mfn2 between cell lines. Since I established that the mitochondrial mass is downregulated, the mitochondrial protein Mfn2 might be upregulated in untreated C9-1+8 CNs, as I saw no reduction of Mfn2.

If this is indeed the case, it would have far-reaching effects, as Mfn2 is essential for multiple mitochondrial processes. First, Mfn2 is responsible for mitochondrial fusion (Eura et al., 2003). Thus, an increase in Mfn2 leads to an increase in mitochondrial fusion. While I was not able to measure any mitochondrial structural changes, other experiments from my group have shown enlarged mitochondria in C9-MNs (Dafinca et al., 2016).

Second, Mfn2 is responsible for mitochondrial tethering to the ER. Disruption in mitochondrial tethering causes various downstream effects, such as a disruption of IP3R signalling (Gomez-Suaga et al., 2022). I found some evidence for oversensitive IP3R signalling in patient cells (Figure 28). Mitochondrial tethering is also essential for Ca^{2+} transfer between the ER and mitochondria (Bernard-Marissal et al., 2015). Thus, an increase in Mfn2 leads to increased mitochondrial Ca^{2+} uptake causing mitochondrial depolarisation, which was present in C9-CNs.

Third, Mfn2 acts as a link between mitochondria and axonal motor proteins (Misko et al., 2010). Thus, increased Mfn2 levels could cause changes in the axonal transport of mitochondria, which manifest as increased speed and fewer pauses, independent of the direction of travel. While I observed a

disruption in axonal transport, I believe it to be a specific upregulation of anterograde transport due to the overexpression of KIF5a (Figure 47, Figure 46). I did not collect enough data to analyse axonal transport speed or pauses.

P-DRP1 levels were significantly downregulated in C9-1+8 CNs treated with $NaAsO_2$. DRP1 levels might be downregulated in stressed cells due to mitophagy. However, the DRP1 protein is mostly cytosolic and only colocalises with mitochondria when it initiates fission. In untreated cells, DRP1 is not downregulated in C9-1+8 patient cells. As dysfunctional mitochondria are fragmented before they are degraded (Y. Wang et al., 2019), stressed cells might attract fission machinery. Thus, P-DRP1 could possibly colocalise with mitochondria more in stressed cells leading to a specific decrease in P-DRP1 levels in stressed cells. However, P-DRP1 seems to be reduced by approx. 64% in stressed cells, while the loss of TOMM20 and COX IV is only significant in untreated cells and is reduced by approx. 35% and 41%, respectively. Therefore, it is more likely that DRP-1 expression is downregulated due to a fission-specific mechanism suggesting that mitochondrial fission is reduced in stressed C9-CNs. This indicates that C9-CNs are unable to upregulate fission as a coping mechanism against mitochondrial stress to generate new mitochondria. This might explain why C9-CNs are more sensitive to mitochondrial stressors.

Additionally, both increased Mfn2 levels and reduced P-DRP1 levels imply that mitochondria are enlarged in C9-CNs. This needs to be confirmed by electron microscopy. Abnormal mitochondrial dynamics can cause mitochondrial transport defects and impair mitochondrial localisation, leading to the depletion of mitochondria in synapses and neurites (J. Gao et al., 2017). Enlarged mitochondria are also observed in combination with mitochondrial depolarisation and increased apoptosis (Dafinca et al., 2016). Thus, there might be a mechanism linking mitochondrial morphology to depolarisation.

In the C9-2 cell line, mitochondrial depolarisation was present, but the mitochondrial mass was not reduced. One explanation for this might be that the mitochondrial fission response to mitochondrial stressors was not impaired in this cell line, enabling C9-2 CNs to generate new mitochondria more

effectively. Additionally, I did not observe a reduction in mitochondrial fission machinery or an increase in axonal transport machinery in this cell line. Differences in mitochondrial phenotype between C9-CN lines could be due to the biological differences between individuals. Alternatively, the chromosomal aberrations identified in the C9-2 and ISO-2 lines might account for differences in phenotype.

To the best of my knowledge, mitochondrial dysfunction has not been previously studied in C9-CNs. However, multiple related studies from C9-MNs exist. A study which quantified mitochondrial DNA in C9-MNs observed no significant differences in mitochondrial mass (Mehta et al., 2021). Experiments from my group in C9-MNs showed structural changes to mitochondria, reduced mitochondrial membrane potential, and decreased basal respiration and ATP production (Dr Ruxandra Dafinca, unpublished; Dr Paola Barbagallo, unpublished; Dafinca et al., 2016). Some studies observed mitochondrial transport impairments, specifically a reduction in motile mitochondria along axons in C9-MNs (Mehta et al., 2021). Preliminary experiments from my research group using C9-MNs did not show any significant changes in the speed or direction of mitochondrial axonal transport (Dr Jakub Scaber, unpublished). Thus, some of my results on mitochondrial dysfunction in C9-CNs equate to findings in C9-MNs. Noticeable differences in mitochondrial phenotypes are the loss of mitochondrial mass in C9-CNs, the lack of significant alteration in mitochondrial respiration, and the specific upregulation of anterograde axonal transport in C9-CNs.

In this work, I established that the C9-FTD phenotype of iPSC-derived CNs includes mitochondrial depolarisation, upregulation of mitophagy, loss of mitochondrial mass as assessed by TOMM20 and COX IV levels, loss of P-DRP1 in stressed CNs, and the upregulation in the expression of the anterograde motor protein KIF5a.

7 Discussion

In genetically and pathologically heterogeneous conditions like FTD and ALS, a major challenge for translational therapeutics is to build realistic and appropriate pre-clinical models for studies of basic pathogenesis and drug discovery. Although the reasons why some patients with the same mutation in the same family develop FTD, while others develop ALS, are not understood, factors specific to the neuronal type are an important area of enquiry. In this thesis, I sought to identify common and divergent phenotypes which might allow a specific approach to FTD caused by hexanucleotide mutations in the *C9orf72* gene.

7.1 Which disease phenotypes did I discover in iPSC-derived C9-CNs?

Table 4: An overview of the molecular pathways studied in this research project and the impairments identified in C9-ALS/FTD patient-derived CNs. UT=untreated, BAF=bafilomycin, TG=thapsigargin, ns=not significant, -=not analysed

MOLECULAR PATHWAY	MARKER/ASSAY	POOLED C9-1 AND C9-8 CORTICAL NEURONS	C9-2 CORTICAL NEURONS
APOPTOSIS	Bcl-2 expression	Reduced (UT, $NaAsO_2$), Increased sensitivity to CCCP	ns
	ClCasp3 levels (by Western blot)	Increased (UT)	ns
	CytC protein levels (by Western blot)	Reduced (UT)	ns
TDP-43 PATHOLOGY	TDP-43 localisation	ns	ns
STRESS GRANULE FORMATION	PABP aggregation	ns	ns
ER STRESS	BiP expression	ns	ns
	CHOP expression	ns	ns
	ATF4 expression	ns	ns
INTRACELLULAR CA^{2+} SIGNALLING	Amplitude after CCh stimulation	ns	-

	Latency after CCh stimulation	Reduced	-
	Ca^{2+} clearance time after CCh stimulation	ns	-
AUTOPHAGY	p62 protein levels	ns	Increased sensitivity to BAF
	LC3BII/LC3BI ratio	ns	ns
	LAMP2A expression	ns	ns
EXCITABILITY	Amplitude after glutamate stimulation	Reduced	Increased
	Latency after glutamate stimulation	Reduced	Increased
	Amplitude after KCl stimulation	Reduced	Reduced
	Latency after KCl stimulation	Reduced	Increased
	GluN1 expression	ns	Increased sensitivity to $NaAsO_2$
	GluA1 expression	Reduced (UT, RAP), Reduced sensitivity to TG and BAF	ns
	PSD95 expression	ns	ns
	CACNA2D1 expression	Increased sensitivity to $NaAsO_2$	ns
CA^{2+} CLEARANCE	Clearance time after glutamate stimulation	Reduced	Increased
	Clearance time after KCl stimulation	Reduced	ns
	MCU expression	ns	ns
MITOCHONDRIAL FUSION AND FISSION APPARATUS	P-DRP1 levels	Reduced ($NaAsO_2$), Reduced sensitivity to $NaAsO_2$	ns
	Mfn2 expression	ns	ns
MITOCHONDRIAL MASS	TOMM20 levels (by Western blot)	Reduced (UT), Reduced sensitivity to $NaAsO_2$, increased sensitivity to CCCP	ns

	COX IV levels	Reduced (UT), Increased sensitivity to $NaAsO_2$	ns
MITOCHONDRIAL MEMBRANE POTENTIAL	MitoTracker Red CMXRos	Reduced (UT)	Reduced (UT)
MITOPHAGY	PINK1 levels	Increased (CCCP), Increased sensitivity to CCCP	ns
	P-Ub (Ser65) levels	Increased sensitivity to CCCP	ns
OXIDATIVE STRESS	ROS Red Assay	ns	ns
MITOCHONDRIAL RESPIRATION	Basal respiration	ns	ns
	Maximum respiration	ns	ns
	ATP production	ns	ns
	Spare respiratory capacity	ns	ns
	H^+ leak	ns	ns
	Non-mitochondrial O_2 consumption	ns	ns
AXONAL MITOCHONDRIAL TRANSPORT	DCTN1 expression	ns	ns
	KIF5a expression	Increased (CCCP), Increased sensitivity to CCCP	ns

As I observed an increase in pro-apoptotic markers in C9-ALS/FTD patient iPSC-derived CNs, I studied a variety of C9-ALS/FTD-associated molecular pathways to identify any misregulation in C9-CNs which might cause the increase in cell death (Table 4).

I did not observe any TDP-43 pathology, ER stress, altered stress granule formation or autophagy in C9-CNs. I did, however, find a significant dysregulation of excitability. In pooled C9-1+8, GluA1 levels were reduced. This led to hypoexcitability and reduced cytosolic Ca^{2+} clearance after glutamate and

KCl stimulation. In another patient line, I identified increased excitability and clearance time after glutamate stimulation, which could cause excitotoxicity.

Moreover, I found various mitochondrial abnormalities. I observed a reduction in the mitochondrial fission protein P-DRP1 in C9-CNs when cells were stressed, which could point toward morphological changes and a reduced ability to generate new mitochondria to cope with mitochondrial stress.

I identified a reduction in multiple mitochondrial proteins in C9-1+8 CNs, which suggests a reduction in mitochondrial mass. I also observed a decrease in mitochondrial potential in all C9-CNs. In addition, when studying mitophagy-associated proteins, I found an increased sensitivity towards mitochondrial depolarisers and an increase in PINK1 levels in stressed C9-1+8 CNs. Thus, the decrease in mitochondrial potential induces mitophagy and leads to mitochondrial loss. Anterograde axonal transport of mitochondria is upregulated in cells treated with CCCP, possibly compensating for the loss of mitochondria. Despite these mitochondrial defects, I did not observe any changes in mitochondrial respiration and ATP production. Still, the observed mitochondrial damage might cause cell death by ROS toxicity. Therefore, the increase in apoptosis might result from either excitotoxicity or mitochondrial damage.

7.2 Which phenotypes might be the primary defect caused by the *C9orf72* hexanucleotide expansion?

In iPSC-derived CNs, the main cellular phenotype of FTD consists of upregulated apoptosis, defective excitation, and mitochondrial impairment. Now I discuss the cellular mechanism for the impairment of those cellular functions. They could be directly dysregulated by the effectors of the C9-HRE, namely C9orf72 haploinsufficiency, DPRs, or RNA foci. Alternatively, the pathways might be affected as a result of a different impaired cellular function. Understanding the causes of these cellular phenotypes is essential for developing therapeutic strategies for FTD.

I observed an increase in pro-apoptotic markers in C9-CNs. Since apoptosis-associated proteins are not known to interact with DPRs directly (Božič et al., 2022; Hartmann et al., 2018; Liu et al., 2022), the increase in apoptosis is most likely due to the dysregulation of other cellular pathways. As described previously, apoptosis may result from excitotoxicity or mitochondrial-associated stress, such as ATP depletion or oxidative stress which damages proteins and DNA.

I identified a dysregulation of excitability in C9-FTD CNs. Various evidence exists that excitability alterations are a direct cause of the effectors of the C9-HRE. An RNAseq study conducted in the C9-2 cell line and its isogenic control determined that the presence of the C9-HRE leads to a dysregulation of the expression of genes associated with synapse organisation, modulation of synaptic transmission, neurotransmitter transport, and chemical synaptic transmission (Ababneh et al., 2020). This might be due to the dysregulation of transcription factors by TDP-43 or RNA foci. Alternatively, DPRs might interfere with excitation. Experiments from my group showed that both $(GA)_{50}$ and $(PR)_{50}$ expression leads to a reduced Ca^{2+} release amplitude after glutamate stimulation. $(PR)_{50}$ also leads to an increased latency and clearance time (Dr Paola Barbagallo, unpublished). While this experiment does not prove a direct interaction between poly-GA and poly-PR with excitability-associated proteins, it suggests potential effectors of the C9-HRE.

Excitation could also be dysregulated as a result of a different cellular pathway. First, previous studies have shown that C9orf72 haploinsufficiency-associated autophagy impairment causes an increase in glutamate receptors (Shi et al., 2018), leading to increased excitability in glutamatergic neurons. As I did not observe any significant changes in autophagy, it is unlikely that excitability is altered as a result of aberrant autophagy. Second, excitation might be dysregulated as a result of mitochondrial impairment (Dafinca et al., 2021). A previous study identified a positive regulation between synaptic activity and ER-mitochondria tethering (Gómez-Suaga et al., 2019). Thus, synaptic activity increases ER-mitochondria contacts and vice versa. The process of synaptic vesicle recycling is tightly regulated by Ca^{2+} signalling and the availability of ATP (Brini et al., 2014). Hence, a loss of connectivity between

the ER and mitochondria and mitochondrial impairment could cause an impairment in excitability (Dafinca et al., 2021). Third, glutamate is synthesised from glutamine in neurons by the mitochondrial protein glutaminase (Cassago et al., 2012; Walker & van der Donk, 2016). Therefore, a loss in mitochondrial mass reduces the capacity of cells to produce glutamate for neurotransmission. This might explain why I saw hypoexcitability in the cell lines, which showed a reduction in mitochondrial proteins, thus mitochondrial mass, but not in the C9-2 line, which did not display any mitochondrial impairment. Since synapses are plastic and regulated by the quantity of action potentials arriving at the post-synapse, the reduced glutamate release correlates with a lower number of post-synaptic glutamate receptors. Thus, a reduction in mitochondrial mass might be responsible for the decrease in GluA1 levels and hypoexcitability in the C9-1 line.

In this study, I observed various signs of mitochondrial impairment in C9-CNs. These could have been caused directly by the effectors of the C9-HRE. Proteomics studies using primary rat neurons and HEK293T cells showed that $(GR)_{149}$ and $(PR)_{175}$ interact with mitochondrial ribosomes (Hartmann et al., 2018). Similarly, $(GR)_{80}$ has been identified to colocalise with mitochondria in iPSC-derived C9-MNs and bind to mitochondrial ribosomal proteins leading to oxidative stress (Lopez-Gonzalez et al., 2016). Thus, the direct interaction between DPRs and mitochondria has been well established.

Still, mitochondrial impairments could also be a secondary effect of the C9-HRE. As explained above, mitochondrial defects might be caused by an aberrant synaptic transmission which affects ER-mitochondria tethering and mitochondrial Ca^{2+} regulation (Dafinca et al., 2021). Reduced calcium uptake impairs mitochondrial polarisation and metabolism (Duchen, 2000). Thus synaptic function regulates mitochondrial function.

In summary, with our current knowledge, it is impossible to draw definitive conclusions on which cellular defects act as primary defects in C9-CNs. Since I did not observe autophagy impairments or ER stress, I can exclude these cellular pathways as primarily affected pathways in C9-CNs, leaving synaptic and mitochondrial impairments as the main pathways leading to cell death. Of those two pathways,

there is currently more evidence available that mitochondrial dysfunction is affected directly by the C9-HRE, while synaptic impairment might result from mitochondrial defects.

7.3 Is the disease phenotype in C9-CNs the same as in C9-MNs?

In this section, I will discuss whether the C9-ALS/FTD phenotype in C9-CNs is the same as the disease phenotype in C9-MNs (Table 5). Due to the genetic heterogeneity of cell lines, I compare my results from C9-CNs primarily with results from similar experiments which use the same cell lines used in this study.

Table 5: Comparison of affected molecular pathways in C9-MNs and C9-CNs. ns=not significant, green=identical impairment.

MOLECULAR PATHWAY	MARKER/ASSAY	C9-MOTOR NEURONS (ONLY CELL LINES USED IN THIS STUDY)	C9-CORTICAL NEURONS (C9-1, C9-2, C9-8)
APOPTOSIS	Bcl-2 expression	Reduced (C9-2)	Reduced (C9-1+8)
	ClCasp3 levels	Increased (C9-2)	Increased (C9-1+8)
	CytC protein levels	ns (C9-2)	Reduced (C9-1+8)
STRESS GRANULE FORMATION	PABP aggregation	Increased (C9-2)	ns
AUTOPHAGY	p62 protein levels	Increased (C9-2)	ns
ER STRESS	BiP expression	ns (C9-2)	ns
	CHOP expression	Reduced (C9-2)	ns
	ATF4 expression	ns (C9-2)	ns
INTRACELLULAR CA^{2+} SIGNALLING	Amplitude after CCh stimulation	Reduced (C9-1, C9-2)	ns
EXCITABILITY	Amplitude after glutamate stimulation	Reduced (C9-1, C9-2)	Reduced (C9-1) Increased (C9-2)
	Amplitude after KCl stimulation	Increased (C9-1, C9-2)	Reduced (C9-1+8, C9-2)
	Latency after KCl stimulation	Increased (C9-1, C9-2)	Reduced (C9-1+8) Increased (C9-2)

	GluA1 expression	Increased (C9-2; RNAseq)	Reduced (C9-1+8; Western blot)
CA^{2+} CLEARANCE	Clearance time after glutamate stimulation	Reduced (C9-1, C9-2)	Reduced (C9-1) Increased (C9-2)
	Clearance time after KCl stimulation	Increased (C9-1, C9-2)	Reduced (C9-1+8)
	MCU expression	Reduced (C9-1, C9-2)	ns
MITOCHONDRIAL MASS	TOMM20 levels	ns	Reduced (C9-1+8)
	COX IV levels	ns	Reduced (C9-1+8)
MITOCHONDRIAL MEMBRANE POTENTIAL	MitoTracker Red CMXRos	Reduced (C9-2)	Reduced (C9-1+8, C9-2)
MITOCHONDRIAL RESPIRATION	Basal respiration	Reduced (C9-2)	ns
	Maximum respiration	ns	ns
	ATP production	Reduced (C9-2)	ns
	Spare respiratory capacity	Reduced (C9-2)	ns
AXONAL MITOCHONDRIAL TRANSPORT	Mitochondrial transport direction	ns	Increased anterograde (preliminary)

Upregulated apoptosis is commonly observed in C9-MNs. A study from my group, which used the C9-2 cell line in addition to other cell lines not used in this project, found a decrease in Bcl-2, Bcl-X_L, and an increase in ClCasp3 in C9-MNs (Dafinca et al., 2016). BAK and CytC levels were also increased in C9-MNs, but differences in the C9-2 line were not significant for these markers (Dafinca et al., 2016). This correlates roughly to my results in C9-CNs in which Bcl-2 levels were reduced and ClCasp3 levels were increased in pooled C9-1+8 CNs. Instead of an increase in CytC levels, I observed a reduction in C9-1+8 CNs, most likely due to the decrease in mitochondrial mass in these C9-FTD cells.

Previous work from my group detected protein-associated cellular stress in C9-MNs. A study using C9-MNs determined an increase in the number of neurons with stress granules in all patient lines, including the C9-2 line used here (Dafinca et al., 2016). The study also observed an increase in p62

levels in C9-lines, including the C9-2 line (Dafinca et al., 2016). I did not find an increase in stress granule formation or p62 levels in any C9-CN. Therefore, the C9-CNs phenotype differs from the C9-MNs phenotype in stress granule formation and autophagy.

In the context of ER stress, the study mentioned above observed an increase in BiP expression in several C9-MNs lines but not the C9-2 line (Dafinca et al., 2016). Further experiments from my group did not detect significant changes in BiP levels in C9-MNs (Dr Paola Barbagallo, unpublished). However, this study identified a significant downregulation of ATF4 in a C9-ALS/FTD patient line which was not used here and a reduction in CHOP and PERK levels in the C9-2 line and another C9-MN line (Dr Paola Barbagallo, unpublished). Since I did not observe any changes in these ER stress markers in C9-CNs, my cortical cultures do not replicate the ER stress phenotype identified in C9-MNs.

The release of ER Ca^{2+} through the IP3R is reduced in C9-1 and C9-2 MNs (Dafinca et al., 2020). I did not observe any differences in the amplitude but a reduced latency of ER Ca^{2+} release in pooled C9-1+8 CNs. Therefore, altered IP3R signalling is present in both C9-MNs and C9-CNs.

Significant defects of neuronal excitation have been identified in C9-MNs. A previous study from my group using C9-MNs identified a reduced Ca^{2+} amplitude and an increased clearance time after glutamate stimulation in C9-1 and C9-2 cell lines (Dafinca et al., 2020). Here, I observed a reduction in the Ca^{2+} amplitude, latency, and clearance time after glutamate stimulation in the C9-1 iPSC-derived CNs. In contrast, I identified an increase in Ca^{2+} amplitude, latency, and increased clearance time after glutamate stimulation in the C9-2 iPSC-derived CNs. In MNs, my group previously observed an increase in the Ca^{2+} amplitude, latency, and recovery time after KCl stimulation in the C9-1 and C9-2 cell lines (Dafinca et al., 2020; Dr Ruxandra Dafinca, unpublished). In CNs, I observed a reduced amplitude in all C9-CNs, a reduced latency and clearance time in pooled C9-1+8 CNs, and an increased latency in C9-2 CNs after KCl stimulation. Thus, my observations on the excitability of C9-CNs differ from many findings in C9-MNs. The heterogeneity of cell lines is seemingly more pronounced in C9-CNs than in C9-MNs in Ca^{2+} imaging experiments.

In C9-MNs, a study using RNAseq presents an increase in the expression of the permeable AMPAR subunits GluA1, GluA2, and GluA3, the permeable NMDA subunit GluN2A, and the metabotropic glutamate receptor subunits mGluR2 and mGluR4 in C9-2 as measured (Dafinca et al., 2020). Additionally, in C9-MNs, the expression of MCU is reduced in the C9-1 and C9-2 lines, such as the expression of Mitochondrial Calcium Uptake 2 (MICU2) in the C9-2 lines, and the calbindin levels in the C9-1 and C9-2 lines (Dafinca et al., 2020; Dr Paola Barbagallo, unpublished). I also found a reduction in GluA1 levels in pooled C9-1+8 CNs but not in the C9-2 cell line. I did not observe any significant changes in MCU expression. Thus, the altered expression of the proteins relevant to the excitation of MNs partially correlates to their expression in CNs.

I observed multiple facets of mitochondrial dysfunction in C9-CNs. Previous experiments in C9-MNs found a decrease in mitochondrial potential in the C9-2 line and other C9-lines, which were not used in these experiments (Dafinca et al., 2020). In CNs, I observed a similar reduction in mitochondrial potential in all C9-FTD lines. Seahorse experiments using C9-MNs show a decrease in basal respiration, ATP production, and maximal respiration in the C9-1 line, as well as a reduction in basal respiration, ATP production, and spare respiratory capacity in the C9-2 line (Dr Ruxandra Dafinca, unpublished; Dr Paola Barbagallo, unpublished). In CNs, however, I did not observe any significant differences in mitochondrial respiration.

Western blot data from C9-MNs show no significant reduction in COX IV or TOMM20 in patient cells (Dr Paola Barbagallo, unpublished). While I did not observe a decrease in the levels of those two proteins in C9-2 CNs, I identified a significant reduction of TOMM20 in pooled C9-1+8 CNs. Another study which quantified mitochondrial DNA in cell lines, different from the cell lines used here, observed no significant differences in mitochondrial mass in C9-MNs (Mehta et al., 2021). The same study observed mitochondrial transport impairments, specifically a reduction in motile mitochondria along axons in C9-MNs (Mehta et al., 2021). Mitochondrial axonal transport experiments from my group showed no significant differences in transport speed or direction. In C9-CNs, I did not observe

a difference in the number of motile mitochondria in the low sample size of my axonal trafficking experiments but rather an increase in anterograde mitochondrial transport and overexpression of KIF5a. Thus, any findings drawn from mitochondrial respiration studies vary widely between C9-MNs and C9-CNs.

7.4 Are iPSC-derived C9-CNs a useful disease model?

While I discussed the general advantages or disadvantages of working with iPSC-derived neurons in the introduction, working with iPSC-derived C9-CNs in this project illuminated some advantages and limitations of this cellular model specific to identifying the phenotype of C9-CNs.

First, we need to establish whether iPSC-derived C9-CNs represent neurons affected by FTD. The human cortex is a complex structure organised into cortical layers. Each layer comprises several types of neurons that differ from other layers and differ between various lobes. In FTD, cortical neurons degenerate specifically in the frontal and temporal lobes. Studies have shown that cell death is most significant in upper cortical layers (II-III) and layer V neurons in frontal regions (Kersaitis et al., 2004; E. J. Kim et al., 2012; Santillo & Englund, 2014). The earliest cellular changes in FTD are the loss of glial cells and the loss of neurons in layers II and III. In late disease stages, layer V and the CA1 sector of the hippocampus will also be affected. While FTD is characterised by the dysregulation of various neurotransmitter systems, studies suggest that glutamate is key in the pathogenesis of FTD. This indicates that glutamatergic pyramidal neurons are the primary affected cell type in FTD. Some studies imply that von Economo neurons (VENs), a type of bipolar pyramidal cell believed to be a primate-specific neuron type, is the most affected type of neuron in layers III, III, and V of the frontal cortex in bvFTD (E. J. Kim et al., 2012; Santillo & Englund, 2014). Therefore, the identity of the main neurons affected by FTD is very specific.

When differentiating iPSCs to cortical neurons, I could control the layer identity of the cortical neuron culture. However, the differentiation protocol is not suited to produce cells with the neuronal identity

of a specific cortical lobe or subgroup. Instead, I characterise the cortical cultures to assess whether they show similar traits as the cortical neurons we believe to be affected by FTD. Similar to VENs, the cultures used here were glutamatergic and a high percentage of cells expressed CTIP2. Additionally, they showed increased cell death. We do not yet understand why VENs are particularly vulnerable in bvFTD and are thus unable to replicate all the characteristics of cortical neurons affected by FTD. However, to our current knowledge, the iPSC-derived CNs used in this project replicate layer V VENs characteristics.

I did, however, observe impurities in the cultures used here. These impurities are particularly common in long differentiation processes, as non-neuronal cells have more time to expand while the neurons are in a post-mitotic stage. Additionally, in this protocol, I could not split the cells after day 32, which means that I could not reduce the number of non-neuronal cells by lifting off neurons, which are more loosely attached to the plate than non-neuronal cells. These impurities deflect the measurements and increase the standard deviation between differentiations, which means that subtle changes in C9-CNs might have been overlooked. Furthermore, difficulties with differentiations made working with a small format such as 96-well plates challenging and the results from these experiments unreliable, limiting the uses of iPSC-derived CNs.

Although layer II and III neurons are more affected in FTD than layer V neurons, I did not differentiate the cells past layer V for multiple reasons. First, differentiating cells for substantially longer than 60 days would have been impractical, as it would have limited the number of differentiations possible in the time available for this project and would have required higher material expenses per differentiation. Second, since I could not split cells after day 32, the Geltrex coating of the plates was noticeably degraded even at day 55, making it impossible to keep cells attached past this time point. Third, differentiating cultures for a long time would have increased non-neuronal impurities in the culture, as described above.

Since FTD is a heterogeneous disease, a large number of patient cell lines is needed. Because of subtle differences in pluripotency due to their reprogramming effectiveness in our iPSC lines, some cell lines differentiated to CNs better than others, and some cell lines were impossible to differentiate to CNs. This reduced the number of cell lines available to us. Therefore, I were only able to use three patient lines for most experiments and observed stark differences in phenotypes with individual patient lines behaving differently from others. Thus, to effectively study C9-CNs, a high number of cell lines is required. Since I observed both differences between patient lines and between control lines, the use of isogenic control lines is strongly recommended to enable a robust statistical analysis. However, generating isogenic control lines of C9-iPSCs is very complex due to the GC-rich nature of the region and the size of the mutation. Therefore, isogenic controls are currently not readily available.

iPSC-derived CNs are a highly valuable research model despite the technical challenges associated with studying C9-CNs. iPSC-derived C9-CNs are the only early-disease model which replicates the genetic background of patients accurately and in which the phenotype is caused by haploinsufficiency, RNA foci, and DPRs. Since the C9-HRE is large and complex, it cannot be induced into healthy cell cultures, e.g. HEK cells or animal models. Other existing models only replicate a subset of the effectors of the C9-HRE, such as one specific DPR. Therefore, a phenotyping study such as this one is only possible with C9-ALS/FTD patient iPSC-derived CNs.

7.5 Which further experiments are needed?

Finally, I will discuss further experiments which would be useful and build upon this study. First, conducting RNAseq experiments with C9-CNs would be useful, as I showed that protein expression in C9-CNs is significantly different from C9-MNs. RNAseq results would provide more clarity on whether the reduction of specific proteins, e.g. mitochondrial proteins, is due to changes in protein expression or changes in folding and degeneration. We could also gain knowledge on which pathways are affected due to altered gene expression in C9-CNs. Second, other pathways are commonly affected in C9-MNs, which I did not study as part of this project, such as nucleocytoplasmic transport. Understanding

whether these pathways are affected in C9-CNs would be useful to gain a more comprehensive picture of the C9-FTD phenotype in CNs. Third, it would be useful to study iPSC-derived CNs from different genetic backgrounds, such as MAPT or GRN mutations or sporadic disease, to investigate if the FTD phenotype in iPSC is similar. Since it is currently unclear how these various genetic causes lead to the same pathology, we might find some clues by comparing cellular phenotypes.

In addition, open questions remain from the pathways which I studied here. Additional experiments should be conducted to better understand morphological changes in mitochondria in C9-CNs and the mechanism behind these alterations, as morphological impairment might be the reason for mitochondrial damage in C9-CNs. Similarly, ROS production needs to be understood better, as oxidative stress might be a cause of cell death. Mitochondrial loss should also be confirmed by measuring mtDNA, and additional data should be gathered to confirm the changes in mitochondrial transport, which I observed in preliminary experiments. Furthermore, since changes in IP3R signalling were observed in both MNs and CNs, this pathway is worth investigating further, as it might be an unknown C9-ALS/FTD phenotype.

As I discovered that excitability issues and mitochondrial impairments are key in the C9-FTD phenotype potentially causing cell death, it should be examined whether methods to improve excitability or mitochondrial function prevent cell death. For example, hypoexcitability might be targeted by increasing AMPAR expression or increasing glutamate availability, e.g. by reducing glutamate uptake from the synapse by astrocytes or increasing the sensitivity of pre-synaptic VGCCs. Hyperexcitability may be targeted by increasing autophagy to reduce the number of AMPARs in the synapse. Mitochondrial loss may be treated by targeting its cause, e.g. targeting pro-oxidative proteins, increasing Mfn2 activity or inhibiting DPR1 activity. By studying the effects of these therapeutic strategies, we could determine whether these pathways might be the basis for future pharmacological treatments. If these phenotypes are found across familial and sporadic forms of FTD, treating cellular phenotypes could have an advantage over the treatments currently in development

which target a specific mutation. Once the pathological mechanisms that lead to the FTD phenotypes I established in this study are better understood, disease-modifying pharmaceutical therapies can be developed.

8 References

Ababneh, N. A., Scaber, J., Flynn, R., Douglas, A., Barbagallo, P., Candalija, A., Turner, M. R., Sims, D., Dafinca, R., Cowley, S. A., & Talbot, K. (2020). Correction of amyotrophic lateral sclerosis related phenotypes in induced pluripotent stem cell-derived motor neurons carrying a hexanucleotide expansion mutation in C9orf72 by CRISPR/Cas9 genome editing using homology-directed repair. *Human Molecular Genetics*, *29*(13), 2200–2217. https://doi.org/10.1093/HMG/DDAA106

Abo-Rady, M., Kalmbach, N., Pal, A., Schludi, C., Janosch, A., Richter, T., Freitag, P., Bickle, M., Kahlert, A. K., Petri, S., Stefanov, S., Glass, H., Staege, S., Just, W., Bhatnagar, R., Edbauer, D., Hermann, A., Wegner, F., & Sterneckert, J. L. (2020). Knocking out C9ORF72 Exacerbates Axonal Trafficking Defects Associated with Hexanucleotide Repeat Expansion and Reduces Levels of Heat Shock Proteins. *Stem Cell Reports*, *14*(3), 390–405. https://doi.org/10.1016/J.STEMCR.2020.01.010

Agilent Technologies Inc. (2019). *XF Cell Mito Stress Test Report Generator*.

Alcamo, E. A., Chirivella, L., Dautzenberg, M., Dobreva, G., Fariñas, I., Grosschedl, R., & McConnell, S. K. (2008). Satb2 Regulates Callosal Projection Neuron Identity in the Developing Cerebral Cortex. *Neuron*, *57*(3), 364–377. https://doi.org/10.1016/J.NEURON.2007.12.012

Allen, S. P., Hall, B., Woof, R., Francis, L., Gatto, N., Shaw, A. C., Myszczynska, M., Hemingway, J., Coldicott, I., Willcock, A., Job, L., Hughes, R. M., Boschian, C., Bayatti, N., Heath, P. R., Bandmann, O., Mortiboys, H., Ferraiuolo, L., & Shaw, P. J. (2019). C9orf72 expansion within astrocytes reduces metabolic flexibility in amyotrophic lateral sclerosis. *Brain*, *142*(12), 3771–3790. https://doi.org/10.1093/BRAIN/AWZ302

Almeida, S., Gascon, E., Tran, H., Jung Chou, H., Gendron, T. F., DeGroot, S., Tapper, A. R., Sellier, C., Charlet-Berguerand, N., Karydas, A., Seeley, W. W., Boxer, A. L., Petrucelli, L., Miller, B. L., & Gao, F.-B. (2013). Modeling key pathological features of frontotemporal dementia with C9ORF72 repeat expansion in iPSC-derived human neurons. *Acta Neuropathol*, *3*, 385–399. https://doi.org/10.1007/s00401-013-1149-y

Altman, T., Ionescu, A., Ibraheem, A., Priesmann, D., Gradus-Pery, T., Farberov, L., Alexandra, G., Shelestovich, N., Dafinca, R., Shomron, N., Rage, F., Talbot, K., Ward, M. E., Dori, A., Krüger, M., & Perlson, E. (2021). Axonal TDP-43 condensates drive neuromuscular junction disruption through inhibition of local synthesis of nuclear encoded mitochondrial proteins. *Nature Communications*, *12*(1). https://doi.org/10.1038/S41467-021-27221-8

Amick, J., Roczniak-Ferguson, A., & Ferguson, S. M. (2016). C9orf72 binds SMCR8, localizes to lysosomes, and regulates mTORC1 signaling. *Molecular Biology of the Cell*, *27*(20), 3040–3051. https://doi.org/10.1091/mbc.E16-01-0003

Anderson, G. W., Goebel, H. H., & Simonati, A. (2013). Human pathology in NCL. In *Biochimica et Biophysica Acta - Molecular Basis of Disease*. https://doi.org/10.1016/j.bbadis.2012.11.014

Andersson, M. K., Ståhlberg, A., Arvidsson, Y., Olofsson, A., Semb, H., Stenman, G., Nilsson, O., & Åman, P. (2008). The multifunctional FUS, EWS and TAF15 proto-oncoproteins show cell type-specific expression patterns and involvement in cell spreading and stress response. *BMC Cell Biology*, *9*(1), 1–17. https://doi.org/10.1186/1471-2121-9-37/FIGURES/7

Arai, T., Hasegawa, M., Akiyama, H., Ikeda, K., Nonaka, T., Mori, H., Mann, D., Tsuchiya, K., Yoshida, M., Hashizume, Y., & Oda, T. (2006). TDP-43 is a component of ubiquitin-positive tau-negative

inclusions in frontotemporal lobar degeneration and amyotrophic lateral sclerosis. *Biochemical and Biophysical Research Communications*. https://doi.org/10.1016/j.bbrc.2006.10.093

Arai, T., Nonaka, T., Hasegawa, M., Akiyama, H., Yoshida, M., Hashizume, Y., Tsuchiya, K., Oda, T., & Ikeda, K. (2003). Neuronal and glial inclusions in frontotemporal dementia with or without motor neuron disease are immunopositive for p62. *Neuroscience Letters*. https://doi.org/10.1016/S0304-3940(03)00216-7

Araya, R. (2014). Input transformation by dendritic spines of pyramidal neurons. *Frontiers in Neuroanatomy*, *8*(DEC), 141. https://doi.org/10.3389/FNANA.2014.00141/BIBTEX

Armstrong, M. J. (2018). Progressive Supranuclear Palsy: an Update. In *Current Neurology and Neuroscience Reports*. https://doi.org/10.1007/s11910-018-0819-5

Armstrong, R. A., Ellis, W., Hamilton, R. L., MacKenzie, I. R. A., Hedreen, J., Gearing, M., Montine, T., Vonsattel, J. P., Head, E., Lieberman, A. P., & Cairns, N. J. (2010). Neuropathological heterogeneity in frontotemporal lobar degeneration with TDP-43 proteinopathy: A quantitative study of 94 cases using principal components analysis. *Journal of Neural Transmission*. https://doi.org/10.1007/s00702-009-0350-6

Bach, D., Pich, S., Soriano, F. X., Vega, N., Baumgartner, B., Oriola, J., Daugaard, J. R., Lloberas, J., Camps, M., Zierath, J. R., Rabasa-Lhoret, R., Wallberg-Henriksson, H., Laville, M., Palacín, M., Vidal, H., Rivera, F., Brand, M., & Zorzano, A. (2003). Mitofusin-2 Determines Mitochondrial Network Architecture and Mitochondrial Metabolism: A NOVEL REGULATORY MECHANISM ALTERED IN OBESITY *. *Journal of Biological Chemistry*, *278*(19), 17190–17197. https://doi.org/10.1074/JBC.M212754200

Baker, M., Mackenzie, I. R., Pickering-Brown, S. M., Gass, J., Rademakers, R., Lindholm, C., Snowden, J., Adamson, J., Sadovnick, A. D., Rollinson, S., Cannon, A., Dwosh, E., Neary, D., Melquist, S., Richardson, A., Dickson, D., Berger, Z., Eriksen, J., Robinson, T., … Hutton, M. (2006). Mutations in progranulin cause tau-negative frontotemporal dementia linked to chromosome 17. *Nature 2006 442:7105*, *442*(7105), 916–919. https://doi.org/10.1038/nature05016

Baldwin, K. R., Godena, V. K., Hewitt, V. L., & Whitworth, A. J. (2016). Axonal transport defects are a common phenotype in Drosophila models of ALS. *Human Molecular Genetics*, *25*(12), 2378–2392. https://doi.org/10.1093/HMG/DDW105

Balendra, R., & Isaacs, A. M. (2018). C9orf72-mediated ALS and FTD: multiple pathways to disease. In *Nature Reviews Neurology*. https://doi.org/10.1038/s41582-018-0047-2

Baradaran-Heravi, Y., Van Broeckhoven, C., & van der Zee, J. (2020). Stress granule mediated protein aggregation and underlying gene defects in the FTD-ALS spectrum. *Neurobiology of Disease*, *134*, 104639. https://doi.org/https://doi.org/10.1016/j.nbd.2019.104639

Barrientos, A., Barros, M. H., Valnot, I., Rötig, A., Rustin, P., & Tzagoloff, A. (2002). Cytochrome oxidase in health and disease. *Gene*, *286*(1), 53–63. https://doi.org/10.1016/S0378-1119(01)00803-4

Batra, R., & Lee, C. W. (2017). Mouse Models of C9orf72 Hexanucleotide Repeat Expansion in Amyotrophic Lateral Sclerosis/ Frontotemporal Dementia. *Frontiers in Cellular Neuroscience*, *11*. https://www.frontiersin.org/article/10.3389/fncel.2017.00196

B'chir, W., Maurin, A.-C., Carraro, V., Averous, J., Jousse, C., Muranishi, Y., Parry, L., Stepien, G., Fafournoux, P., & Bruhat, A. (2013). The eIF2α/ATF4 pathway is essential for stress-induced

autophagy gene expression. *Nucleic Acids Research*, *41*(16), 7683–7699. https://doi.org/10.1093/nar/gkt563

Beckers, J., Tharkeshwar, A. K., & van Damme, P. (2021). C9orf72 ALS-FTD: recent evidence for dysregulation of the autophagy-lysosome pathway at multiple levels. *Https://Doi.Org/10.1080/15548627.2021.1872189*, *17*(11), 3306–3322. https://doi.org/10.1080/15548627.2021.1872189

Behrouzi, R., Liu, X., Wu, D., Robinson, A. C., Tanaguchi-Watanabe, S., Rollinson, S., Shi, J., Tian, J., Hamdalla, H. H. M., Ealing, J., Richardson, A., Jones, M., Pickering-Brown, S., Davidson, Y. S., Strong, M. J., Hasegawa, M., Snowden, J. S., & Mann, D. M. A. (2016). Pathological tau deposition in Motor Neurone Disease and frontotemporal lobar degeneration associated with TDP-43 proteinopathy. *Acta Neuropathologica Communications*, *4*(1), 33. https://doi.org/10.1186/S40478-016-0301-Z/FIGURES/5

Belcastro, V., Siciliano, V., Gregoretti, F., Mithbaokar, P., Dharmalingam, G., Berlingieri, S., Iorio, F., Oliva, G., Polishchuck, R., Brunetti-Pierri, N., & Di Bernardo, D. (2011). Transcriptional gene network inference from a massive dataset elucidates transcriptome organization and gene function. *Nucleic Acids Research*. https://doi.org/10.1093/nar/gkr593

Belkacemi, A., Hui, X., Wardas, B., Laschke, M. W., Wissenbach, U., Menger, M. D., Lipp, P., Beck, A., & Flockerzi, V. (2018). IP 3 Receptor-Dependent Cytoplasmic Ca 2+ Signals Are Tightly Controlled by Cavβ3. *Cell Reports*, *22*(5), 1339–1349. https://doi.org/10.1016/J.CELREP.2018.01.010/ATTACHMENT/A4BEED0A-C955-4644-A651-CB5E4F975D6A/MMC1.PDF

Belzil, V. v., Bauer, P. O., Prudencio, M., Gendron, T. F., Stetler, C. T., Yan, I. K., Pregent, L., Daughrity, L., Baker, M. C., Rademakers, R., Boylan, K., Patel, T. C., Dickson, D. W., & Petrucelli, L. (2013). Reduced C9orf72 gene expression in c9FTD/ALS is caused by histone trimethylation, an epigenetic event detectable in blood. *Acta Neuropathologica*, *126*(6), 895–905. https://doi.org/10.1007/S00401-013-1199-1/FIGURES/5

Bernard-Marissal, N., Médard, J. J., Azzedine, H., & Chrast, R. (2015). Dysfunction in endoplasmic reticulum-mitochondria crosstalk underlies SIGMAR1 loss of function mediated motor neuron degeneration. *Brain*, *138*(4), 875–890. https://doi.org/10.1093/BRAIN/AWV008

Berridge, M. J. (2016). The inositol trisphosphate/calcium signaling pathway in health and disease. *Physiological Reviews*, *96*(4), 1261–1296. https://doi.org/10.1152/PHYSREV.00006.2016/ASSET/IMAGES/LARGE/Z9J00416277300007.JPEG

Bieniek, K. F., Murray, M. E., Rutherford, N. J., Castanedes-Casey, M., Dejesus-Hernandez, M., Liesinger, A. M., Baker, M. C., Boylan, K. B., Rademakers, R., & Dickson, D. W. (2013). Tau Pathology in Frontotemporal Lobar Degeneration with C9ORF72 Hexanucleotide Repeat Expansion. *Acta Neuropathologica*, *125*(2), 289. https://doi.org/10.1007/S00401-012-1048-7

Biogen Inc., & Ionis Pharmaceuticals Inc. (2022). *Biogen and Ionis Announce Topline Phase 1 Study Results of Investigational Drug in C9orf72 Amyotrophic Lateral Sclerosis*. Globe Newswire. https://investors.biogen.com/news-releases/news-release-details/biogen-and-ionis-announce-topline-phase-1-study-results

Birger, A., Ben-Dor, I., Ottolenghi, M., Turetsky, T., Gil, Y., Sweetat, S., Perez, L., Belzer, V., Casden, N., Steiner, D., Izrael, M., Galun, E., Feldman, E., Behar, O., & Reubinoff, B. (2019). Human iPSC-

derived astrocytes from ALS patients with mutated C9ORF72 show increased oxidative stress and neurotoxicity. *EBioMedicine*, *50*, 274–289. https://doi.org/10.1016/J.EBIOM.2019.11.026

Bodansky, A., Kim, J. M. H., Tempest, L., Velagapudi, A., Libby, R., & Ravits, J. (2010). TDP-43 and ubiquitinated cytoplasmic aggregates in sporadic ALS are low frequency and widely distributed in the lower motor neuron columns independent of disease spread. *Amyotrophic Lateral Sclerosis*. https://doi.org/10.3109/17482961003602363

Boeynaems, S., Bogaert, E., Kovacs, D., Konijnenberg, A., Timmerman, E., Volkov, A., Guharoy, M., De Decker, M., Jaspers, T., Ryan, V. H., Janke, A. M., Baatsen, P., Vercruysse, T., Kolaitis, R.-M., Daelemans, D., Taylor, J. P., Kedersha, N., Anderson, P., Impens, F., … Van Den Bosch, L. (2017). Phase Separation of C9orf72 Dipeptide Repeats Perturbs Stress Granule Dynamics. *Molecular Cell*, *65*(6), 1044-1055.e5. https://doi.org/10.1016/j.molcel.2017.02.013

Boivin, M., Pfister, V., Gaucherot, A., Ruffenach, F., Negroni, L., Sellier, C., & Charlet-Berguerand, N. (2020). Reduced autophagy upon C9ORF72 loss synergizes with dipeptide repeat protein toxicity in G4C2 repeat expansion disorders. *The EMBO Journal*, *39*(4), e100574. https://doi.org/10.15252/EMBJ.2018100574

Boros, B. D., Schoch, K. M., Kreple, C. J., & Miller, T. M. (2022). Antisense Oligonucleotides for the Study and Treatment of ALS. *Neurotherapeutics 2022*, *1*, 1–14. https://doi.org/10.1007/S13311-022-01247-2

Božič, J., Motaln, H., Janež, A. P., Markič, L., Tripathi, P., Yamoah, A., Aronica, E., Lee, Y.-B., Heilig, R., Fischer, R., Thompson, A. J., Goswami, A., & Rogelj, B. (2022). Interactome screening of C9orf72 dipeptide repeats reveals VCP sequestration and functional impairment by polyGA. *Brain : A Journal of Neurology*, *145*(2), 684–699. https://doi.org/10.1093/BRAIN/AWAB300

Brini, M., Calì, T., Ottolini, D., & Carafoli, E. (2014). Neuronal calcium signaling: Function and dysfunction. *Cellular and Molecular Life Sciences*, *71*(15), 2787–2814. https://doi.org/10.1007/S00018-013-1550-7/FIGURES/3

Bruijn, L. I., Becher, M. W., Lee, M. K., Anderson, K. L., Jenkins, N. A., Copeland, N. G., Sisodia, S. S., Rothstein, J. D., Borchelt, D. R., Price, D. L., & Cleveland, D. W. (1997). ALS-Linked SOD1 Mutant G85R Mediates Damage to Astrocytes and Promotes Rapidly Progressive Disease with SOD1-Containing Inclusions. *Neuron*, *18*(2), 327–338. https://doi.org/10.1016/S0896-6273(00)80272-X

Buratti, E., Dörk, T., Zuccato, E., Pagani, F., Romano, M., & Baralle, F. E. (2001). Nuclear factor TDP-43 and SR proteins promote in vitro and in vivo CFTR exon 9 skipping. *EMBO Journal*. https://doi.org/10.1093/emboj/20.7.1774

Burk, K., & Pasterkamp, R. J. (2019). Disrupted neuronal trafficking in amyotrophic lateral sclerosis. *Acta Neuropathologica 2019 137:6*, *137*(6), 859–877. https://doi.org/10.1007/S00401-019-01964-7

Burman, J. L., Yu, S., Poole, A. C., Decal, R. B., & Pallanck, L. (2012). Analysis of neural subtypes reveals selective mitochondrial dysfunction in dopaminergic neurons from parkin mutants. *Proceedings of the National Academy of Sciences of the United States of America*, *109*(26), 10438–10443. https://doi.org/10.1073/PNAS.1120688109/-/DCSUPPLEMENTAL

Cai, Q., Zakaria, H. M., Simone, A., & Sheng, Z. H. (2012). Spatial Parkin Translocation and Degradation of Damaged Mitochondria via Mitophagy in Live Cortical Neurons. *Current Biology*, *22*(6), 545–552. https://doi.org/10.1016/J.CUB.2012.02.005

Cairns, N. J., Neumann, M., Bigio, E. H., Holm, I. E., Troost, D., Hatanpaa, K. J., Foong, C., White, C. L., Schneider, J. A., Kretzschmar, H. A., Carter, D., Taylor-Reinwald, L., Paulsmeyer, K., Strider, J., Gitcho, M., Goate, A. M., Morris, J. C., Mishra, M., Kwong, L. K., … Mackenzie, I. R. A. (2007). TDP-43 in familial and sporadic frontotemporal lobar degeneration with ubiquitin inclusions. *American Journal of Pathology*. https://doi.org/10.2353/ajpath.2007.070182

Cárdenas, C., Miller, R. A., Smith, I., Bui, T., Molgó, J., Müller, M., Vais, H., Cheung, K. H., Yang, J., Parker, I., Thompson, C. B., Birnbaum, M. J., Hallows, K. R., & Foskett, J. K. (2010). Essential Regulation of Cell Bioenergetics by Constitutive InsP3 Receptor Ca2+ Transfer to Mitochondria. *Cell*, *142*(2), 270–283. https://doi.org/10.1016/J.CELL.2010.06.007

Caroppo, P., Camuzat, A., Guillot-Noel, L., Thomas-Antérion, C., Couratier, P., Wong, T. H., Teichmann, M., Golfier, V., Auriacombe, S., Belliard, S., Laurent, B., Lattante, S., Millecamps, S., Clot, F., Dubois, B., Van Swieten, J. C., Brice, A., & Le Ber, I. (2016). Defining the spectrum of frontotemporal dementias associated with TARDBP mutations. *Neurology: Genetics*. https://doi.org/10.1212/NXG.0000000000000080

Casellas-D Iaz, S., Larramona-Arcas, R., Riqu E-Pujol, G., Tena-Morraja, P., M€ Uller-S Anchez, C., Segarra-Mondejar, M., Gavald A-Navarro, A., Villarroya, F., Reina, M., Mart Inez-Estrada, O. M., & Soriano, F. X. (2021). Mfn2 localization in the ER is necessary for its bioenergetic function and neuritic development. *EMBO Reports*, *22*(9), e51954. https://doi.org/10.15252/EMBR.202051954

Cassago, A., Ferreira, A. P. S., Ferreira, I. M., Fornezari, C., Gomes, E. R. M., Greene, K. S., Pereira, H. M., Garratt, R. C., Dias, S. M. G., & Ambrosio, A. L. B. (2012). Mitochondrial localization and structure-based phosphate activation mechanism of Glutaminase C with implications for cancer metabolism. *Proceedings of the National Academy of Sciences of the United States of America*, *109*(4), 1092–1097. https://doi.org/10.1073/PNAS.1112495109/SUPPL_FILE/PNAS.1112495109_SI.PDF

Cha, M. Y., Kim, D. K. yu, & Mook-Jung, I. (2015). The role of mitochondrial DNA mutation on neurodegenerative diseases. *Experimental & Molecular Medicine 2015 47:3*, *47*(3), e150–e150. https://doi.org/10.1038/emm.2014.122

Chang, Y. J., Jeng, U. S., Chiang, Y. L., Hwang, I. S., & Chen, Y. R. (2016). The glycine-alanine dipeptide repeat from C9 or f72 hexanucleotide expansions forms toxic amyloids possessing cell-to-cell transmission properties. *Journal of Biological Chemistry*. https://doi.org/10.1074/jbc.M115.694273

Chen, C., Gu, S., Jiang, X., & Zhang, Z. (2017). Arsenite-induced endoplasmic reticulum-dependent apoptosis through disturbance of calcium homeostasis in HBE cell line. *Environmental Toxicology*, *32*(1), 197–216. https://doi.org/10.1002/TOX.22226

Chen, H., Detmer, S. A., Ewald, A. J., Griffin, E. E., Fraser, S. E., & Chan, D. C. (2003). Mitofusins Mfn1 and Mfn2 coordinately regulate mitochondrial fusion and are essential for embryonic development. *The Journal of Cell Biology*, *160*(2), 189–200. https://doi.org/10.1083/JCB.200211046

Chen, H., Vermulst, M., Wang, Y. E., Chomyn, A., Prolla, T. A., McCaffery, J. M., & Chan, D. C. (2010). Mitochondrial Fusion Is Required for mtDNA Stability in Skeletal Muscle and Tolerance of mtDNA Mutations. *Cell*, *141*(2), 280–289. https://doi.org/10.1016/J.CELL.2010.02.026

Chen, X., Guo, C., & Kong, J. (2012). Oxidative stress in neurodegenerative diseases. *Neural Regeneration Research*, *7*(5), 376. https://doi.org/10.3969/J.ISSN.1673-5374.2012.05.009

Chen, Y., Aon, M. A., Hsu, Y. te, Soane, L., Teng, X., McCaffery, J. M., Cheng, W. C., Qi, B., Li, H., Alavian, K. N., Dayhoff-Brannigan, M., Zou, S., Pineda, F. J., O'Rourke, B., Ko, Y. H., Pedersen, P. L., Kaczmarek, L. K., Jonas, E. A., & Hardwick, J. M. (2011). Bcl-xL regulates mitochondrial energetics by stabilizing the inner membrane potential. *Journal of Cell Biology*, *195*(2), 263–276. https://doi.org/10.1083/JCB.201108059

Chen, Y., Deng, J., Wang, P., Yang, M., Chen, X., Zhu, L., Liu, J., Lu, B., Shen, Y., Fushimi, K., Xu, Q., & Wu, J. Y. (2016). PINK1 and Parkin are genetic modifiers for FUS-induced neurodegeneration. *Human Molecular Genetics*, *25*(23), 5059. https://doi.org/10.1093/HMG/DDW310

Cheng, W., Wang, S., Mestre, A. A., Fu, C., Makarem, A., Xian, F., Hayes, L. R., Lopez-Gonzalez, R., Drenner, K., Jiang, J., Cleveland, D. W., & Sun, S. (2018). C9ORF72 GGGGCC repeat-associated non-AUG translation is upregulated by stress through eIF2α phosphorylation. *Nature Communications*, *9*(1), 51. https://doi.org/10.1038/s41467-017-02495-z

Cheng, W., Wang, S., Zhang, Z., Morgens, D. W., Hayes, L. R., Lee, S., Portz, B., Xie, Y., Nguyen, B. v., Haney, M. S., Yan, S., Dong, D., Coyne, A. N., Yang, J., Xian, F., Cleveland, D. W., Qiu, Z., Rothstein, J. D., Shorter, J., … Sun, S. (2019). CRISPR-Cas9 Screens Identify the RNA Helicase DDX3X as a Repressor of C9ORF72 (GGGGCC)n Repeat-Associated Non-AUG Translation. *Neuron*, *104*(5), 885-898.e8. https://doi.org/10.1016/J.NEURON.2019.09.003

Chew, J., Cook, C., Gendron, T. F., Jansen-West, K., del Rosso, G., Daughrity, L. M., Castanedes-Casey, M., Kurti, A., Stankowski, J. N., Disney, M. D., Rothstein, J. D., Dickson, D. W., Fryer, J. D., Zhang, Y.-J., & Petrucelli, L. (2019). Aberrant deposition of stress granule-resident proteins linked to C9orf72-associated TDP-43 proteinopathy. *Molecular Neurodegeneration*, *14*(1), 9. https://doi.org/10.1186/s13024-019-0310-z

Ciura, S., Lattante, S., le Ber, I., Latouche, M., Tostivint, H., Brice, A., & Kabashi, E. (2013). Loss of function of C9orf72 causes motor deficits in a zebrafish model of Amyotrophic Lateral Sclerosis. *Annals of Neurology*, *74*(2), 180–187. https://doi.org/10.1002/ana.23946

Clarke, J. P., Thibault, P. A., Salapa, H. E., & Levin, M. C. (2021). A Comprehensive Analysis of the Role of hnRNP A1 Function and Dysfunction in the Pathogenesis of Neurodegenerative Disease. *Frontiers in Molecular Biosciences*, *8*, 217. https://doi.org/10.3389/FMOLB.2021.659610/BIBTEX

Colpo, G. D., Ribeiro, F. M., Rocha, N. P., & Teixeira, A. L. (2017). Animal Models for the Study of Human Neurodegenerative Diseases. *Animal Models for the Study of Human Disease: Second Edition*, 1109–1129. https://doi.org/10.1016/B978-0-12-809468-6.00042-5

Conlon, E. G., Lu, L., Sharma, A., Yamazaki, T., Tang, T., Shneider, N. A., & Manley, J. L. (2016). The C9ORF72 GGGGCC expansion forms RNA G-quadruplex inclusions and sequesters hnRNP H to disrupt splicing in ALS brains. *ELife*, *5*(September2016). https://doi.org/10.7554/ELIFE.17820

Constantinides, V. C., Paraskevas, G. P., Paraskevas, P. G., Stefanis, L., & Kapaki, E. (2019). Corticobasal degeneration and corticobasal syndrome: A review. *Clinical Parkinsonism & Related Disorders*, *1*, 66–71. https://doi.org/https://doi.org/10.1016/j.prdoa.2019.08.005

Contractor, A., Mulle, C., & Swanson, G. T. (2011). Kainate receptors coming of age: milestones of two decades of research. *Trends in Neurosciences*, *34*(3), 154–163. https://doi.org/10.1016/J.TINS.2010.12.002

Cox, L. E., Ferraiuolo, L., Goodall, E. F., Heath, P. R., Higginbottom, A., Mortiboys, H., Hollinger, H. C., Hartley, J. A., Brockington, A., Burness, C. E., Morrison, K. E., Wharton, S. B., Grierson, A. J., Ince, P. G., Kirby, J., & Shaw, P. J. (2010). Mutations in CHMP2B in Lower Motor Neuron Predominant Amyotrophic Lateral Sclerosis (ALS). *PLoS ONE*, *5*(3). https://doi.org/10.1371/JOURNAL.PONE.0009872

Coyne, A. N., Lorenzini, I., Chou, C. C., Torvund, M., Rogers, R. S., Starr, A., Zaepfel, B. L., Levy, J., Johannesmeyer, J., Schwartz, J. C., Nishimune, H., Zinsmaier, K., Rossoll, W., Sattler, R., & Zarnescu, D. C. (2017). Post-transcriptional Inhibition of Hsc70-4/HSPA8 Expression Leads to Synaptic Vesicle Cycling Defects in Multiple Models of ALS. *Cell Reports*, *21*(1), 110–125. https://doi.org/10.1016/J.CELREP.2017.09.028

Cozzolino, M., Pesaresi, M. G., Amori, I., Crosio, C., Ferri, A., Nencini, M., & Carrì, M. T. (2009). Oligomerization of Mutant SOD1 in Mitochondria of Motoneuronal Cells Drives Mitochondrial Damage and Cell Toxicity. *Https://Home.Liebertpub.Com/Ars*, *11*(7), 1547–1558. https://doi.org/10.1089/ARS.2009.2545

Cristofani, R., Crippa, V., Vezzoli, G., Rusmini, P., Galbiati, M., Cicardi, M. E., Meroni, M., Ferrari, V., Tedesco, B., Piccolella, M., Messi, E., Carra, S., & Poletti, A. (2018). The small heat shock protein B8 (HSPB8) efficiently removes aggregating species of dipeptides produced in C9ORF72-related neurodegenerative diseases. *Cell Stress & Chaperones*, *23*(1), 1. https://doi.org/10.1007/S12192-017-0806-9

Cruts, M., Gijselinck, I., van der Zee, J., Engelborghs, S., Wils, H., Pirici, D., Rademakers, R., Vandenberghe, R., Dermaut, B., Martin, J. J., van Duijn, C., Peeters, K., Sciot, R., Santens, P., de Pooter, T., Mattheijssens, M., van den Broeck, M., Cuijt, I., Vennekens, K., … van Broeckhoven, C. (2006). Null mutations in progranulin cause ubiquitin-positive frontotemporal dementia linked to chromosome 17q21. *Nature 2006 442:7105*, *442*(7105), 920–924. https://doi.org/10.1038/nature05017

Dafinca, R., Barbagallo, P., Farrimond, L., Candalija, A., Scaber, J., Ababneh, N. A., Sathyaprakash, C., Vowles, J., Cowley, S. A., & Talbot, K. (2020). Impairment of Mitochondrial Calcium Buffering Links Mutations in C9ORF72 and TARDBP in iPS-Derived Motor Neurons from Patients with ALS/FTD. *Stem Cell Reports*, *14*(5), 892–908. https://doi.org/10.1016/J.STEMCR.2020.03.023

Dafinca, R., Barbagallo, P., & Talbot, K. (2021). The Role of Mitochondrial Dysfunction and ER Stress in TDP-43 and C9ORF72 ALS. *Frontiers in Cellular Neuroscience*, *15*, 97. https://doi.org/10.3389/FNCEL.2021.653688/BIBTEX

Dafinca, R., Scaber, J., Ababneh, N., Lalic, T., Weir, G., Christian, H., Vowles, J., Douglas, A. G. L., Fletcher-Jones, A., Browne, C., Nakanishi, M., Turner, M. R., Wade-Martins, R., Cowley, S. A., & Talbot, K. (2016). C9orf72 Hexanucleotide Expansions Are Associated with Altered Endoplasmic Reticulum Calcium Homeostasis and Stress Granule Formation in Induced Pluripotent Stem Cell-Derived Neurons from Patients with Amyotrophic Lateral Sclerosis and Frontotemporal Demen. *Stem Cells*. https://doi.org/10.1002/stem.2388

Darling, A. L., Breydo, L., Rivas, E. G., Gebru, N. T., Zheng, D., Baker, J. D., Blair, L. J., Dickey, C. A., Koren, J., & Uversky, V. N. (2019). Repeated repeat problems: Combinatorial effect of C9orf72-derived

dipeptide repeat proteins. *International Journal of Biological Macromolecules*. https://doi.org/10.1016/j.ijbiomac.2019.01.035

Davidson, Y., Kelley, T., Mackenzie, I. R. A., Pickering-Brown, S., Du Plessis, D., Neary, D., Snowden, J. S., & Mann, D. M. A. (2007). Ubiquitinated pathological lesions in frontotemporal lobar degeneration contain the TAR DNA-binding protein, TDP-43. *Acta Neuropathologica*. https://doi.org/10.1007/s00401-006-0189-y

de Brito, O. M., & Scorrano, L. (2008). Mitofusin 2 tethers endoplasmic reticulum to mitochondria. *Nature 2008 456:7222*, *456*(7222), 605–610. https://doi.org/10.1038/nature07534

de Vos, K. J., & Hafezparast, M. (2017). Neurobiology of axonal transport defects in motor neuron diseases: Opportunities for translational research? *Neurobiology of Disease*, *105*, 283. https://doi.org/10.1016/J.NBD.2017.02.004

DeJesus-Hernandez, M., Mackenzie, I. R., Boeve, B. F., Boxer, A. L., Baker, M., Rutherford, N. J., Nicholson, A. M., Finch, N. C. A., Flynn, H., Adamson, J., Kouri, N., Wojtas, A., Sengdy, P., Hsiung, G. Y. R., Karydas, A., Seeley, W. W., Josephs, K. A., Coppola, G., Geschwind, D. H., … Rademakers, R. (2011). Expanded GGGGCC Hexanucleotide Repeat in Noncoding Region of C9ORF72 Causes Chromosome 9p-Linked FTD and ALS. *Neuron*. https://doi.org/10.1016/j.neuron.2011.09.011

Demine, S., Renard, P., & Arnould, T. (2019). Mitochondrial Uncoupling: A Key Controller of Biological Processes in Physiology and Diseases. *Cells*, *8*(8). https://doi.org/10.3390/CELLS8080795

Deng, J., Yang, M., Chen, Y., Chen, X., Liu, J., Sun, S., Cheng, H., Li, Y., Bigio, E. H., Mesulam, M., Xu, Q., Du, S., Fushimi, K., Zhu, L., & Wu, J. Y. (2015). FUS Interacts with HSP60 to Promote Mitochondrial Damage. *PLoS Genetics*, *11*(9), 1005357. https://doi.org/10.1371/JOURNAL.PGEN.1005357

Desai, S., Juncker, M., & Kim, C. (2018). Regulation of mitophagy by the ubiquitin pathway in neurodegenerative diseases. *Experimental Biology and Medicine*, *243*(6), 554. https://doi.org/10.1177/1535370217752351

Devlin, A. C., Burr, K., Borooah, S., Foster, J. D., Cleary, E. M., Geti, I., Vallier, L., Shaw, C. E., Chandran, S., & Miles, G. B. (2015). Human iPSC-derived motoneurons harbouring TARDBP or C9ORF72 ALS mutations are dysfunctional despite maintaining viability. *Nature Communications 2015 6:1*, *6*(1), 1–12. https://doi.org/10.1038/ncomms6999

Dong, X. X., Wang, Y., & Qin, Z. H. (2009). Molecular mechanisms of excitotoxicity and their relevance to pathogenesis of neurodegenerative diseases. *Acta Pharmacologica Sinica*, *30*(4), 379. https://doi.org/10.1038/APS.2009.24

Donnelly, C. J., Zhang, P. W., Pham, J. T., Heusler, A. R., Mistry, N. A., Vidensky, S., Daley, E. L., Poth, E. M., Hoover, B., Fines, D. M., Maragakis, N., Tienari, P. J., Petrucelli, L., Traynor, B. J., Wang, J., Rigo, F., Bennett, C. F., Blackshaw, S., Sattler, R., & Rothstein, J. D. (2013). RNA Toxicity from the ALS/FTD C9ORF72 Expansion Is Mitigated by Antisense Intervention. *Neuron*. https://doi.org/10.1016/j.neuron.2013.10.015

Dossou, A. S., & Basu, A. (2019). The Emerging Roles of mTORC1 in Macromanaging Autophagy. *Cancers 2019, Vol. 11, Page 1422*, *11*(10), 1422. https://doi.org/10.3390/CANCERS11101422

Duchen, M. R. (2000). Mitochondria and calcium: from cell signalling to cell death. *The Journal of Physiology*, *529 Pt 1*(Pt 1), 57–68. https://doi.org/10.1111/j.1469-7793.2000.00057.x

Ehlers, M. D. (2000). Reinsertion or Degradation of AMPA Receptors Determined by Activity-Dependent Endocytic Sorting. *Neuron*, *28*(2), 511–525. https://doi.org/10.1016/S0896-6273(00)00129-X

Elamin, M., Phukan, J., Bede, P., Jordan, N., Byrne, S., Pender, N., & Hardiman, O. (2011). Executive dysfunction is a negative prognostic indicator in patients with ALS without dementia. *Neurology*. https://doi.org/10.1212/WNL.0b013e318214359f

Enogieru, A. B., Omoruyi, S. I., Hiss, D. C., & Ekpo, O. E. (2019). GRP78/BIP/HSPA5 as a Therapeutic Target in Models of Parkinson's Disease: A Mini Review. *Advances in Pharmacological Sciences*, *2019*, 2706783. https://doi.org/10.1155/2019/2706783

Eura, Y., Ishihara, N., Yokota, S., & Mihara, K. (2003). Two Mitofusin Proteins, Mammalian Homologues of FZO, with Distinct Functions Are Both Required for Mitochondrial Fusion. *The Journal of Biochemistry*, *134*(3), 333–344. https://doi.org/10.1093/JB/MVG150

Evans, C. S., & Holzbaur, E. L. F. (2019). Autophagy and mitophagy in ALS. *Neurobiology of Disease*, *122*, 35–40. https://doi.org/10.1016/J.NBD.2018.07.005

Fan, M. M. Y., & Raymond, L. A. (2007). N-Methyl-d-aspartate (NMDA) receptor function and excitotoxicity in Huntington's disease. *Progress in Neurobiology*, *81*(5–6), 272–293. https://doi.org/10.1016/J.PNEUROBIO.2006.11.003

Ferrari, R., Kapogiannis, D., Huey, E. D., & Momeni, P. (2011). FTD and ALS: a tale of two diseases. *Current Alzheimer Research*, *8*(3), 273. https://doi.org/10.2174/156720511795563700

Filler, K., Lyon, D., Bennett, J., McCain, N., Elswick, R., Lukkahatai, N., & Saligan, L. N. (2014). Association of mitochondrial dysfunction and fatigue: A review of the literature. *BBA Clinical*, *1*, 12. https://doi.org/10.1016/J.BBACLI.2014.04.001

Fischer, L. R., Culver, D. G., Tennant, P., Davis, A. A., Wang, M., Castellano-Sanchez, A., Khan, J., Polak, M. A., & Glass, J. D. (2004). Amyotrophic lateral sclerosis is a distal axonopathy: evidence in mice and man. *Experimental Neurology*, *185*(2), 232–240. https://doi.org/10.1016/J.EXPNEUROL.2003.10.004

Fischer, L. R., & Glass, J. D. (2007). Axonal Degeneration in Motor Neuron Disease. *Neurodegenerative Diseases*, *4*(6), 431–442. https://doi.org/10.1159/000107704

Fischer-Hayes, L. R., Brotherton, T., & Glass, J. D. (2013). Axonal degeneration in the peripheral nervous system: Implications for the pathogenesis of amyotrophic lateral sclerosis. *Experimental Neurology*, *246*, 6–13. https://doi.org/10.1016/J.EXPNEUROL.2013.05.001

Floris, G., Borghero, G., Cannas, A., Di Stefano, F., Murru, M. R., Corongiu, D., Cuccu, S., Tranquilli, S., Cherchi, M. V., Serra, A., Loi, G., Marrosu, M. G., Chiò, A., & Marrosu, F. (2015). Clinical phenotypes and radiological findings in frontotemporal dementia related to TARDBP mutations. *Journal of Neurology*. https://doi.org/10.1007/s00415-014-7575-5

Fomin, V., Richard, P., Hoque, M., Li, C., Gu, Z., Fissore-O'Leary, M., Tian, B., Prives, C., & Manley, J. L. (2018). The C9ORF72 Gene, Implicated in Amyotrophic Lateral Sclerosis and Frontotemporal Dementia, Encodes a Protein That Functions in Control of Endothelin and Glutamate Signaling . *Molecular and Cellular Biology*, *38*(22). https://doi.org/10.1128/MCB.00155-18/SUPPL_FILE/ZMB999101858SM3.AVI

Fonseca, T. B., Sánchez-Guerrero, Á., Milosevic, I., & Raimundo, N. (2019). Mitochondrial fission requires DRP1 but not dynamins. *Nature 2019 570:7761*, *570*(7761), E34–E42. https://doi.org/10.1038/s41586-019-1296-y

Fortier, G., Butti, Z., & Patten, S. A. (2020). Modelling C9orf72-Related Amyotrophic Lateral Sclerosis in Zebrafish. *Biomedicines*, *8*(10), 440. https://doi.org/10.3390/biomedicines8100440

Fransson, Å., Ruusala, A., & Aspenström, P. (2006). The atypical Rho GTPases Miro-1 and Miro-2 have essential roles in mitochondrial trafficking. *Biochemical and Biophysical Research Communications*, *344*(2), 500–510. https://doi.org/10.1016/J.BBRC.2006.03.163

Freibaum, B. D., Lu, Y., Lopez-Gonzalez, R., Kim, N. C., Almeida, S., Lee, K. H., Badders, N., Valentine, M., Miller, B. L., Wong, P. C., Petrucelli, L., Kim, H. J., Gao, F. B., & Taylor, J. P. (2015). GGGGCC repeat expansion in C9orf72 compromises nucleocytoplasmic transport. *Nature 2015 525:7567*, *525*(7567), 129–133. https://doi.org/10.1038/nature14974

Freibaum, B. D., & Taylor, J. P. (2017). The role of dipeptide repeats in C9ORF72-related ALS-FTD. In *Frontiers in Molecular Neuroscience*. https://doi.org/10.3389/fnmol.2017.00035

Frottin, F., Pérez-Berlanga, M., Hartl, F. U., & Hipp, M. S. (2021). Multiple pathways of toxicity induced by C9orf72 dipeptide repeat aggregates and G4C2 RNA in a cellular model. *ELife*, *10*. https://doi.org/10.7554/ELIFE.62718

Galluzzi, L., Bravo-San Pedro, J. M., & Kroemer, G. (2014). Organelle-specific initiation of cell death. *Nature Cell Biology 2014 16:8*, *16*(8), 728–736. https://doi.org/10.1038/ncb3005

Galluzzi, L., Vitale, I., Aaronson, S. A., Abrams, J. M., Adam, D., Agostinis, P., Alnemri, E. S., Altucci, L., Amelio, I., Andrews, D. W., Annicchiarico-Petruzzelli, M., Antonov, A. v., Arama, E., Baehrecke, E. H., Barlev, N. A., Bazan, N. G., Bernassola, F., Bertrand, M. J. M., Bianchi, K., … Kroemer, G. (2018). Molecular mechanisms of cell death: recommendations of the Nomenclature Committee on Cell Death 2018. *Cell Death & Differentiation 2018 25:3*, *25*(3), 486–541. https://doi.org/10.1038/s41418-017-0012-4

Galvan, A., & Wichmann, T. (2008). Pathophysiology of Parkinsonism. *Clinical Neurophysiology*, *119*(7), 1459–1474. https://doi.org/https://doi.org/10.1016/j.clinph.2008.03.017

Gao, F., Almeida, S., & Lopez-Gonzalez, R. (2017). Dysregulated molecular pathways in amyotrophic lateral sclerosis–frontotemporal dementia spectrum disorder. *The EMBO Journal*. https://doi.org/10.15252/embj.201797568

Gao, J., Wang, L., Liu, J., Xie, F., Su, B., & Wang, X. (2017). Abnormalities of Mitochondrial Dynamics in Neurodegenerative Diseases. *Antioxidants 2017, Vol. 6, Page 25*, *6*(2), 25. https://doi.org/10.3390/ANTIOX6020025

Gascon, E., Lynch, K., Ruan, H., Almeida, S., Verheyden, J. M., Seeley, W. W., Dickson, D. W., Petrucelli, L., Sun, D., Jiao, J., Zhou, H., Jakovcevski, M., Akbarian, S., Yao, W. D., & Gao, F. B. (2014). Alterations in microRNA-124 and AMPA receptors contribute to social behavioral deficits in frontotemporal dementia. *Nature Medicine 2014 20:12*, *20*(12), 1444–1451. https://doi.org/10.1038/nm.3717

Gass, J., Cannon, A., Mackenzie, I. R., Boeve, B., Baker, M., Adamson, J., Crook, R., Melquist, S., Kuntz, K., Petersen, R., Josephs, K., Pickering-Brown, S. M., Graff-Radford, N., Uitti, R., Dickson, D., Wszolek, Z., Gonzalez, J., Beach, T. G., Bigio, E., … Rademakers, R. (2006). Mutations in

progranulin are a major cause of ubiquitin-positive frontotemporal lobar degeneration. *Human Molecular Genetics*, *15*(20), 2988–3001. https://doi.org/10.1093/HMG/DDL241

Geevasinga, N., Menon, P., Nicholson, G. A., Ng, K., Howells, J., Kril, J. J., Yiannikas, C., Kiernan, M. C., & Vucic, S. (2015). Cortical Function in Asymptomatic Carriers and Patients With C9orf72 Amyotrophic Lateral Sclerosis. *JAMA Neurology*, *72*(11), 1268–1274. https://doi.org/10.1001/JAMANEUROL.2015.1872

Gendron, T. F., Bieniek, K. F., Zhang, Y.-J., Jansen-West, K., Ash, P. E. A., Caulfield, T., Daughrity, L., Dunmore, J. H., Castanedes-Casey, M., Chew, J., Cosio, D. M., van Blitterswijk, M., Lee, W. C., Rademakers, R., Boylan, K. B., Dickson, D. W., & Petrucelli, L. (2013). Antisense transcripts of the expanded C9ORF72 hexanucleotide repeat form nuclear RNA foci and undergo repeat-associated non-ATG translation in c9FTD/ALS. *Acta Neuropathologica*, *126*(6), 829–844. https://doi.org/10.1007/s00401-013-1192-8

Ghasemi, M., Keyhanian, K., & Douthwright, C. (2021). Glial Cell Dysfunction in C9orf72-Related Amyotrophic Lateral Sclerosis and Frontotemporal Dementia. *Cells 2021, Vol. 10, Page 249*, *10*(2), 249. https://doi.org/10.3390/CELLS10020249

Giacomelli, E., Vahsen, B. F., Calder, E. L., Xu, Y., Scaber, J., Gray, E., Dafinca, R., Talbot, K., & Studer, L. (2022). Human stem cell models of neurodegeneration: From basic science of amyotrophic lateral sclerosis to clinical translation. *Cell Stem Cell*, *29*(1), 11–35. https://doi.org/10.1016/J.STEM.2021.12.008

Gijselinck, I., van Mossevelde, S., van der Zee, J., Sieben, A., Engelborghs, S., de Bleecker, J., Ivanoiu, A., Deryck, O., Edbauer, D., Zhang, M., Heeman, B., Bäumer, V., van den Broeck, M., Mattheijssens, M., Peeters, K., Rogaeva, E., de Jonghe, P., Cras, P., Martin, J. J., … van Broeckhoven, C. (2015). The C9orf72 repeat size correlates with onset age of disease, DNA methylation and transcriptional downregulation of the promoter. *Molecular Psychiatry 2016 21:8*, *21*(8), 1112–1124. https://doi.org/10.1038/mp.2015.159

Gilkerson, R., de La Torre, P., & st. Vallier, S. (2021). Mitochondrial OMA1 and OPA1 as Gatekeepers of Organellar Structure/Function and Cellular Stress Response. *Frontiers in Cell and Developmental Biology*, *9*, 527. https://doi.org/10.3389/FCELL.2021.626117/BIBTEX

Gilks, N., Kedersha, N., Ayodele, M., Shen, L., Stoecklin, G., Dember, L. M., & Anderson, P. (2004). Stress Granule Assembly Is Mediated by Prion-like Aggregation of TIA-1. *Https://Doi.Org/10.1091/Mbc.E04-08-0715*, *15*(12), 5383–5398. https://doi.org/10.1091/MBC.E04-08-0715

Gittings, L. M., & Sattler, R. (2020). Recent advances in understanding amyotrophic lateral sclerosis and emerging therapies. *Faculty Reviews*, *9*, 12. https://doi.org/10.12703/b/9-12

Glick, D., Barth, S., & Macleod, K. F. (2010). Autophagy: cellular and molecular mechanisms. *The Journal of Pathology*, *221*(1), 3. https://doi.org/10.1002/PATH.2697

Gomez-Suaga, P., Mórotz, G. M., Markovinovic, A., Martín-Guerrero, S. M., Preza, E., Arias, N., Mayl, K., Aabdien, A., Gesheva, V., Nishimura, A., Annibali, A., Lee, Y., Mitchell, J. C., Wray, S., Shaw, C., Noble, W., & Miller, C. C. J. (2022). Disruption of ER-mitochondria tethering and signalling in C9orf72-associated amyotrophic lateral sclerosis and frontotemporal dementia. *Aging Cell*, *21*(2), e13549. https://doi.org/10.1111/ACEL.13549

Gómez-Suaga, P., Pérez-Nievas, B. G., Glennon, E. B., Lau, D. H. W., Paillusson, S., Mórotz, G. M., Calì, T., Pizzo, P., Noble, W., & Miller, C. C. J. (2019). The VAPB-PTPIP51 endoplasmic reticulum-mitochondria tethering proteins are present in neuronal synapses and regulate synaptic activity. *Acta Neuropathologica Communications*, *7*(1), 35. https://doi.org/10.1186/S40478-019-0688-4

Götzl, J. K., Lang, C. M., Haass, C., & Capell, A. (2016). Impaired protein degradation in FTLD and related disorders. In *Ageing Research Reviews*. https://doi.org/10.1016/j.arr.2016.04.008

Götzl, J. K., Mori, K., Damme, M., Fellerer, K., Tahirovic, S., Kleinberger, G., Janssens, J., Van Der Zee, J., Lang, C. M., Kremmer, E., Martin, J. J., Engelborghs, S., Kretzschmar, H. A., Arzberger, T., Van Broeckhoven, C., Haass, C., & Capell, A. (2014). Common pathobiochemical hallmarks of progranulin-associated frontotemporal lobar degeneration and neuronal ceroid lipofuscinosis. *Acta Neuropathologica*. https://doi.org/10.1007/s00401-014-1262-6

Greaves, C. V., & Rohrer, J. D. (2019). An update on genetic frontotemporal dementia. In *Journal of Neurology*. https://doi.org/10.1007/s00415-019-09363-4

Green, K. M., Glineburg, M. R., Kearse, M. G., Flores, B. N., Linsalata, A. E., Fedak, S. J., Goldstrohm, A. C., Barmada, S. J., & Todd, P. K. (2017). RAN translation at C9orf72-associated repeat expansions is selectively enhanced by the integrated stress response. *Nature Communications*, *8*(1), 2005. https://doi.org/10.1038/s41467-017-02200-0

Greene, J. C., Whitworth, A. J., Kuo, I., Andrews, L. A., Feany, M. B., & Pallanck, L. J. (2003). Mitochondrial pathology and apoptotic muscle degeneration in Drosophila parkin mutants. *Proceedings of the National Academy of Sciences*, *100*(7), 4078–4083. https://doi.org/10.1073/PNAS.0737556100

Guan, B.-J., Krokowski, D., Majumder, M., Schmotzer, C. L., Kimball, S. R., Merrick, W. C., Koromilas, A. E., & Hatzoglou, M. (2014). Translational control during endoplasmic reticulum stress beyond phosphorylation of the translation initiation factor eIF2α. *The Journal of Biological Chemistry*, *289*(18), 12593–12611. https://doi.org/10.1074/jbc.M113.543215

Guo, C. Y., Sun, L., Chen, X. P., & Zhang, D. S. (2013). Oxidative stress, mitochondrial damage and neurodegenerative diseases. *Neural Regeneration Research*, *8*(21), 2003. https://doi.org/10.3969/J.ISSN.1673-5374.2013.21.009

Guo, W., Naujock, M., Fumagalli, L., Vandoorne, T., Baatsen, P., Boon, R., Ordovás, L., Patel, A., Welters, M., Vanwelden, T., Geens, N., Tricot, T., Benoy, V., Steyaert, J., Lefebvre-Omar, C., Boesmans, W., Jarpe, M., Sterneckert, J., Wegner, F., … van den Bosch, L. (2017). HDAC6 inhibition reverses axonal transport defects in motor neurons derived from FUS-ALS patients. *Nature Communications 2017 8:1*, *8*(1), 1–15. https://doi.org/10.1038/s41467-017-00911-y

Guo, W., Stoklund Dittlau, K., & van den Bosch, L. (2020). Axonal transport defects and neurodegeneration: Molecular mechanisms and therapeutic implications. *Seminars in Cell & Developmental Biology*, *99*, 133–150. https://doi.org/10.1016/J.SEMCDB.2019.07.010

Haeusler, A. R., Donnelly, C. J., & Rothstein, J. D. (2016). The expanding biology of the C9orf72 nucleotide repeat expansion in neurodegenerative disease. *Nature Reviews. Neuroscience*, *17*(6), 383–395. https://doi.org/10.1038/NRN.2016.38

Haghnia, M., Cavalli, V., Shah, S. B., Schimmelpfeng, K., Brusch, R., Yang, G., Herrera, C., Pilling, A., & Goldstein, L. S. B. (2007). Dynactin is required for coordinated bidirectional motility, but not for

dynein membrane attachment. *Molecular Biology of the Cell*, *18*(6), 2081–2089. https://doi.org/10.1091/MBC.E06-08-0695/ASSET/IMAGES/LARGE/ZMK0060780690004.JPEG

Hao, Z., Liu, L., Tao, Z., Wang, R., Ren, H., Sun, H., Lin, Z., Zhang, Z., Mu, C., Zhou, J., & Wang, G. (2019). Motor dysfunction and neurodegeneration in a C9orf72 mouse line expressing poly-PR. *Nature Communications 2019 10:1*, *10*(1), 1–11. https://doi.org/10.1038/s41467-019-10956-w

Hardiman, O., Al-Chalabi, A., Chio, A., Corr, E. M., Logroscino, G., Robberecht, W., Shaw, P. J., Simmons, Z., & van den Berg, L. H. (2017). Amyotrophic lateral sclerosis. *Nature Reviews Disease Primers 2017 3:1*, *3*(1), 1–19. https://doi.org/10.1038/nrdp.2017.71

Hartmann, H., Hornburg, D., Czuppa, M., Bader, J., Michaelsen, M., Farny, D., Arzberger, T., Mann, M., Meissner, F., & Edbauer, D. (2018). Proteomics and C9orf72 neuropathology identify ribosomes as poly-GR/PR interactors driving toxicity. *Life Science Alliance*, *1*(2). https://doi.org/10.26508/LSA.201800070

Hautbergue, G. M., Castelli, L. M., Ferraiuolo, L., Sanchez-Martinez, A., Cooper-Knock, J., Higginbottom, A., Lin, Y. H., Bauer, C. S., Dodd, J. E., Myszczynska, M. A., Alam, S. M., Garneret, P., Chandran, J. S., Karyka, E., Stopford, M. J., Smith, E. F., Kirby, J., Meyer, K., Kaspar, B. K., … Shaw, P. J. (2017). SRSF1-dependent nuclear export inhibition of C9ORF72 repeat transcripts prevents neurodegeneration and associated motor deficits. *Nature Communications 2017 8:1*, *8*(1), 1–18. https://doi.org/10.1038/ncomms16063

Hautbergue, G. M., Cleary, J. D., Guo, S., & Ranum, L. P. W. (2021). Therapeutic strategies for C9orf72 amyotrophic lateral sclerosis and frontotemporal dementia. *Current Opinion in Neurology*, *34*(5), 748–755. https://doi.org/10.1097/WCO.0000000000000984

He, Z., Ong, C. H. P., Halper, J., & Bateman, A. (2003). Progranulin is a mediator of the wound response. *Nature Medicine*. https://doi.org/10.1038/nm816

Hegedus, J., Putman, C. T., & Gordon, T. (2007). Time course of preferential motor unit loss in the SOD1G93A mouse model of amyotrophic lateral sclerosis. *Neurobiology of Disease*, *28*(2), 154–164. https://doi.org/10.1016/J.NBD.2007.07.003

Hernandez-Resendiz, S., Prunier, F., Girao, H., Dorn, G., & Hausenloy, D. J. (2020). Targeting mitochondrial fusion and fission proteins for cardioprotection. *Journal of Cellular and Molecular Medicine*, *24*(12), 6571–6585. https://doi.org/10.1111/JCMM.15384

Herzog, E., Bellenchi, G. C., Gras, C., Bernard, V., Ravassard, P., Bedet, C., Gasnier, B., Giros, B., & El Mestikawy, S. (2001). The existence of a second vesicular glutamate transporter specifies subpopulations of glutamatergic neurons. *The Journal of Neuroscience : The Official Journal of the Society for Neuroscience*, *21*(22), RC181. https://doi.org/10.1523/JNEUROSCI.21-22-j0001.2001

Herzog, J. J., Xu, W., Deshpande, M., Rahman, R., Suib, H., Rodal, A. A., Rosbash, M., & Paradis, S. (2020). TDP-43 dysfunction restricts dendritic complexity by inhibiting CREB activation and altering gene expression. *Proceedings of the National Academy of Sciences of the United States of America*, *117*(21). https://doi.org/10.1073/PNAS.1917038117/-/DCSUPPLEMENTAL

Hetz, C. (2012). The unfolded protein response: controlling cell fate decisions under ER stress and beyond. *Nature Reviews Molecular Cell Biology*, *13*(2), 89–102. https://doi.org/10.1038/nrm3270

Hiji Masanori, M., Takahashi, T., Fukuba, H., Yamashita, H., Kohriyama, T., & Matsumoto, M. (2008). White matter lesions in the brain with frontotemporal lobar degeneration with motor neuron disease: TDP-43-immunopositive inclusions co-localize with p62, but not ubiquitin. *Acta Neuropathologica*. https://doi.org/10.1007/s00401-008-0402-2

Hirokawa, N., Niwa, S., & Tanaka, Y. (2010). Molecular Motors in Neurons: Transport Mechanisms and Roles in Brain Function, Development, and Disease. *Neuron*, *68*(4), 610–638. https://doi.org/10.1016/J.NEURON.2010.09.039

Hirokawa, N., Sato-Yoshitake, R., Yoshida, T., & Kawashima, T. (1990). Brain dynein (MAP1C) localizes on both anterogradely and retrogradely transported membranous organelles in vivo. *Journal of Cell Biology*, *111*(3), 1027–1037. https://doi.org/10.1083/JCB.111.3.1027

Hjerpe, R., Bett, J. S., Keuss, M. J., Solovyova, A., McWilliams, T. G., Johnson, C., Sahu, I., Varghese, J., Wood, N., Wightman, M., Osborne, G., Bates, G. P., Glickman, M. H., Trost, M., Knebel, A., Marchesi, F., & Kurz, T. (2016). UBQLN2 Mediates Autophagy-Independent Protein Aggregate Clearance by the Proteasome. *Cell*, *166*(4), 935–949. https://doi.org/10.1016/J.CELL.2016.07.001

Ho, W. Y., Tai, Y. K., Chang, J. C., Liang, J., Tyan, S. H., Chen, S., Guan, J. L., Zhou, H., Shen, H. M., Koo, E., & Ling, S. C. (2019). The ALS-FTD-linked gene product, C9orf72, regulates neuronal morphogenesis via autophagy. *Autophagy*. https://doi.org/10.1080/15548627.2019.1569441

Hong, S., & Pedersen, P. L. (2008). ATP Synthase and the Actions of Inhibitors Utilized To Study Its Roles in Human Health, Disease, and Other Scientific Areas. *Microbiology and Molecular Biology Reviews*, *72*(4), 590–641. https://doi.org/10.1128/MMBR.00016-08

Howland, D. S., Liu, J., She, Y., Goad, B., Maragakis, N. J., Kim, B., Erickson, J., Kulik, J., DeVito, L., Psaltis, G., DeGennaro, L. J., Cleveland, D. W., & Rothstein, J. D. (2002). Focal loss of the glutamate transporter EAAT2 in a transgenic rat model of SOD1 mutant-mediated amyotrophic lateral sclerosis (ALS). *Proceedings of the National Academy of Sciences*, *99*(3), 1604–1609. https://doi.org/10.1073/PNAS.032539299

Hu, F., Padukkavidana, T., Vægter, C. B., Brady, O. A., Zheng, Y., Mackenzie, I. R., Feldman, H. H., Nykjaer, A., & Strittmatter, S. M. (2010). Sortilin-mediated endocytosis determines levels of the frontotemporal dementia protein, progranulin. *Neuron*. https://doi.org/10.1016/j.neuron.2010.09.034

Huganir, R. L., & Nicoll, R. A. (2013). AMPARs and synaptic plasticity: the last 25 years. *Neuron*, *80*(3), 704–717. https://doi.org/10.1016/J.NEURON.2013.10.025

Ioakeimidis, F., Ott, C., Kozjak-Pavlovic, V., Violitzi, F., Rinotas, V., Makrinou, E., Eliopoulos, E., Fasseas, C., Kollias, G., & Douni, E. (2014). A Splicing Mutation in the Novel Mitochondrial Protein DNAJC11 Causes Motor Neuron Pathology Associated with Cristae Disorganization, and Lymphoid Abnormalities in Mice. *PLoS ONE*, *9*(8), 104237. https://doi.org/10.1371/JOURNAL.PONE.0104237

Islam, M. T. (2016). Oxidative stress and mitochondrial dysfunction-linked neurodegenerative disorders. *Https://Doi.Org/10.1080/01616412.2016.1251711*, *39*(1), 73–82. https://doi.org/10.1080/01616412.2016.1251711

Itakura, E., Zavodszky, E., Shao, S., Wohlever, M. L., Keenan, R. J., & Hegde, R. S. (2016). Ubiquilins Chaperone and Triage Mitochondrial Membrane Proteins for Degradation. *Molecular Cell*, *63*(1), 21–33. https://doi.org/10.1016/J.MOLCEL.2016.05.020

Ivannikov, M. v., Sugimori, M., & Llinás, R. R. (2010). Calcium clearance and its energy requirements in cerebellar neurons. *Cell Calcium*, *47*(6), 507. https://doi.org/10.1016/J.CECA.2010.04.004

Jeong, J., Pandey, S., Li, Y., Badger, J. D., Lu, W., & Roche, K. W. (2019). PSD-95 binding dynamically regulates NLGN1 trafficking and function. *Proceedings of the National Academy of Sciences of the United States of America*, *116*(24), 12035–12044. https://doi.org/10.1073/PNAS.1821775116/-/DCSUPPLEMENTAL

Ji, A. L., Zhang, X., Chen, W. W., & Huang, W. J. (2017). Genetics insight into the amyotrophic lateral sclerosis/frontotemporal dementia spectrum. *Journal of Medical Genetics*. https://doi.org/10.1136/jmedgenet-2016-104271

Ji, Y. J., Ugolino, J., Brady, N. R., Hamacher-Brady, A., & Wang, J. (2017). Systemic deregulation of autophagy upon loss of ALS- and FTD-linked C9orf72. *Https://Doi.Org/10.1080/15548627.2017.1299312*, *13*(7), 1254–1255. https://doi.org/10.1080/15548627.2017.1299312

Jiang, J., Zhu, Q., Gendron, T. F., Saberi, S., McAlonis-Downes, M., Seelman, A., Stauffer, J. E., Jafar-nejad, P., Drenner, K., Schulte, D., Chun, S., Sun, S., Ling, S. C., Myers, B., Engelhardt, J., Katz, M., Baughn, M., Platoshyn, O., Marsala, M., … Lagier-Tourenne, C. (2016). Gain of Toxicity from ALS/FTD-Linked Repeat Expansions in C9ORF72 Is Alleviated by Antisense Oligonucleotides Targeting GGGGCC-Containing RNAs. *Neuron*, *90*(3), 535–550. https://doi.org/10.1016/J.NEURON.2016.04.006

Jiang, X., Chen, C., Zhao, W., & Zhang, Z. (2013). Sodium arsenite and arsenic trioxide differently affect the oxidative stress, genotoxicity and apoptosis in A549 cells: An implication for the paradoxical mechanism. *Environmental Toxicology and Pharmacology*, *36*(3), 891–902. https://doi.org/10.1016/J.ETAP.2013.08.002

Jicha, G. A., & Nelson, P. T. (2011). Management of frontotemporal dementia: targeting symptom management in such a heterogeneous disease requires a wide range of therapeutic options. *Neurodegenerative Disease Management*, *1*(2), 141. https://doi.org/10.2217/NMT.11.9

Jo, Y., Cho, H. M., Sun, W., & Ryu, J. R. (2017). Localization of dynamin-related protein 1 and its potential role in lamellipodia formation. *Histochemistry and Cell Biology*, *148*(1), 13–20. https://doi.org/10.1007/S00418-017-1554-8

Johri, A., & Beal, M. F. (2012). Mitochondrial Dysfunction in Neurodegenerative Diseases. *Journal of Pharmacology and Experimental Therapeutics*, *342*(3), 619–630. https://doi.org/10.1124/JPET.112.192138

Joselin, A. P., Hewitt, S. J., Callaghan, S. M., Kim, R. H., Chung, Y. H., Mak, T. W., Shen, J., Slack, R. S., & Park, D. S. (2012). ROS-dependent regulation of Parkin and DJ-1 localization during oxidative stress in neurons. *Human Molecular Genetics*, *21*(22), 4888–4903. https://doi.org/10.1093/HMG/DDS325

Julien, O., & Wells, J. A. (2017). Caspases and their substrates. *Cell Death & Differentiation 2017 24:8*, *24*(8), 1380–1389. https://doi.org/10.1038/cdd.2017.44

Kabashi, E., Lin, L., Tradewell, M. L., Dion, P. A., Bercier, V., Bourgouin, P., Rochefort, D., Bel Hadj, S., Durham, H. D., Velde, C. Vande, Rouleau, G. A., & Drapeau, P. (2009). Gain and loss of function of ALS-related mutations of TARDBP (TDP-43) cause motor deficits in vivo. *Human Molecular Genetics*. https://doi.org/10.1093/hmg/ddp534

Kadowaki, M., & Karim, M. R. (2009). Chapter 13 Cytosolic LC3 Ratio as a Quantitative Index of Macroautophagy. *Methods in Enzymology*, *452*(C), 199–213. https://doi.org/10.1016/S0076-6879(08)03613-6

Kaneko, T., & Fujiyama, F. (2002). Complementary distribution of vesicular glutamate transporters in the central nervous system. *Neuroscience Research*, *42*(4), 243–250. https://doi.org/10.1016/s0168-0102(02)00009-3

Kang, S. H., Li, Y., Fukaya, M., Lorenzini, I., Cleveland, D. W., Ostrow, L. W., Rothstein, J. D., & Bergles, D. E. (2013). Degeneration and impaired regeneration of gray matter oligodendrocytes in amyotrophic lateral sclerosis. *Nature Neuroscience 2013 16:5*, *16*(5), 571–579. https://doi.org/10.1038/nn.3357

Kania, E., Roest, G., Vervliet, T., Parys, J. B., & Bultynck, G. (2017). IP3 receptor-mediated calcium signaling and its role in autophagy in cancer. *Frontiers in Oncology*, *7*(JUL), 140. https://doi.org/10.3389/FONC.2017.00140/BIBTEX

Kann, O., & Kovács, R. (2007). Mitochondria and neuronal activity. *American Journal of Physiology - Cell Physiology*, *292*(2), 641–657. https://doi.org/10.1152/AJPCELL.00222.2006/ASSET/IMAGES/LARGE/ZH00020750970002.JPEG

Kansal, K., Mareddy, M., Sloane, K. L., Minc, A. A., Rabins, P. V., McGready, J. B., & Onyike, C. U. (2016). Survival in Frontotemporal Dementia Phenotypes: A Meta-Analysis. In *Dementia and Geriatric Cognitive Disorders*. https://doi.org/10.1159/000443205

Katsetos, C. D., Legido, A., Perentes, E., & Mörk, S. J. (2003). Class III beta-tubulin isotype: a key cytoskeletal protein at the crossroads of developmental neurobiology and tumor neuropathology. *Journal of Child Neurology*, *18*(12), 851–866. https://doi.org/10.1177/088307380301801205

Katz, J. S., Katzberg, H. D., Woolley, S. C., Marklund, S. L., & Andersen, P. M. (2012). Combined fulminant frontotemporal dementia and amyotrophic lateral sclerosis associated with an I113T SOD1 mutation. *Amyotrophic Lateral Sclerosis*, *13*(6), 567–569. https://doi.org/10.3109/17482968.2012.678365

Kaufmann, T., Tai, L., Ekert, P. G., Huang, D. C. S., Norris, F., Lindemann, R. K., Johnstone, R. W., Dixit, V. M., & Strasser, A. (2007). The BH3-Only Protein Bid Is Dispensable for DNA Damage- and Replicative Stress-Induced Apoptosis or Cell-Cycle Arrest. *Cell*, *129*(2), 423–433. https://doi.org/10.1016/J.CELL.2007.03.017

Kawahara, Y., & Mieda-Sato, A. (2012). TDP-43 promotes microRNA biogenesis as a component of the Drosha and Dicer complexes. *Proceedings of the National Academy of Sciences of the United States of America*. https://doi.org/10.1073/pnas.1112427109

Kedersha, N., Cho, M. R., Li, W., Yacono, P. W., Chen, S., Gilks, N., Golan, D. E., & Anderson, P. (2000). Dynamic Shuttling of Tia-1 Accompanies the Recruitment of mRNA to Mammalian Stress Granules. *Journal of Cell Biology*, *151*(6), 1257–1268. https://doi.org/10.1083/JCB.151.6.1257

Kersaitis, C., Halliday, G. M., & Kril, J. J. (2004). Regional and cellular pathology in frontotemporal dementia: Relationship to stage of disease in cases with and without Pick bodies. *Acta Neuropathologica*, *108*(6), 515–523. https://doi.org/10.1007/S00401-004-0917-0/FIGURES/3

Khoury, R., Liu, Y., Sheheryar, Q., & Grossberg, G. T. (2021). Pharmacotherapy for Frontotemporal Dementia. *CNS Drugs*, *35*(4), 425–438. https://doi.org/10.1007/S40263-021-00813-0/TABLES/3

Kilpinen, H., Goncalves, A., Leha, A., Afzal, V., Alasoo, K., Ashford, S., Bala, S., Bensaddek, D., Casale, F. P., Culley, O. J., Danecek, P., Faulconbridge, A., Harrison, P. W., Kathuria, A., McCarthy, D., McCarthy, S. A., Meleckyte, R., Memari, Y., Moens, N., … Gaffney, D. J. (2017). Common genetic variation drives molecular heterogeneity in human iPSCs. *Nature 2017 546:7658*, *546*(7658), 370–375. https://doi.org/10.1038/nature22403

Kim, E. J., Sidhu, M., Gaus, S. E., Huang, E. J., Hof, P. R., Miller, B. L., DeArmond, S. J., & Seeley, W. W. (2012). Selective Frontoinsular von Economo Neuron and Fork Cell Loss in Early Behavioral Variant Frontotemporal Dementia. *Cerebral Cortex*, *22*(2), 251–259. https://doi.org/10.1093/CERCOR/BHR004

Kim, N. C., Tresse, E., Kolaitis, R. M., Molliex, A., Thomas, R. E., Alami, N. H., Wang, B., Joshi, A., Smith, R. B., Ritson, G. P., Winborn, B. J., Moore, J., Lee, J. Y., Yao, T. P., Pallanck, L., Kundu, M., & Taylor, J. P. (2013). VCP Is Essential for Mitochondrial Quality Control by PINK1/Parkin and this Function Is Impaired by VCP Mutations. *Neuron*, *78*(1), 65–80. https://doi.org/10.1016/J.NEURON.2013.02.029

Kirk, K., Gennings, C., Hupf, J. C., Tadesse, S., D'Aurelio, M., Kawamata, H., Valsecchi, F., Mitsumoto, H., & Manfredi, G. (2014). Bioenergetic markers in skin fibroblasts of sporadic amyotrophic lateral sclerosis and progressive lateral sclerosis patients. *Annals of Neurology*, *76*(4), 620–624. https://doi.org/10.1002/ANA.24244

Kishi, S., Slack, B. E., Uchiyama, J., & Zhdanova, I. v. (2009). Zebrafish as a Genetic Model in Biological and Behavioral Gerontology: Where Development Meets Aging in Vertebrates – A Mini-Review. *Gerontology*, *55*(4), 430. https://doi.org/10.1159/000228892

Koppers, M., van Blitterswijk, M. M., Vlam, L., Rowicka, P. A., van Vught, P. W. J., Groen, E. J. N., Spliet, W. G. M., Engelen-Lee, J. Y., Schelhaas, H. J., de Visser, M., van der Kooi, A. J., van der Pol, W. L., Pasterkamp, R. J., Veldink, J. H., & van den Berg, L. H. (2012). VCP mutations in familial and sporadic amyotrophic lateral sclerosis. *Neurobiology of Aging*, *33*(4), 837.e7-837.e13. https://doi.org/10.1016/J.NEUROBIOLAGING.2011.10.006

Koyano, F., Okatsu, K., Kosako, H., Tamura, Y., Go, E., Kimura, M., Kimura, Y., Tsuchiya, H., Yoshihara, H., Hirokawa, T., Endo, T., Fon, E. A., Trempe, J. F., Saeki, Y., Tanaka, K., & Matsuda, N. (2014). Ubiquitin is phosphorylated by PINK1 to activate parkin. *Nature*, *510*(7503), 162–166. https://doi.org/10.1038/NATURE13392

Krishnan, G., Zhang, Y., Gu, Y., Kankel, M. W., Gao, F. B., & Almeida, S. (2020). CRISPR deletion of the C9ORF72 promoter in ALS/FTD patient motor neurons abolishes production of dipeptide repeat proteins and rescues neurodegeneration. *Acta Neuropathologica*, *140*(1), 81. https://doi.org/10.1007/S00401-020-02154-6

Kurd, D. D., & Saxton, W. M. (1996). Kinesin Mutations Cause Motor Neuron Disease Phenotypes by Disrupting Fast Axonal Transport in Drosophila. *Genetics*, *144*(3), 1075–1085. https://doi.org/10.1093/GENETICS/144.3.1075

LaClair, K. D., Zhou, Q., Michaelsen, M., Wefers, B., Brill, M. S., Janjic, A., Rathkolb, B., Farny, D., Cygan, M., de Angelis, M. H., Wurst, W., Neumann, M., Enard, W., Misgeld, T., Arzberger, T., & Edbauer, D. (2020). Congenic expression of poly-GA but not poly-PR in mice triggers selective neuron loss and interferon responses found in C9orf72 ALS. *Acta Neuropathologica*, *140*(2), 121–142. https://doi.org/10.1007/S00401-020-02176-0/FIGURES/6

Lagier-Tourenne, C., Polymenidou, M., & Cleveland, D. W. (2010). TDP-43 and FUS/TLS: Emerging roles in RNA processing and neurodegeneration. *Human Molecular Genetics*. https://doi.org/10.1093/hmg/ddq137

Lagier-Tourenne, C., Polymenidou, M., Hutt, K. R., Vu, A. Q., Baughn, M., Huelga, S. C., Clutario, K. M., Ling, S. C., Liang, T. Y., Mazur, C., Wancewicz, E., Kim, A. S., Watt, A., Freier, S., Hicks, G. G., Donohue, J. P., Shiue, L., Bennett, C. F., Ravits, J., … Yeo, G. W. (2012). Divergent roles of ALS-linked proteins FUS/TLS and TDP-43 intersect in processing long pre-mRNAs. *Nature Neuroscience 2012 15:11*, *15*(11), 1488–1497. https://doi.org/10.1038/nn.3230

Lamark, T., Svenning, S., & Johansen, T. (2017). Regulation of selective autophagy: The p62/SQSTM1 paradigm. In *Essays in Biochemistry*. https://doi.org/10.1042/EBC20170035

Langseth, A. J., Kim, J., Ugolino, J. E., Shah, Y., Hwang, H. Y., Wang, J., Bergles, D. E., & Brown, S. P. (2017). Cell-type specific differences in promoter activity of the ALS-linked C9orf72 mouse ortholog. *Scientific Reports 2017 7:1*, *7*(1), 1–13. https://doi.org/10.1038/s41598-017-05864-2

Lazarou, M., Sliter, D. A., Kane, L. A., Sarraf, S. A., Wang, C., Burman, J. L., Sideris, D. P., Fogel, A. I., & Youle, R. J. (2015). The ubiquitin kinase PINK1 recruits autophagy receptors to induce mitophagy. *Nature*, *524*(7565), 309. https://doi.org/10.1038/NATURE14893

Le Ber, I. (2013). Genetics of frontotemporal lobar degeneration: An up-date and diagnosis algorithm. *Revue Neurologique*. https://doi.org/10.1016/j.neurol.2013.07.014

le Bras, A. (2021). Modeling ALS/FTD in mice: Updates on the C9orf72 BAC transgenic mice. *Lab Animal*, *50*(1), 13. https://doi.org/10.1038/s41684-020-00693-9

Lee, E. B., Lee, V. M. Y., & Trojanowski, J. Q. (2012). Gains or losses: Molecular mechanisms of TDP43-mediated neurodegeneration. In *Nature Reviews Neuroscience*. https://doi.org/10.1038/nrn3121

Lee, K. H., Zhang, P., Kim, H. J., Mitrea, D. M., Sarkar, M., Freibaum, B. D., Cika, J., Coughlin, M., Messing, J., Molliex, A., Maxwell, B. A., Kim, N. C., Temirov, J., Moore, J., Kolaitis, R. M., Shaw, T. I., Bai, B., Peng, J., Kriwacki, R. W., & Taylor, J. P. (2016). C9orf72 Dipeptide Repeats Impair the Assembly, Dynamics, and Function of Membrane-Less Organelles. *Cell*. https://doi.org/10.1016/j.cell.2016.10.002

Lee, Y.-B., Chen, H.-J., Peres, J. N., Gomez-Deza, J., Attig, J., Štalekar, M., Troakes, C., Nishimura, A. L., Scotter, E. L., Vance, C., Adachi, Y., Sardone, V., Miller, J. W., Smith, B. N., Gallo, J.-M., Ule, J., Hirth, F., Rogelj, B., Houart, C., & Shaw, C. E. (2013). Hexanucleotide Repeats in ALS/FTD Form Length-Dependent RNA Foci, Sequester RNA Binding Proteins, and Are Neurotoxic. *Cell Reports*, *5*(5), 1178–1186. https://doi.org/https://doi.org/10.1016/j.celrep.2013.10.049

Li, P., Nijhawan, D., Budihardjo, I., Srinivasula, S. M., Ahmad, M., Alnemri, E. S., & Wang, X. (1997). Cytochrome c and dATP-Dependent Formation of Apaf-1/Caspase-9 Complex Initiates an Apoptotic Protease Cascade. *Cell*, *91*(4), 479–489. https://doi.org/10.1016/S0092-8674(00)80434-1

Lin, M. Y., & Sheng, Z. H. (2015). Regulation of Mitochondrial Transport in Neurons. *Experimental Cell Research*, *334*(1), 35. https://doi.org/10.1016/J.YEXCR.2015.01.004

Lin, Y., Mori, E., Kato, M., Xiang, S., Wu, L., Kwon, I., & McKnight, S. L. (2016). Toxic PR Poly-Dipeptides Encoded by the C9orf72 Repeat Expansion Target LC Domain Polymers. *Cell*. https://doi.org/10.1016/j.cell.2016.10.003

Ling, S. C., Polymenidou, M., & Cleveland, D. W. (2013). Converging Mechanisms in ALS and FTD: Disrupted RNA and Protein Homeostasis. *Neuron*, *79*(3), 416–438. https://doi.org/10.1016/J.NEURON.2013.07.033

Lipscombe, D., Helton, T. D., & Xu, W. (2004). L-type calcium channels: The low down. *Journal of Neurophysiology*, *92*(5), 2633–2641. https://doi.org/10.1152/JN.00486.2004/ASSET/IMAGES/LARGE/Z9K0100441740003.JPEG

Liu, F., Morderer, D., Wren, M. C., Vettleson-Trutza, S. A., Wang, Y., Rabichow, B. E., Salemi, M. R., Phinney, B. S., Oskarsson, B., Dickson, D. W., & Rossoll, W. (2022). Proximity proteomics of C9orf72 dipeptide repeat proteins identifies molecular chaperones as modifiers of poly-GA aggregation. *Acta Neuropathologica Communications 2022 10:1*, *10*(1), 1–18. https://doi.org/10.1186/S40478-022-01322-X

Lopez-Gonzalez, R., Lu, Y., Gendron, T. F., Karydas, A., Tran, H., Yang, D., Petrucelli, L., Miller, B. L., Almeida, S., & Gao, F. B. (2016). Poly(GR) in C9ORF72-Related ALS/FTD Compromises Mitochondrial Function and Increases Oxidative Stress and DNA Damage in iPSC-Derived Motor Neurons. *Neuron*, *92*(2), 383. https://doi.org/10.1016/J.NEURON.2016.09.015

Lu, B., & Guo, S. (2020). Mechanisms Linking Mitochondria Dysfunction and Proteostasis Failure. *Trends in Cell Biology*, *30*(4), 317. https://doi.org/10.1016/J.TCB.2020.01.008

Lu, T., Pan, Y., Kao, S. Y., Li, C., Kohane, I., Chan, J., & Yankner, B. A. (2004). Gene regulation and DNA damage in the ageing human brain. *Nature 2004 429:6994*, *429*(6994), 883–891. https://doi.org/10.1038/nature02661

Luz, A. L., Godebo, T. R., Bhatt, D. P., Ilkayeva, O. R., Maurer, L. L., Hirschey, M. D., & Meyer, J. N. (2016). From the Cover: Arsenite Uncouples Mitochondrial Respiration and Induces a Warburg-like Effect in Caenorhabditis elegans. *Toxicological Sciences*, *152*(2), 349. https://doi.org/10.1093/TOXSCI/KFW093

Mackenzie, I. R. A., Bigio, E. H., Ince, P. G., Geser, F., Neumann, M., Cairns, N. J., Kwong, L. K., Forman, M. S., Ravits, J., Stewart, H., Eisen, A., McClusky, L., Kretzschmar, H. A., Monoranu, C. M., Highley, J. R., Kirby, J., Siddique, T., Shaw, P. J., Lee, V. M. Y., & Trojanowski, J. Q. (2007). Pathological TDP-43 distinguishes sporadic amyotrophic lateral sclerosis from amyotrophic lateral sclerosis with SOD1 mutations. *Annals of Neurology*. https://doi.org/10.1002/ana.21147

Mackenzie, I. R. A., Frick, P., Grässer, F. A., Gendron, T. F., Petrucelli, L., Cashman, N. R., Edbauer, D., Kremmer, E., Prudlo, J., Troost, D., & Neumann, M. (2015). Quantitative analysis and clinico-pathological correlations of different dipeptide repeat protein pathologies in C9ORF72 mutation carriers. *Acta Neuropathologica*. https://doi.org/10.1007/s00401-015-1476-2

MacKenzie, I. R. A., & Neumann, M. (2012). FET proteins in frontotemporal dementia and amyotrophic lateral sclerosis. *Brain Research*, *1462*, 40–43. https://doi.org/10.1016/J.BRAINRES.2011.12.010

Mackenzie, I. R. A., & Neumann, M. (2017). Fused in Sarcoma Neuropathology in Neurodegenerative Disease. *Cold Spring Harbor Perspectives in Medicine*, *7*(12), a024299. https://doi.org/10.1101/CSHPERSPECT.A024299

MacKenzie, I. R., Arzberger, T., Kremmer, E., Troost, D., Lorenzl, S., Mori, K., Weng, S. M., Haass, C., Kretzschmar, H. A., Edbauer, D., & Neumann, M. (2013). Dipeptide repeat protein pathology in C9ORF72 mutation cases: Clinico-pathological correlations. *Acta Neuropathologica*, *126*(6), 859–879. https://doi.org/10.1007/S00401-013-1181-Y/TABLES/4

Mackenzie, I. R., Nicholson, A. M., Sarkar, M., Messing, J., Purice, M. D., Pottier, C., Annu, K., Baker, M., Perkerson, R. B., Kurti, A., Matchett, B. J., Mittag, T., Temirov, J., Hsiung, G. Y. R., Krieger, C., Murray, M. E., Kato, M., Fryer, J. D., Petrucelli, L., … Rademakers, R. (2017). TIA1 Mutations in Amyotrophic Lateral Sclerosis and Frontotemporal Dementia Promote Phase Separation and Alter Stress Granule Dynamics. *Neuron*, *95*(4), 808-816.e9. https://doi.org/10.1016/J.NEURON.2017.07.025

Maday, S., Wallace, K. E., & Holzbaur, E. L. F. (2012). Autophagosomes initiate distally and mature during transport toward the cell soma in primary neurons. *Journal of Cell Biology*, *196*(4), 407–417. https://doi.org/10.1083/JCB.201106120/VIDEO-5

Maharjan, N., Künzli, C., Buthey, K., & Saxena, S. (2016). C9ORF72 Regulates Stress Granule Formation and Its Deficiency Impairs Stress Granule Assembly, Hypersensitizing Cells to Stress. *Molecular Neurobiology 2016 54:4*, *54*(4), 3062–3077. https://doi.org/10.1007/S12035-016-9850-1

Majounie, E., Renton, A. E., Mok, K., Dopper, E. G. P., Waite, A., Rollinson, S., Chiò, A., Restagno, G., Nicolaou, N., Simon-Sanchez, J., van Swieten, J. C., Abramzon, Y., Johnson, J. O., Sendtner, M., Pamphlett, R., Orrell, R. W., Mead, S., Sidle, K. C., Houlden, H., … Logroscino, G. (2012). Frequency of the C9orf72 hexanucleotide repeat expansion in patients with amyotrophic lateral sclerosis and frontotemporal dementia: A cross-sectional study. *The Lancet Neurology*. https://doi.org/10.1016/S1474-4422(12)70043-1

Martier, R., Liefhebber, J. M., García-Osta, A., Miniarikova, J., Cuadrado-Tejedor, M., Espelosin, M., Ursua, S., Petry, H., van Deventer, S. J., Evers, M. M., & Konstantinova, P. (2019). Targeting RNA-Mediated Toxicity in C9orf72 ALS and/or FTD by RNAi-Based Gene Therapy. *Molecular Therapy. Nucleic Acids*, *16*, 26–37. https://doi.org/10.1016/J.OMTN.2019.02.001

Martinez-Vicente, M. (2017). Neuronal mitophagy in neurodegenerative diseases. *Frontiers in Molecular Neuroscience*, *10*, 64. https://doi.org/10.3389/FNMOL.2017.00064/BIBTEX

Mauvezin, C., & Neufeld, T. P. (2015). Bafilomycin A1 disrupts autophagic flux by inhibiting both V-ATPase-dependent acidification and Ca-P60A/SERCA-dependent autophagosome-lysosome fusion. *Autophagy*, *11*(8), 1437. https://doi.org/10.1080/15548627.2015.1066957

May, S., Hornburg, D., Schludi, M. H., Arzberger, T., Rentzsch, K., Schwenk, B. M., Grässer, F. A., Mori, K., Kremmer, E., Banzhaf-Strathmann, J., Mann, M., Meissner, F., & Edbauer, D. (2014). C9orf72 FTLD/ALS-associated Gly-Ala dipeptide repeat proteins cause neuronal toxicity and Unc119 sequestration. *Acta Neuropathologica*. https://doi.org/10.1007/s00401-014-1329-4

McCord, J. M., & Fridovich, I. (1969). Superoxide Dismutase: AN ENZYMIC FUNCTION FOR ERYTHROCUPREIN (HEMOCUPREIN). *Journal of Biological Chemistry*, *244*(22), 6049–6055. https://doi.org/10.1016/S0021-9258(18)63504-5

McLelland, G. L., Goiran, T., Yi, W., Dorval, G., Chen, C. X., Lauinger, N. D., Krahn, A. I., Valimehr, S., Rakovic, A., Rouiller, I., Durcan, T. M., Trempe, J. F., & Fon, E. A. (2018). Mfn2 ubiquitination by PINK1/parkin gates the p97-dependent release of ER from mitochondria to drive mitophagy. *ELife*, *7*. https://doi.org/10.7554/ELIFE.32866

Mehta, A. R., Gregory, J. M., Dando, O., Carter, R. N., Burr, K., Nanda, J., Story, D., McDade, K., Smith, C., Morton, N. M., Mahad, D. J., Hardingham, G. E., Chandran, S., & Selvaraj, B. T. (2021). Mitochondrial bioenergetic deficits in C9orf72 amyotrophic lateral sclerosis motor neurons cause dysfunctional axonal homeostasis. *Acta Neuropathologica 2021 141:2*, *141*(2), 257–279. https://doi.org/10.1007/S00401-020-02252-5

Mejzini, R., Flynn, L. L., Pitout, I. L., Fletcher, S., Wilton, S. D., & Akkari, P. A. (2019). ALS Genetics, Mechanisms, and Therapeutics: Where Are We Now? . In *Frontiers in Neuroscience* (Vol. 13, p. 1310).

Misko, A., Jiang, S., Wegorzewska, I., Milbrandt, J., & Baloh, R. H. (2010). Mitofusin 2 Is Necessary for Transport of Axonal Mitochondria and Interacts with the Miro/Milton Complex. *The Journal of Neuroscience*, *30*(12), 4232. https://doi.org/10.1523/JNEUROSCI.6248-09.2010

Mizielinska, S., Grönke, S., Niccoli, T., Ridler, C. E., Clayton, E. L., Devoy, A., Moens, T., Norona, F. E., Woollacott, I. O. C., Pietrzyk, J., Cleverley, K., Nicoll, A. J., Pickering-Brown, S., Dols, J., Cabecinha, M., Hendrich, O., Fratta, P., Fisher, E. M. C., Partridge, L., & Isaacs, A. M. (2014). *C9orf72* repeat expansions cause neurodegeneration in *Drosophila* through arginine-rich proteins. *Science*, *345*(6201), 1192–1194. https://doi.org/10.1126/science.1256800

Mizielinska, S., Lashley, T., Norona, F. E., Clayton, E. L., Ridler, C. E., Fratta, P., & Isaacs, A. M. (2013). C9orf72 frontotemporal lobar degeneration is characterised by frequent neuronal sense and antisense RNA foci. *Acta Neuropathologica*, *126*(6), 845–857. https://doi.org/10.1007/S00401-013-1200-Z/FIGURES/8

Mizuno, Y., Amari, M., Takatama, M., Aizawa, H., Mihara, B., & Okamoto, K. (2006). Immunoreactivities of p62, an ubiqutin-binding protein, in the spinal anterior horn cells of patients with amyotrophic lateral sclerosis. *Journal of the Neurological Sciences*. https://doi.org/10.1016/j.jns.2006.05.060

Moens, T. G., Mizielinska, S., Niccoli, T., Mitchell, J. S., Thoeng, A., Ridler, C. E., Grönke, S., Esser, J., Heslegrave, A., Zetterberg, H., Partridge, L., & Isaacs, A. M. (2018). Sense and antisense RNA are not toxic in Drosophila models of C9orf72-associated ALS/FTD. *Acta Neuropathologica*, *135*(3), 445–457. https://doi.org/10.1007/s00401-017-1798-3

Mokas, S., Mills, J. R., Garreau, C., Fournier, M. J., Robert, F., Arya, P., Kaufman, R. J., Pelletier, J., & Mazroui, R. (2009). Uncoupling stress granule assembly and translation initiation inhibition. *Molecular Biology of the Cell*, *20*(11), 2673–2683. https://doi.org/10.1091/MBC.E08-10-1061/ASSET/IMAGES/LARGE/ZMK0110990680007.JPEG

Monaco, G., van Dam, S., Casal Novo Ribeiro, J. L., Larbi, A., & de Magalhães, J. P. (2015). A comparison of human and mouse gene co-expression networks reveals conservation and divergence at the tissue, pathway and disease levels. *BMC Evolutionary Biology*, *15*, 259. https://doi.org/10.1186/s12862-015-0534-7

Mori, K., Arzberger, T., Grässer, F. A., Gijselinck, I., May, S., Rentzsch, K., Weng, S. M., Schludi, M. H., Van Der Zee, J., Cruts, M., Van Broeckhoven, C., Kremmer, E., Kretzschmar, H. A., Haass, C., & Edbauer, D. (2013). Bidirectional transcripts of the expanded C9orf72 hexanucleotide repeat are

translated into aggregating dipeptide repeat proteins. *Acta Neuropathologica*. https://doi.org/10.1007/s00401-013-1189-3

Mori, K., Nihei, Y., Arzberger, T., Zhou, Q., Mackenzie, I. R., Hermann, A., Hanisch, F., Brain Banking Alliance, B., Kamp, F., Nuscher, B., Orozco, D., Edbauer, D., & Haass, C. (2016). Reduced hnRNPA3 increases C9orf72 repeat RNA levels and dipeptide-repeat protein deposition. *EMBO Reports*, *17*(9), 1314–1325. https://doi.org/10.15252/EMBR.201541724

Mukhtar, T., & Taylor, V. (2018). Untangling Cortical Complexity During Development. *Journal of Experimental Neuroscience*, *12*. https://doi.org/10.1177/1179069518759332

National Records of Scotland. (2018). *Vital Events Reference Tables 2017*. https://webarchive.nrscotland.gov.uk/20210314055427/

Neisch, A. L., Neufeld, T. P., & Hays, T. S. (2017). A STR IPAK complex mediates axonal transport of autophagosomes and dense core vesicles through PP2A regulation. *Journal of Cell Biology*, *216*(2), 441–461. https://doi.org/10.1083/JCB.201606082/VIDEO-1

Neumann, M., Rademakers, R., Roeber, S., Baker, M., Kretzschmar, H. A., & MacKenzie, I. R. A. (2009). A new subtype of frontotemporal lobar degeneration with FUS pathology. *Brain*, *132*(11), 2922–2931. https://doi.org/10.1093/BRAIN/AWP214

Neumann, M., Sampathu, D. M., Kwong, L. K., Truax, A. C., Micsenyi, M. C., Chou, T. T., Bruce, J., Schuck, T., Grossman, M., Clark, C. M., McCluskey, L. F., Miller, B. L., Masliah, E., Mackenzie, I. R., Feldman, H., Feiden, W., Kretzschmar, H. A., Trojanowski, J. Q., & Lee, V. M. Y. (2006). Ubiquitinated TDP-43 in frontotemporal lobar degeneration and amyotrophic lateral sclerosis. *Science*. https://doi.org/10.1126/science.1134108

Nguyen, H. P., Van Broeckhoven, C., & van der Zee, J. (2018). ALS Genes in the Genomic Era and their Implications for FTD. In *Trends in Genetics*. https://doi.org/10.1016/j.tig.2018.03.001

Nguyen, L., Montrasio, F., Pattamatta, A., Tusi, S. K., Bardhi, O., Meyer, K. D., Hayes, L., Nakamura, K., Banez-Coronel, M., Coyne, A., Guo, S., Laboissonniere, L. A., Gu, Y., Narayanan, S., Smith, B., Nitsch, R. M., Kankel, M. W., Rushe, M., Rothstein, J., … Ranum, L. P. W. (2020). Antibody Therapy Targeting RAN Proteins Rescues C9 ALS/FTD Phenotypes in C9orf72 Mouse Model. *Neuron*, *105*(4), 645-662.e11. https://doi.org/10.1016/J.NEURON.2019.11.007

Nimmerjahn, A., Kirchhoff, F., & Helmchen, F. (2005). Neuroscience: Resting microglial cells are highly dynamic surveillants of brain parenchyma in vivo. *Science*, *308*(5726), 1314–1318. https://doi.org/10.1126/SCIENCE.1110647/SUPPL_FILE/1110647S9.MOV

Nolan, M., Scott, C., Gamarallage, M. P., Lunn, D., Carpenter, K., McDonough, E., Meyer, D., Kaanumalle, S., Santamaria-Pang, A., Turner, M. R., Talbot, K., & Ansorge, O. (2020). Quantitative patterns of motor cortex proteinopathy across ALS genotypes. *Acta Neuropathologica Communications*, *8*(1), 1–20. https://doi.org/10.1186/S40478-020-00961-2/FIGURES/6

Nonaka, T., Masuda-Suzukake, M., Arai, T., Hasegawa, Y., Akatsu, H., Obi, T., Yoshida, M., Murayama, S., Mann, D. M. A., Akiyama, H., & Hasegawa, M. (2013). Prion-like Properties of Pathological TDP-43 Aggregates from Diseased Brains. *Cell Reports*. https://doi.org/10.1016/j.celrep.2013.06.007

Northern Ireland Statistics and Research Agency. (2018). *Registrar General Northern Ireland Annual Report 2017*. www.nisra.gov.uk

Nowicka, U., Chroscicki, P., Stroobants, K., Sladowska, M., Turek, M., Uszczynska-Ratajczak, B., Kundra, R., Goral, T., Perni, M., Dobson, C. M., Vendruscolo, M., & Chacinska, A. (2021). Cytosolic aggregation of mitochondrial proteins disrupts cellular homeostasis by stimulating the aggregation of other proteins. *ELife*, *10*. https://doi.org/10.7554/ELIFE.65484

Oakes, J. A., Davies, M. C., & Collins, M. O. (2017). TBK1: a new player in ALS linking autophagy and neuroinflammation. *Molecular Brain*, *10*(1), 1–10. https://doi.org/10.1186/S13041-017-0287-X/FIGURES/3

Office for National Statistics. (2018). *Deaths registered in England and Wales (series DR): 2017*. https://www.ons.gov.uk/peoplepopulationandcommunity/birthsdeathsandmarriages/deaths/bulletins/deathsregisteredinenglandandwalesseriesdr/2017#continued-increases-in-deaths-to-dementia-and-alzheimer-disease-at-ages-80-years-and-over

Oh, E., Akopian, D., & Rape, M. (2018). Principles of Ubiquitin-Dependent Signaling. *Https://Ezproxy-Prd.Bodleian.Ox.Ac.Uk:2102/10.1146/Annurev-Cellbio-100617-062802*, *34*, 137–162. https://doi.org/10.1146/ANNUREV-CELLBIO-100617-062802

Ohki, Y., Wenninger-Weinzierl, A., Hruscha, A., Asakawa, K., Kawakami, K., Haass, C., Edbauer, D., & Schmid, B. (2017). Glycine-alanine dipeptide repeat protein contributes to toxicity in a zebrafish model of C9orf72 associated neurodegeneration. *Molecular Neurodegeneration*, *12*(1), 6. https://doi.org/10.1186/s13024-016-0146-8

Öijerstedt, L., Chiang, H. H., Björkström, J., Forsell, C., Lilius, L., Lindström, A. K., Thonberg, H., & Graff, C. (2019). Confirmation of high frequency of C9orf72 mutations in patients with frontotemporal dementia from Sweden. *Neurobiology of Aging*. https://doi.org/10.1016/j.neurobiolaging.2019.03.009

Olney, N. T., Spina, S., & Miller, B. L. (2017). Frontotemporal Dementia. *Neurologic Clinics*, *35*(2), 339–374. https://doi.org/10.1016/J.NCL.2017.01.008

Olszewska, D. A., Lonergan, R., Fallon, E. M., & Lynch, T. (2016). Genetics of Frontotemporal Dementia. *Current Neurology and Neuroscience Reports*, *16*(12), 107. https://doi.org/10.1007/s11910-016-0707-9

Onesto, E., Colombrita, C., Gumina, V., Borghi, M. O., Dusi, S., Doretti, A., Fagiolari, G., Invernizzi, F., Moggio, M., Tiranti, V., Silani, V., & Ratti, A. (2016). Gene-specific mitochondria dysfunctions in human TARDBP and C9ORF72 fibroblasts. *Acta Neuropathologica Communications*, *4*(1), 47. https://doi.org/10.1186/S40478-016-0316-5/FIGURES/5

O'Rourke, J. G., Bogdanik, L., Yáñez, A., Lall, D., Wolf, A. J., Muhammad, A. K. M. G., Ho, R., Carmona, S., Vit, J. P., Zarrow, J., Kim, K. J., Bell, S., Harms, M. B., Miller, T. M., Dangler, C. A., Underhill, D. M., Goodridge, H. S., Lutz, C. M., & Baloh, R. H. (2016). C9orf72 is required for proper macrophage and microglial function in mice. *Science*, *351*(6279), 1324–1329. https://doi.org/10.1126/SCIENCE.AAF1064/SUPPL_FILE/AAF1064-OROURKE-SM.PDF

Ou, S. H., Wu, F., Harrich, D., García-Martínez, L. F., & Gaynor, R. B. (1995). Cloning and characterization of a novel cellular protein, TDP-43, that binds to human immunodeficiency virus type 1 TAR DNA sequence motifs. *Journal of Virology*. https://doi.org/10.1128/jvi.69.6.3584-3596.1995

Palikaras, K., Lionaki, E., & Tavernarakis, N. (2018). Mechanisms of mitophagy in cellular homeostasis, physiology and pathology. *Nature Cell Biology 2018 20:9*, *20*(9), 1013–1022. https://doi.org/10.1038/s41556-018-0176-2

Panas, M. D., Ivanov, P., & Anderson, P. (2016). Mechanistic insights into mammalian stress granule dynamics. *Journal of Cell Biology*, *215*(3), 313–323. https://doi.org/10.1083/jcb.201609081

Panza, F., Lozupone, M., Seripa, D., Daniele, A., Watling, M., Giannelli, G., & Imbimbo, B. P. (2020). Development of disease-modifying drugs for frontotemporal dementia spectrum disorders. *Nature Reviews Neurology*, *16*(4), 213–228. https://doi.org/10.1038/s41582-020-0330-x

Perkins, E. M., Burr, K., Banerjee, P., Mehta, A. R., Dando, O., Selvaraj, B. T., Suminaite, D., Nanda, J., Henstridge, C. M., Gillingwater, T. H., Hardingham, G. E., Wyllie, D. J. A., Chandran, S., & Livesey, M. R. (2021). Altered network properties in C9ORF72 repeat expansion cortical neurons are due to synaptic dysfunction. *Molecular Neurodegeneration*, *16*(1), 1–16. https://doi.org/10.1186/S13024-021-00433-8/FIGURES/4

Pesah, Y., Pham, T., Burgess, H., Middlebrooks, B., Verstreken, P., Zhou, Y., Harding, M., Bellen, H., & Mardon, G. (2004). Drosophila parkin mutants have decreased mass and cell size and increased sensitivity to oxygen radical stress. *Development*, *131*(9), 2183–2194. https://doi.org/10.1242/DEV.01095

Phukan, J., Elamin, M., Bede, P., Jordan, N., Gallagher, L., Byrne, S., Lynch, C., Pender, N., & Hardiman, O. (2012). The syndrome of cognitive impairment in amyotrophic lateral sclerosis: A population-based study. *Journal of Neurology, Neurosurgery and Psychiatry*. https://doi.org/10.1136/jnnp-2011-300188

Pich, S., Bach, D., Briones, P., Liesa, M., Camps, M., Testar, X., Palacín, M., & Zorzano, A. (2005). The Charcot–Marie–Tooth type 2A gene product, Mfn2, up-regulates fuel oxidation through expression of OXPHOS system. *Human Molecular Genetics*, *14*(11), 1405–1415. https://doi.org/10.1093/HMG/DDI149

Pieczenik, S. R., & Neustadt, J. (2007). Mitochondrial dysfunction and molecular pathways of disease. *Experimental and Molecular Pathology*, *83*(1), 84–92. https://doi.org/10.1016/J.YEXMP.2006.09.008

Pihán, P., Carreras-Sureda, A., & Hetz, C. (2017). BCL-2 family: integrating stress responses at the ER to control cell demise. *Cell Death & Differentiation 2017 24:9*, *24*(9), 1478–1487. https://doi.org/10.1038/cdd.2017.82

Pilling, A. D., Horiuchi, D., Lively, C. M., & Saxton, W. M. (2006). Kinesin-1 and dynein are the primary motors for fast transport of mitochondria in Drosophila motor axons. *Molecular Biology of the Cell*, *17*(4), 2057–2068. https://doi.org/10.1091/MBC.E05-06-0526/ASSET/IMAGES/LARGE/ZMK0040675970008.JPEG

Pinto, B. S., Saxena, T., Oliveira, R., Méndez-Gómez, H. R., Cleary, J. D., Denes, L. T., McConnell, O., Arboleda, J., Xia, G., Swanson, M. S., & Wang, E. T. (2017). Impeding Transcription of Expanded Microsatellite Repeats by Deactivated Cas9. *Molecular Cell*, *68*(3), 479-490.e5. https://doi.org/10.1016/J.MOLCEL.2017.09.033

Popgeorgiev, N., Jabbour, L., & Gillet, G. (2018). Subcellular Localization and Dynamics of the Bcl-2 Family of Proteins. *Frontiers in Cell and Developmental Biology*, *6*(FEB). https://doi.org/10.3389/FCELL.2018.00013

Popoli, M., Yan, Z., McEwen, B. S., & Sanacora, G. (2011). The stressed synapse: the impact of stress and glucocorticoids on glutamate transmission. *Nature Reviews Neuroscience 2011 13:1*, *13*(1), 22–37. https://doi.org/10.1038/NRN3138

Prentice, H., Modi, J. P., & Wu, J. Y. (2015). Mechanisms of Neuronal Protection against Excitotoxicity, Endoplasmic Reticulum Stress, and Mitochondrial Dysfunction in Stroke and Neurodegenerative Diseases. *Oxidative Medicine and Cellular Longevity*, *2015*. https://doi.org/10.1155/2015/964518

Prpar Mihevc, S., Baralle, M., Buratti, E., & Rogelj, B. (2016). TDP-43 aggregation mirrors TDP-43 knockdown, affecting the expression levels of a common set of proteins. *Scientific Reports*. https://doi.org/10.1038/srep33996

Quaegebeur, A., Glaria, I., Lashley, T., & Isaacs, A. M. (2020). Soluble and insoluble dipeptide repeat protein measurements in C9orf72-frontotemporal dementia brains show regional differential solubility and correlation of poly-GR with clinical severity. *Acta Neuropathologica Communications*, *8*(1), 184. https://doi.org/10.1186/S40478-020-01036-Y/TABLES/4

Raffaele, S., Boccazzi, M., & Fumagalli, M. (2021). Oligodendrocyte Dysfunction in Amyotrophic Lateral Sclerosis: Mechanisms and Therapeutic Perspectives. *Cells*, *10*(3), 1–32. https://doi.org/10.3390/CELLS10030565

Renaud, L., Picher-Martel, V., Codron, P., & Julien, J. P. (2019). Key role of UBQLN2 in pathogenesis of amyotrophic lateral sclerosis and frontotemporal dementia. *Acta Neuropathologica Communications*, *7*(1), 1–11. https://doi.org/10.1186/S40478-019-0758-7/TABLES/2

Renton, A. E., Majounie, E., Waite, A., Simón-Sánchez, J., Rollinson, S., Gibbs, J. R., Schymick, J. C., Laaksovirta, H., van Swieten, J. C., Myllykangas, L., Kalimo, H., Paetau, A., Abramzon, Y., Remes, A. M., Kaganovich, A., Scholz, S. W., Duckworth, J., Ding, J., Harmer, D. W., … Traynor, B. J. (2011). A hexanucleotide repeat expansion in C9ORF72 is the cause of chromosome 9p21-linked ALS-FTD. *Neuron*. https://doi.org/10.1016/j.neuron.2011.09.010

Riemslagh, F. W., Verhagen, R. F. M., van der Toorn, E. C., Smits, D. J., Quint, W. H., van der Linde, H. C., van Ham, T. J., & Willemsen, R. (2021). Reduction of oxidative stress suppresses poly-GR-mediated toxicity in zebrafish embryos. *Disease Models & Mechanisms*, *14*(11). https://doi.org/10.1242/DMM.049092

Rojas-Rivera, D., & Hetz, C. (2014). TMBIM protein family: ancestral regulators of cell death. *Oncogene 2015 34:3*, *34*(3), 269–280. https://doi.org/10.1038/onc.2014.6

Ron, D., & Walter, P. (2007). Signal integration in the endoplasmic reticulum unfolded protein response. *Nature Reviews Molecular Cell Biology*, *8*(7), 519–529. https://doi.org/10.1038/nrm2199

Rong, Y., & Distelhorst, C. W. (2008). Bcl-2 Protein Family Members: Versatile Regulators of Calcium Signaling in Cell Survival and Apoptosis. *Http://Dx.Doi.Org/10.1146/Annurev.Physiol.70.021507.105852*, *70*, 73–91. https://doi.org/10.1146/ANNUREV.PHYSIOL.70.021507.105852

Rong, Y. P., Bultynck, G., Aromolaran, A. S., Zhong, F., Parys, J. B., de Smedt, H., Mignery, G. A., Roderick, H. L., Bootman, M. D., & Distelhorst, C. W. (2009). The BH4 domain of Bcl-2 inhibits ER calcium release and apoptosis by binding the regulatory and coupling domain of the IP3 receptor.

Proceedings of the National Academy of Sciences of the United States of America, *106*(34), 14397–14402. https://doi.org/10.1073/PNAS.0907555106/SUPPL_FILE/0907555106SI.PDF

Rosa, N., Ivanova, H., Wagner, L. E., Kale, J., la Rovere, R., Welkenhuyzen, K., Louros, N., Karamanou, S., Shabardina, V., Lemmens, I., Vandermarliere, E., Hamada, K., Ando, H., Rousseau, F., Schymkowitz, J., Tavernier, J., Mikoshiba, K., Economou, A., Andrews, D. W., … Bultynck, G. (2021). Bcl-xL acts as an inhibitor of IP3R channels, thereby antagonizing Ca2+-driven apoptosis. *Cell Death & Differentiation 2021*, 1–18. https://doi.org/10.1038/s41418-021-00894-w

Rothstein, J. D., van Kammen, M., Levey, A. I., Martin, L. J., & Kuncl, R. W. (1995). Selective loss of glial glutamate transporter GLT-1 in amyotrophic lateral sclerosis. *Annals of Neurology*, *38*(1), 73–84. https://doi.org/10.1002/ANA.410380114

Rusten, T. E., & Stenmark, H. (2010). P62, an autophagy hero or culprit? *Nature Cell Biology*, *12*(3), 207–209. https://doi.org/10.1038/NCB0310-207

Saftig, P., Beertsen, W., & Eskelinen, E. L. (2008). LAMP-2: A control step for phagosome and autophagosome maturation. *Autophagy*, *4*(4), 510–512. https://doi.org/10.4161/AUTO.5724

Salameh, J. S., Brown, R. H., & Berry, J. D. (2015). Amyotrophic Lateral Sclerosis: Review. *Seminars in Neurology*. https://doi.org/10.1055/s-0035-1558984

Salussolia, C. L., Prodromou, M. L., Borker, P., & Wollmuth, L. P. (2011). Arrangement of Subunits in Functional NMDA Receptors. *Journal of Neuroscience*, *31*(31), 11295–11304. https://doi.org/10.1523/JNEUROSCI.5612-10.2011

Santillo, A. F., & Englund, E. (2014). Greater loss of von Economo neurons than loss of layer II and III neurons in behavioral variant frontotemporal dementia. *American Journal of Neurodegenerative Disease*, *3*(2), 64. /pmc/articles/PMC4162587/

Sareen, D., O'Rourke, J. G., Meera, P., Muhammad, A. K. M. G., Grant, S., Simpkinson, M., Bell, S., Carmona, S., Ornelas, L., Sahabian, A., Gendron, T., Petrucelli, L., Baughn, M., Ravits, J., Harms, M. B., Rigo, F., Frank Bennett, C., Otis, T. S., Svendsen, C. N., & Baloh, R. H. (2013). Targeting RNA foci in iPSC-derived motor neurons from ALS patients with a C9ORF72 repeat expansion. *Science Translational Medicine*, *5*(208). https://doi.org/10.1126/SCITRANSLMED.3007529/SUPPL_FILE/5-208RA149_SM.PDF

Sarkar, S., Ravikumar, B., Floto, R. A., & Rubinsztein, D. C. (2008). Rapamycin and mTOR-independent autophagy inducers ameliorate toxicity of polyglutamine-expanded huntingtin and related proteinopathies. *Cell Death & Differentiation 2009 16:1*, *16*(1), 46–56. https://doi.org/10.1038/cdd.2008.110

Scaber, J., & Talbot, K. (2016). What is the role of TDP-43 in C9orf72-related amyotrophic lateral sclerosis and frontemporal dementia? *Brain*, *139*(12), 3057–3059. https://doi.org/10.1093/BRAIN/AWW264

Schludi, M. H., May, S., Grässer, F. A., Rentzsch, K., Kremmer, E., Küpper, C., Klopstock, T., Ceballos-Baumann, A., Danek, A., Diehl-Schmid, J., Fassbender, K., Förstl, H., Kornhuber, J., Otto, M., Dieterich, M., Feuerecker, R., Giese, A., Klünemann, H., Kurz, A., … Roeber, S. (2015). Distribution of dipeptide repeat proteins in cellular models and C9orf72 mutation cases suggests link to transcriptional silencing. *Acta Neuropathologica*, *130*(4), 537–555. https://doi.org/10.1007/S00401-015-1450-Z/FIGURES/8

Schmitz, A., Pinheiro Marques, J., Oertig, I., Maharjan, N., & Saxena, S. (2021). Emerging Perspectives on Dipeptide Repeat Proteins in C9ORF72 ALS/FTD. *Frontiers in Cellular Neuroscience*, *15*, 3. https://doi.org/10.3389/FNCEL.2021.637548/BIBTEX

Sellier, C., Campanari, M., Julie Corbier, C., Gaucherot, A., Kolb-Cheynel, I., Oulad-Abdelghani, M., Ruffenach, F., Page, A., Ciura, S., Kabashi, E., & Charlet-Berguerand, N. (2016). Loss of C9 ORF 72 impairs autophagy and synergizes with polyQ Ataxin-2 to induce motor neuron dysfunction and cell death . *The EMBO Journal*. https://doi.org/10.15252/embj.201593350

Selvaraj, B. T., Livesey, M. R., Zhao, C., Gregory, J. M., James, O. T., Cleary, E. M., Chouhan, A. K., Gane, A. B., Perkins, E. M., Dando, O., Lillico, S. G., Lee, Y. B., Nishimura, A. L., Poreci, U., Thankamony, S., Pray, M., Vasistha, N. A., Magnani, D., Borooah, S., … Chandran, S. (2018). C9ORF72 repeat expansion causes vulnerability of motor neurons to Ca2+-permeable AMPA receptor-mediated excitotoxicity. *Nature Communications 2018 9:1*, *9*(1), 1–14. https://doi.org/10.1038/s41467-017-02729-0

Shankaran, S. S., Capell, A., Hruscha, A. T., Fellerer, K., Neumann, M., Schmid, B., & Haass, C. (2008). Missense Mutations in the Progranulin Gene Linked to Frontotemporal Lobar Degeneration with Ubiquitin-immunoreactive Inclusions Reduce Progranulin Production and Secretion *. *Journal of Biological Chemistry*, *283*(3), 1744–1753. https://doi.org/10.1074/JBC.M705115200

Sharpe, J. L., Harper, N. S., Garner, D. R., & West, R. J. H. (2021). Modeling C9orf72-Related Frontotemporal Dementia and Amyotrophic Lateral Sclerosis in Drosophila. *Frontiers in Cellular Neuroscience*, *15*, 424. https://doi.org/10.3389/FNCEL.2021.770937/BIBTEX

Shi, Y., Kirwan, P., & Livesey, F. J. (2012). Directed differentiation of human pluripotent stem cells to cerebral cortex neurons and neural networks. *Nature Protocols*. https://doi.org/10.1038/nprot.2012.116

Shi, Y., Lin, S., Staats, K. A., Li, Y., Chang, W. H., Hung, S. T., Hendricks, E., Linares, G. R., Wang, Y., Son, E. Y., Wen, X., Kisler, K., Wilkinson, B., Menendez, L., Sugawara, T., Woolwine, P., Huang, M., Cowan, M. J., Ge, B., … Ichida, J. K. (2018). Haploinsufficiency leads to neurodegeneration in C9ORF72 ALS/FTD human induced motor neurons. *Nature Medicine 2018 24:3*, *24*(3), 313–325. https://doi.org/10.1038/nm.4490

Sleeman, K. E., de Brito, M., Etkind, S., Nkhoma, K., Guo, P., Higginson, I. J., Gomes, B., & Harding, R. (2019). The escalating global burden of serious health-related suffering: projections to 2060 by world regions, age groups, and health conditions. *The Lancet Global Health*, *7*(7), e883–e892. https://doi.org/10.1016/S2214-109X(19)30172-X

Smethurst, P., Newcombe, J., Troakes, C., Simone, R., Chen, Y. R., Patani, R., & Sidle, K. (2016). In vitro prion-like behaviour of TDP-43 in ALS. *Neurobiology of Disease*. https://doi.org/10.1016/j.nbd.2016.08.007

Smith, K. R., Damiano, J., Franceschetti, S., Carpenter, S., Canafoglia, L., Morbin, M., Rossi, G., Pareyson, D., Mole, S. E., Staropoli, J. F., Sims, K. B., Lewis, J., Lin, W. L., Dickson, D. W., Dahl, H. H., Bahlo, M., & Berkovic, S. F. (2012). Strikingly different clinicopathological phenotypes determined by progranulin-mutation dosage. *American Journal of Human Genetics*. https://doi.org/10.1016/j.ajhg.2012.04.021

Soutar, M. P. M., Kempthorne, L., Miyakawa, S., Annuario, E., Melandri, D., Harley, J., O'Sullivan, G. A., Wray, S., Hancock, D. C., Cookson, M. R., Downward, J., Carlton, M., & Plun-Favreau, H. (2018).

AKT signalling selectively regulates PINK1 mitophagy in SHSY5Y cells and human iPSC-derived neurons. *Scientific Reports 2018 8:1*, *8*(1), 1–11. https://doi.org/10.1038/s41598-018-26949-6

Staats, K. A., Bogaert, E., Hersmus, N., Jaspers, T., Luyten, T., Bultynck, G., Parys, J. B., Hisatsune, C., Mikoshiba, K., van Damme, P., Robberecht, W., & van den Bosch, L. (2012). Neuronal overexpression of IP3 receptor 2 is detrimental in mutant SOD1 mice. *Biochemical and Biophysical Research Communications*, *429*(3–4), 210–213. https://doi.org/10.1016/J.BBRC.2012.10.094

Staats, K. A., van Helleputte, L., Jones, A. R., Bento-Abreu, A., van Hoecke, A., Shatunov, A., Simpson, C. L., Lemmens, R., Jaspers, T., Fukami, K., Nakamura, Y., Brown, R. H., van Damme, P., Liston, A., Robberecht, W., Al-Chalabi, A., & van den Bosch, L. (2013). Genetic ablation of phospholipase C delta 1 increases survival in SOD1G93A mice. *Neurobiology of Disease*, *60*, 11–17. https://doi.org/10.1016/J.NBD.2013.08.006

Starr, A., & Sattler, R. (2018). Synaptic dysfunction and altered excitability in C9ORF72 ALS/FTD. *Brain Research*, *1693*, 98–108. https://doi.org/10.1016/J.BRAINRES.2018.02.011

Straub, I. R., Janer, A., Weraarpachai, W., Zinman, L., Robertson, J., Rogaeva, E., & Shoubridge, E. A. (2018). Loss of CHCHD10–CHCHD2 complexes required for respiration underlies the pathogenicity of a CHCHD10 mutation in ALS. *Human Molecular Genetics*, *27*(1), 178. https://doi.org/10.1093/HMG/DDX393

Strong, M. J., Abrahams, S., Goldstein, L. H., Woolley, S., Mclaughlin, P., Snowden, J., Mioshi, E., Roberts-South, A., Benatar, M., HortobáGyi, T., Rosenfeld, J., Silani, V., Ince, P. G., & Turner, M. R. (2017). Amyotrophic lateral sclerosis - frontotemporal spectrum disorder (ALS-FTSD): Revised diagnostic criteria. *Amyotrophic Lateral Sclerosis and Frontotemporal Degeneration*. https://doi.org/10.1080/21678421.2016.1267768

Strong, M. J., Volkening, K., Hammond, R., Yang, W., Strong, W., Leystra-Lantz, C., & Shoesmith, C. (2007). TDP43 is a human low molecular weight neurofilament (hNFL) mRNA-binding protein. *Molecular and Cellular Neuroscience*. https://doi.org/10.1016/j.mcn.2007.03.007

Sullivan, P. M., Zhou, X., Robins, A. M., Paushter, D. H., Kim, D., Smolka, M. B., & Hu, F. (2016). The ALS/FTLD associated protein C9orf72 associates with SMCR8 and WDR41 to regulate the autophagy-lysosome pathway. *Acta Neuropathologica Communications*. https://doi.org/10.1186/s40478-016-0324-5

Sun, D., Wu, R., Zheng, J., Li, P., & Yu, L. (2018). Polyubiquitin chain-induced p62 phase separation drives autophagic cargo segregation. *Cell Research*. https://doi.org/10.1038/s41422-018-0017-7

Tafuri, F., Ronchi, D., Magri, F., Comi, G. P., & Corti, S. (2015). SOD1 misplacing and mitochondrial dysfunction in amyotrophic lateral sclerosis pathogenesis. *Frontiers in Cellular Neuroscience*, *9*(AUGUST). https://doi.org/10.3389/FNCEL.2015.00336

Takamori, S., Rhec, J. S., Rosenmund, C., & Jahn, R. (2000). Identification of a vesicular glutamate transporter that defines a glutamatergic phenotype in neurons. *Nature*. https://doi.org/10.1038/35025070

Tanaka, Y., Kanai, Y., Okada, Y., Nonaka, S., Takeda, S., Harada, A., & Hirokawa, N. (1998). Targeted Disruption of Mouse Conventional Kinesin Heavy Chain kif5B, Results in Abnormal Perinuclear Clustering of Mitochondria. *Cell*, *93*(7), 1147–1158. https://doi.org/10.1016/S0092-8674(00)81459-2

Tanida, I., Ueno, T., & Kominami, E. (2004). LC3 conjugation system in mammalian autophagy. *The International Journal of Biochemistry & Cell Biology*, *36*(12), 2503–2518. https://doi.org/10.1016/J.BIOCEL.2004.05.009

Tao, Z., Wang, H., Xia, Q., Li, K., Li, K., Jiang, X., Xu, G., Wang, G., & Ying, Z. (2015). Nucleolar stress and impaired stress granule formation contribute to C9orf72 RAN translation-induced cytotoxicity. *Human Molecular Genetics*. https://doi.org/10.1093/hmg/ddv005

Taylor, J. P., Brown, R. H., & Cleveland, D. W. (2016). Decoding ALS: from genes to mechanism. *Nature 2016 539:7628*, *539*(7628), 197–206. https://doi.org/10.1038/nature20413

Tee, A. R., Sampson, J. R., Pal, D. K., & Bateman, J. M. (2016). The role of mTOR signalling in neurogenesis, insights from tuberous sclerosis complex. *Seminars in Cell & Developmental Biology*, *52*, 12. https://doi.org/10.1016/J.SEMCDB.2016.01.040

Toth, R. P., & Atkin, J. D. (2018). Dysfunction of optineurin in amyotrophic lateral sclerosis and glaucoma. *Frontiers in Immunology*, *9*(MAY), 1017. https://doi.org/10.3389/FIMMU.2018.01017/BIBTEX

Tsai, R. M., & Boxer, A. L. (2014). Treatment of Frontotemporal Dementia. *Current Treatment Options in Neurology*, *16*(11), 319. https://doi.org/10.1007/S11940-014-0319-0

Tsai, R. M., & Boxer, A. L. (2016). Therapy and clinical trials in frontotemporal dementia: past, present, and future. *Journal of Neurochemistry*, *138*, 211–221. https://doi.org/10.1111/JNC.13640

Urwin, H., Josephs, K. A., Rohrer, J. D., MacKenzie, I. R., Neumann, M., Authier, A., Seelaar, H., van Swieten, J. C., Brown, J. M., Johannsen, P., Nielsen, J. E., Holm, I. E., Dickson, D. W., Rademakers, R., Graff-Radford, N. R., Parisi, J. E., Petersen, R. C., Hatanpaa, K. J., White, C. L., … Isaacs, A. M. (2010). FUS pathology defines the majority of tau- and TDP-43-negative frontotemporal lobar degeneration. *Acta Neuropathologica*, *120*(1), 33. https://doi.org/10.1007/S00401-010-0698-6

Vahsen, B. (2021). *Role of autophagic protein ULK1 in axonal degeneration and regeneration in rat cortical neurons in vitro*. Georg-August-Universität .

Vahsen, B. F., Gray, E., Thompson, A. G., Ansorge, O., Anthony, D. C., Cowley, S. A., Talbot, K., & Turner, M. R. (2021). Non-neuronal cells in amyotrophic lateral sclerosis — from pathogenesis to biomarkers. *Nature Reviews Neurology 2021 17:6*, *17*(6), 333–348. https://doi.org/10.1038/s41582-021-00487-8

van Damme, P., Bogaert, E., Dewil, M., Hersmus, N., Kiraly, D., Scheveneels, W., Bockx, I., Braeken, D., Verpoorten, N., Verhoeven, K., Timmerman, V., Herijgers, P., Callewaert, G., Carmeliet, P., van Bosch, L. den, & Robberecht, W. (2007). Astrocytes regulate GluR2 expression in motor neurons and their vulnerability to excitotoxicity. *Proceedings of the National Academy of Sciences*, *104*(37), 14825–14830. https://doi.org/10.1073/PNAS.0705046104

Van Damme, P., Van Hoecke, A., Lambrechts, D., Vanacker, P., Bogaert, E., Van Swieten, J., Carmeliet, P., Van Den Bosch, L., & Robberecht, W. (2008). Progranulin functions as a neurotrophic factor to regulate neurite outgrowth and enhance neuronal survival. *Journal of Cell Biology*. https://doi.org/10.1083/jcb.200712039

Van Deerlin, V. M., Leverenz, J. B., Bekris, L. M., Bird, T. D., Yuan, W., Elman, L. B., Clay, D., Wood, E. M. C., Chen-Plotkin, A. S., Martinez-Lage, M., Steinbart, E., McCluskey, L., Grossman, M., Neumann, M., Wu, I. L., Yang, W. S., Kalb, R., Galasko, D. R., Montine, T. J., … Yu, C. E. (2008).

TARDBP mutations in amyotrophic lateral sclerosis with TDP-43 neuropathology: a genetic and histopathological analysis. *The Lancet Neurology*. https://doi.org/10.1016/S1474-4422(08)70071-1

Vatsavayai, S. C., Yoon, S. J., Gardner, R. C., Gendron, T. F., Vargas, J. N. S., Trujillo, A., Pribadi, M., Phillips, J. J., Gaus, S. E., Hixson, J. D., Garcia, P. A., Rabinovici, G. D., Coppola, G., Geschwind, D. H., Petrucelli, L., Miller, B. L., & Seeley, W. W. (2016). Timing and significance of pathological features in C9orf72 expansion-associated frontotemporal dementia. *Brain*, *139*(12), 3202–3216. https://doi.org/10.1093/BRAIN/AWW250

Verdone, B. M., Cicardi, M. E., Wen, X., Sriramoji, S., Russell, K., Markandaiah, S. S., Jensen, B. K., Krishnamurthy, K., Haeusler, A. R., Pasinelli, P., & Trotti, D. (2022). A mouse model with widespread expression of the C9orf72-linked glycine–arginine dipeptide displays non-lethal ALS/FTD-like phenotypes. *Scientific Reports*, *12*(1), 5644. https://doi.org/10.1038/s41598-022-09593-z

Verkhratsky, A., & Nedergaard, M. (2018). Physiology of astroglia. *Physiological Reviews*, *98*(1), 239–389. https://doi.org/10.1152/PHYSREV.00042.2016/ASSET/IMAGES/LARGE/Z9J0041728140034.JPEG

Vitale, I., Manic, G., de Maria, R., Kroemer, G., & Galluzzi, L. (2017). DNA Damage in Stem Cells. *Molecular Cell*, *66*(3), 306–319. https://doi.org/10.1016/J.MOLCEL.2017.04.006

Wainger, B. J., Kiskinis, E., Mellin, C., Wiskow, O., Han, S. S. W., Sandoe, J., Perez, N. P., Williams, L. A., Lee, S., Boulting, G., Berry, J. D., Brown, R. H., Cudkowicz, M. E., Bean, B. P., Eggan, K., & Woolf, C. J. (2014). Intrinsic Membrane Hyperexcitability of Amyotrophic Lateral Sclerosis Patient-Derived Motor Neurons. *Cell Reports*, *7*(1), 1–11. https://doi.org/10.1016/J.CELREP.2014.03.019

Waite, A. J., Bäumer, D., East, S., Neal, J., Morris, H. R., Ansorge, O., & Blake, D. J. (2014). Reduced C9orf72 protein levels in frontal cortex of amyotrophic lateral sclerosis and frontotemporal degeneration brain with the C9ORF72 hexanucleotide repeat expansion. *Neurobiology of Aging*. https://doi.org/10.1016/j.neurobiolaging.2014.01.016

Walker, M. C., & van der Donk, W. A. (2016). The Many Roles of Glutamate in Metabolism. *Journal of Industrial Microbiology & Biotechnology*, *43*(0), 419. https://doi.org/10.1007/S10295-015-1665-Y

Wang, G., Gilbert, J., & Man, H. Y. (2012). AMPA receptor trafficking in homeostatic synaptic plasticity: Functional molecules and signaling cascades. *Neural Plasticity*, *2012*. https://doi.org/10.1155/2012/825364

Wang, H., Song, P., Du, L., Tian, W., Yue, W., Liu, M., Li, D., Wang, B., Zhu, Y., Cao, C., Zhou, J., & Chen, Q. (2011). Parkin ubiquitinates Drp1 for proteasome-dependent degradation: implication of dysregulated mitochondrial dynamics in Parkinson disease. *The Journal of Biological Chemistry*, *286*(13), 11649–11658. https://doi.org/10.1074/JBC.M110.144238

Wang, I. F., Wu, L. S., Chang, H. Y., & Shen, C. K. J. (2008). TDP-43, the signature protein of FTLD-U, is a neuronal activity-responsive factor. *Journal of Neurochemistry*. https://doi.org/10.1111/j.1471-4159.2007.05190.x

Wang, W., Li, L., Lin, W. L., Dickson, D. W., Petrucelli, L., Zhang, T., & Wang, X. (2013). The ALS disease-associated mutant TDP-43 impairs mitochondrial dynamics and function in motor neurons. *Human Molecular Genetics*, *22*(23), 4706–4719. https://doi.org/10.1093/HMG/DDT319

Wang, Y., & Mandelkow, E. (2016). Tau in physiology and pathology. *Nature Reviews Neuroscience*, *17*(1), 22–35. https://doi.org/10.1038/nrn.2015.1

Wang, Y., Xu, E., Musich, P. R., & Lin, F. (2019). Mitochondrial dysfunction in neurodegenerative diseases and the potential countermeasure. *CNS Neuroscience & Therapeutics*, *25*(7), 816–824. https://doi.org/10.1111/CNS.13116

Warren, J. D., Rohrer, J. D., & Rossor, M. N. (2013). Clinical review. Frontotemporal dementia. *BMJ (Clinical Research Ed.)*. https://doi.org/10.1136/bmj.f4827

WAVE Life Science Ltd. (2022). *Wave Life Sciences Announces Positive Update to Ongoing Phase 1b/2a FOCUS-C9 Study Driven by Potent, Durable Reductions of Poly(GP) with Low, Single Doses of WVE-004 | BioSpace*. Globe Newswire. https://www.biospace.com/article/releases/wave-life-sciences-announces-positive-update-to-ongoing-phase-1b-2a-focus-c9-study-driven-by-potent-durable-reductions-of-poly-gp-with-low-single-doses-of-wve-004/

Weber, A. M., Wong, F. K., Tufford, A. R., Schlichter, L. C., Matveev, V., & Stanley, E. F. (2010). N-type Ca2+ channels carry the largest current: implications for nanodomains and transmitter release. *Nature Neuroscience 2010 13:11*, *13*(11), 1348–1350. https://doi.org/10.1038/NN.2657

Webster, C. P., Smith, E. F., Bauer, C. S., Moller, A., Hautbergue, G. M., Ferraiuolo, L., Myszczynska, M. A., Higginbottom, A., Walsh, M. J., Whitworth, A. J., Kaspar, B. K., Meyer, K., Shaw, P. J., Grierson, A. J., & Vos, K. J. de. (2016). The C9orf72 protein interacts with Rab1a and the ULK1 complex to regulate initiation of autophagy. *The EMBO Journal*, *35*(15), 1656–1676. https://doi.org/10.15252/EMBJ.201694401

Weil, R., Laplantine, E., Curic, S., & Génin, P. (2018). Role of Optineurin in the Mitochondrial Dysfunction: Potential Implications in Neurodegenerative Diseases and Cancer. *Frontiers in Immunology*, *9*(JUN), 1. https://doi.org/10.3389/FIMMU.2018.01243

Wen, X., Tan, W., Westergard, T., Krishnamurthy, K., Markandaiah, S. S., Shi, Y., Lin, S., Shneider, N. A., Monaghan, J., Pandey, U. B., Pasinelli, P., Ichida, J. K., & Trotti, D. (2014). Antisense proline-arginine RAN dipeptides linked to C9ORF72-ALS/FTD form toxic nuclear aggregates that initiate invitro and invivo neuronal death. *Neuron*. https://doi.org/10.1016/j.neuron.2014.12.010

West, R. J. H., Sharpe, J. L., Voelzmann, A., Munro, A. L., Hahn, I., Baines, R. A., & Pickering-Brown, S. (2020). Co-expression of C9orf72 related dipeptide-repeats over 1000 repeat units reveals age- and combination-specific phenotypic profiles in Drosophila. *Acta Neuropathologica Communications*, *8*(1), 158. https://doi.org/10.1186/s40478-020-01028-y

Westergard, T., McAvoy, K., Russell, K., Wen, X., Pang, Y., Morris, B., Pasinelli, P., Trotti, D., & Haeusler, A. (2019). Repeat-associated non-AUG translation in C9orf72-ALS/FTD is driven by neuronal excitation and stress. *EMBO Molecular Medicine*, *11*(2), e9423. https://doi.org/https://doi.org/10.15252/emmm.201809423

Westermann, B. (2012). Bioenergetic role of mitochondrial fusion and fission. *Biochimica et Biophysica Acta (BBA) - Bioenergetics*, *1817*(10), 1833–1838. https://doi.org/10.1016/J.BBABIO.2012.02.033

White, M. A., Kim, E., Duffy, A., Adalbert, R., Phillips, B. U., Peters, O. M., Stephenson, J., Yang, S., Massenzio, F., Lin, Z., Andrews, S., Segonds-Pichon, A., Metterville, J., Saksida, L. M., Mead, R., Ribchester, R. R., Barhomi, Y., Serre, T., Coleman, M. P., … Sreedharan, J. (2018). TDP-43 gains function due to perturbed autoregulation in a Tardbp knock-in mouse model of ALS-FTD. *Nature Neuroscience*. https://doi.org/10.1038/s41593-018-0113-5

Wicks, P., Abrahams, S., Papps, B., Al-Chalabi, A., Shaw, C., Leigh, P., & Goldstein, L. (2009). SOD1 and cognitive dysfunction in familial amyotrophic lateral sclerosis. *Journal of Neurology*, *256*(2), 234–241. https://doi.org/10.1007/S00415-009-0078-0

Woerner, A. C., Frottin, F., Hornburg, D., Feng, L. R., Meissner, F., Patra, M., Tatzelt, J., Mann, M., Winklhofer, K. F., Hartl, F. U., & Hipp, M. S. (2016). Cytoplasmic protein aggregates interfere with nucleocytoplasmic transport of protein and RNA. *Science*. https://doi.org/10.1126/science.aad2033

Woodworth, M. B., Greig, L. C., Liu, K. X., Ippolito, G. C., Tucker, H. O., & Macklis, J. D. (2016). Ctip1 regulates the balance between specification of distinct projection neuron subtypes in deep cortical layers. *Cell Reports*, *15*(5), 999. https://doi.org/10.1016/J.CELREP.2016.03.064

Woollacott, I. O. C., & Rohrer, J. D. (2016). The clinical spectrum of sporadic and familial forms of frontotemporal dementia. In *Journal of Neurochemistry*. https://doi.org/10.1111/jnc.13654

Wright, A., & Vissel, B. (2012). The essential role of AMPA receptor GluA2 subunit RNA editing in the normal and diseased brain. *Frontiers in Molecular Neuroscience*, *0*(APRIL), 34. https://doi.org/10.3389/FNMOL.2012.00034/BIBTEX

Wright, M. F., Bowdridge, E., McDermott, E. L., Richardson, S., Scheidler, J., Syed, Q., Bush, T., Inskeep, E. K., & Flores, J. A. (2014). Mechanisms of intracellular calcium homeostasis in developing and mature bovine corpora lutea. *Biology of Reproduction*, *90*(3), 1–12. https://doi.org/10.1095/BIOLREPROD.113.113662/2514196

Xi, Z., Zinman, L., Moreno, D., Schymick, J., Liang, Y., Sato, C., Zheng, Y., Ghani, M., Dib, S., Keith, J., Robertson, J., & Rogaeva, E. (2013). Hypermethylation of the CpG Island Near the G4C2 Repeat in ALS with a C9orf72 Expansion. *The American Journal of Human Genetics*, *92*(6), 981–989. https://doi.org/10.1016/J.AJHG.2013.04.017

Xiao, S., McKeever, P. M., Lau, A., & Robertson, J. (2019). Synaptic localization of C9orf72 regulates post-synaptic glutamate receptor 1 levels. *Acta Neuropathologica Communications*, *7*(1), 1–13. https://doi.org/10.1186/S40478-019-0812-5/FIGURES/5

Xin, W. K., Kwan, C. L., Zhao, X. H., Xu, J., Ellen, R. P., McCulloch, C. A. G., & Yu, X. M. (2005). A Functional Interaction of Sodium and Calcium in the Regulation of NMDA Receptor Activity by Remote NMDA Receptors. *Journal of Neuroscience*, *25*(1), 139–148. https://doi.org/10.1523/JNEUROSCI.3791-04.2005

Yamashita, S., & Ando, Y. (2015). Genotype-phenotype relationship in hereditary amyotrophic lateral sclerosis. *Translational Neurodegeneration 2015 4:1*, *4*(1), 1–13. https://doi.org/10.1186/S40035-015-0036-Y

Yang, Y., Gehrke, S., Imai, Y., Huang, Z., Ouyang, Y., Wang, J. W., Yang, L., Beal, M. F., Vogel, H., & Lu, B. (2006). Mitochondrial pathology and muscle and dopaminergic neuron degeneration caused by inactivation of Drosophila Pink1 is rescued by Parkin. *Proceedings of the National Academy of Sciences*, *103*(28), 10793–10798. https://doi.org/10.1073/PNAS.0602493103

Yang, Z., & Wang, K. K. W. (2015). Glial fibrillary acidic protein: from intermediate filament assembly and gliosis to neurobiomarker. *Trends in Neurosciences*, *38*(6), 364–374. https://doi.org/10.1016/J.TINS.2015.04.003

Yih, L., Huang, H., Jan, K., & Lee, T. (1991). Sodium arsenite induces ATP depletion and mitochondrial damage in HeLa cells. *Cell Biology International Reports*, *15*(3), 253–264.

Yin, X. M., Oltvai, Z. N., & Korsmeyer, S. J. (1994). BH1 and BH2 domains of Bcl-2 are required for inhibition of apoptosis and heterodimerization with Bax. *Nature 1994 369:6478*, *369*(6478), 321–323. https://doi.org/10.1038/369321a0

Youle, R. J., & van der Bliek, A. M. (2012). Mitochondrial Fission, Fusion, and Stress. *Science (New York, N.Y.)*, *337*(6098), 1062. https://doi.org/10.1126/SCIENCE.1219855

Yu, C. E., Bird, T. D., Bekris, L. M., Montine, T. J., Leverenz, J. B., Steinbart, E., Galloway, N. M., Feldman, H., Woltjer, R., Miller, C. A., Wood, E. M. C., Grossman, M., McCluskey, L., Clark, C. M., Neumann, M., Danek, A., Galasko, D. R., Arnold, S. E., Chen-Plotkin, A., … Van Deerlin, V. M. (2010). The spectrum of mutations in progranulin: A collaborative study screening 545 cases of neurodegeneration. *Archives of Neurology*. https://doi.org/10.1001/archneurol.2009.328

Yu, R., Jin, S., Lendahl, U., Nistér, M., & Zhao, J. (2019). Human Fis1 regulates mitochondrial dynamics through inhibition of the fusion machinery. *The EMBO Journal*, *38*(8). https://doi.org/10.15252/EMBJ.201899748

Zenisek, D., & Matthews, G. (2000). The Role of Mitochondria in Presynaptic Calcium Handling at a Ribbon Synapse clamp and Ca 2 imaging techniques. The results demon-strate that PMCA is of primary importance in regulating basal Ca 2 and in clearing Ca 2 after depolarization-evoked influx. Mitochondrial Ca 2 uptake plays some role, especially when [Ca 2] i exceeds 800 nM, but the. *Neuron*, *25*, 229–237.

Zhang, X., Gao, F., Wang, D., Li, C., Fu, Y., He, W., & Zhang, J. (2018). Tau Pathology in Parkinson's Disease. *Frontiers in Neurology*, *9*(OCT), 809. https://doi.org/10.3389/FNEUR.2018.00809

Zhang, Y. J., Gendron, T. F., Grima, J. C., Sasaguri, H., Jansen-West, K., Xu, Y. F., Katzman, R. B., Gass, J., Murray, M. E., Shinohara, M., Lin, W. L., Garrett, A., Stankowski, J. N., Daughrity, L., Tong, J., Perkerson, E. A., Yue, M., Chew, J., Castanedes-Casey, M., … Petrucelli, L. (2016). C9ORF72 poly(GA) aggregates sequester and impair HR23 and nucleocytoplasmic transport proteins. *Nature Neuroscience*, *19*(5), 668. https://doi.org/10.1038/NN.4272

Zhang, Y. J., Jansen-West, K., Xu, Y. F., Gendron, T. F., Bieniek, K. F., Lin, W. L., Sasaguri, H., Caulfield, T., Hubbard, J., Daughrity, L., Chew, J., Belzil, V. v., Prudencio, M., Stankowski, J. N., Castanedes-Casey, M., Whitelaw, E., Ash, P. E. A., DeTure, M., Rademakers, R., … Petrucelli, L. (2014). Aggregation-prone c9FTD/ALS poly(GA) RAN-translated proteins cause neurotoxicity by inducing ER stress. *Acta Neuropathologica*, *128*(4), 505. https://doi.org/10.1007/S00401-014-1336-5

Zhao, C., Devlin, A. C., Chouhan, A. K., Selvaraj, B. T., Stavrou, M., Burr, K., Brivio, V., He, X., Mehta, A. R., Story, D., Shaw, C. E., Dando, O., Hardingham, G. E., Miles, G. B., & Chandran, S. (2020). Mutant C9orf72 human iPSC-derived astrocytes cause non-cell autonomous motor neuron pathophysiology. *Glia*, *68*(5), 1046–1064. https://doi.org/10.1002/GLIA.23761

Zheng, N., Jeyifous, O., Munro, C., Montgomery, J. M., & Green, W. N. (2015). Synaptic activity regulates AMPA receptor trafficking through different recycling pathways. *ELife*, *4*(MAY). https://doi.org/10.7554/ELIFE.06878

Zheng, X., Boyer, L., Jin, M., Mertens, J., Kim, Y., Ma, L., Ma, L., Hamm, M., Gage, F. H., & Hunter, T. (2016). Metabolic reprogramming during neuronal differentiation from aerobic glycolysis to neuronal oxidative phosphorylation. *ELife*, *5*(JUN2016). https://doi.org/10.7554/ELIFE.13374

Zhou, Q., Lehmer, C., Michaelsen, M., Mori, K., Alterauge, D., Baumjohann, D., Schludi, M. H., Greiling, J., Farny, D., Flatley, A., Feederle, R., May, S., Schreiber, F., Arzberger, T., Kuhm, C., Klopstock, T., Hermann, A., Haass, C., & Edbauer, D. (2017). Antibodies inhibit transmission and aggregation of C9orf72 poly-GA dipeptide repeat proteins. *EMBO Molecular Medicine*, *9*(5), 687–702. https://doi.org/10.15252/EMMM.201607054

Zhu, J., Nathan, C., Jin, W., Sim, D., Ashcroft, G. S., Wahl, S. M., Lacomis, L., Erdjument-Bromage, H., Tempst, P., Wright, C. D., & Ding, A. (2002). Conversion of proepithelin to epithelins: Roles of SLPI and elastase in host defense and wound repair. In *Cell*. https://doi.org/10.1016/S0092-8674(02)01141-8

Zhu, Q., Jiang, J., Gendron, T. F., McAlonis-Downes, M., Jiang, L., Taylor, A., Diaz Garcia, S., Ghosh Dastidar, S., Rodriguez, M. J., King, P., Zhang, Y., la Spada, A. R., Xu, H., Petrucelli, L., Ravits, J., da Cruz, S., Lagier-Tourenne, C., & Cleveland, D. W. (2020). Reduced C9ORF72 function exacerbates gain of toxicity from ALS/FTD-causing repeat expansion in C9orf72. *Nature Neuroscience 2020 23:5*, *23*(5), 615–624. https://doi.org/10.1038/s41593-020-0619-5

Zou, Z.-Y., Zhou, Z.-R., Che, C.-H., Liu, C.-Y., He, R.-L., & Huang, H.-P. (2017). Genetic epidemiology of amyotrophic lateral sclerosis: a systematic review and meta-analysis. *Journal of Neurology, Neurosurgery & Psychiatry*, *88*(7), 540–549. https://doi.org/10.1136/JNNP-2016-315018

Zu, T., Guo, S., Bardhi, O., Ryskamp, D. A., Li, J., Tusi, S. K., Engelbrecht, A., Klippel, K., Chakrabarty, P., Nguyen, L., Golde, T. E., Sonenberg, N., & Ranum, L. P. W. (2020). Metformin inhibits RAN translation through PKR pathway and mitigates disease in C9orf72 ALS/FTD mice. *Proceedings of the National Academy of Sciences of the United States of America*, *117*(31), 18591–18599. https://doi.org/10.1073/PNAS.2005748117/SUPPL_FILE/PNAS.2005748117.SAPP.PDF

9 Appendices

9.1 Appendix 1: Chromosomal aberrations in iPSCs

I conducted these experiments with iPSCs between October 2018 and November 2021. I received the results of routine quality control of these cell lines in November 2021 which showed major chromosomal aberrations in some of the cell lines (see Table 6).

For the ISO-2 control line, I used both the 59-2 and 59-3 clones at a ratio of approximately 70% to 30%. 14% of 59-2 cells were identified to be tetraploid, while all cells of the 59-3 line have a likely 2/17 translocation and 10% of cells have an additional rearranged chromosome. The C9-02-02 also had major chromosomal aberrations as 75% of cells carry a duplication of chromosome 1 while another 2% of cells are tetraploid. These chromosomal aberrations are likely to affect molecular processes in these cells.

All WT control lines had no chromosomal aberrations. For the C9-1 patient line, I used both C9-01-06 and C9-01-07 clones at a ratio of about 20% to 80%. All cells of the C9-01-06 cell line contain a rearranged chromosome 2, while 1/54 of cells of the C9-01-07 cell line carry an extra chromosome, most likely chromosome 12. The C9-8 cell line SFC-853 was not tested here. This cell line is much younger than the other cell lines I used, as it was reprogrammed not long before I started my experimental work and underwent thorough quality testing back then. Therefore, I do not expect any major chromosomal aberrations in this cell line. As the percentage of aberrant cells in the C9-01-07 line is very low and the C9-01-06 line was not used much, results from the pooled C9-1+8 patient lines compared to WT controls are more reliable than from the C9-2 patient compared to ISO-2 controls.

Table 6: Results of quality testing of iPSC lines from 2021.

LINE	PASSAGE NUMBER TESTED	PASSAGE NUMBER USED IN EXPERIMENTS	DETAILS
SFC180-01-01	24	27 and 29	No chromosomal deficit
SFC840-03-03	25	24, 25, and 31	No chromosomal deficit
SFC856-03-04	23	30	No chromosomal deficit
59-2		46 and 48	14% tetraploid
59-3	44	46 and 48	**All** cells have likely 2/17 Translocation, 10% of cells have and additional rearranged chromosome, unclear origin
C9-01-06	18 and 21	24 and 26	**All** cells contain rearranged Chr 2 **(analysed twice)**
C9-01-07		24 and 26	1/54 cells had extra chromosome (most likely chr12)
C9-02-02		31 and 48	2% tetraploid + 75% duplication of Chr1

9.2 Appendix 2: Optimising the concentration of treatments

In several experiments in this study, cells were treated with compounds. The aim was to induce cellular stress which might exacerbate molecular deficits in patient cells. Thus, the concentration of compounds was aimed at inducing cellular stress rather than apoptosis. Specifically, thapsigargin was used to induce ER stress, sodium arsenite was used to induce stress granules and mitochondrial stress, CCCP was used to induce mitochondrial depolarisation, while bafilomycin and rapamycin were used to study autophagic flux. Using the correct concentration of the compound was essential, as it should be high enough to induce a measurable effect but not high enough to kill CN cultures.

My first approach was to use the same concentration of these compounds as were optimised for iPSC-derived motor neurons. This approach worked for $NaAsO_2$ as measured by the significant induction of stress granules (see Figure 25). However, after several differentiations, it became clear that these

concentrations were not high enough for thapsigargin, bafilomycin, and rapamycin to induce a significant effect. Thus, the concentration of these compounds had to be optimised in iPSC-derived CNs. Due to time constraints, I designed the optimisation experiment with only two WT cell lines on day 50. Therefore, the number of replicates was too low to analyse any meaningful statistics. I pooled the measurements and chose the concentration with the strongest effect.

9.2.1 Thapsigargin treatment

The concentration of thapsigargin used for iPSC-derived MNs in similar experiments to the ones conducted in this study is 1 µM. The concentration of thapsigargin used for calcium imaging in iPSC-derived MNs to induce the immediate and complete emptying of ER Ca^{2+} stores is 10 µM (Dafinca et al., 2016). Since my iPSC-derived CNs were incubated with thapsigargin for 24h to induce measurable changes in protein expression, I expected to use a concentration far below 10 µM to avoid inducing widespread cell death. Therefore, I treated iPSC-derived CNs with the following concentrations of thapsigargin for 24h: 0 µM, 1 µM, 1.5 µM, 2 µM, 2.5 µM, and 3 µM.

I chose to assess thapsigargin efficacy by testing BiP expression. BiP is a protein of the UPR which is upregulated in cells with ER stress. Since thapsigargin induces ER stress, I expect BiP levels to rise in cells treated with thapsigargin. I found that BiP levels were highest at a low concentration of thapsigargin and seemed to be closer to normal levels in cells treated with a high concentration of thapsigargin. I concluded that this might be due to cell death in cells treated with a high concentration of thapsigargin. As cells treated with 1.5 µM had the most consistent upregulation of BiP, I selected a concentration of 1.5 µM for future thapsigargin treatment. This concentration did not cause an increase in apoptosis as measured by ClCasp3 levels in any cell line (Figure 21, data not shown).

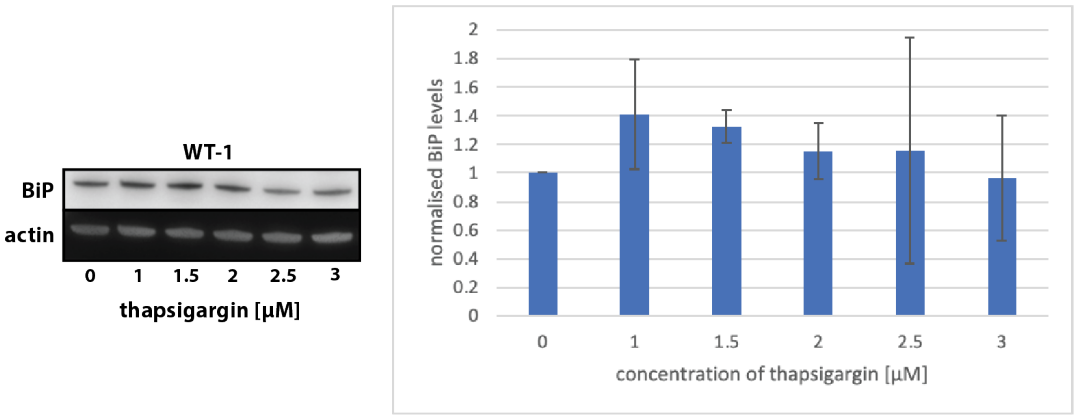


Figure 48: Optimisation of the concentration of thapsigargin measuring BiP expression in pooled WT-1 and WT-2 cell lines. iPSC-derived CNs on day 50 were treated with various concentrations of thapsigargin for 24h. Left: representative example of Western blot. Right: quantification of Western blots. Bars represent means, error bars represent the standard deviation. n=2.

I later found that a concentration of 1.5 µM thapsigargin did not induce the upregulation of UPR proteins, suggesting that the concentration of thapsigargin might not have been high enough. However, using 1.5 µM thapsigargin I observed a significant downregulation of GluA1 expression in WT control lines (see Figure 33), suggesting that thapsigargin caused a molecular deficit in iPSC-derived CNs.

9.2.2 Bafilomycin treatment

The concentration of bafilomycin used for iPSC-derived MNs in similar experiments to the ones conducted in this study is 100 nM (Dr. Paola Barbagallo, unpublished). Since this concentration did not appear to have any measurable effect on iPSC-derived CNs, I treated iPSC-derived CNs with the following concentrations of bafilomycin for 24h: 0 nM, 150 nM, 200 nM, 250 nM, and 300 nM. I chose to test autophagic flux by measuring p62 levels. p62 is essential for autophagy and is degraded in autophagosomes. As bafilomycin inhibits autophagic flux, we expect p62 levels to rise. This experiment was conducted with only one cell line (n=1). p62 levels were at their highest when iPSC-

derived CNs were incubated with 250 nM bafilomycin for 24h (Figure 49). Thus, this concentration was used for all the following experiments.

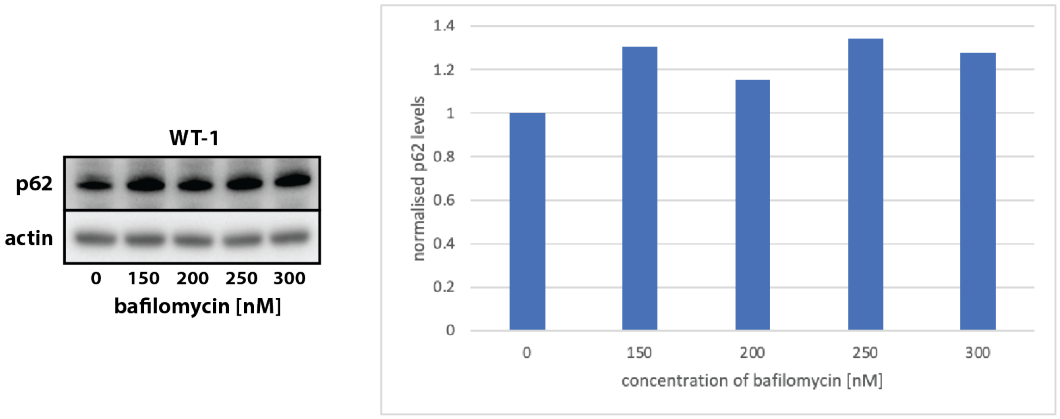


Figure 49: Optimisation of the concentration of bafilomycin measuring p62 expression in the WT-1 cell line. iPSC-derived CNs on day 50 were treated with various concentrations of bafilomycin for 24h. Picture and quantification of Western blot. n=1.

Further experiments showed that 250 nM bafilomycin did not significantly inhibit autophagic flux in WT cell lines according to p62 levels, but significantly increased p62 levels in the C9-2 patient line, suggesting an increased sensitivity to autophagy inhibition in patient cells (see Figure 29A). It was also sufficient to induce a significant upregulation of the LC3BII/LC3BI ratio in WT controls and pooled C9-1+8 cells, which is an additional readout of autophagic flux (see Figure 29B). Therefore, the treatment with 250 nM bafilomycin for 24h was useful to study autophagic defects in C9-CNs.

9.2.3 Rapamycin treatment

The concentration of rapamycin used for iPSC-derived MNs in similar experiments to the ones conducted in this study is 40 nM (Dr. Paola Barbagallo, unpublished). Since this concentration did not appear to have any measurable effect on iPSC-derived CNs, I treated iPSC-derived CNs with the following concentrations of rapamycin for 24h: 0 nM, 40 nM, 80 nM, 100 nM, and 120 nM. Again, I chose to test autophagic flux by measuring p62 levels, expecting a drop in p62 levels as a result of the

stimulation of autophagy by rapamycin. p62 levels first dropped at the addition of a low concentration of rapamycin, then rose, and then dropped again (Figure 50).

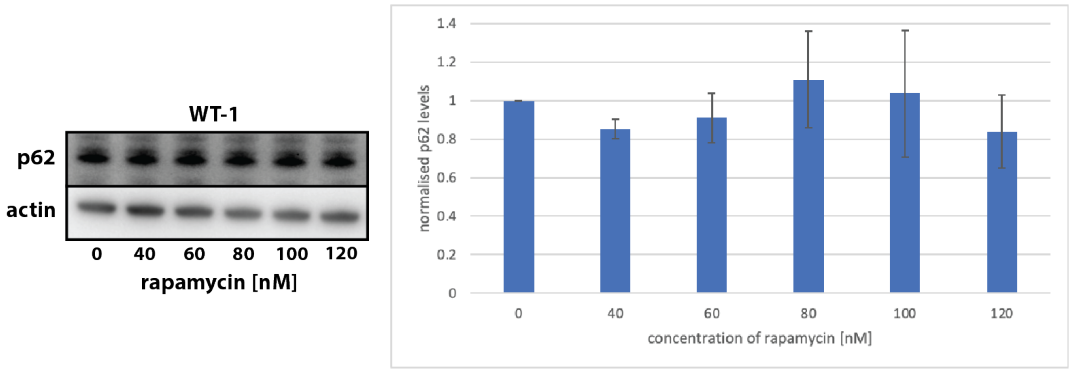


Figure 50: Optimisation of the concentration of rapamycin measuring p62 expression in the pooled WT-1 and WT-2 cell lines. iPSC-derived CNs on day 50 were treated with various concentrations of rapamycin for 24h. Left: representative example of Western blot. Right: quantification of Western blots. Bars represent means, error bars represent the standard deviation. n=2.

Since these concentrations did not cause a robust drop in p62 levels at any concentration, I tried to find a working concentration in the literature. One study optimised the concentration of rapamycin in primary cortical neurons and found that the addition of 250 nM rapamycin causes a moderate effect in cells treated for 6h as measured by studying the LC3BII/LC3BI ratio (B. Vahsen, 2021). Since I aimed to treat cells for 24h and did not have time to repeat the optimisation experiment, I used 200 nM of rapamycin for all following experiments. With this concentration, I measured no significant effects on autophagic flux in iPSC-derived CNs. However, I observed a potential exacerbation of GluA1 loss in rapamycin-treated pooled C9-1+8 CNs (Figure 33), implying that 200 nM rapamycin affects molecular mechanisms in C9-CNs.

9.2.4 $NaAsO_2$ treatment

For $NaAsO_2$, I used the same concentrations as used in iPSC-derived MNs (Ababneh et al., 2020). I observed a significant upregulation of the number of stress granules per neuron in response to 1h of treatment with 0.5 mM $NaAsO_2$ (see Figure 25). Therefore, this concentration effectively induced

cellular stress and did not require optimisation. Further effects of this treatment are an increase in GluN1 expression and P-DRP1 levels amongst others.

9.2.5 CCCP treatment

Several papers found a significant initiation of mitophagy in cortical neurons treated with 10 µM CCCP for 1h to 24h (Cai et al., 2012; Joselin et al., 2012; Soutar et al., 2018). One study found that Parkin translocation is highest at 24h in mouse primary neurons (Cai et al., 2012). Another found that treating iPSC-derived CNs with 10 µM CCCP for 16h caused a significant reduction in the protein levels of the mitochondrial proteins TOMM20, TIM23, PMPCB, and AKT pSer473 (Soutar et al., 2018).

I decided to study mitophagy with CCCP treatment halfway through my experimental time once I established a robust loss of mitochondrial mass. As my experimental time was limited and the above mentioned studies found a robust initiation of mitophagy using 10 µM CCCP in cortical neurons, I decided to use this concentration of CCCP without optimising the concentration first to ensure getting a high enough number of technical replicates to find statistically significant effects. In my experiments, treating cells with 10 µM CCCP significantly induced mitophagy according to PINK1 levels and pUb (Ser65) levels in pooled C9-CNs suggesting an increased sensitivity to mitochondrial stressors (Figure 43). Therefore, the chosen concentration of CCCP was effective in exacerbating mitochondrial defects in patient CNs.

9.3 Appendix 3: Materials

Table 7: The materials used in this study for cell culture, immunocytochemistry, Western blotting, calcium imaging, and cellular assays.

Item	**Supplier**	Catalogue number
Cell Culture		
mTeSR1	Stemcell technologies	85850
Y-26732	Tocris	1254
UltraPure 0.5M EDTA	Invitrogen	15575020
Dimethy sulfoxide (DMSO)	Sigma-Aldrich	D8418
ES-grade serum	Gibco	16141-061
DMEM/F12 GlutaMAX™	Gibco	10565-018
Neurobasal®	Gibco	21103-049
N2 supplement	Gibco	17502048
B27 supplement minus vitamin A	Gibco	12587010
Insulin	Sigma-Aldrich	I9278-5ML
MEM Non-Essential Amino Acids Solution	Gibco	11140050
2-mercaptoethanol	Gibco	31350-010
Antibiotic-Antimycotic	Gibco	15240-096
Dorsomorphin	Cayman Chemical Company	21207
SB-431542	Millipore	616461-5mg
StemPro® Accutase®	Gibco	A11105-01
FGF2	Ray biotech	268-10059
BDNF	Peprotech	450-02-100ug

GDNF	Peprotech	450-10-100ug
Bafilomycin	Sigma-Aldrich	B1793-2ug
Rapamycin	Sigma-Aldrich	R0395-1mg
Thapsigargin	Tocris	1138
Sodium arsenite ($NaArO_2$)	Sigma	S7400
CCCP	Tocris Bioscience	0452
Immunocytochemistry		
Paraformaldehyde (PFA)	TAAB Laboratories Equipment	F003
Normal Goat Serum (NGS)	Sigma	NS02L
Triton X-100	Sigma-Aldrich	X-100-500mL
4',6-Diamidino-2-Phenylindole (DAPI)	Sigma-Aldrich	D8417
Dako	Agilent	S3023
Western blotting		
PBS	Gibco	10010023
Pierce® RIPA buffer	Thermo Scientific	89900
Protease inhibitor	Roche	04693159
Phosphatase inhibitor	Thermo Scientific	A32957
Pierce™ BCA Protein Assay	Thermo Scientific	23225
NuPAGE™ LDS sample buffer	Invitrogen	NP0007
NuPAGE™ Sample Reducing Agent	Invitrogen	11569166
NuPAGE™ 4-12% Bis-Tris Gel	Invitrogen	NP0322BOX
NanoPAC-500 Mini Power Supply	Cleaver Scientific	NANOPAC-500
NuPAGE™ MES running buffer	Life Technologies	NP0002

XCell SureLock™ Mini-Cell	Thermo Fisher	EI0001
iBlot 2 Dry Blotting System	Thermo Fisher	IB21001
iBlot®2 PVDF Regular Stacks	Invitrogen	IB24001
Skim Milk Powder	Sigma-Aldrich	70166-500G
Tris Buffered Saline (TBS)	Sigma-Aldrich	T5912
Tween® 20	Fisher Bioreagents	10113103
Immobilon Western Chemiluminescent HRP substrate	Millipore	WBKLS0500
ChemiDoc MP Imaging System	Bio-Rad	17001402
Restore™ PLUS Western Blot Stripping Buffer	Thermo Scientific	46430
Protein ladder Spectra Multicolor Broad Range	Thermo Scientific	26634
Calcium imaging		
Fluo 4-AM	Invitrogen	F14217
Hank's Balanced Salts Solution (HBSS) with Ca^{2+} and Mg^{2+}	Gibco	14025092
Hank's Balanced Salts Solution (HBSS) without Ca^{2+} and Mg^{2+}	Gibco	14175095
L-glutamic acid	Sigma-Aldrich	128430
KCl	Sigma-Aldrich	P9541
Carbamoylcholine chloride (CCh)	Sigma-Aldrich	C4382
Assays and Chemicals		
MitoTracker™ Red CMXRos	Invitrogen	M7512
MitoTracker™ Green FM	Invitrogen	M7514

Seahorse XF Cell Mito Stress Test	Agilent	103015-100
CyQUANT GR Cell Proliferation Assay	Invitrogen	C7026
Cellular ROS Assay (Red)	Abcam	ab186027

Table 8: Supplier and concentration of antibodies used in this study. ICC=immunocytochemistry, WB=Western blotting.

Target	Supplier	Catalogue number	Concentration used (ICC)	Concentration used (WB)
Primary antibodies				
Tuj1 (ms)	Sigma	A5441	1:5000	
Tuj1 (rb)	Abcam	ab227387	1:5000	
Tuj1 (chk)	Millipore	AB9354	1:1000	
VGluT1	Invitrogen	48-2400	1:1000	
GFAP	Cell Signalling Technologies	80788	1:500	
Tbr1	Abcam	ab183032	1:100	
CTIP1	OriGene	TA590410	1:300	
CTIP2	Abcam	ab18465	1:300	
Bcl-2	Agilent	M0887		1:1000
ClCasp3	Cell Signalling Technologies	9661S	1:500	1:500
Cytochrome C	Abcam	ab110325	1:1000	1:1000
TOMM20	Abcam	ab78547	1:1000	1:1000
TDP-43	Proteintech	10782-2AP	1:500	1:1000

BiP	Abcam	ab21685		1:500
CHOP	Santa Cruz Biotechnology	sc-793		1:1000
ATF4	Abcam	ab184909		1:1000
PABP	Abcam	ab21060	1:1000	
GluN1	Abcam	ab253190		1:1000
GluA1	Abcam	ab31232		1:1000
PSD95	Abcam	Ab2723	1:1000	
CACNA2D1	Abcam	ab253190		1:1000
p62	BD Transduction Laboratories	BD610333		1:1000
LC3B	Novus Biologicals	NB100-2220		1:1000
Lamp2A	Abcam	ab18528		1:1000
MCU	Abcam	ab219827		1:1000
COX IV	Abcam	ab14744		1:1000
P-DRP1	Cell Signalling Technologies	8570		1:1000
Mfn2	Cell Signalling Technologies	11925S		1:1000
PINK1	Cell Signalling Technologies	6946		1:1000
pUb (Ser65)	Millipore	ABS1513-I		1:1000
DCTN1	Thermo Fisher	PA521289		1:1000
KIF5a	Abcam	ab5628		1:1000
β-actin (ms)	Sigma	A5441		1:10000
β-actin (rb)	abcam	ab15568		1:10000
GAPDH	Millipore	ABS16		1:1000

Secondary antibodies				
488 goat-anti-rabbit	Invitrogen	A11034	1:500	
488 goat-anti-mouse	Abcam	A11001	1:2000	
488 goat-anti-chicken	Abcam	ab150169	1:500	
488 goat-anti-rat	Abcam	A11006	1:500	
568 goat-anti-rabbit	Abcam	A11011	1:1000	
568 goat-anti-mouse	Invitrogen	A11004	1:1000	
647 donkey-anti-mouse	Abcam	A31571	1:1000	
647 goat-anti-chicken	Abcam	ab150171	1:500	
ECL anti-rabbit IgG	Cytiva	NA934V		1:5000
ECL anti-mouse IgG	Cytiva	NA931V		1:5000
680RD donkey-anti-mouse	Licor	925-68072		1:5000
800CW donkey-anti-rabbit	Licor	925-32213		1:5000